New Carboxylate and Hydroxamate Inhibitors of Prostaglandin-H-Synthase and their Metal Complexes

A thesis for the degree of
Doctor of Philosophy

Presented to

THE NATIONAL UNIVERSITY OF IRELAND

By

Ahmed Al Agha, BSc, MSc

Research carried out at
Centre for Synthesis and Chemical Biology
The Department of Pharmaceutical and Medicinal Chemistry
Royal College of Surgeons in Ireland,
123 St. Stephen's Green
Dublin 2

PhD 2009

Dedication

To my family

Acknowledgements

Firstly, I would like to thank my supervisor Professor Kevin B. Nolan for all his help, patience and encouragement over the past four years and especially for being so generous with his time and advice throughout my PhD. He has given me the opportunity to work on an important project and has allowed me the freedom to make my own decisions regarding the work and develop my own ideas. If I had another chance to select a supervisor I would have no doubt in selecting him again.
I would also like to give a very special thanks to my advisor Dr. Mauro Adamo who has taught me a lot of organic chemistry and has developed my enthusiasm in this area. He is also a great friend as well as advisor.

Thanks to my special friends in the laboratory Dr. Darren Griffith and Dr Murali Nagabelli for all their time and advice and for teaching me so many practical skills and how to face the problems during my work. Thanks also to Dr. Anthony Chubb, for his molecular modelling expertise, for testing my compounds and for being such a good friend. Also, thanks to other staff members of the Chemistry Department, Dr. Celine Marmion, Dr. Marc Devocelle, Professor Oswaldo Nunez, Dr. James Barlow, Dr Hasan Nimir, Dr. Edelmiro Moman, Mr Terry Murphy, Mr Emmet Campion, Ms Patricia Whyte and Ms Rosemary O' Donoghue for all their help and encouragement.

Many thanks to the rest of the gang in the research laboratory, past and present for making RCSI a very enjoyable and entertaining place to work. These are Linda Piras, Krystyna Krot, Dr Vivek Konda, Aoife Flanagan, Michael Thai, James Parker, Simone Bruschi, Giovanni Campi, Dr Francesco Fini, Stephane Desgranges, Paolo Disetti, Dr. Suresh Surisetti, Sumanth Peraka, David Kennedy, Celine Petit, Jean Lee, Sara Secco, Lisa Taco, Eva Torres Costa, Dr. Ravendra, Robert James Wells, Daria Rosso, Dr. Elise Bernard, Dr. Vivienne, Peter Cully, Colin McElduff, Clodagh Mulcahy, Laura Kennedy, Eleanor Duffy. Gia Bellini and Dr Maria Moccia. A very special thanks to Christine Mara for always being so helpful and accommodating especially in technical matters! I wish you all the best in your future. Suzanne Donnelly was a great help with laboratory matters and looking after me in the lab.

Thanks also to Dr. Helge Müller-Bunz, University College Dublin for the X-ray crystallographic results, Dr. Dilip Rai at University College Dublin for MS analysis, Dr. John O'Brien in Trinity College Dublin for the numerous NMR spectra and to Ann Connolly at University College Dublin for the elemental analysis. Without their help this thesis would not exist. I would like to also thank Dr Zebiune Ramtola, Dr Fiona O'Brien, for their help and patience while they introduced me to the pharmacy laboratory techniques, tutorials and lectures. A very special thanks to Dr Helen McVeigh and Ms Bernadette Kearney in the School of Postgraduate Studies.

Finally I would like to thank my family who have been so wonderfully supportive over the years, particularly my parents, for their help, support, patience, encouragement, love and understanding and for motivating me at the right times. Special thanks to my big brother Dr Rani for looking after me over the past four years and creating for me an environment which made following this path all the more easy. Also to my sisters Amira, Amani and Eman. To all my friends and relatives. You are always behind me and never let me down. I am forever in your debt.

Abstract

The thesis describes new carboxylate and hydroxamate inhibitors of prostaglandin-H-synthase (PGHS) as well as the synthesis and structures of metal complexes of the hydroxamates which were synthesised. This enzyme, also called cyclooxygenase (COX), has two active sites a cyclooxygenase (COX) active site which is the target for aspirin and a peroxidase (POX) active site, upon which the COX site depends.

The thesis is divided in to three chapters. The first chapter describes the attempted synthesis of aspirin derivatives, specifically designed by molecular modelling to fit better into the COX active site of PGHS. These derivatives possess O-acetylsalicylate moieties with an additional alkylcarboxylate substituent which allows simultaneous interaction with Arg120 and Tyr385 at the COX site whilst locating the acetyl group in close proximity to Ser530. The most active compound synthesised was an O-acetylsalicylate ester with an alkylcarboxylate ester substituent which is non-acidic and may act as a lead for further research. An introduction to platelets, thrombosis, prostaglandins and PGHS is given in this chapter prior to a description and discussion of the compounds synthesised.

Chapter 2 describes acetylated salicylhydroxamic acids as PGHS inhibitors. Previous work in our laboratory led to mono- and tri-acetylated salicylhydroxamate derivatives as inhibitors of the COX site of PGHS. The first of these, N-acetoxy-2-hydroxybenzamide (SalAc, **2**), is less potent than aspirin while N-acetoxy-N-acetyl-2-acetoxybenzamide ($SalAc_3$, **4**) is 4-fold more potent. A mechanism of action for SalAc, **2**, similar to that of aspirin and for $SalAc_3$, **4**, involving N-deacetylation followed by transfer of an acetyl group to Ser530 from the diacetylated metabolite N-acetoxy-2-acetoxybenzamide, $SalAc_2$, **3**. The synthesis, crystal structure and PGHS inhibitory activity of **3**, which is 6-fold more active than aspirin, is reported in Chapter 2. The crystal structure of **2** is also reported as well as improved synthesis of **2** and **3**.

Chapter 3 describes the attempted synthesis of acetylated anthranilic hydroxamic acid as a dual COX and POX site inhibitor of PGHS. Unfortunately the product was the cyclic hydroxamic acid, 3-hydroxy-2-methyl-3H-quinazolin-4-one (ChaH). The formation and structure of this and of the complexes $Fe(Cha)_2(Cl)(H_2O).^7/_2H_2O$, $Co(Cha)_2(C_2H_5OH)_2$, $Ni(Cha)_2(C_2H_5OH)_2$, $Cu(Cha)H_2O(Cl)$ and $[Zn(Cha)_2].2H_2O$ are described. The synthesis and structure of the 4-aminophenylhydroxamic acid complex $[Fe^{III}(4\text{-}Apha)_3].C_2H_5OH$ is also described here.

Chapter 1

Design, synthesis and evaluation of aspirin analogues having an additional carboxylate substituent for antithrombotic activity

1.1	Chapter Overview	1
1.2	Thrombosis	4
	1.2.1 Introduction	4
	1.2.2 Sustained responses of platelets	4
	1.2.3 The role of platelets in thrombus formation	6
	1.2.4 Potential antiplatelet targets	7
	1.2.5 Antiplatelet drugs	8
1.3	Prostaglandins	10
	1.3.1 Formation and structures of prostaglandins	10
	1.3.2 Synthesis of prostaglandins	12
	1.3.3 Prostaglandin functions	14
	1.3.4 Prostaglandin receptors	15
1.4	Crystal structure of PGHS	16
	1.4.1 Description of structure	
	1.4.2 The cyclooxygenase active site	18
	1.4.3 The peroxidase active site	20
1.5	PGHS isoforms	21
	1.5.1 Discovery of a second isoform	21
	1.5.2 Discovery of a third isoform	22
	1.5.4 Properties of PGHS-1 and PGHS-2	22
1.6	PGHS catalysis	23
	1.6.1 Arachidonic acid metabolism	23

1.6.2 Cyclooxygenase activity 25
1.6.3 Cyclooxygenase substrate specificity 28
1.6.4 Peroxidase activity 28
1.6.5 Peroxidase kinetics 29
1.6.6 Peroxidase substrate specificity 30
1.6.7 Mechanism of catalysis 31

1.7 Inhibitors ofPGHS: NSAIDs 33
1.7.1 Classification and inhibitory activity 33
1.7.2 Amino acid residues important for NSAID activity and selectivity 35
1.7.3 Side effects of NSAIDs and PGHS (COX-2) selective inhibitors 37

1.8 Aims of the work 40

1.9 Results and Discussion 42

1.10 Conclusions 56

1.11 General Experimental Details 57

1.12 Experimental 58

1.13 References 67

Chapter 2

Acetylated Hydroxamic Acids as Prostaglandin-H-Synthase Inhibitors: Mode of Action Explained using Crystallography and *ex vivo* Studies

2.1 Chapter Overview 77

2.2 Aspirin 78

2.2.1 Biological Activity 78

2.2.2 Pharmacology and Pharmacokinetics 79

2.2.3 Side effects of aspirin 80

2.2.4 Inhibition of PGHS by aspirin, N-acetoxy-2-hydroxy-benzamide (SalAc), 2, and N-acetoxy-N-acetyl-2-acetoxybenzamide ($SalAc_3$), 4 80

2.2.5 Towards 'Super Aspirin' 83

2.3 Acetylated pyridoxine (vitamin B6) derivatives as PGHS inhibitors 86

2.4 Experimental – synthesis 87

2.4.1 Salicylhydroxamic acid, 1. 87

2.4.2 N-acetoxy-2-hydroxybenzamide (SalAc), 2, and N-acetoxy-2-acetoxybenzamide ($SalAc_2$), 3. 87

2.4.3 N-acetoxy-N-acetyl-2-acetoxybenzamide ($SalAc_3$), 4. 89

2.4.4 Acetic acid 4-acetoxymethyl-5-hydroxy-6-methyl-pyridin-3-ylmethyl ester, 9. 89

2.4.5 Acetic acid 3-acetoxy-5-acetoxymethyl-2-methyl-pyridin-4-ylmethyl ester, 10. 90

2.5 Instrumentation 90

2.5.1 Infrared spectroscopy 90

2.5.2 ^{1}H, ^{13}C NMR spectroscopy 90

2.5.3 Single X-ray diffraction measurements 91

2.5.4 Mass spectroscopy 91
2.5.5 Elemental analysis 91

2.6 Results and Discussion 91
2.6.1 Salicylhydroxamic acid, 1. 91
2.6.2 N-acetoxy-2-hydroxybenzamide (SalAc), 2, and N-acetoxy-2-acetoxybenzamide ($SalAc_2$), 3. 92
2.6.3 N-acetoxy-N-acetyl-2-acetoxybenzamide ($SalAc_3$), 4. 97
2.6.4 Platelet aggregation studies 97
2.6.5 Acetic acid 4-acetoxymethyl-5-hydroxy-6-methyl-pyridin-3-ylmethyl ester, 9. 99
2.6.6 Acetic acid 3-acetoxy-5-acetoxymethyl-2-methyl-pyridin-4-ylmethyl ester, 10. 100

2.7 Conclusions 101

2.8 References 102

Chapter 3

Attempted Synthesis of a Dual POX/COX Site Inhibitor of PGHS. Synthesis and Crystal Structures of the Cyclic Hydroxamic Acid, 3-Hydroxy-2-methyl-3H-quinazolin-4-one (ChaH) and of its Fe(III), Co(II), Ni(II), Cu(II) and Zn(II) Complexes

3.1	Chapter overview	107
3.2	Metals in medicine – general	107
3.3	Metals in medicine and physiology	109
	3.3.1 Iron	110
	3.3.2 Cobalt	113
	3.3.3 Nickel	115
	3.3.4 Copper	116
	3.3.5 Zinc	118
3.4	Hydroxamic acids	121
	3.4.1 The chemistry of hydroxamic acids	121
	3.4.2 Hydroxamic acids in biology and medicine	127
	3.4.3 Cyclic hydroxamic acids	129
	3.4.4 Aims of the work in this chapter	129
3.5	Experimental - synthesis	131
	3.5.1 Methyl 4-aminobenzoate, 5.	131
	3.5.2 4-Aminophenylhydroxamic acid, 4-AphaH, 6.	131
	3.5.3 Anthranilic hydroxamic acid, 2-AphaH, 2.	132
	3.5.4 3-Hydroxy-2-methyl-3H-quinazolin-4-one (ChaH), 4.	133
	3.5.5 $Fe^{III}(4\text{-Apha})_3.C_2H_5OH$, 8.	133
	3.5.6 $Fe(Cha)_2(Cl)(H_2O).7/2H_2O$, 9.	134

3.5.7 $Co(Cha)_2(C_2H_5OH)_2.H_2O$, 10 and $Co(Cha)_2(C_2H_5OH)_2$, 11. 134

3.5.8 $Ni(Cha)_2(C_2H_5OH)_2$, 12. 135

3.5.9 $Cu(Cha)_2$, 13 and $Cu(Cha)H_2O(Cl)$, 14. 135

3.5.10 $[Zn(Cha)_2].2H_2O$, 15. 135

3.6 Experimental – instrumentation 136

3.6.1 Infrared spectroscopy 136

3.6.2 ^1H, ^{13}C NMR spectroscopy 136

3.6.3 Single crystal X-ray diffraction measurements 136

3.6.4 Mass spectrometry 136

3.6.5 Elemental analysis 137

3.7 Results and Discussion 137

3.7.1 Anthranilic hydroxamic acid, 2, and 4-Aminophenylhydroxamic acid, 6. 137

3.7.2 3-Hydroxy-2-methyl-3H-quinazolin-4-one (ChaH), 4. 139

3.7.3 $[Fe^{III}(4\text{-Apha})_3].C_2H_5OH$, 8. 143

3.7.4 Metal Complexes of the Cyclic Hydroxamic Acid, 3-Hydroxy-2-methyl-3H-quinazolin-4-one (ChaH), 4. 146

3.7.4.1 $Fe(Cha)_2(Cl)(H_2O).^7/_2H_2O$, 9. 147

3.7.4.2 $Co(Cha)_2(C_2H_5OH)_2.H_2O$, 10 and $Co(Cha)_2(C_2H_5OH)_2$, 11. 150

3.7.4.3 $Ni(Cha)_2(C_2H_5OH)_2$, 12. 152

3.7.4.4 $Cu(Cha)_2$, 13 and $Cu(Cha)H_2O(Cl)$, 14. 154

3.7.4.5 $[Zn(Cha)_2].2H_2O$, 15. 156

3.8 Conclusions 158

3.9 References 159

Abbreviations

AA	Arachidonic acid
AcSHA	Acetylsalicylhydroxamic acid
ADP	Adenosine diphosphate
AMP	Adenosine monophosphate
AHA	Anthranilic hydroxamic acid
ASA	Acetylsalicylic acid (Aspirin)
BHA	Benzohydroxamic acid
cAMP	Cyclic adenosine monophosphate
cGMP	Cyclic guanosine monophosphate
CD	Catalytic domain
$CHCl_3$	Chloroform
COX	Cyclooxygenase
DCM	Dichloromethane
DIEA	*N,N*-Diisopropylethylamine
DHLA	Dihomo-γ-linolenic acid
DMF	Dimethylformamide
DMSO	Dimethyl sulfoxide
EET	Epoxyeicosatrienoic acid
EGF	Epidermal growth factor
EP	Endoperoxide
ER	Endoplasmic reticulum
EtOAc	Ethyl acetate
GI	Gastrointestinal
GP	Glycoprotein
GPCR	G-protein-coupled seven-transmembrane domain receptors
GSH	Reduced glutathione
HCl	Hydrochloric acid
HETE	Hydroxyeicosatetraenoic acid
H_2O_2	Hydrogen peroxide
HOBt	Hydroxybenzotriazole

HPETE	Hydroperoxyeicosatetraenoic acid
HRP	Horseradish peroxidase
IC_{50}	Half maximal nhibitory concentration
LC/MS	Liquid Chromatograph/Mass Spectrometry
LOX	Lipoxygenase
LPO	Lactoperoxidase
MBD	Membrane binding domain
MeOH	Methanol
Na_2SO_4	Sodium sulphate
MI	Myocardial infarction
MPO	Myeloperoxidase
MS	Mass spectrometry
NADPH	Nicotinamide adenine dinucleotide
NSAID	Nonsteroidal anti-inflammatory drug
ORTEP	Oak Ridge Thermal Ellipsoid programme
PAR	Protease activation receptor
PDGF	Platelet-derived growth factor
PG	Prostaglandin
PGE_2	Prostaglandin E_2
PGG_2	Prostaglandin G_2
PGH_2	Prostaglandin H_2
PGHS	Prostaglandin H_2 synthase
PGI_2	Prostacyclin
PKC	Protein kinase C
PKA	Protein kinase A
PLA_2	Phospholipase A_2
PLC	Phospholipase C
PLD	Phospholipase D
PLP	Pyridoxal 5'-phosphate
POX	Peroxidase
PPA	*trans*-5-phenyl-pent-4-en-ol, PPA
PPIX	Protoporphyrin IX

PPh_3	Triphenylphosphine
PPHP	*trans*-5-phenyl-pent-4-en-1-yl hydroperoxide
PPP	Platelet poor plasma
PRP	Platelet rich plasma
SEM	Standard error of the mean
SA	Salicylic acid
SHA	Salicylhydroxamic acid
TFA	Trifluoroacetic acid
THF	Tetrahydrofuran
TLC	Thin Layer Chromatography
TMPD	*N,N,N',N'*-tetramethyl-*p*-phenylenediamine
TP receptor	Thromboxane A_2/prostanoid receptor
TRAP	Thrombin receptor activating peptide
TxA_2	Thromboxane A_2
TxB_2	Thromboxane B_2
VEGF	Vascular endothelial growth factor
vWf	von Willebrand factor
NOE	Nuclear Overhauser Effect
DNA	Deoxy ribonucleic acid

Chapter 1

Design, synthesis and evaluation of aspirin analogues having an additional carboxylate substituent for antithrombotic activity

1.4	Chapter Overview	1
1.5	Thrombosis	4
	1.5.1 Introduction	4
	1.5.2 Sustained responses of platelets	4
	1.5.3 The role of platelets in thrombus formation	6
	1.5.4 Potential antiplatelet targets	7
	1.5.5 Antiplatelet drugs	8
1.6	Prostaglandins	10
	1.6.1 Formation and structures of prostaglandins	10
	1.6.2 Synthesis of prostaglandins	12
	1.6.3 Prostaglandin functions	14
	1.6.4 Prostaglandin receptors	15
1.4	Crystal structure of PGHS	16
	1.4.1 Description of structure	
	1.4.2 The cyclooxygenase active site	18
	1.4.3 The peroxidase active site	20
1.5	PGHS isoforms	21
	1.5.1 Discovery of a second isoform	21
	1.5.2 Discovery of a third isoform	22
	1.5.4 Properties of PGHS-1 and PGHS-2	22
1.6	PGHS catalysis	23
	1.6.1 Arachidonic acid metabolism	23

1.6.2 Cyclooxygenase activity 25
1.6.3 Cyclooxygenase substrate specificity 28
1.6.4 Peroxidase activity 28
1.6.5 Peroxidase kinetics 29
1.6.6 Peroxidase substrate specificity 30
1.6.7 Mechanism of catalysis 31

1.7 Inhibitors ofPGHS: NSAIDs 33
1.7.1 Classification and inhibitory activity 33
1.7.2 Amino acid residues important for NSAID activity and selectivity 35
1.7.4 Side effects of NSAIDs and PGHS (COX-2) selective inhibitors 37

1.8 Aims of the work 40

1.9 Results and Discussion 42

1.10 Conclusions 56

1.11 General Experimental Details 57

1.12 Experimental 58

1.13 References 67

1.1 Chapter Overview

Aspirin is an analgesic, anti-pyretic and anti-thrombotic agent which inhibits prostaglandin-H-synthase, PGHS, also called cyclooxygenase, COX. This enzyme has two active sites a cyclooxygenase (COX) and a peroxidase (POX). The antithrombotic action of aspirin is due to blocking of the production of thromboxane A_2, an important prothrombotic agent which causes activation and aggregation of platelets, an early step in thrombosis. An introduction to platelets, thrombosis, prostaglandins and PGHS is given at the beginning of this chapter. The chapter also describes the synthesis of aspirin derivatives which have been specifically designed by molecular modelling to fit better than aspirin into the COX active site of PGHS. The proposed mechanism of aspirin action involves formation of a salt linkage with Arg120 and irreversible acetylation of Ser530 at the COX active site of PGHS, **Fig. 1(a).** But docking experiments show that if the aspirin carboxylate is bound to Arg120, the acetyl group and Ser530 are separated by ~6 Å. The newly designed aspirin analogues contain alkylcarboxylate substituents which form the salt linkage and allow the acetyl group to be much closer to Ser530, **Fig. 1(b).**

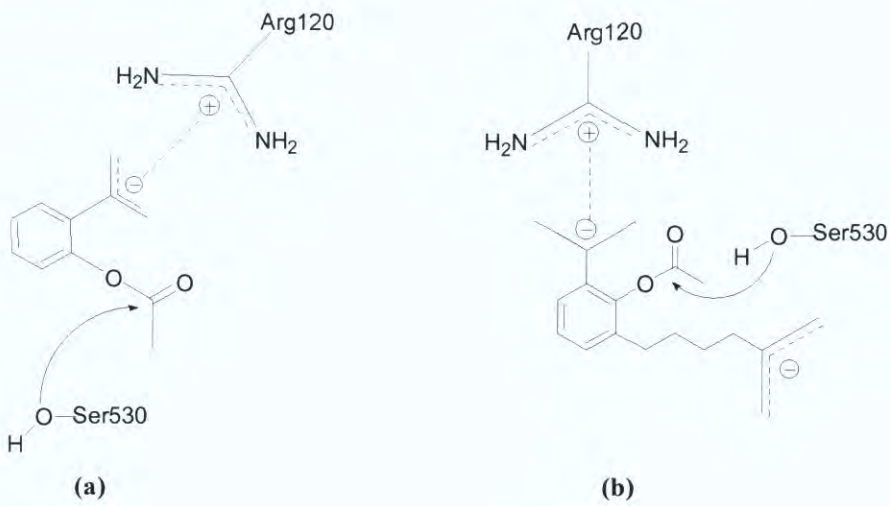

Fig. 1: Mechanisms of inhibition of PGHS by aspirin (a) and by designed aspirin analogues (b)

1.2 Thrombosis

1.2.1 Platelets

When blood vessels are damaged due to rupture or erosion of a lesion, transport of oxygen and carbon dioxide through the bloodstream is reduced because of diminished blood supply and this leads to conditions such as blood clots, stroke, coma and death.[1] Blood platelets are important for the vascular system because they stop bleeding (haemostasis) and repair damaged blood vessels.[2] This happens by adhesion of platelets to the exposed sub-endothelium, they then aggregate by platelet-platelet adherence following pro-thrombotic signals. This gives rise to a platelet plug which seals the damaged vessel wall.[3] Platelets are also important in thrombosis, inflammation as well as maintaining haemostasis,[4] and also play a role in atherosclerosis.

1.2.2 Sustained responses of platelets

Platelets are fragments of blood cells produced in the cytoplasm of megakaryocytes in the bone marrow and circulate in blood where they play important roles in haemostasis and in thrombus formation following endothelial injury.[5] Platelets have a simple structure and are small in size. This enables them to be transported to the edge of vessels, putting them in the ideal position to maintain the integrity of the vasculature.[4] Platelets consist of a plasma membrane, internal membranes, a cytoskeleton (microtubules and microfilaments), mitochondria, glycogen granules, storage granules lysosomes, and peroxisomes. In the resting state platelets circulate as discs, **Fig. 1.1 (a).** The lifetime of platelets is typically 8-10 days.[1] Platelets play an important role in clotting by formation of a platelet plug. This is shown in **Fig. 1.2.**[6] Platelets rapidly stick to the endothelium of atherosclerotic vessels (injured site) and then respond to agonist stimulation. The platelets are then converted into an active conformation losing their disc-like shape, and becoming spherical. This causes the release of mediators which activate surrounding platelets **Fig. 1.1 (b)**, giving rise to aggregation.[1] This process is promoted by receptors which bind agonists that stimulate platelet response. The interactions between the platelet agonist and its receptor activate other signals in the platelet which commence and terminate changes in shape and aggregation. This is also associated with the presence of calcium and vitamin K in the blood, along with the

formation of fibrin from the protein fibrinogen.[7] The most critical clinical outcome is production of a thrombus or blood clot leading to myocardial infraction or stroke.[8]

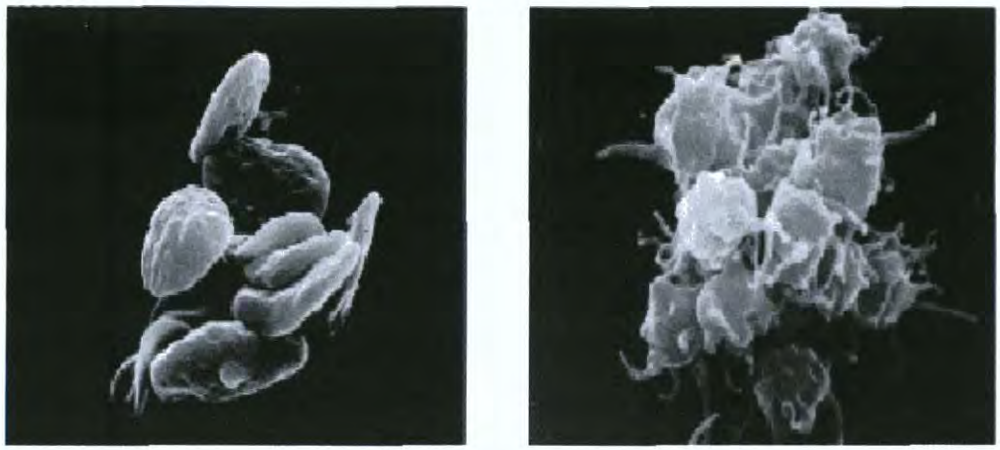

(a) (b)

Fig. 1.1: (a) Resting platelets, (b) activated platelets. Reproduced from S. Willoughby, A. Holmes, J. Loscalzo, *Eur J. Cardio. Nurs.*, 2002, **1**, 273-288.

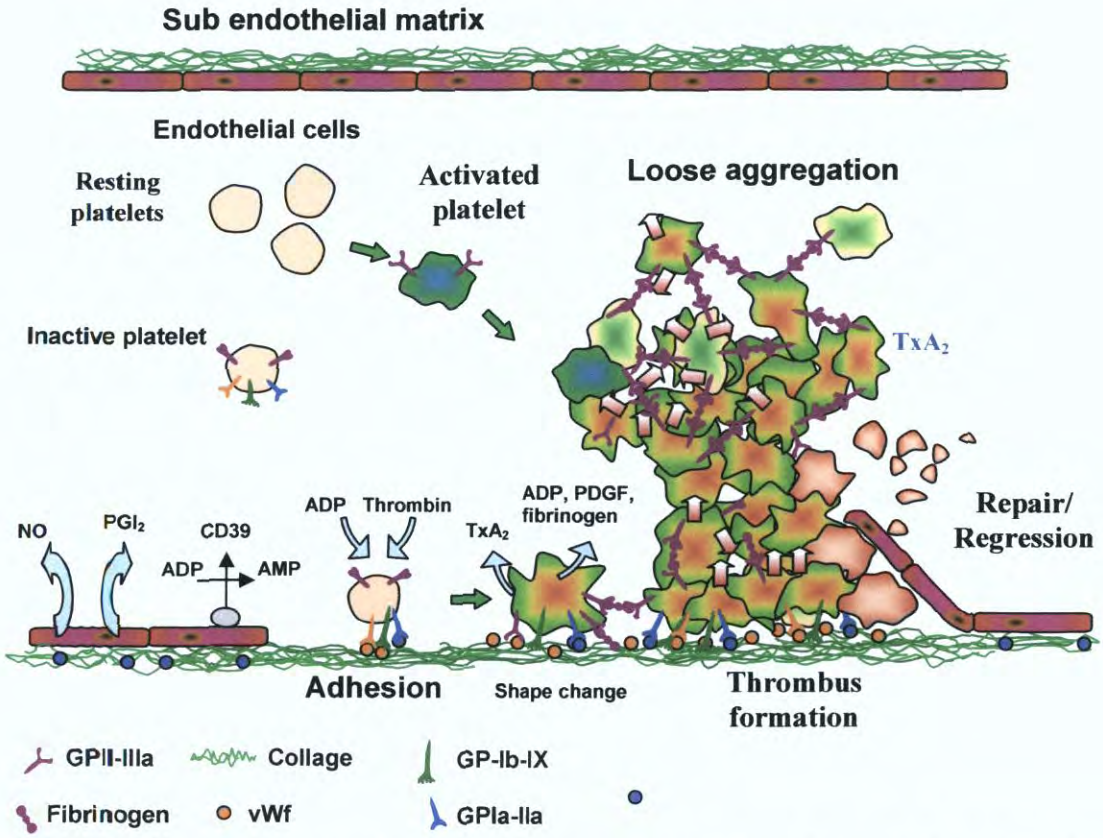

Fig. 1.2: Distinct mechanisms regulating platelet aggregation and thrombus growth: Interaction of platelets with sub-endothelium and platelet activating factors. Reproduced from D. L. Bhatt, E. J. Topol, *J. Nat. Rev. Drug Discov.*, 2003, **2**, 15-28.

1.2.3 The role of platelets in thrombus formation

In haemostasis, platelets circulate near the endothelial cell lining of the vessel wall without sticking to it and they are kept in this state by prostacyclin and nitric oxide, released by the endothelium cells that line the blood vessel walls.[6] Nitric oxide is a powerful endothelial factor that plays a key role in the anti-thrombotic effects of the endothelium by preventing platelet adhesion, platelet granule secretion, and platelet aggregation.[9] Nitric oxide coordinates to the iron of the haem group of soluble guanylyl cyclase. This haem coordination activates guanylyl cyclase and promotes formation of cyclic guanosine monophosphate (cGMP) which decreases intracellular calcium levels and inhibits the active state of glycoprotein GPIIb-IIIa.[10] Endothelial cells contain prostacyclin synthase, which can produce prostacyclin PGI_2 from PGH_2. Prostaglandin I_2 binds to a specific receptor on the platelet surface and activates adenylyl cyclase, causing calcium reuptake which inhibits platelet activation and aggregation.[1] In addition, endothelial cells express the enzyme CD39 on their surface which inhibits platelet activation by converting adenosine di-phosphate (ADP), an inducer of platelet activation released by platelets, into adenosine monophosphate (AMP). The initial adhesion of platelets to the damaged arterial vessel wall involves a wide array of ligands and receptors. Both thrombin and ADP cause platelets to change into an active conformation. Activated platelets secrete ADP, platelet derived growth factor and fibrinogen from storage granules in the platelet, and thromboxane A_2 (TxA_2), produced by immediate biosynthesis. ADP and TxA_2 are powerful platelet agonists, and interact with their specific receptors causing circulating platelets to alter shape and become activated.[6,11] The glycoprotein (GP) IIb-IIIa, also known as integrin $\alpha IIb\beta 3$, is found in high concentrations in platelet membrane. This receptor has a role in promoting thrombus formation by binding fibrinogen and forming fibrinogen bridges between platelets, resulting in platelet aggregation.[12,13]

Platelets also contain thromboxane synthase, which produces thromboxane A_2 (TxA_2) an important mediator of platelet aggregation and thrombosis.[13-15] Thromboxane A_2 causes an increase in calcium concentration in the platelet cytosol and a decrease in platelet cAMP levels by inhibition of adenylyl cyclase.[16] In the presence of PGHS inhibitors such as aspirin, TxA_2 synthesis is completely blocked by inhibition of the conversion of

arachidonic acid (AA) to prostaglandin endoperoxides and subsequently thromboxane A_2 (TxA_2).[17-18] The platelet activation is dependent on the interaction between vWf and its platelet receptor GPIb/V/IX complex.[19] The vWf-GPIb interaction is the only known receptor-ligand interaction that can cause platelet interactions throughout all regions of the vasculature, which explains its unique role in haemostasis and thrombosis.[20] Also GPIb-α subunit is primarily expressed on platelets and there is evidence that this subunit acts as a counter-receptor to one or more endothelial cell-adhesion molecules.[21] Deficiency of GPIb in humans or mice lead to a severe bleeding diathesis.[22]

1.2.4 Potential antiplatelet targets

Activation of platelets needs many input signals, involving adhesive proteins and soluble agonists,[23] that induce platelet activation through protein coupled receptors linked to the regulation of phospholipase C (PLC), phosphatidylinositol 3-kinase (PI3K), adenylyl cyclase and GTPases, whereas platelet adhesion receptors initiate platelet activation through one or more non-receptor tyrosine kinases.[24] A number of anti-thrombotic targets have been identified, **Table. 1** and this has led to the development of a diverse range of anti-platelet agents.[1]

Table 1: Potential anti-platelet targets. Reproduced from D. L. Bhatt, E. J. Topol, *J. Nat. Rev Drug Discov.*, 2003, **2**, 15-28.

- $P2Y_1$ receptor
- $P2Y_{12}$ receptor
- $P2Y_1$ and $P2Y_{12}$ receptors
- CD40-CD40 ligand system
- RANTES
- P-selectin
- CD39-ATPDase
- GPIb-V-IX complex-von Willebrand factor
- Protease-activated receptors (PARs)
- Pepducins
- Platelet leptin receptor
- Arp2/3 complex
- Growth-arrest specific gene 6(Gas6)

The principal factor regulating the adhesiveness of platelets is the activation state of GPIIb-IIIa. The affinity of this receptor is controlled by activating and inhibitory signals.

The antithrombotic effects of thrombin antagonists are primarily due to the inhibition of fibrin formation.[24] Platelet activation and aggregation contribute to thrombus formation and therefore anti-platelet therapy is important for both the treatment and prevention of cardiovascular disease. Understanding the role of platelets in haemostasis and disorders caused by abnormal platelet function has led to important new therapies for thrombotic disease.[6,13]

1.2.5 Antiplatelet drugs

Anti-platelet drugs act against myocardial infarction, stroke and cardiovascular disease.[25] Aspirin, (acetylsalicylic acid) the most widely used antiplatelet agent, inhibits platelet cyclooxygenase and the conversion of arachidonic acid to the platelet agonist thromboxaneA_2, but does not block platelet activation occurring by various signalling pathways that are independent of TxA_2 release. Therefore a number of drugs have been developed to complement aspirin's beneficial effects. These include the thienopyridines, *i.e.* ticlopidine, clopidogrel, dipyridamole and GPIIb-IIIa antagonists.[12] Aspirin acts by irreversibly acetylating a serine residue Ser530 in platelet COX-1 and Ser516 of COX-2. Most work has been carried out on ovine COX and Ser530 in the ovine sequence corresponds to Ser529 in the human system. Aspirin therapy blocks TxA_2 synthesis compared with other NSAIDs (non-steroidal anti-inflammatory drugs) that inhibit platelets in a reversible and incomplete manner via COX-1 inhibition.[26] Aspirin reduces the risk of acute myocardial infraction by approximately one third.[27] In order to prevent thrombotic disorders, aspirin daily doses of 75 mg or below have been considered to be more effective than higher doses because such low doses may spare prostacyclin (a platelet anti-aggregant and vasodilator) and cause less gastrointestinal toxicity.[28] In addition, long term therapy with aspirin appears to cause an increase in gastrointestinal haemorrhage.[26]

The second widely used group of antiplatelet drugs are ticlopidine and clopidogrel, thienopyridines, which act by causing irreversible inhibition of ADP binding to the $P2Y_{12}$ receptor. Both of these are prodrugs, and are metabolised by cytochrome P450 in the liver to the active metabolites.[29] Ticlopidine is effective in preventing cardiovascular disease and works as well as aspirin. However, its use is associated with neutropenia and bone marrow aplasia.[30] Due to these side effects and its slow onset of

action it has been replaced by the safer clopidogrel, which reduces by 10% the risk of serious vascular side-effects among high risk patients compared to aspirin.[25] Clopidogrel is slightly more effective than aspirin in reducing ischaemic complications but overall, the safety and tolerability of aspirin and clopidogrel are similar. Therefore clopidogrel is an alternative to aspirin for secondary prevention in patients who cannot tolerate the latter.[31]

Thromboxane A_2 (TxA_2) is a key mediator of platelet aggregation and smooth muscle contraction.[32] An overproduction of TxA_2 has been associated with many diseases such as MI, thrombosis, pulmonary embolism, atherosclerosis and asthma.[17] Its action is mediated through G protein-coupled-receptors of which two isoforms, TP-α and TP-β, occur in humans. Therefore, TP receptor antagonists, thromboxane synthase inhibitors and drugs containing both properties have been developed to suppress the formation or the action of thromboxane A_2.[15,32] The inhibition of thromboxane synthase prevents the conversion of PGH_2 to TxA_2, resulting in an accumulation of TxA_2 precursor, PGH_2, which is chemically more stable than TxA_2.[33] BM-573, a torsemide derivative is a novel non-carboxylic dual TxA_2 synthase inhibitor and TP receptor antagonist. The pharmacological profile of the drug is characterised by a higher affinity for the thromboxane receptor and complete prevention of human platelet aggregation induced by arachidonic acid at lower dose.[70] The chemically related BM-573, BM-613, is a newly developed combined TxA_2 receptor antagonist and TxA_2 synthase inhibitor characterised by strong antiplatelet and anti-thrombotic potency. Therefore, TxA_2 inhibitors could be drug candidates for thrombotic disorders.[32]

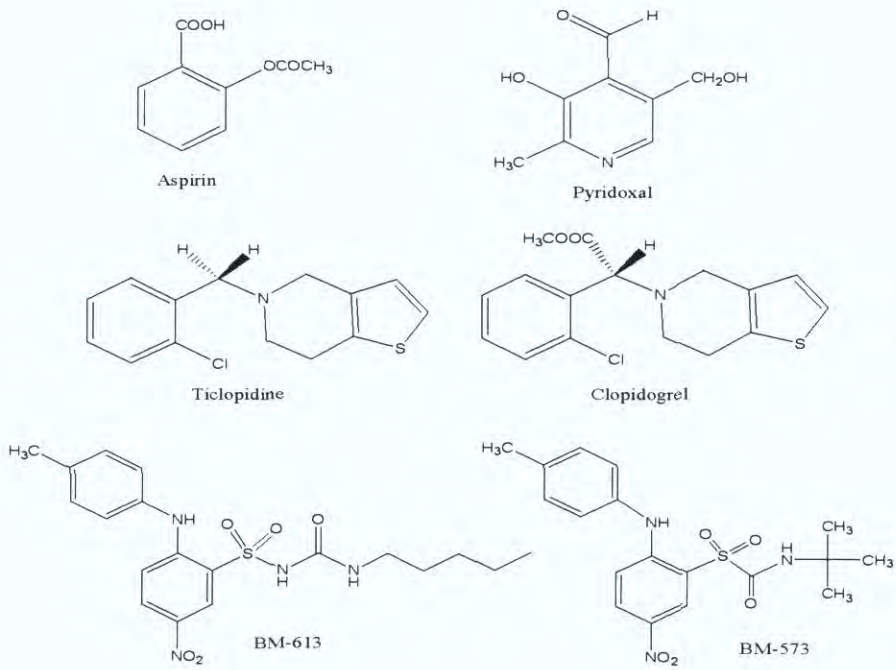

Fig. 1.3: Structures of antiplatelet agents. Repreduced from M. J. Quinn, D. J. Fitzgerald, *Circulation*, 1999, **100**, 1667-1672.

1.3 Prostaglandins

1.3.1 Formation and structures of prostaglandins

Although discovered in the 1930's by Ulf von Euler, prostaglandins (PGs), because of their low concentrations and instability,[34] were not identified or characterised for almost 30 years afterwards. Following this it was established that prostaglandins are formed from polyunsaturated fatty acids by a complex series of reactions involving oxygenation, cyclisation and the generation of five chiral centers from a chiral substrate.[35] Prostaglandin biosynthesis was described by Hamberg and Samuelsson in 1967. The enzyme responsible for the synthesis of prostaglandins was called prostaglandin-H-synthase (PGHS).[36] In 1991 it was recognised that there are two isoforms of the enzyme, PGHS-1 also called COX-1 and a second inducible isoform, PGHS-2, also called COX-2.[37] PGHS-1 and PGHS-2 catalyse the first committed step in the biosynthesis of prostaglandins and thromboxanes.[38] PGHS is a haemoprotein, active as a homodimer, which contains two distinct catalytic sites, a cyclooxygenase (COX) site and a peroxidase (POX) site. At the cyclooxygenase site, arachidonic acid is converted to the hydroperoxy endoperoxide prostaglandin G_2 (PGG_2), before it is further reduced by the peroxidase (POX) site to the hydroxy endoperoxide prostaglandin-H_2 (PGH_2), the

common intermediate in all prostaglandin synthesis.[39] In 1971, Sir John Vane demonstrated that the inhibition of prostaglandin synthesis was the target for non-steroidal anti-inflammatory drugs (NSAIDS) such as aspirin.[40] Later it was reported that the inhibitory effects of most current NSAIDs are limited to the COX site and had no effect on the POX site. Therefore, after treatment with NSAIDs, peroxidase (POX) activity can continue to generate damaging free radical species, which are implicated in many pathological conditions including atherosclerosis. The need for a dual COX and POX site inhibitor was recognised and the hydroxamic acid Tepoxalin is such as inhibitor.[41]

Prostaglandins or prostanoids are a large group of fatty acid derivatives containing 18 to 22 carbons, collectively known as eicosanoids that are derived from n-3 and n-6 polyunsaturated fatty acids.[42] PGs contain a cyclopentane ring with two side chains named α, containing a carboxylic acid moiety, and ω, while thromboxanes contain a fused cyclohexane (oxane) ring. Prostaglandins are divided into the D, E, and the F series; both the E and F series have three members i.e. E_1, E_2, E_3 and $F_1\alpha$, $F_1\beta$, $F_2\alpha$ and $F_3\alpha$ where numbers represent the number of double bonds and α and β represent the orientation of the hydroxyl group at C_9, **Fig. 1.4.** Prostaglandin E contains a keto oxygen at C_9 and a hydroxyl group at C_{11}, whereas prostaglandin F has a hydroxyl group at the C_9 and C_{11} positions of the cyclopentane ring. PGA, PGB and PGC are unsaturated ketones that are produced non-enzymatically from PGE during extraction procedures. Based on the number of double bonds in their side chains, prostaglandins are further divided into three groups, (a) PGs possessing a 13-*trans* double bond, (b) PGs possessing 5-*cis* and 13-*trans* double bonds, and (c) PGs possessing 5-*cis*, 13-*trans*, and 17-*cis* double bonds. The PGs in these groups are synthesised from γ-homolinolenic acid (8,11,14-eicosatrienoic acid), arachidonic acid (5,8,11,14-eicosatetraenoic acid), and 5,8,11,14,17-eicosapentaenoic acid, respectively. Hence, eicosatrienoic acid is the precursor of PGE_1 and PGF_1, arachidonic acid is the precursor of PGE_2 and PGF_2, and eicosapentaenoic acid is a precursor of PGE_3 and PGF_3. Arachidonic acid is the most abundant C_{20} polyenoic fatty acid in the lipids of most tissues and because of that it is not surprising that PGF_2 and PGE_2 are the most common prostaglandins.[16,43]

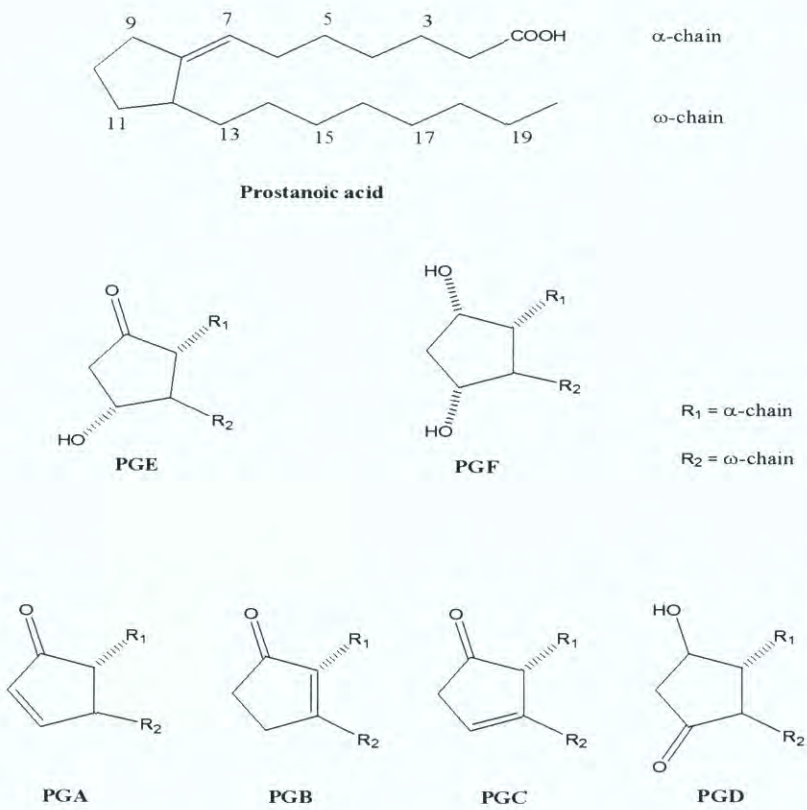

Fig. 1.4: Structures of prostaglandins. Reproduced from W. L. Smith, *J. Biochem*, 1989, **259** (2), 315-24.

1.3.2 Synthesis of prostaglandins

Arachidonic acid is released from membrane phospholipids by phospholipase A_2 (PLA_2). It is then converted to prostaglandins by PGHS, a bifunctional enzyme that first converts arachidonic acid into the hydroperoxide prostaglandin G_2 (PGG_2) in the cyclooxygenase (COX) active site followed by reduction of PGG_2 at position 15 to the corresponding alcohol (PGH_2) in the peroxidase (POX) active site. This is the precursor for the synthesis of all prostaglandins and thromboxanes **Scheme 1.1.**[16,44] PGD_2 is formed by a rearrangement of PGH_2 while PGE_2 and its homologue PGE_1 are formed by rearrangement of the endoperoxide group of PGH_2.[43] PGA_2 is a dehydration product of PGE_2 formed by the action of a dehydrase enzyme found in human serum. Further PGA_2 isomerisation gives PGB_2. PGA_2 has been reported to inhibit the growth of cancer cells *via* activation of apoptosis. While PGD_2, PGE_2, PGI_2 and TxA_2 are all synthesised by non-oxidative rearrangement, PGF_2 and its metabolites are formed by a 2-e^- reduction of PGH_2. Two biologically active forms of PGF_2 are known, $PGF_2\alpha$ and 9α-11β-PGF_2 and both cause contraction of smooth muscles.[43] There are three individual pathways for the

synthesis of PGF_2 stereoisomers; (a) reduction of PGH_2 to $PGF_{2\alpha}$ by an endoperoxide reductase, (b) reduction of PGE_2 to $PGF_{2\alpha}$ by a 9-keto-reductase and (c) reduction of PGD_2 to 9α,11β-PGF_2 by an 11-keto-reductase. A PGF synthase from bovine lung is known to have both 11-keto-PGD_2 and PGH_2 reductase activity, catalyzing the formation of $PGF_{2\alpha}$ and 9α-11β-PGF_2 respectively.[45]

The formation of the platelet inhibitory prostaglandin, prostacyclin PGI_2 from PGH_2 involves an acid catalysed heterolytic cleavage of the endoperoxide PGH_2 followed by oxycylisation of the transiently positive oxygen at C-6. The enzyme that catalyses the conversion is called PGI_2 synthase, a haem protein found in high concentrations in both vascular and nonvascular smooth muscles and vascular endothelial cells.[46] TxA_2 is synthesised in the platelets and is a powerful vasoconstrictor and thrombogenic agent. Like PGI_2 it is unstable and its stable hydrolysis metabolite is TxB_2 which is inactive. The conversion of PGH_2 to TxA_2 is catalysed by thromboxane A synthase.[43]

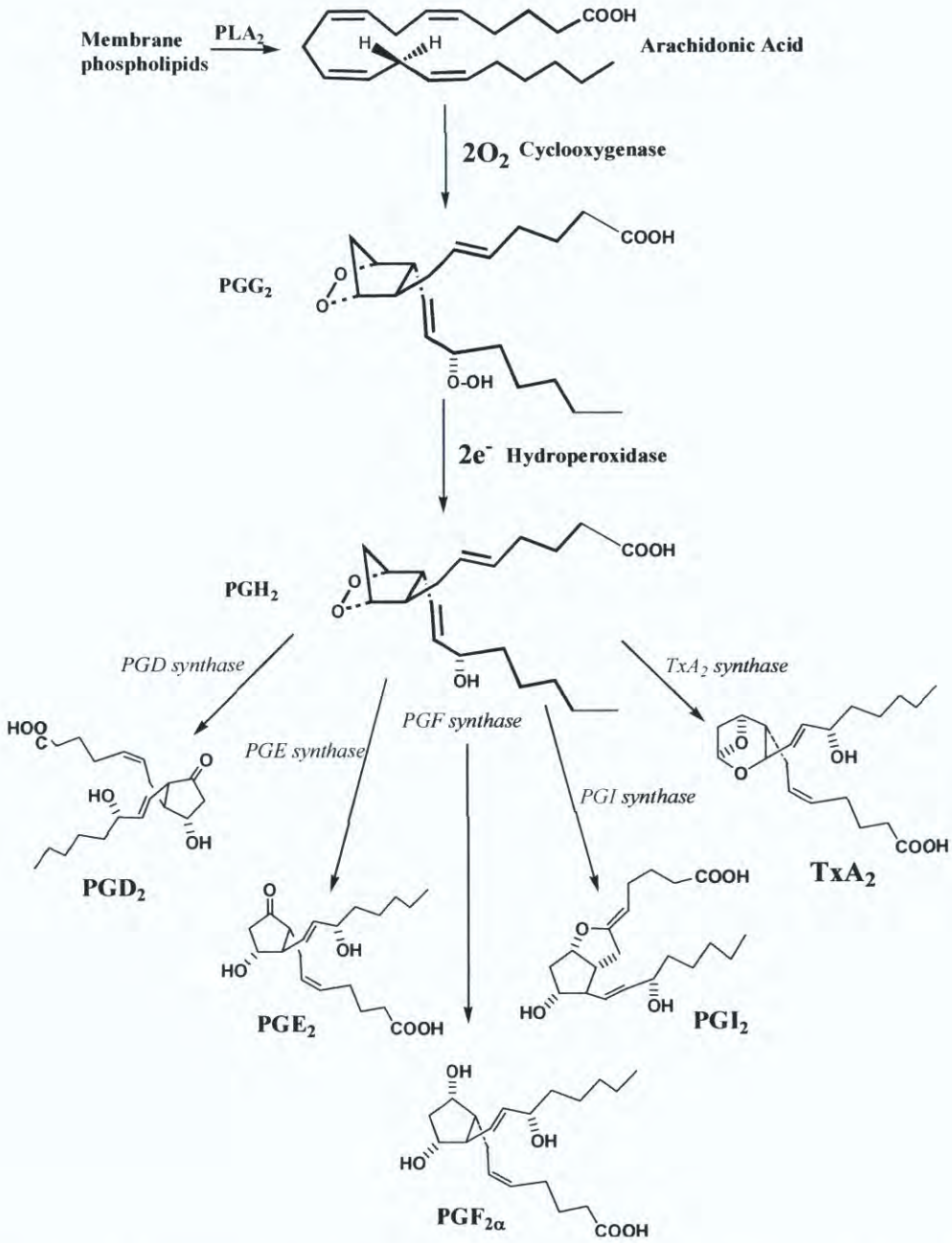

Scheme 1.1: Cycloogenase biosynthetic pathway and structures of arachidonic acid, prostaglandins endoperoxides (PGG_2 and PGH_2), prostaglandins (PGE_2, PGD_2, PGF_{2a}), prostacyclin (PGI_2) and thromboxane A_2 (TxA_2). Reproduced from J. M. Dogne, X. de Leval, J. Hanson, M. Frederick, B. Lambermont, A. Ghuysen, A. Casini, B. Maserreel, K. Ruan, B. Pirotte, P. Kolh, *Curr. Med. Chem.*, 2004, **11**, 1223-1241.

1.3.3 Prostaglandin functions

Prostaglandins are made in human tissues and cells in response to a wide range of stimuli and they are involved in a number of functions, such as haemostasis and

protection of the gastric mucosa as well as a number of pathological conditions, such as cancer, cardiovascular diseases, rheumatoid arthritis and osteoarthritis.[47] PGD_2, the most abundant prostaglandin in the central nervous system, is known to act as an anticoagulant vasodilator. PGEs maintain the gastric mucosa by inhibiting gastric acid secretion.[48] PGFs are associated with contraction of bronchial and tracheal muscles.[49] Prostacyclin PGI_2 is a potent vasodilator and along with inflammatory mediators such as bradykinin and histamine causes an increase in vascular permeability and oedema.[50] Furthermore PGI_2 acts as anti-thrombotic agent.[51] In contrast to PGI_2, its physiological antagonist, thromboxane A_2 is a potent vasoconstrictor and platelet aggregator. The balance between PGI_2 and TxA_2 systems is important in preventing thrombosis while performing efficient haemostasis.[52] In the kidney, PGI_2 stimulates cAMP mediated rennin release and modulates renovascular tone, PGE_2 inhibits water and chloride reabsorbion and TxA_2 decreases renal blood flow and the rate of the glomerular filtrate.[53] Production of thromboxane TxA_2 and prostacyclin PGI_2 is increased in patients with atherosclerosis. TxA_2 promotes and PGI_2 prevents atherogenesis through control of platelet activation and leukocyte-endothelial cell interaction.[54]

1.3.4 Prostaglandin receptors

Prostaglandins are hydrophobic and do not easily cross the cell membrane. Once formed, they act through G-protein-coupled receptors on the surface of the target cells. Eleven receptors are known; the PGD receptors, four subtypes of PGE receptors, the PGF receptors, the PGI receptor and the TxA_2 receptors. All of these are G protein-coupled receptors with seven transmembrane domains encoded by different genes.[55]

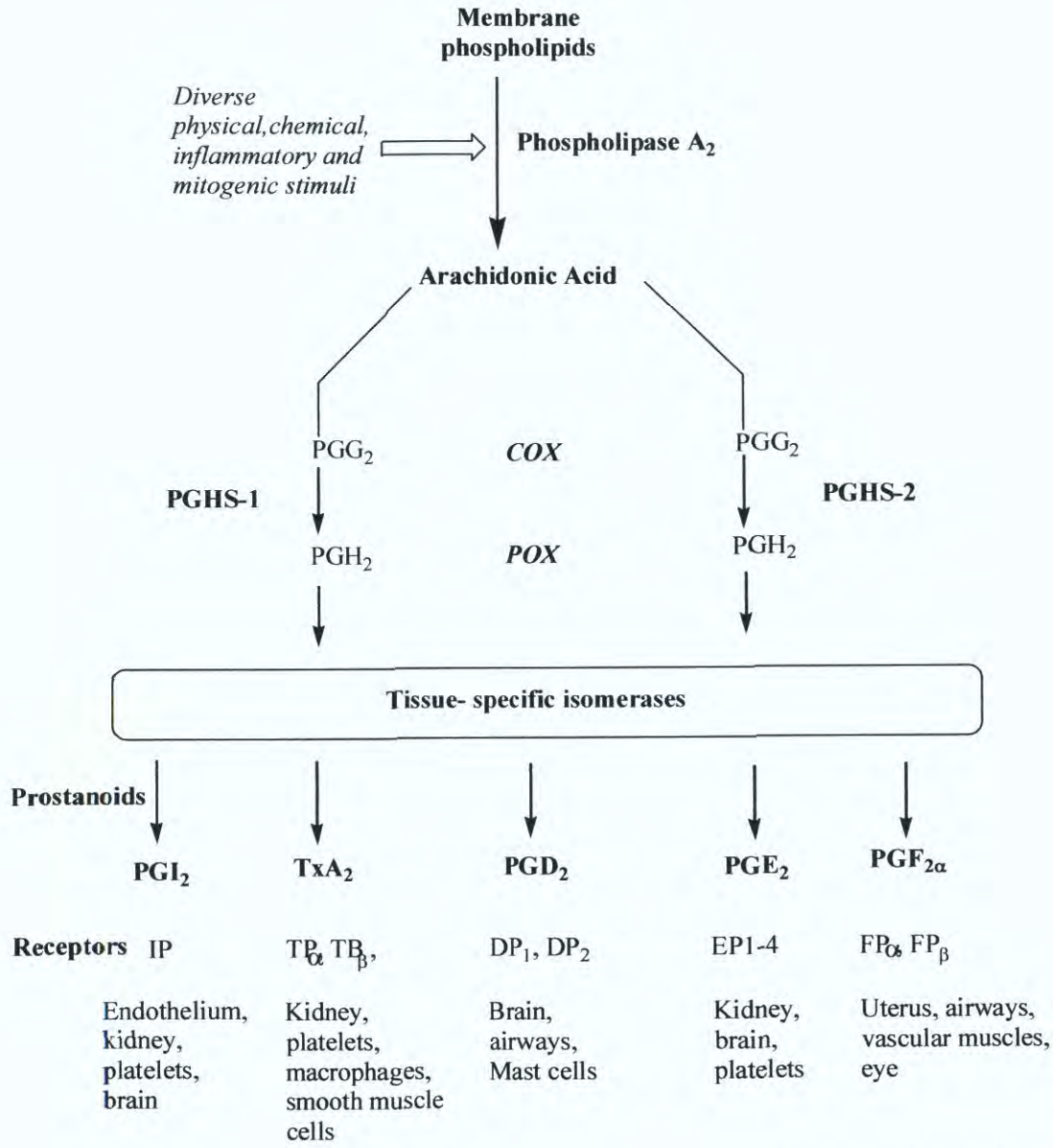

Scheme 1.2: Production and actions of prostaglandins and thromboxane. Reproduced from J. M. Dogne, X. de Leval, J. Hanson, M. Frederick, B. Lambermont, A. Ghuysen, A. Casini, B. Maserreel, K. Ruan, B. Pirotte, P. Kolh, *Curr. Med. Chem.*, 2004, **11**, 1223-1241.

1.4 Crystal structure of PGHS

1.4.1 General description

PGHS is the first enzyme involved in the biotransformation of arachidonic acid to prostaglandins.[35,38,56] Two isoforms of the enzyme are known, the constitutively expressed PGHS-1, regarded as a housekeeping isoform and the inducible PGHS-2. PGHS-1 is widely distributed throughout the body and is the only form which produces

thromboxane, while PGHS-2 is found mainly at sites of inflammation in response to specific stimuli, in tumours and in the central nervous system.[35,57]

The PGHS-1 and -2 enzymes are glycosylated, integral membrane proteins bound to the luminal surface of the endoplasmic reticulum with a relative molecular mass of ~ 140 kDa. PGHS is a dimeric protein made up of two identical subunits. Each monomer has two distinct catalytic sites, a cyclooxygenase (COX) and a peroxidase (POX) active site.[57] Crystal structures of both isoforms from human,[58] murine[59] and ovine[60] sources have been determined. The crystal structures of PGHS-1 and -2, show that each monomer consists of three structural domains: the epidermal growth factor (EGF) domain of 50 amino acids at the N terminus, the α-helical membrane binding domain (MBD) of about 50 amino acids, and a large *C*-terminal globular catalytic domain with about 460 amino acids which contains the POX and COX active sites, **Figs. 1.5** and **1.6.**[39] PGHS-1 is glycosylated at three asparagine residues, Asn68, Asn144, Asn410, whereas PGHS-2 may be glycosylated at up to four asparagine residues, Asn53, Asn130, Asn396, Asn580. The glycosylation of Asn410 in PGHS-1 is essential for COX and POX activities.[61]

The catalytic domain is the largest part of the polypeptide in PGHS-1 and -2. It is almost completely made up of α-helices with a direct homology to other members of the myeloperoxidase family of proteins but with a hydrophobic channel protruding into the core of this domain. The catalytic domain is a single unit in both isoforms but can be divided into two distinct regions, the cyclooxygenase (COX) and peroxidase (POX) active site areas.[57] The COX active site resides at the apex of a 25 Å-long hydrophobic channel extending from the membrane-binding domain to the center of the protein **Fig. 1.6.** In contrast, the POX active site is located in a large groove on the opposite side at the haem binding site, away from the membrane-binding domain **Fig. 1.5.**[57,62]

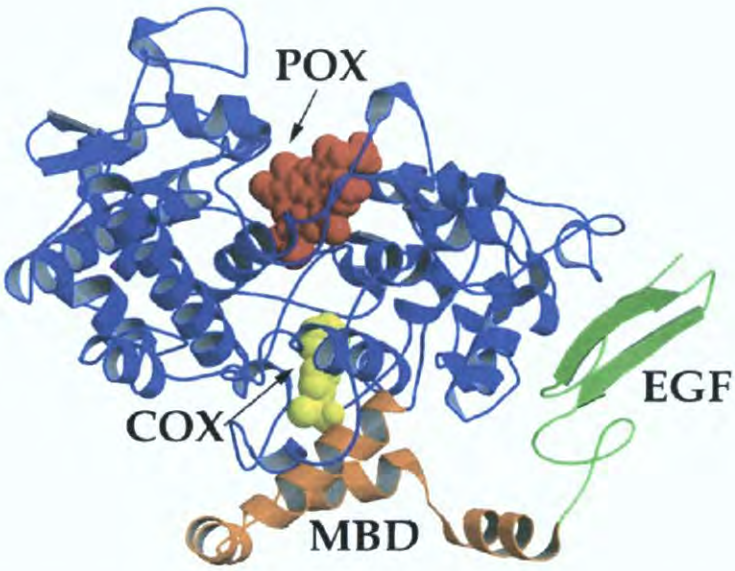

Fig. 1.5: A ribbon drawing of PGHS-1 monomer viewed from the dimer interface. The catalytic, EGF and MBD domains are coloured blue, green and gold respectively. Bound arachidonic acid is coloured yellow and is positioned in the COX active site. The heme can be seen in red, in the POX active site. Reproduced from W. L. Smith, D. L. DeWitt, R. M. Garavito, *Annu. Rev. Biochem.*, 2000, **69**, 145-182.

The cyclooxygenase active site

The cyclooxygenase active site of PGHS-1 and -2 is made up of a hydrophobic channel of dimensions ca. 8 x 25 Å that extends from the outer surface of the membrane binding domain (MBD) into the core of the globular region.[57,63] The MBD forms the mouth of the channel through which arachidonate and O_2 enter directly from the polar compartment of the lipid bilayer. The COX channel mouth is a relatively open structure in all reported PGHS crystal structures. The COX catalytic site of PGHS-1 incorporates the upper part of this channel, extending from Arg120 to Tyr385 and makes up the binding site for fatty acids and competitive COX inhibitors. At Arg120 and Tyr355, the channel narrows to form a constriction or "aperture" in all reported crystal structures.[56]

The cyclooxygenase active site channel is lined by 24 amino acid residues. PGHS-1 differs from PGHS-2 mainly because it possesses isoleucine at position 523 while this residue is replaced by valine in PGHS-2.[35,39] This single difference opens a polar side pocket in PGHS-2 that has been exploited in the synthesis of PGHS-2 selective drugs.[64] Only three of the channel residues are polar, Arg120, Ser353, and Ser530. Ser530 is the site of acetylation by aspirin and Arg120 binds to the carboxylate groups of fatty acids and many NSAIDs molecules in PGHS-1 but is not essential in PGHS-2.[65,66]

The COX active site of PGHS-2 is about 20% larger than that of PGHS-1 and has slightly different shape and size.[39] This is due to differences in three amino acid residues between both isoforms, Ile523, Ile434 and His513 in PGHS-1 are replaced respectively by Val523, Val434 and Arg513 in PGHS-2. These differences influence inhibitor binding and provide more substrate flexibility in the PGHS-2 COX site and a slightly enlarged PGHS-2 active site relative to PGHS-1. The other difference is the position of helix D, the last of the four helices of the MBD. In PGHS-2 this helical segment is positioned "upwards" and not in the MBD thus providing a larger opening in the MBD.[58]

The binding of arachidonic acid within the COX active site of PGHS-1 is in an extended "L-shaped" conformation **Fig. 1.6.** Val349, Trp387, Leu534 are critical for positioning AA in this conformation so that when hydrogen abstraction at C-13 occurs, the molecule is optimally arranged to yield PGG_2. The residues Gly533 and Tyr384 are essential for positioning C-13 of arachidonate for hydrogen abstraction.[67] Carbons 7-14 of AA are in an S-shaped conformation that twists the substrate chain around the side chain of Ser530, which is the residue acetylated by aspirin. The residues forming the AA and COX active sites are close together, and interactions within 4 Å between both of these occur.[65] Of the 49 interactions between the substrate and the enzyme only two involve carboxylates while Arg120 and Tyr355 give hydrophilic interactions and the remaining are hydrophobic. Site directed mutagenesis studies have indicated that the guanidinium side chain of Arg120 is important for high affinity binding of AA to PGHS-1 through salt bridge formation. Arachidonic acid is placed with its carbon 13 oriented near the phenolic oxygen of Tyr385, where the *proS* hydrogen can be abstracted to initiate COX reaction. The carbons 14-20 of AA bind in a hydrophobic groove above Ser530, where its conformation is stabilized by Phe205, Phe209, Val344, Phe381 and Leu534 through substrate-protein interactions.[67] This facilitates conversion to PGG_2 as opposed to alternative fatty acid substrates such as the hydroxy eicosatetraenoic acids (HETEs).[68]

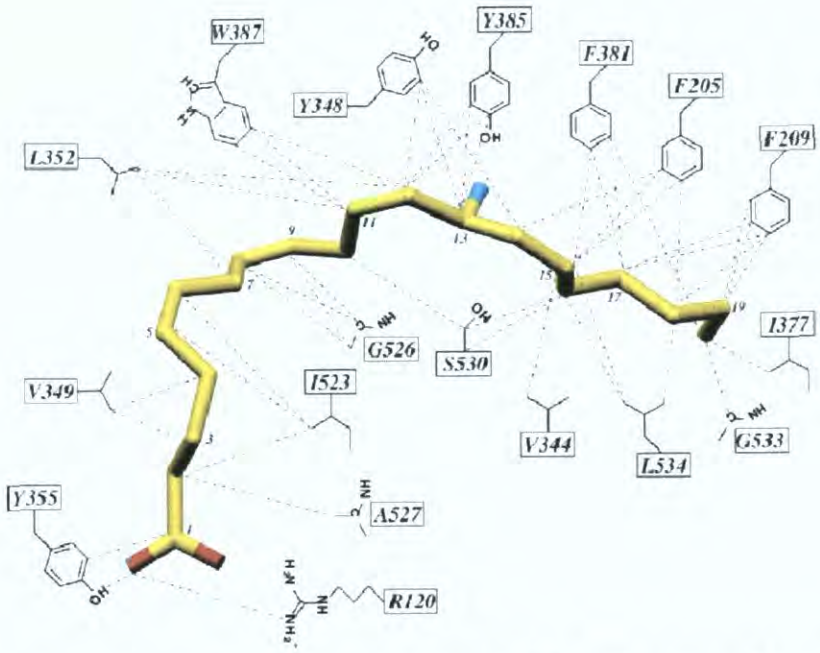

Fig. 1.6: Interactions between arachidonic acid (AA) and COX active site residues of PGHS-1. Carbon atoms of AA are yellow, oxygen atoms red, and the 13 proS hydrogen blue. All dashed lines represent interactions within 4.0 Å between the specific side chain atom of the protein and AA. Reproduced from M. G. Malkowski, S. L. Ginell, W. L. Smith, R. M. Garavito, *Science*., 2000, **289**, 1933-1937.

1.4.2 The peroxidase active site

The structure of the POX active site in PGHS, is similar to those of other haem peroxidases.[57] It is located at the interface between the large and small lobes of the catalytic domain, in a shallow cleft on the upper surface of the enzyme. This active site contains a haem group which possesses high spin Fe (III) complexed to a protoporphyrin IX prosthetic group. The haem group is essential for catalytic activity **Fig. 1.7.** The haem iron is complexed to a proximal histidine, His388. A distal water molecule is also present above the iron atom. The crystal structure shows that the imidazole *Nδ* of His388 participates in a hydrogen bond network *via* a water molecule with Tyr504. In PGHS-2, the same interaction is seen but the existence of a proximal water molecule has not been observed.

On the distal haem surface, His207 is thought to play a role in the deprotonation of the hydroperoxide substrate PGG_2 and subsequent protonation of the alkoxide ion to form the alcohol. Gln203 is important in catalysis, as the side chain of the distal histidine seems to be oriented by hydrogen bonding to the glutamine main chain carbonyl. In both PGHS and MPO, a glutamine side chain (Gln203 in PGHS-1) instead of the arginine

residue in non-mammalian peroxidases is near the distal histidine. Mutations of Gln203, distal His207 or proximal His388 in *ovine* PGHS-1 and human PGHS-2 lead to a reduction or elimination of POX activity. The POX site although partially protected by a shield lying above His207 and Gln203, has its haem group much more exposed to the solvent than other peroxidases.[64]

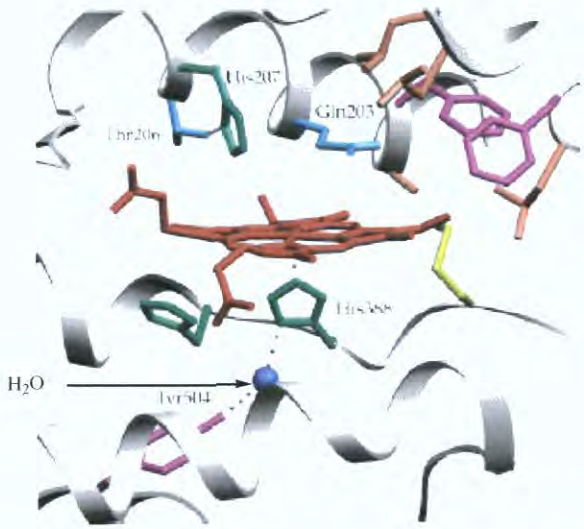

Fig. 1.7: Peroxidase Active Site of PGHS-1. The haem group is in red. The proximal His388 (green), is hydrogen-bonded to a water molecule (blue) and Tyr504 (magenta). The distal His207 (green) and Glu203 (blue) can also be observed. Reproduced from R. M. Garavito, M. G. Malkowski, D. L. DeWitt, *Prostaglandins & Other Lipid Mediat*ors, 2002, **68-69**, 129-152.

1.5 PGHS isoforms

1.5.1 Discovery of a second isoform

Up until the late 1980s, it was thought that only one PGHS existed and that this was expressed in most cells. However, it was noted that the concentration of PGHS increased in response to stimuli at inflammation sites, indicating the existence of an inducible form of the enzyme.[69] This proved to be the case when in 1991 a second isoform of the enzyme PGHS-2 was cloned.[70] It soon was established that two isoforms of PGHS existed, PGHS-1 (COX-1) and PGHS-2 (COX-2). PGHS-1, first cloned in 1988 by Merlie *et al.*,[71] is located on chromosome 9 and is responsible for the biosynthesis of PGs in the gastric mucosa and in the kidney for "house-keeping" physiological functions. In contrast, PGHS-2, discovered in 1989 by Simmons *et al.*,[66] is inducible, is

located on chromosome 1 and is expressed in response to a host of growth factors, cytokines and mitogens. There is approximately 60-65% homology between the amino acid structures of PGHS-1 and -2 from the same species and 85-90% from different species. Both aspirin and other NSAIDs inhibit the two isoforms to different degrees.[39]

1.5.2 Discovery of a third isoform

In 1999 Simmons *et al.* identified a novel PGHS-1 mRNA variant derived from the PGHS-1 gene located in canine brain, which they named PGHS-3 (COX-3). This is co-regulated with PGHS-2 during NSAID- induced apoptosis.[72] In humans, PGHS-3 mainly occurs in cerebral cortex and in other tissues. PGHS-3, which is glycosylated, possesses a glycosylation-dependent cyclooxygenase activity and seems to have a different mechanism of action to PGHS-1 and -2. Comparison of canine COX-3 activity with murine COX-1 and -2 indicates that paracetamol (acetaminophen) does not directly inhibit PGHS-1 or -2 but is active against PGHS-3. Some NSAIDs such as indomethacin, ibuprofen and aspirin are potent inhibitors of this isoform. Thus, inhibition of PGHS-3 could be the way in which these drugs reduce pain and fever.[73]

1.5.3 Properties of PGHS-1 and PGHS-2

There are small structural differences between PGHS-1 and PGHS-2 which are responsible for important pharmacological and biological variations. The active site of PGHS-1 is smaller than that of PGHS-2 and this size difference has been exploited in developing PGHS-2 (COX-2) specific inhibitors. Moreover, the size difference between the active sites is consistent with the fact that PGHS-1 is totally inhibited by aspirin acetylation, whereas PGHS-2 retains ability to convert arachidonic acid to 15-R-HETE after aspirin treatment. In addition, the difference in size is consistent with the fact that dihomo-γ-linolenic acid and eicosapentaenoic acid are improved substrates for human PGHS-2 relative to PGHS-1. Furthermore the difference in size does not affect the gross kinetic properties (e.g. K_m, V_{max}) of the two isozymes PGHS-1 and PGHS-2. Due to the similarities in kinetics between PGHS-1 and -2, prostaglandins can be formed by both isoforms in cells and tissues.[74]

1.6 PGHS catalysis

1.6.1 Arachidonic acid metabolism

Arachidonic acid (AA) is a linear unsaturated hydrocarbon containing 20 carbon atoms and four *cis* double bonds per molecule.[75] Arachidonic acid is converted to a hydroperoxide PGG_2, by prostaglandin-H-synthase. PGG_2 then undergoes a 2-e^- reduction at the POX site of the enzyme to give PGH_2, which is the precursor of prostaglandins, thromboxanes and prostacyclin. Arachidonic acid can be metabolised by three different pathways; (a) prostaglandin-H-synthase (PGHS) (b) lipoxygenase (LOX) and (c) cytochrome P-450.

Phospholipase A_2 (PLA_2) is the major pathway for arachidonic acid liberation. PLA_2 cleaves the glycerophospholipid backbone at the fatty acid composition sn-2 position to yield free arachidonic acid and lysophospholipid. Lipoxygenases form hydroperoxyeicosatetraenoic acids (HPETEs), as primary products, which are reduced to hydroxyl-acids ($HETE_S$), or converted into leukotrienes and lipoxins **Fig. 1.8**,[16,43] which play a major role in inflammation.[43] The epoxygenase pathway forms epoxyeicosatrienoic acid (EETs) Fig. 1.12. Cytochrome P-450 catalyses the conversion of arachidonic acid (AA) into epoxyeicosatrienoic acids (EETs), which are hydrolysed to the corresponding diols by epoxide hydrolase. EETs have potent effects on peptide hormone secretion, vascular and bronchial smooth muscle tone and ionic fluxes, thus playing an important role in the kidney and the cardiovascular system.[76] All three pathways require molecular oxygen and are outlined in **Scheme 1.3.**[16] Arachidonic acid is stored in cell membranes and esterified in the sn-2 position of glycerophospholipids. Arachidonic acid is either consumed in the diet or formed from linoleic acid. Metabolism of arachidonic acid is initiated by its release from membrane phospholipids, in response to certain extracellular stimuli. Release of arachidonic acid from three phospholipids classes, phosphatidylinositol (PI), phosphatidylethanolamine (PE), and phosphatidylcholine (PC), involves two major pathways; the phospholipase C and the phospholipase A_2 pathways.[43]

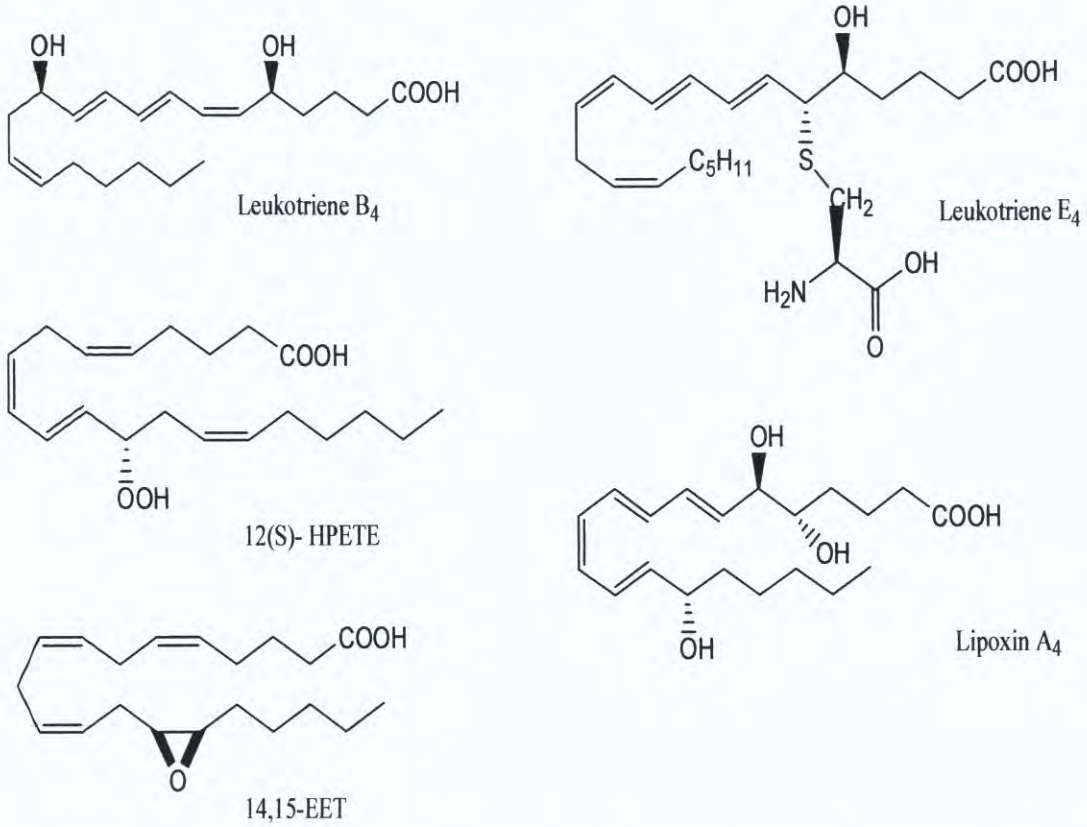

Fig. 1.8: Products formed as a result of lipoxygenase and epoxygenase pathways. Reproduced from W. L. Smith, *Biochem J.*, 1989, **259** (2), 315-24.

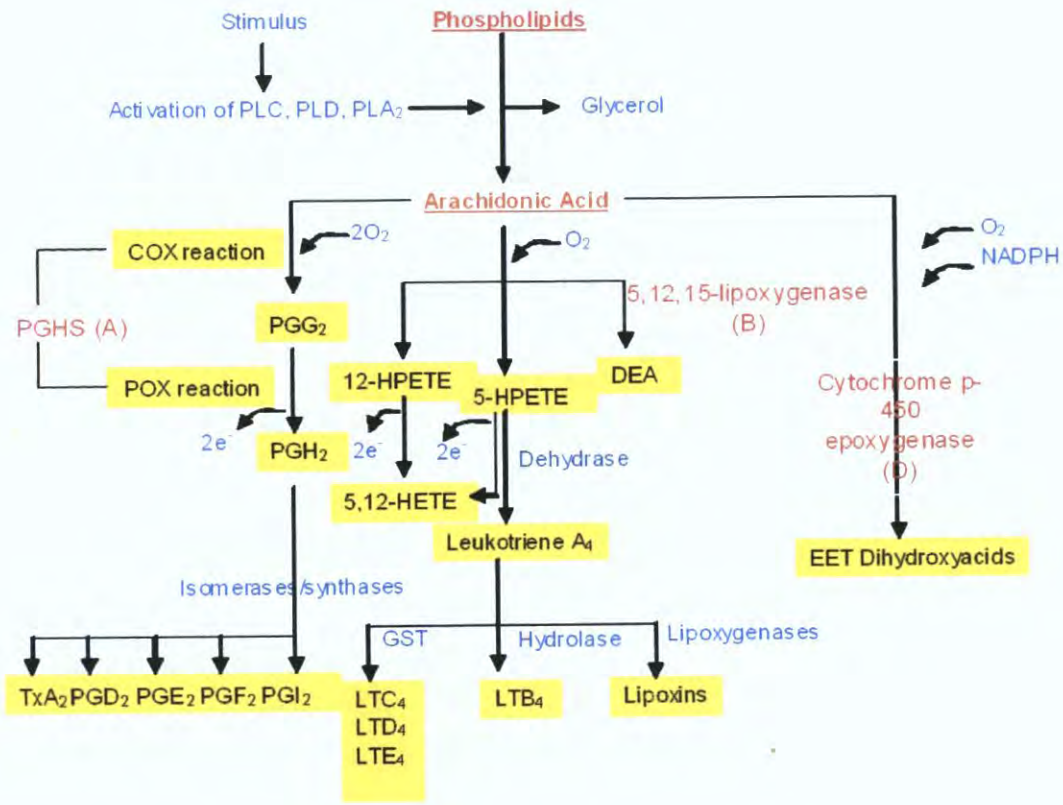

Scheme. 1.3: Major pathways involved in arachnidonic acid metabolism

(A) Prostaglandin H_2 synthase pathway: The formation of hormonally active prostaglandins by isomerases or synthases; **(B) Lipoxygenase pathway:** The formation of HPETEs and DEAs by lipoxygenase and the subsequent formation of 5- and 12-HETE by peroxidases, leukotrienes by hydrase and tranferases and lipoxins by lipoxygenases ; **(C) Epoxygenase pathway:** The formation of EETs and dihydroxyacids by cytochrome p450 epoxygenase pathway. All three pathways require molecular oxygen Abbreviations: HPETE: hydroperoxyeicosatetraenoic acids, HETE: hydroxyeicosatetraenoic acids, DEA: dihydroxyeicosatetraenoic acids, EET: epoxyeicosatrienoic acid. Reproduced from W. L. Smith, *Biochem J*, 1989, **259** (2), 315-24.

1.6.2 Cyclooxygenase activity

The cyclooxygenase reaction catalyses the addition of two oxygen molecules to C-11 and C-15 of arachidonic acid to form PGG_2, **Scheme 1.4.** The COX reaction is initiated by abstraction of the 13-*Pro-S* hydrogen atom from arachidonic acid by a Tyr385 phenolic radical produced during reaction with peroxide, giving an arachidonyl radical. This is followed by attack on the arachidonyl radical at C-11 by molecular oxygen. In

order to do this oxygen moves from the lipid bilayer into a small pocket created by Val349, Ala527, Ser530 and Leu531. C-11 of arachodinic acid is located above this pocket and yields an 11-R-peroxyl radical intermediate. The resulting peroxy radical was thought to attack C-9 to form the endoperoxide bridge, resulting in a localized radical at C-8, which in turn reacts with the conjugated diene spanning C12-C15. Since arachidonic acid binds in an extended L-shaped conformation, ring closure between C-8 and C-12, is not possible at this stage as the distance of 5Å is too far. In order to facilitate this, a reconfiguration of arachidonic acid is essential for reaction to occur. It is thought that the conformational transition requires a movement of the ω-end, C_{13}–C_{20}, of the AA towards the carboxyl portion above Ser530 and Leu534. The loss of the C-11/12 double bond with the formation of the 11R- peroxyl radical allows more freedom for attack on C-9. The 11R-hydroperoxyl radical could attack C-9 from the R-side by swinging over C-8 and causing rotation of the C-10 to C-11 bond, moving C-12 closer to C-8, thus facilitating ring closure. Carbons 13-20 are repositioned and C-15 is then ideally placed for the addition of a second oxygen molecule to form the 15-S-peroxyl radical. The 15-S-peroxyl radical is aligned below Tyr385 for donation of the radical to complete cyclooxygenase catalysis.[64] The donation of a hydrogen atom back to the substrate from Tyr385 creates PGG_2 with retention of stereochemistry. This final step regenerates a Tyr385 radical for the next round of cyclooxygenase catalysis. Thus, multiple turnovers per activation event allow accumulation of PGG_2.[35,77]

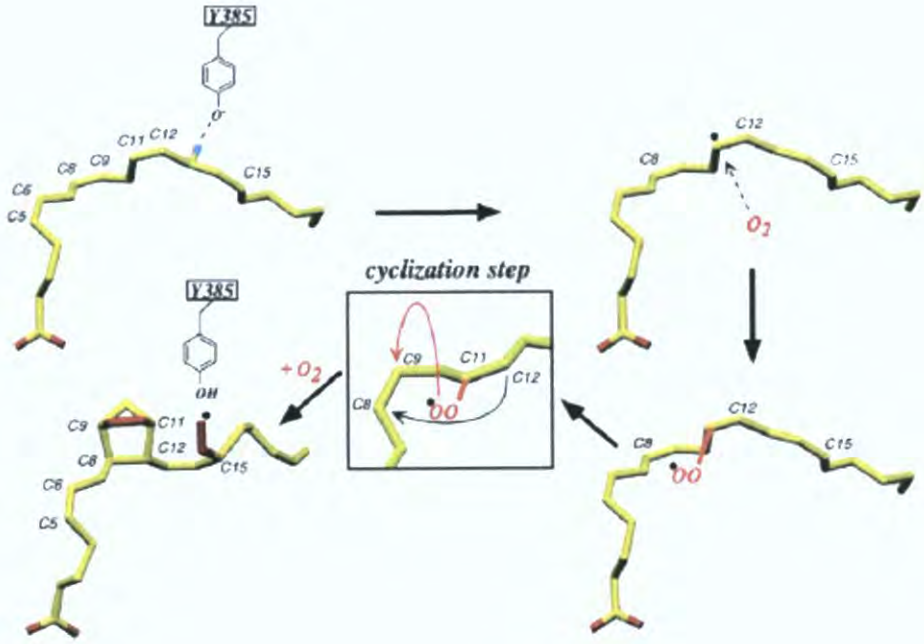

Scheme 1.4: A schematic representation of the COX reaction. Reproduced from R. M. Garavito, M. G. Malkowski, D. L. DeWitt, *Prostaglandins & Other Lipid Mediators*., 2002, **68-69**, 129-152.

The COX reaction is peroxidase dependent,[78] and requires the haem group at the peroxidase active site to undergo a two electron oxidation. The oxidized haem then oxidizes Tyr385 to a tyrosyl radical which abstracts the 13-S-hydrogen from arachidonic acid in order to initiate the COX reaction. Differences in thresholds for hydroperoxide activation between PGHS-1 and -2 may contribute to their individual actions.[64] The COX activity of PGHS-2 requires a 10-fold lower concentration of hydroperoxide than PGHS-1, and this allows PGHS-2 to function independently within the same cell.[39] PGHS-1 and -2 isoforms mainly catalyze formation of PGG_2 from AA within the COX site, but they also produce a significant amount of other oxygenated products such as, 11*R*-HETE, 15*R*-HETE and 15*S*-HETE, which are produced by native ovine PGHS-1. The syntheses are always initiated by abstraction of the 13-*Pro-S* hydrogen (15*S*-HETE) or 13-*Pro-R* hydrogen (15*R*-HETE) depending on the stereochemistry around C_{15} at the time of oxygen addition. This implies tha AA can assume up to three catalytically competent arrangements in the COX active site of o-PGHS-1.[64]

1.6.3 Cyclooxygenase substrate specificity

Despite their similarities, PGHS-1 and -2 exhibit differences in their substrate specificity. PGHS-1 shows a strong preference for 20-C fatty acids with three or four double bonds, whereas PGHS-2 has a higher affinity for 18-C substrates. Arachidonic acid is the preferred substrate for the COX activity of PGHS-1 and -2. The ability of PGHS-2 to accommodate 18- and 20-carbon polyunsaturated fatty acids is larger than PGHS-1 and this may be due to the fact that PGHS-2 has a lager active site than PGHS-1. Site directed mutagenesis studies have shown that Arg513 in PGHS-2 plays an important role in PGHS-2 metabolism.[79]

1.6.4 Peroxidase activity

Redox reactions involving the haem iron are crucial to the peroxidase reaction of both isoforms. The first step involves 2-e^- reduction of hydroperoxides to the corresponding alcohol and the production of compound I, an oxyferryl-protoporphyrin(IX) cation radical, $O{=}Fe^{IV}$- $PPIX^+$, reaction 1, **Scheme 1.5.** A 1-e^- reduction of the porphyrin radical in compound I by an electron donor generates compound II, an O=Fe(IV)-PPIX species, reaction 2, **Scheme 1.5.** Further one electron reduction of compound II, regenerates the resting Fe (III) state of the enzyme, reaction 3, **Scheme 1.5.** PGHS peroxidase activity reduces the cyclooxygenase hydroperoxy endoperoxide product, PGG_2 to the hydroxy endoperoxide, PGH_2. For PGHS, two electron reduction of a hydroperoxide to form compound I, followed by an intramolecular electron transfer generates the tyrosyl radical that initiates cyclooxygenase activity, serving as the COX oxidant. Reducing co-substrates function as electron donors to generate compound II and hence the free radical substrates.[80]

Overall Reaction: $ROOH + XH_2 \longrightarrow ROH + XH_2O$

Reaction 1: Fe^{III} - PPIX + ROOH $\longrightarrow$ $O{=}Fe^{IV}$ - $PPIX^{+\cdot}$ + ROH
Compound I

Reaction 2: $O{=}Fe^{IV}$ – $PPIX^{+\cdot} + e^-$ $\longrightarrow$ $O{=}Fe^{IV}$ - PPIX
Compound II

Reaction 3: $O{=}Fe^{IV}$ - PPIX + e^- $\longrightarrow$ Fe^{III} - PPIX + H_2O

(PPIX = protoporphyrin IX)

Scheme 1.5: Scheme of Peroxidase mechanism of action. Reproduced from L. M. Landino, B. C. Crews, J. K. Gierse, S. D. Hauser, L. J. Marnett, *J. Biol.* Chem., 1997, **272**, 21565-21574.

The peroxidase activity of PGHS is also necessary to activate the cyclooxygenase activity of PGHS.[81] Although COX catalysis requires an initial oxidation of the haem group at the POX site, peroxidase catalysis can operate maximally in the absence of COX turnover or occupancy of the COX active site.[82] The structure of PGHS-1 peroxidase is very similar to that of myeloperoxidase and horseradish peroxidase. The feature that distinguishes classical haem peroxidases from other haemoproteins is their ability to break peroxide bonds heterolytically which is facilitated by the distal histidine acting as a general acid-base catalyst. This causes deprotonation of the hydroperoxide substrate and subsequent protonation of the incipient alkoxide ion during generation of compound I, while a neighbouring arginine stabilises the developing hydroxide or alkoxide ion. In PGHS, the distal histidine, His207, side chain seems to be orientated by hydrogen bonding to the Glu203 main chain carbonyl. Interactions on the proximal side of the haem iron are thought to affect the reactivity of the haem group.[83] Mutations of Glu203, His207, or His388 in *ovine* PGHS-1 and human PGHS-2 lead to a reduction or elimination of POX activity.

1.6.5 Peroxidase kinetics

Peroxidase activities of PGHS-1 and -2 have been investigated by measuring the rate of oxidation of reducing co-substrates such as guaiacol,[80] and *N,N,N',N'*-tetra-*p*-methylphenylenediamine dihydrochloride, TMPD.[84] There are two important differences between the POX activities of PGHS-1 and -2. While PGHS-1 catalyses

almost exclusively a $2e^-$-reduction of hydroperoxide substrates, PGHS-2 catalyses 60% $2e^-$- and 40% $1e^-$-reductions.[80] Also the rate of formation of compound II from compound I, is much faster in PGHS-2 at lower peroxide concentrations. Therefore, PGHS-2 COX activity is stimulated at lower concentrations of hydroperoxide compared to PGHS-1. Even when PGHS-1 is not able to function, PGHS-2 can function independently and in the presence of PGHS-1.

1.6.6 Peroxidase substrate specificity

Peroxidase substrate specificity has been studied by a number of groups.[85-89] The peroxidase sites of both PGHS isoforms can reduce a range of peroxides such as lipophilic primary or secondary peroxides e.g. 15-HETE and 5-phenyl-4-pentenyl-1-hydroperoxide (PPHP), small hydrophilic peroxides like H_2O_2 and sterically hindered tertiary peroxides such as *t*BuOOH.[85] Both isoforms have a preference for secondary alkyl hydroperoxides and the natural substrate PGG_2.[85] The turnover for POX activity is higher than for COX activity and is approximately 14 times that of arachidonic acid turnover in the presence of peroxidase-reducing co-substrates.[86] There are a number of compounds which can act as reducing co-substrates for PGHS with efficiencies which depend on lipid solubility and redox potential.[87] Thus, all lipophilic compounds with low oxidation potentials can act as co-substrates for the POX reaction. These include aromatic amines and phenols. Markey *et al.* indicated that there was no correlation between the ability of the compound to inhibit COX and to cause peroxidase hydroperoxide reduction.[86] Therefore phenolic compounds can stimulate COX activity at low concentrations by quenching the active enzyme back to its resting state.[88]

Physiological compounds, which have the ability to act as reducing cosubstrate, include L-epinephrine as well as ascorbic acid, uric acid, lipoic acid, indoleacetic acid and others, **Fig. 1.10.**

Nitric oxide (NO) can act as a reducing co-substrate for the POX activity of platelet PGHS-1 according to recent studies. The reaction of PGHS-1 with NO results in the inhibition of soluble guanylate cyclase and therefore the platelets lose the anti-aggregatory effect of NO. Thus, catalytic utilisation of NO during the eicosanoid

synthesis reveals a second pro-aggregatory activity of the enzyme besides the production of TxA_2.[89]

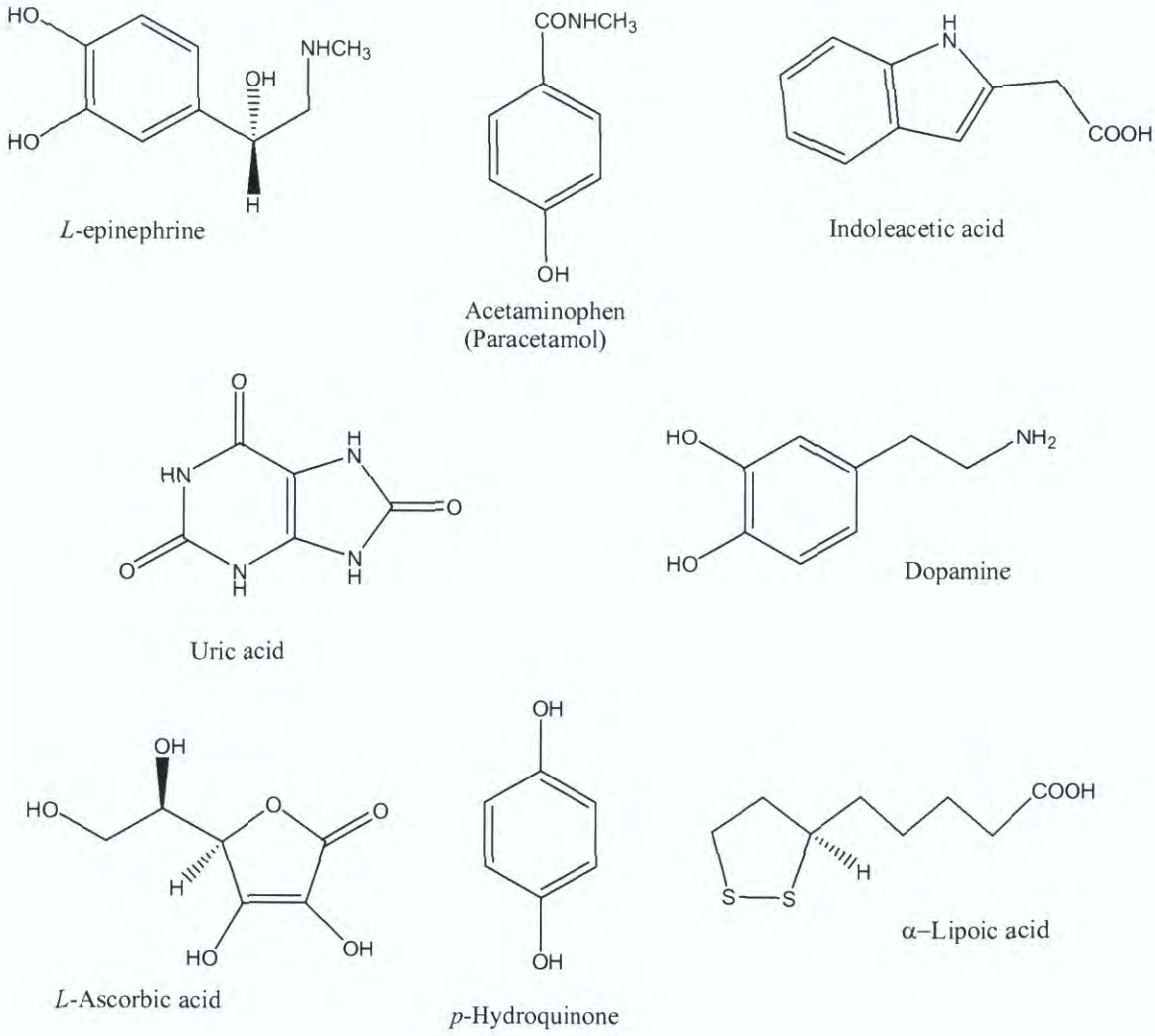

Fig. 1.10: Compounds that can act as reducing co-substrates for PGHS. Reproduced from V. B. O'Donnell, B. Coles, M. J. Lewis, B. C. Crews, L. J. Marnett, B. A. Freeman, *J. Biol. Chem.*, 2000, **275**, 38239-38244.

1.6.7 Mechanism of catalysis

The COX site reaction is initiated by the POX site reaction *via* the generation of a reactive tyrosyl radical and once initiated becomes autocatalytic. In contrast, the peroxidase haem requires a co-reductant to return the haem iron to its resting state before peroxide cleavage can occur again. POX catalysis is initiated when a peroxide reacts with the haem group **Fig. 1.11(a)**, giving compounds I and II. Another

intermediate, called intermediate II, **Fig. 1.11(b)**, has been recognized by electron paramagnetic resonance (EPR) spectroscopy and is formed from compound I by a single electron traveling from Tyr385 along the peptide chain to the proximal ligand, His388, and finally to the haem group, reducing the porphyrin radical. Intermediate II therefore contains an oxyferryl group with a neutral protoporphyrin IX and a Tyr385 radical and is two oxidizing equivalents above the resting enzyme.[91] Compound I can undergoes a $1e^-$ reduction by an exogenous electron donor to produce Compound II, **Fig. 1.11(c).**[85] Compound I and Intermediate II can be returned to the resting state in two steps, *via* Compound II with the aid of reducing co-substrates **Fig. 1.11(c, d, h).** Intermediate II and Compound II are can be differentiated by EPR spectroscopy.[91]

In cyclooxygenase catalysis, Intermediate II, with its tyrosyl radical, it thought to be the initial oxidant in the COX catalysis, abstracting the 13-pro-S hydrogen from arachidonate. This initiates the oxygenation reaction and regenerates the tyrosine residue. If the PGG_2 radical abstracts a hydrogen atom from the tyrosyl residue to form PGG_2 then the tyrosyl radical is regenerated and a chain reaction could occur, **Fig. 1.11 (e, f, g).** This is a branched-chain mechanism with autocatalytic characteristics; for every intermediate I converted to the Fe (IV) =O-tyrosyl radical another chain can be started, this leads to the accumulation of large amounts of PGG_2, instead of PGH_2, the precursor of all other prostaglandins.[92]

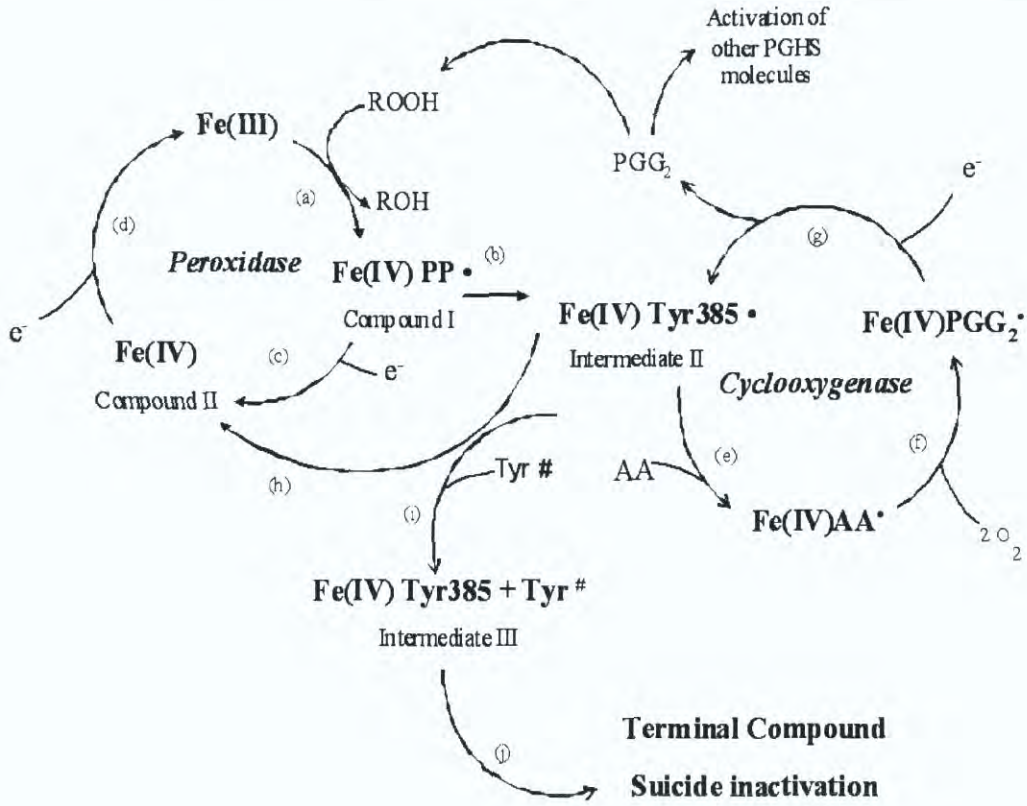

Fig. 1.11: PGHS branched-chain tyrosyl radical mechanism. Steps (a) through (h) are based on the catalytic mechanism; steps (i) and (j) reflect the self-inactivation mechanism. The oxidation state of the heme iron is indicated by Roman numerals; Intermediates II (a Tyr385 radical and the oxyferryl heme) and III (Tyr385 radical and the oxyferryl heme and a second tyrosyl radical); Compound I and II: peroxidase Compounds I and II; ROOH and ROH: hydroperoxide and the corresponding alcohol; PP•: protoporphyrin π-cation radical; Tyr•: tyrosyl radical; AA•: arachidonate radical; and $PGG_2^{\bullet}$: prostaglandin G_2 with peroxyl radical on C_{15}. Reproduced from W. L. Smith, D. L. DeWitt, R. M. Garavito, *Annu. Rev. Biochem*, 2000, **69**, 145-182.

1.7 Inhibitors of PGHS: NSAIDs

1.7.1 Classification and inhibitory activity

NSAIDs, non-steroidal anti-inflammatory drugs, are the most widely used drugs and have broad applications. A number of these are shown in **Fig. 1.12.** These agents are used therapeutically as anti-inflammatories, antipyretics and analgesics.[93] In 1971, the mode of action of NSAIDs through the inhibition of PGHS was proposed by Vane.[40] NSAIDs can be subdivided into two classes of drug behaviour: (a) classical, 'isoform nonspecific' NSAIDs and (b) COX-2 (PGHS-2) inhibitors. All classical NSAIDs can inhibit both PGHS-1 and -2 but in general bind more tightly to PGHS-1. In contrast, COX-2 inhibitors are selective. All NSAIDs compete with arachidonate for the COX

active site, and they are commonly classified according to their mode of inhibition of PGHS. These include (a) rapid, reversible binding e.g. ibuprofen, (b) rapid, lower affinity reversible binding followed by time-dependent, higher affinity, slow reversible binding e.g. flurbiprofen or (c) rapid, reversible binding followed by covalent modification e.g. aspirin.[94]

Aspirin is the only commercially available irreversible inhibitor of both PGHS-1 and –2 which covalently modifies the enzyme through acetylation of Ser530, in the COX active site, thus blocking substrate access to the upper section of the channel. When the purified enzyme is acetylated, only the COX and not the POX activity is inhibited.[65] Recently described NSAIDs selectively inhibit PGHS-2 whereas selective PGHS-1 inhibitors are in the developmental process. These NSAIDs inhibit PGHS-2 in a slow, time-dependent manner but are also weak competitive inhibitors of PGHS-1. The reason for this is when the blood concentration of a PGHS-2 selective NSAID is below the IC_{50} for PGHS-1 inhibition, the activity of PGHS-1 will be slightly affected, while PGHS-2 is completely inhibited.[95]

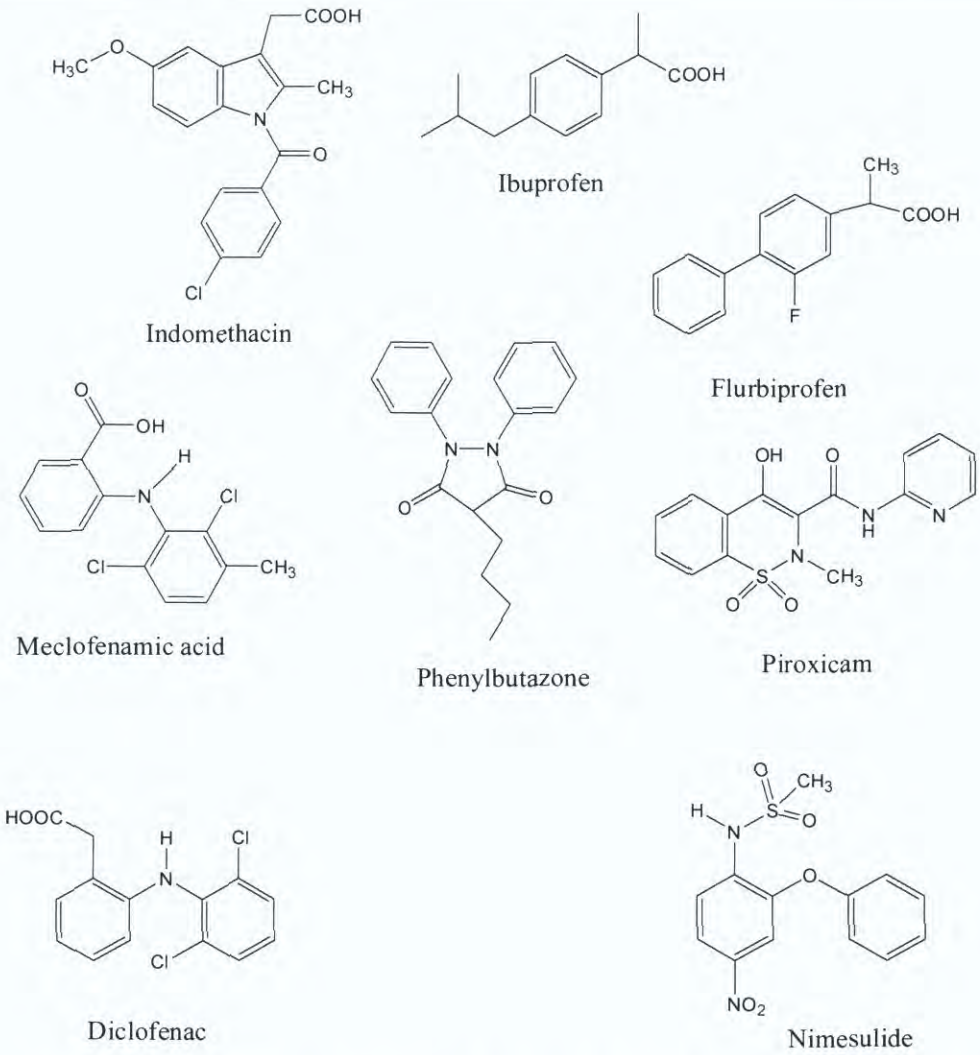

Fig. 1.12: Structures of some common NSAIDs. Reproduced from R. A. Copeland, J. M. Williams, J. Giannaras, S. Nurnberg, M. Covington, D. Pinto, S. Pick, J. M. Trzaskos, *Proc. Natl. Acad. Sci., U S A* 1994, **91**, 11202-11206.

1.7.2 Amino acid residues important for NSAID activity and selectivity

In the PGHS-1 cyclooxygenase active site, amino acid residues such as Val349, Gly533, Ser530, Arg120 and Tyr355 are important with respect to substrate binding.[58] The hydrophobic residues present in the COX active site function to position arachidonic acid and inhibitors. The guanidinium group of Arg120 forms a salt linkage with the carboxylate group of arachidonic acid and carboxylate containing NSAIDs such as flurbiprofen. It has been shown that the carboxylate group interaction with Arg120 is more important for aracidonic acid than for inhibitor binding to PGHS-1. In contrast the mutation of Arg120 in human PGHS-2 suggested that the guanidinium

group of Arg120 in this isoform forms a less important interaction with the arachidonate of the substrate.

X-ray crystal analysis has reported that Tyr355 lies on the opposite side from Arg120 of the COX channel and creates important interactions with NSAIDs and the substrate arachidonic acid. An enzyme modification has shown that this residue dictates the stereospecificity but not the reactivity of PGHSs toward NSAIDs especially those of the 2-phenylpropionic class such as ibuprofen and flurbiprofen **Fig. 1.12.** The COX channel ends with Tyr385 and together with Ser530, which is also important for NSAIDs interactions, these residues have the ability to interact with negatively charged groups in both arachidonic acid and NSAIDs such as aspirin.[39,64] The crystal structure of ovine PGHS-1 shows that the PGHS substrate arachidonic acid binds Arg120 by a salt linkage.[67] Most non-steroidal anti-inflammatory drugs (NSAIDs) containing aromatic carboxylic acids interact similarly, and orientate the aromatic functionality of the drug towards Tyr385 in the COX site.[96] Interestingly, Tyr385 is critical for aspirin acetylation of Ser530, as confirmed by the mutation of Tyr385 to Phe which reduces activity by over 90%.[97] The role of Tyr385 is to stabilize the negatively charged tetrahedral intermediate formed during acetylation. It follows that a more effective inhibitor might result by simultaneous interaction with both Arg120 and Tyr385, while orientating an acetyl group in close proximity to the hydroxyl oxygen of Ser530.[98] Although recent evidence suggests that Ser530 is essential in time-dependent inhibition by both nimesulide and piroxicam **Fig. 1.12**, this residue is not involved in COX catalysis of PGHS-1, as the Ser530 mutant retains the activity of the native enzyme.[99]

The main differences between the COX active sites of PGHS-1 and -2 have allowed the development of a new class of NSAIDs, the COX-2 inhibitors. The substitution of Ile523 in PGHS-1 with Val523 in PGHS-2 results in a small side pocket adjacent to the active site channel which increases the size of NSAID binding by approximately 20% in the COX active site compared to PGHS-1.[96] Also the substitution of Ile434 in PGHS-1 by Val434 in PGHS-2 can further increase the effective size of the active site channel.[39,58]

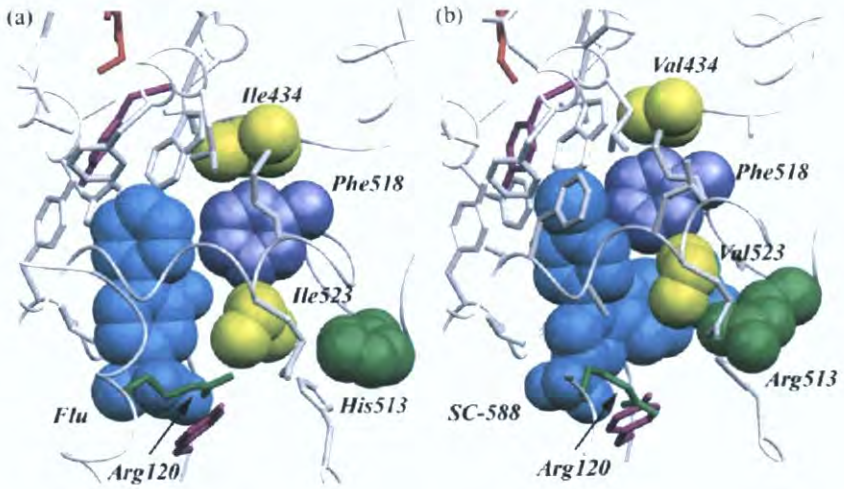

Fig. 1.13: A view of NSAIDs binding to the COX active site. Flurbiprofen (light blue) is bound in the COX active site channel in ovine PGHS-1. The COX-2 inhibitor SC-588 (light blue) is bound in the COX active site channel of mouse PGHS-2. The phenylsulfonamide group of SC-588 extends into the side pocket made accessible by Val523 and interacts with Arg513. Reproduced from R. M. Garavito, M. G. Malkowski, D. L. DeWitt, *Prostaglandins & Other Lipid Mediators*, 2002, **68-69**, 129-152.

The larger size of the central channel in PGHS-2 can reduce ionic and steric crowding by the positively charged Arg120, thus enhancing the binding of nonacidic NSAIDs such as SC-588 **Fig. 1.14.** The substitution of His513 in PGHS-1 with Arg513 in PGHS-2 alters the chemical environment of the side pocket.[100] This substitution results in a positive charge being located at the center of this pocket, which can interact with polar groups of molecules entering the pocket.[96]

1.7.3 Side effects of NSAIDs and PGHS-2 (COX-2) selective inhibitors

The main therapeutic effect of nonsteroidal anti-inflammatory drugs (NSAIDs) is to inhibit the overproduction of prostaglandins, which are responsible for pathological effects, by COX-2 in response to inflammatory stimuli. Despite the therapeutic effects, there are several side effects associated with their use. These side effects occur mainly when NSAIDs are used in the treatment of arthritis or chronic inflammatory disease. For example approximately 1% of chronic users of NSAIDs, usually those with arthritis or chronic inflammatory disease get ulcers or develop other serious gastro-intestinal problems each year. These side effects result from inhibition of PGHS-1 the isoform present in the stomach lining and which produces prostaglandins which protect the

gastric mucosa.[39] Chronic use of NSAIDs produces gastro-duodenal mucosal injury in 35-60% of patients, ulcerations in 10-25%, and severe haemorrhages or perforations in < 1%. Side-effects are mainly reported in the upper gastrointestinal tract and less frequently in the liver, kidney and bone marrow. Gastric ulceration is the most common side effect associated with acute exposure to NSAIDs. Acute mucosal damage induced by aspirin in humans occurs within 60 minutes.[101] Side effects associated with the renal system is due to the inhibition of the biosynthesis of prostaglandins PGE_2 and PGI_2 involved in the maintenance of renal blood dynamics. Thus NSAID-induced kidney damage is associated with a disruption of the adrenergic-angiotensin systems, or reduced renal blood flow due to the inhibition of prostaglandins that protect kidney function.[102] Skin reactions are also observed with the use of NSAIDs, such as mefenamic acid.[103] These include mild rashes and urticaria to photosensitivity.[104] Liver problems are associated with some NSAIDs such as diclofenac (Voltaren).[105]

The development of selective COX-2 inhibitors was intended to inhibit only the production of COX-2 dependent inflammatory prostaglandins, without affecting COX-1 and its gastro-protective and platelet functions. Therefore it was anticipated that selective PGHS-2 inhibitors should reduce pain, fever and inflammation without causing gastric damage compared to conventional non-selective NSAIDs (*e.g.* naproxen, ibuprofen, flurbiprofen or diclofenac).[106] PGHS-2 inhibitors can be categorised into three main groups **Fig. 1.14:** (a) acidic sulfonamides *e.g.* NS-398, nimesulide[107] and flosulide,[99] (b) diarylheterocyclic (or tricyclics) *e.g.* Dup697,[108] rofecoxib (vioxx),[109] celecoxib (celebrex),[110] etoricoxib,[111] and (c) alterations to traditional NSAID's such as meclofenamic acid,[112] ketoprofen, piroxicam, aspirin and indomethacin derivatives (non-selective inhibitors).[113] Other classes of selective PGHS-2 inhibitors e,g. naphthalene derivatives also exist.[114] The tricyclics are the most diverse group of PGHS-2 inhibitors. These include rofecoxib (vioxx) and celecoxib (celebrex), the first PGHS-2 inhibitors approved for clinical use.[110] Rofecoxib is a methylsulfone, which has a longer $t_{1/2}$, and is slightly more potent and selective *in vivo* than celecoxib.[109]

Although initial experiences with selective COX-2 inhibitors were positive problems particularly of a cardiovascular nature became apparent following large-scale clinical use. Rofecoxib (Vioxx) was withdrawn from the market in 2004, following the doubling of heart attacks in patients being treated with this drug for colon cancer.[115] Celecoxib (celebrex), an effective anti-inflammatory and analgesic,[110] which was the first PGHS-2 selective inhibitor approved for human use, also gave rise to concerns and because of the increased occurrence of heart attacks associated with the use of this drug the National Cancer Institute terminated the Adenoma Prevention with Celecoxib (APC) trial. In addition, Valdecoxib which has higher selectively and potency than celecoxib for inhibition of PGHS-2 and was used for the treatment of osteoarthritis,[116] was in 2004 the subject of a serious FDA warning regarding reported cardiovascular side effects as well as adverse skin reactions.[117] It now appears that there is an increase of adverse cardiovascular events, with PGHS-2 selective NSAIDs, compared to classical NSAIDs. This was observed in the Celecoxib Long-term Arthritis Safety Study (CLASS) and the Vioxx Gastrointestinal Outcomes Research (VIGOR) studies, which reported that PGHS-2 selective inhibitors do not reduce the incidence of gastric ulcers and can cause more morbidity than non-selective NSAID as a result of prostacyclin suppression and impaired blood flow due to accumulation of thromboxane A_2.[116]

Selective inhibition of PGHS-2 has been linked to kidney disorders, as kidney expresses large amounts of PGHS-2; its inhibition can result in hypertension and salt and water retention. Furthermore, PGHS-2 plays an important role in wound healing in the cornea and blocking this enzyme may inhibit this healing.[118] The anti-inflammatory effects of selective COX-2 inhibitors have been documented. Since inflammation constitutes an important feature in ischemic heart failure, it was reported that inhibition of pro-inflammatory prostanoids through use of selective COX-2 inhibitor could significantly ameliorate myocardial injury and hence improve myocardial function.[119]

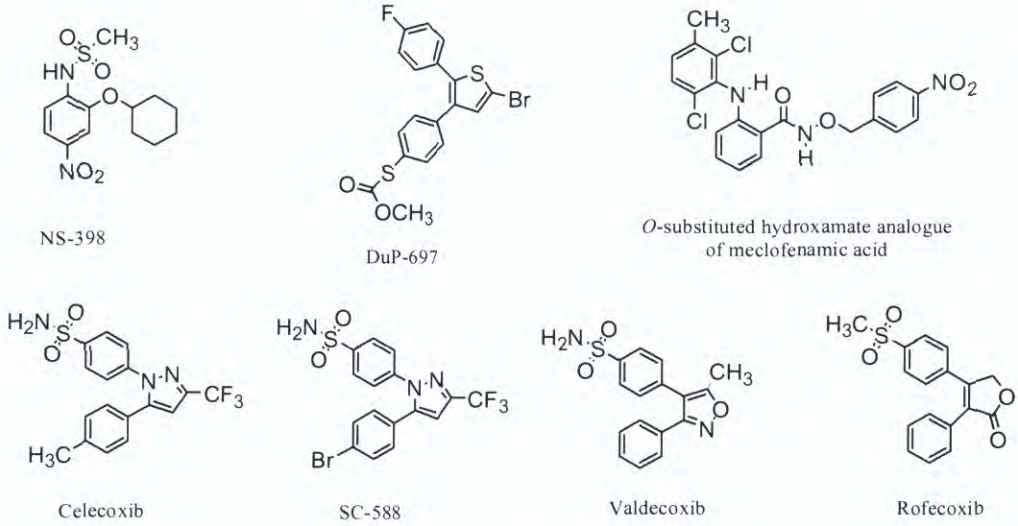

Fig. 1.14: Structures of common PGHS-2 inhibitors or Coxibs. Reproduced from C. S. Li, C. Brideau, C. C. Chan, C. Savoie, D. Claveau, et al, *Bioorganic & Medicinal Chemistry Letters*., 2003, **13** (4), 597-600.

1.8 Aims of the work described in this chapter

Acetylsalicylic acid (aspirin), **Fig 1.16** is an effective long-term prophylaxis of thrombotic events such as heart attacks and strokes. It covalently inhibits prostaglandin-H-synthase by interacting with Arg120 or Tyr385 at the active site allowing delivery of its acetyl group to Ser530. However molecular modelling studies carried out by Dr E. Moman and Dr A. Chubb in our laboratory have shown that the structure has not been optimized to fit the active site. They have designed acetylsalicylate analogues with an additional carboxylate substituent which allows simultaneous interaction with Arg120 and Tyr385 whilst positioning the acetyl group in close proximity to Ser530. This has led to an active ester derivative which unlike acetylsalicylate is non-acidic and which may act a useful lead compound for further exploitation of this approach.[120-122]

In the work carried out by Drs Moman and Chubb, docking using the MOE-Dock program allowing receptor flexibility,[123,124] accurately predicted the crystallographic placement of arachidonate in the crystal structure of ovine PGHS-1,[67,125] PDB:1DIY **Fig. 1.15 A**, with a root mean square deviation (RMSD) of 1.11 Å and a binding energy of -14.3 kcal/mol. Similar docking of acetylsalicylate showed carboxylate binding to either Arg120 or Tyr385, but not both simultaneously **Fig. 1.15 B.** With an optimal

binding energy at -8.8 kcal/mol, although this is compensated for by irreversible inhibition. If bound to Arg120, the distance between the acetyl group and Ser530 is 5.88 Å, which is too far for acetyl group transfer. This is corroborated by the crystallographic position of salicylate in PDB:1PTH [65] which is bound to Arg120 and is separated from Ser530 by 5.54 Å.

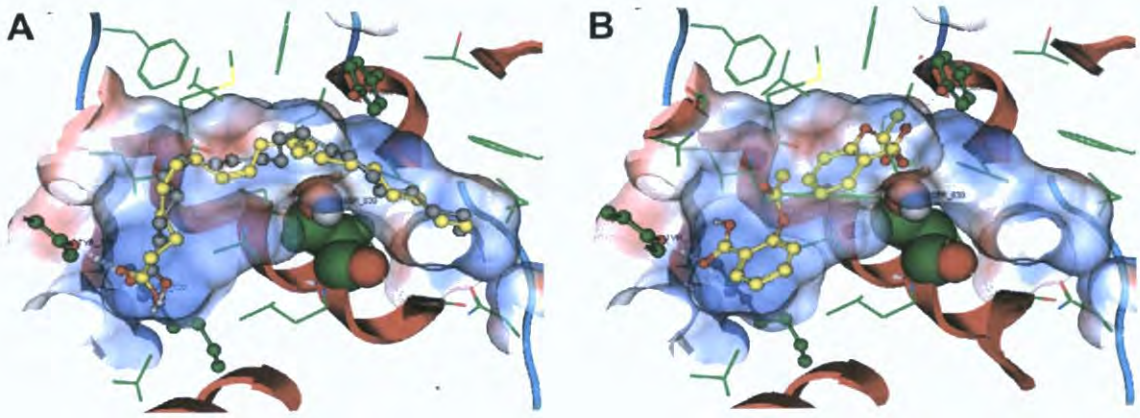

Fig. 1.15: Docked conformations of arachidonate and aspirin in the PGHS-1 cyclooxygenase site. MOE-Dock was used to place arachidonate **(A)** and aspirin **(B)** in the active site of the ovine PGHS-1 COX site crystal structure 1DIY. The PGHS-COX site isoelectric surface is shown semi-transparent, where negative regions are red, positive regions blue, and neutral regions white. Receptor carbons are green, the crystallographic arachidonate carbons are grey, and the binding pose found using MOE-Dock has yellow carbons. Nitrogens are blue, oxygens are red. Non-polar hydrogens (white) were removed for clarity. Ser530 is shown in space fill, Arg120, Tyr355 and Tyr385 are shown in ball-and-stick, and other Cox site residues are shown in line notation. The isolated backbone alpha helix is shown in red ribbon, while the loop regions are depicted with cyan. Half the site has been cropped for visualization. Light green lines indicate distance measures mentioned in the text. In **(B)**, aspirin bound to Arg120 is shown with yellow carbons. Reproduced from A. Alagha, E. Moman, M. F. M. Adamo, K. B. Nolan, A. J. Chubb, *Bioorg Med Chem Lett.*, 2009, **19** (15), 4213-6.

To allow the acetylsalicylate moiety to advance further down the COX active site channel, while retaining a salt bridge with Arg120, we introduced an *n*-pentanoate chain at the *meta* position, giving **2 Fig 1.16**, as a target molecule for synthesis and study of anti-platelet activity.[122] In **2** the *n*-pentanoate group is capable of interacting with the active site Arg120, while the salicylate carboxylate interacts with Tyr385, and the acetyl group is in close proximity to Ser530. MOE-docking showed that **2** could indeed form a salt bridge with Arg120, and a hydrogen bond to Tyr385, while allowing the acetyl group to interact favorably with Ser530 **Fig. 1.17 A.** The binding energy of -13.7 kcal/mol is similar to that of the substrate, and significantly lower than that for aspirin. Based on the results of enzyme inhibition by **2** compounds **3-5** were also synthesised and PGHS-2 was chosen as the target enzyme for inhibition studies.

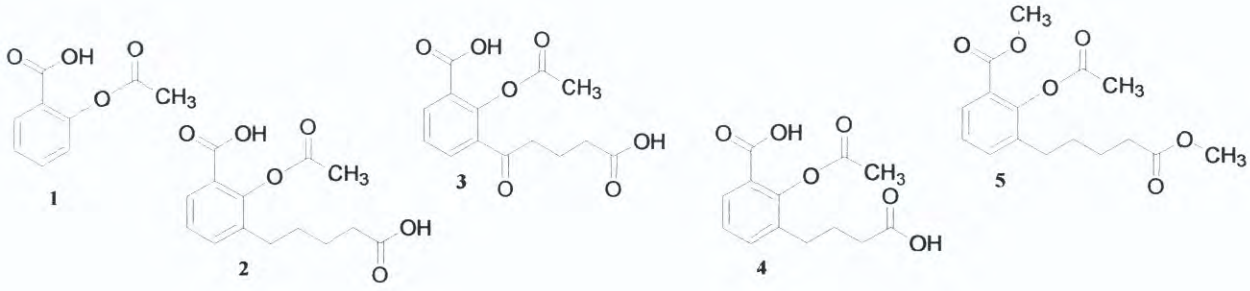

Fig. 1.16: Compounds synthesised and tested for anti-platelet activity

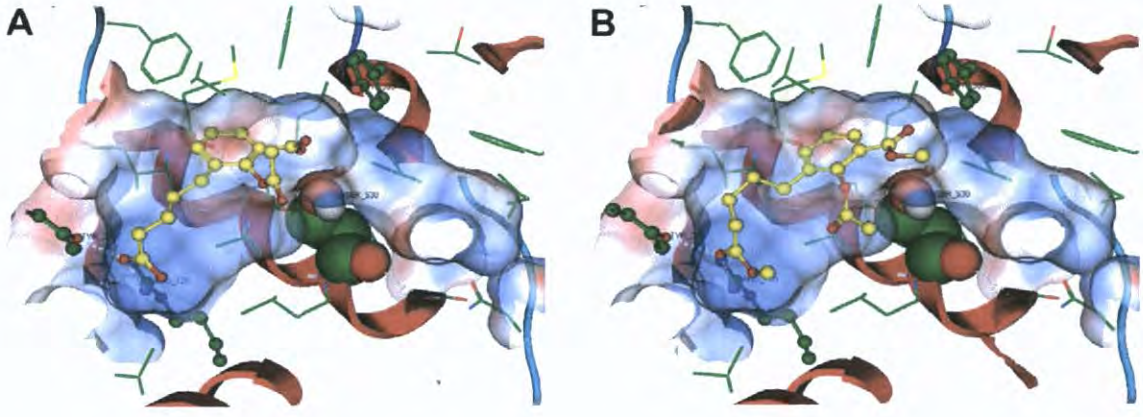

Fig. 1.17: Docked conformations of **2** and **5** in the PGHS-1 cyclooxygenase site. MOE-Dock was used to place **2 (A)** and **5 (B)** in the active site of the ovine PGHS-1 COX site crystal structure 1DIY. Key as per **Fig. 1.15** In **(A)**, the interatomic distances between **2** and Arg120, Ser530 and Tyr385 are 2.34 Å, 2.53 Å and 3.60 Å, respectively. In **(B)**, the interatomic distances between **5** and Arg120, Ser530 and Tyr385 are 2.51 Å, 3.21 Å, and 2.53 Å, respectively. Arg120 forms hydrogen bonds with either the *n*-pentanoate or ester groups, while the salicylate carboxylate or ester groups interact with Tyr385. The acetyl group is in close proximity to Ser530 in both **2** and **5**. Reproduced from A. Alagha, E. Moman, M. F. M. Adamo, K. B. Nolan, A. J. Chubb, *Bioorg Med Chem Lett.*, 2009, **19** (15), 4213-6.

1.9 Results and Discussion

Results of molecular modelling studies led us to select compound **2** as a target for PGHS-2 inhibition, **Fig. 1.16.** A retro-synthetic analysis of compound **2** is outlined in **Scheme 1.6.**

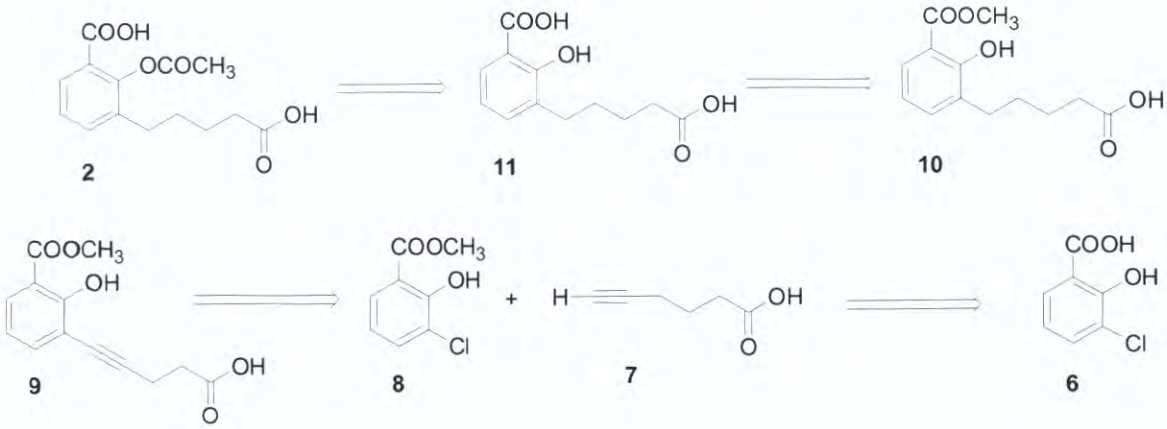

Scheme 1.6: Retrosynthesis of target molecule **2**

Product **2** is formed by acetylation of the phenolic group in **11** which is obtained by hydrolysis of **10.** This is obtained by catalytic hydrogenation of **9**, the product of Sonogashira coupling of 5-pentynoic acid, **7** and methyl 3-chloro-2-hydroxybenzoate, **8**, which is obtained from the readily available starting material 3-chloro-2-hydroxybenzoic acid, **6.**

Sonogashira coupling is used to couple terminal alkynes with aryl or vinyl halides using Pd^0 as the active catalyst. The reaction is performed in the presence of base and copper iodide is used as a co-catalyst, **equation 1**, **Scheme 1.7.**

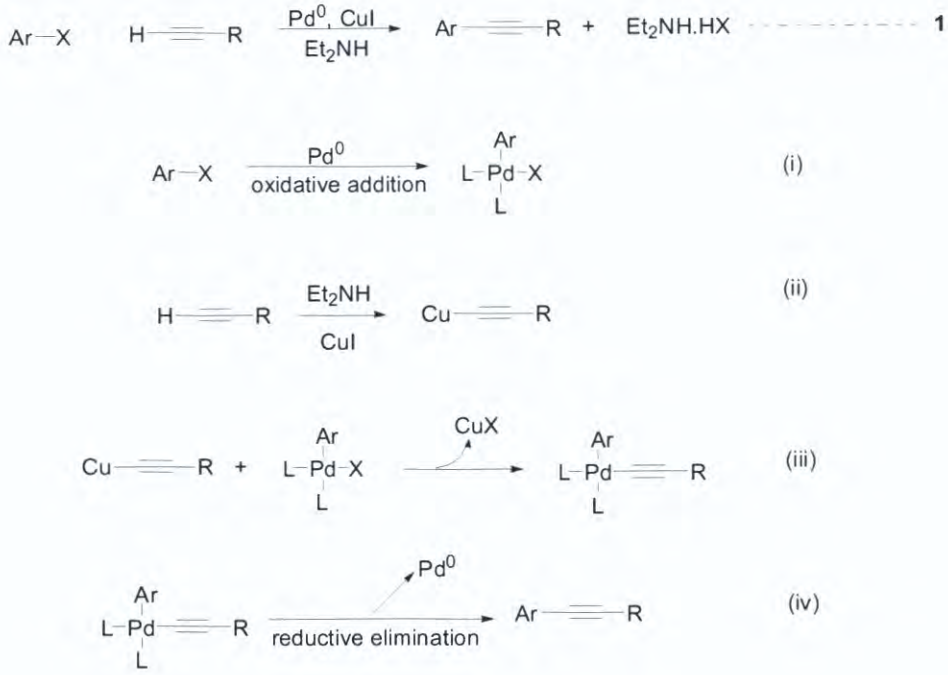

Scheme 1.7: Sonogashira coupling reaction mechanism

Oxidative addition of the organic halide to the palladium complex gives a Pd^{II} intermediate, **Scheme 1.7**, step (i). This intermediate undergoes transmetallation with the alkynyl copper, step (ii), which is generated from the terminal alkyne, base and copper iodide, step (i). Reductive elimination from the alkynylpalladium(II) intermediate gives the product and regenerates the Pd^0 catalyst, step (iv). In the Sonogashira reaction it is more convenient to use a soluble Pd^{II} derivative such as $(PPh_3)_2PdCl_2$ instead of Pd^0 as catalyst. This is rapidly reduced *in situ* to give a coordinatively unsaturated, catalytically active, Pd^0 species.[126,127]

In our initial attempt at the synthesis of **2,** we reacted **6** (unesterified) directly with pentynoic acid, **7,** in the presence of $(PPh_3)_2PdCl_2$, CuI and $N(Pr^i)_2Et$ (DIPEA) in anhydrous DMF solvent, **Scheme 1.8.** This reaction was performed using various reaction conditions as outlined in **Table 3**, but ^1H NMR analysis of the reaction product mixtures showed no evidence of product **9** and so this approach was not pursued further. This disappointing result was thought to be due to the presence of a free carboxylic acid group in **6** which may have interfered with the catalyst by 'salicylate-

type' complexation. It was then decided to protect the acid by esterification and attempt the Sonogashira coupling on this as outlined in **Scheme 1.9.** Esterification of **6** using dry HCl in refluxing methanol gave methyl ester **8** in very good yield and excellent purity (86%). This was reacted with two equivalents of pentynoic acid, **7**, in the presence of CuI, $(PPh_3)_2PdCl_2$ and DIPEA in dry DMF under N_2 for 24 h at room temperature and for 72 h at 80 °C but both attempts proved unsuccessful, as confirmed by ^{1}H NMR analysis of the reaction mixtures, **Table 3 (Entry 7).**

Scheme 1.8

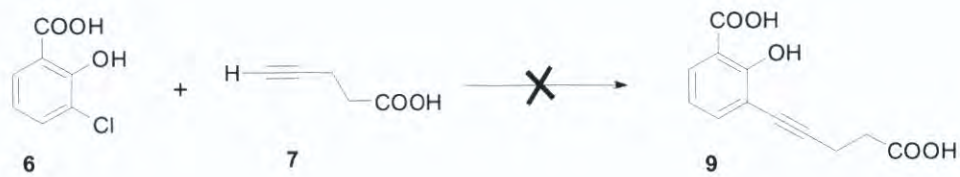

Scheme 1.9

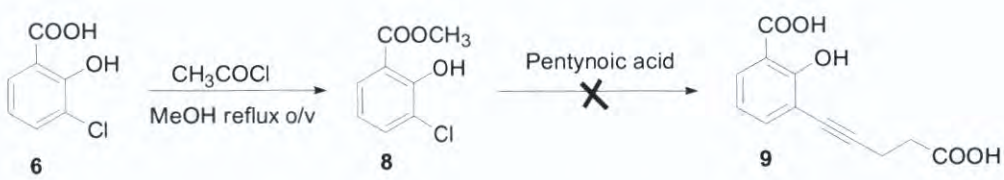

The suspected reason for the failure of **6** and **8** to undergo Sonogashira coupling was that chloro compounds may be less reactive in these reactions and may require more harsh coupling reactions. We therefore decided to use bromo instead of chloro derivatives as starting materials and attempted the synthesis of **14a**, methyl 3-bromo-2-hydroxybenzoate, by bromination of methyl salicylate, **13**, using bromine in chloroform **Scheme 1.10.** This reaction produced, not the desired compound, but its unwanted regeo-isomer, methyl 5-bromo-2-hydroxybenzoate, **14.** Nevertheless we proceeded to investigate Sonogashira coupling of this. However, as with the previous reactions, this reaction did not give the required product.

Table 3: Attempted synthesis of compound 9 using various reaction conditions

Entry	Reactant	Reactant	Conditions	Results
1	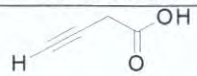 1.5 eq.	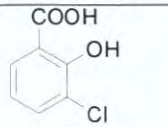 1 eq.	10 mol.% CuI, 5 mol.% $PdCl_2(PPh_3)_2$, DIPEA in excess, Dry DMF, N_2 atmosphere, 1 h @ r.t. to 2 days @ 40 °C.	Not expected compound
2	1.5 eq.	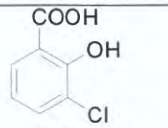 1 eq.	0.36 eq. CuI, 5 mol.% $PdCl_2(PPh_3)_2$, DIPEA in excess, Dry DMF, N_2 atmosphere, 1 h @ r.t. to 3 days @ 40 °C.	Not expected compound
3	1.5 eq.	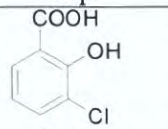 1 eq.	10 mol.% CuI, 5 mol.% $PdCl_2(PPh_3)_2$, DIPEA in excess, Dry ACN, N_2 atmosphere, 1 h @ r.t. to 3 days @ 50 °C.	Not expected compound
4	1.5 eq.	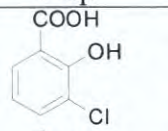 1 eq.	10 mol.% CuI, 5 mol.% $PdCl_2(PPh_3)_2$,DIPEA in excess, Dry DMF, N_2 atmosphere, 1 h @ r.t. to 4 days @ 40 °C.	Not expected compound
5	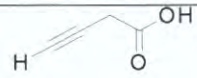 1.5 eq.	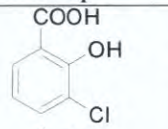 1 eq.	CuI, $PdCl_2(PPh_3)_2$ and DIPEA),Dry DMF,N_2 atmosphere,1 h @ r.t. to 2 days @ 80 °C.	Not expected compound
6	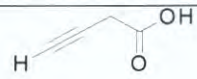 2 eq.	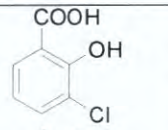 1 eq.	Excess of (CuI, $PdCl_2(PPh_3)_2$ and DIPEA),Dry DMF,N_2 atmosphere, 5 days @ r.t.	Not expected compound
7	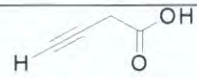 2 eq.	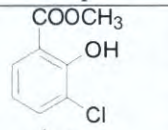 1 eq.	0.017 eq. CuI, 3 eq. DIPEA, 0.0022 eq. $PdCl_2(pph_3)_2$, dry DMF,N_2 atmosphere, 24 h @ r.t. to 3 days @ 80 °C.	Not expected compound
8	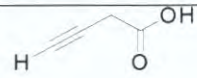 1.5 eq.	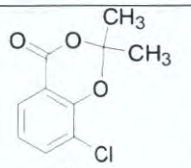 1 eq.	1 eq. CuI, 5 mol.% $PdCl_2(pph_3)_2$, DIPEA in excess, Dry DMF, N_2atmosphere, 1 h @ r.t. to 24 hrs @ 50 °C to 5 days @ 80 °C.	Not expected compound

Scheme 1.10

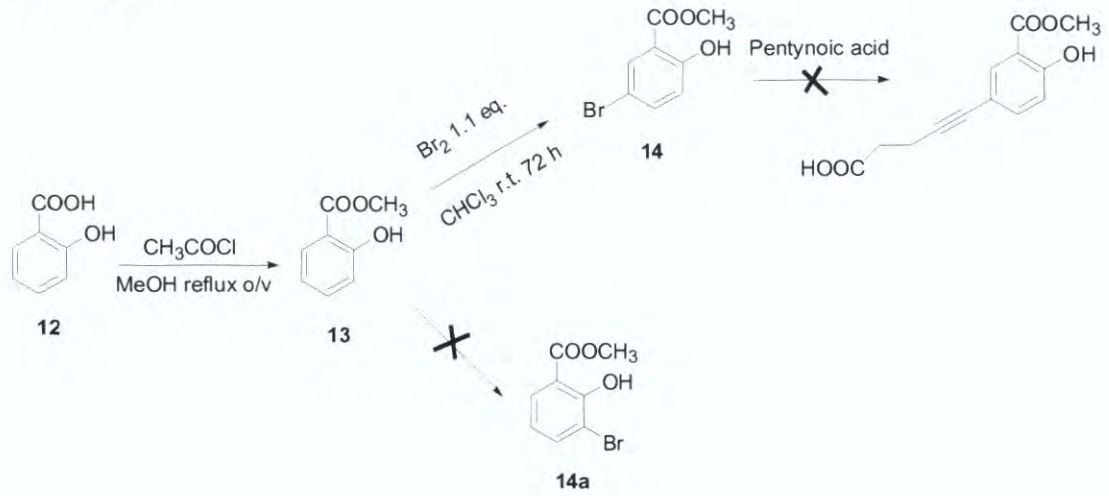

Scheme 1.11

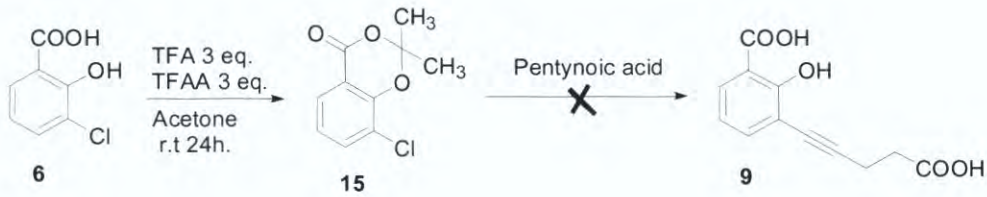

In order to avoid interference from 'salicylate-type' complexation of starting materials with the catalyst we decided to protect the salicylate by acetal formation. Hence reaction of 3-chloro-2-hydroxybenzoic acid, **6**, with acetone in the presence of trifluoroacetic acid-trifluoroacetic anhydride afforded compound **15**, in good yield, **Scheme 1.11.**[128] This intermediate when reacted with 5-pentynoic acid under Sonogashira conditions, **Table 3 (Entry 8)**, yielded several products which unfortunately could not be separated and characterized.

At this stage considering the obtained results, we decided to use an alternative approach and came to the conclusion that a Fries rearrangement was the best way to introduce an *n*-pentanoate chain at the *meta* position. A Fries rearrangement involves the conversion of phenyl esters to *o*-acylphenols in the presence of $AlCl_3$ catalyst. The reaction is catalyzed by Lewis acids such as $AlCl_3$, BF_3, $TiCl_4$ or $SnCl_4$. The Lewis acid forms a complex with the phenyl ester which dissociates to form an acylium ion. Depending on the solvent an ion pair can form and the ionic species can react with each other within

the solvent system. A hydrolysis reaction gives the final product. The reaction is *ortho, para*-selective so that the site of acylation can be regulated by the choice of temperature. Only sterically unhindered arenes are suitable substrates, since substituents will interfere with this reaction, **Scheme 1.12.**[129]

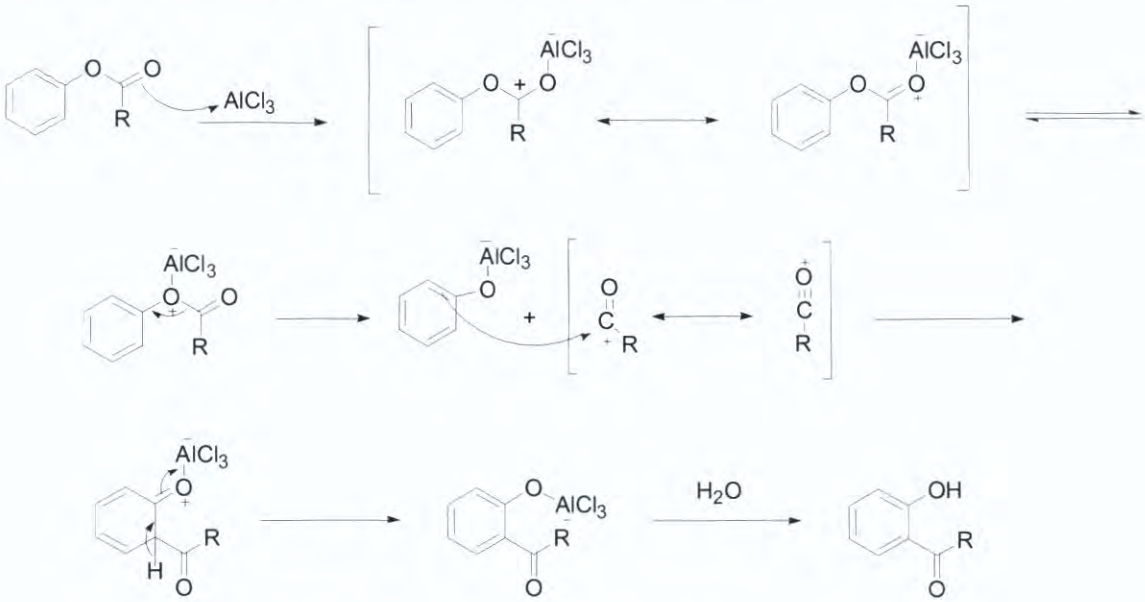

Scheme 1.12: Mechanism of the Fries Rearrangement

In order to carry out a Fries rearrangement to arrive at the desired product we first synthesised phenyl ester **17**, in quantitative yield, by acylation of **13** with 4-Chlorocarbonyl-butyric acid methyl ester, **Scheme 1.13.** A Fries rearrangement of **17** in the presence of $AlCl_3$ catalyst in tetrachloroethane gave **16** in high purity but low yield, 34%. Reaction of **13** with glutaric anhydride and $AlCl_3$ catalyst in tetrachloroethane gave **16** as a key intermediate.[130]

Scheme 1.13

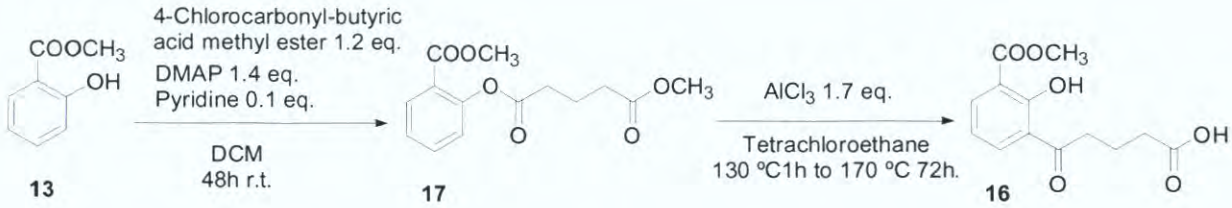

Compound **16** was also obtained in one step, albeit in slightly lower yield, 29%,[131,132] by reaction of **13** with glutaric anhydride in the presence of $AlCl_3$ in tetrachloroethane, **Scheme 1.14.** The structure of **16** was confirmed by microanalytical, HRMS, ^{1}H-NMR, ^{13}C-NMR and IR data. The product gave satisfactory C, H microanalysis and HRMS; found 267.0858 [M+H$^+$], $C_{13}H_{15}O_6$ requires 267.0869. The ^{1}H NMR spectrum of a solution of **16** in d^6-DMSO showed signals at δ 1.82 ppm (2H, quintet) corresponding to the aliphatic chain CH_2 at C(3), δ 2.30 ppm (2H, triplet) corresponding to the aliphatic chain CH_2 at C(4), δ 3.00 ppm (2H, t) corresponding to the aliphatic chain CH_2 at C(2), and δ 3.92 ppm (3H, singlet) for the methyl protons of the ester group. Three signals in the aromatic region at δ 7.09 (1H, doublet), 8.10 (1H, double of doublets) and 8.35 (1H, doublet) ppm are observed. The signal for the phenolic –OH group occurs at 11.03 (1H, singlet) ppm and for the carboxylic –OH group at 12.09 (1H, singlet). The^{13}C-NMR spectrum of **16** in d^6-DMSO showed signals at 197.8 ppm (ketone), δ174.8 (acid), 168.5 ppm (ester), 163.5-114.4 (aromatic CH groups), 37.14, 33.25, 19.64 (aliphatic –CH_2 groups) and at 53.1 ppm (ester CH_3). The IR spectrum of the product showed two υ(C=O) bands, one which is very broad at 1698 cm^{-1}and which contains overlapping ester and acid carbonyl bands and one at 1669 cm^{-1} which is due to the ketone.

Scheme 1.14

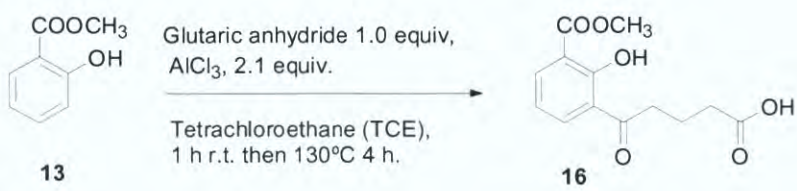

Having obtained compound **16**, it was relatively easy to synthesise our target compound

2, **Scheme 1.15.** Reduction of ketone **16** with triethylsilane / trifluoroacetic acid at room temperature,[133] afforded **10** (79% yield), base hydrolysis of which gave **11** (93% yield). Acetylation of the phenolic group in **11** with acetic anhydride and base in dry DMF afforded the target compound **2** in 60% yield.[134] The overall yield of **2** in the 5-step process from salicylic acid **12**, is 13%.

Scheme 1.15

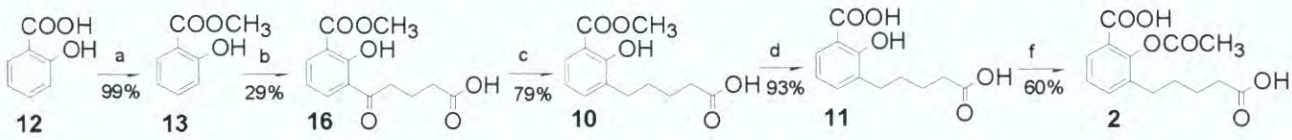

Scheme 1.15: Reagents and conditions: (a) CH_3COCl, MeOH, reflux 12 h; (b) Glutaric anhydride 1.0 equiv $AlCl_3$, 2.1 equiv tetrachloroethane (TCE), 1 h rt then 130 °C 4 h; (c) $(C_2H_5)_3SiH$ 3.0 equiv TFA, 48 h rt; (d) NaOH 4.0 equiv H_2O, reflux 2 h; (e) Ac_2O 10 equiv pyridine 100 equiv DMF dry, 3 h rt.

The structure of **2** was confirmed by microanalytical, HRMS, ^{1}H-NMR, ^{13}C-NMR and IR data. The product gave satisfactory C, H microanalysis and HRMS; found 279.0882 [M-H$^+$], $C_{14}H_{15}O_6$ requires 279.0869. The ^{1}H NMR spectrum of a solution of **2** in d^6-DMSO showed signals at δ 1.59-1.51 ppm (4H, multiplet) corresponding to the aliphatic chain CH_2 at C(3) and CH_2 at C(4), δ 2.24 ppm (5H, multiplet) corresponding to the aliphatic chain CH_2 at C(5) and the methyl group, δ 2.63 ppm (2H, triplet) corresponding to the aliphatic chain CH_2 at C(2). Three signals in the aromatic region at δ 7.12-7.07 (1H, multiplet), 7.45 (1H, double of doublets) and 7.73 (1H, doublet) ppm are observed. The signal for the carboxylic –OH group occurs at δ12.59 ppm (2H, singlet). The ^{13}C-NMR spectrum of **2** in d^6-DMSO showed signals at δ 174.4 ppm (ketone), δ169.3 ppm (acid), δ165.7 ppm (acid), δ148.2-123.5 ppm (aromatic CH groups), δ 33.9, 33.4, 30.2, and 24.0 ppm (aliphatic –CH_2 groups) and at δ 20.8 ppm (CH_3). The IR spectrum of the product showed a broad O-H stretching band at 3435 cm^{-1}, an ester υ(C=O) band at 1754 cm^{-1} and an acid υ(C=O) band at 1695 cm^{-1}.

The activity of **2** with respect to platelet aggregation was investigated by Dr Anthony Chubb, Molecular & Cellular Therapeutics Department, RCSI. Unfortunately compound **2** was found to be inactive in platelet aggregation assays at the highest

concentration tested (1000 μM). In this assay, arachidonate was used to stimulate human platelets to form aggregates, as would occur at sites of vascular injury, atherosclerotic plaque rupture and thrombosis formation. As PGHS-1 is the main form of prostaglandin H_2 synthase in anucleate platelets, it is a convenient and physiologically relevant model for PGHS-1 activity.[135]

Following this result which may have been due to suboptimal polarity in **2** or in the length of the alkycarboxylate chain it was decided to synthesize a number of other compounds. These included the more polar **3,** the less polar **5** and the shorter chain alkyl carboxylate-containing **4.** Compound **3** was obtained by hydrolysis of **16** to give **18** (95% yield) followed by acetylation (81% yield), **Scheme 1.16.**

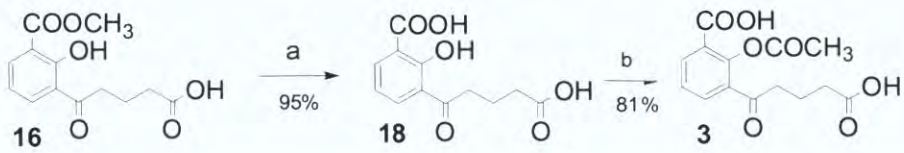

Scheme 1.16: Reagents and conditions: (a) NaOH 2.0 equiv H_2O, reflux 2 h; (b) Ac_2O 10 equiv pyridine 100 equiv DMF dry, 24 h rt.

The structure of **3** was confirmed by microanalytical, HRMS, ^{1}H-NMR, ^{13}C-NMR and IR data. The product gave satisfactory C, H microanalysis and HRMS; found 293.0674 [M-H$^+$], $C_{14}H_{13}O_7$ requires 293.0661. The ^{1}H NMR spectrum of a solution of **3** in d^6-DMSO showed signals (ppm) at δ 1.84 (2H, quintet) corresponding to the aliphatic chain CH_2 at C(3), δ 2.28 (3H, singlet) corresponding to the methyl group, δ 2.32 (2H, triplet) corresponding to the aliphatic chain CH_2 at C(4), δ 3.10 (2H, triplet) corresponding to the aliphatic chain CH_2 at C(2). Three signals in the aromatic region at δ 7.37 (1H, doublet), δ 8.17 (1H, double of doublets) and δ 8.45 (1H, doublet) are observed. The signal for the carboxylic –OH group occurs at δ12.6 (1H, singlet). The^{13}C-NMR spectrum of **3** in d^6-DMSO showed signals at δ198.5 (aliphatic acid), δ174.7 (acetyl carbonyl), δ169.4 (aromatic acid), δ165.5 (aliphatic carbonyl), δ153.9-124.9 (aromatic CH groups) δ 37.6, 33.2, 21.3 (aliphatic $-CH_2$ groups) and at δ19.5(CH_3). The IR spectrum of the product showed two υ(C=O) bands, one which is very broad at 1707 cm^{-1} due to the carboxylic acid group and one at 1783 cm^{-1} which is

due to the acetyl group. The υ(OH) stretch of the carboxylic acid group appears as a broad band at 3386 cm^{-1}.

The synthesis of target compound **4** was carried out as illustrated in **Scheme 1.17.** Reaction of **13** with maleic anhydride using two equivalents of $AlCl_3$ in tetrachloroethane gave **19** (44% yield),[131] which upon catalytic hydrogenation gave **20** (97% yield),[136] followed by hydrolysis gave **21** (90% yield) and finally acetylation gave target compound **4** (40% yield).

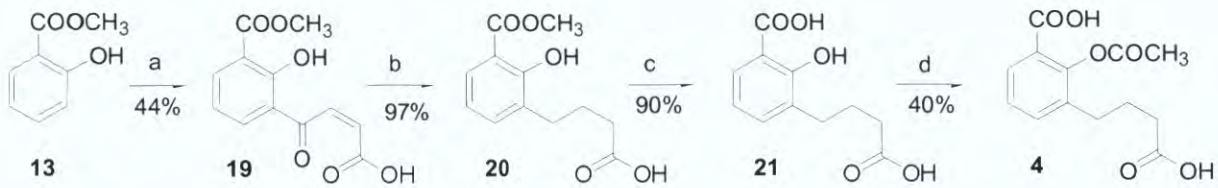

Scheme 1.17: Reagents and conditions: (a) maleic anhydride 1.0 equiv $AlCl_3$ 2.1equiv Tetrachloroethane (TCE), 1 h rt then 130 ^{0}C 2 h; (b) H_2, Pd/C 0.1 equiv MeOH, 12 h rt; (c) NaOH 2 equiv H_2O reflux 12 h; (d) Ac_2O 4 equiv pyridine 3.3 equiv DMF dry, 24 h rt

The structure of **19** was confirmed by HRMS, ^{1}H-NMR, ^{13}C-NMR and IR data. HRMS; found 249.0408 [M-H$^+$], $C_{12}H_9O_6$ requires 249.0399. The ^{1}H NMR spectrum of a solution of **19** in d^6-DMSO showed signals (ppm) at δ 3.92 (3H, singlet) corresponding to the methyl protons of the ester group. δ 6.67 (1H, doublet) corresponding to the aliphatic chain CH at C(3) and at δ 7.86 (1H, doublet) corresponding to the aliphatic chain CH at C(2). Three signals in the aromatic region at δ 7.13 (1H, doublet), δ 8.17 (1H, double of doublets) and δ 8.38 (1H, doublet) are observed. The signal for the phenolic –OH group occurs at δ 11.21 (1H, singlet) and for the carboxylic –OH group at δ 13.19 (1H, singlet). The^{13}C-NMR spectrum of **19** in d^6-DMSO showed signals at δ186.9 (ketone), δ167.6 ppm (acid), δ166.3 ppm (ester), δ 135.8, δ 132.1 (aliphatic –CH groups) ppm, δ163.6, 135.4, 132.6, 127.7, 118.2 and 114.5 (aromatic CH groups) ppm, δ 52.6 ppm (ester CH_3). IR spectrum of the product **19** showed two υ(C=O) bands, one which is sharp at 1710 cm^{-1} and due to the ester and the other broad at 1666 cm^{-1} and due to the acid.

The structure of **4** was confirmed by HRMS, ^{1}H-NMR, ^{13}C-NMR and IR data. HRMS; found 265.0720 [M-H^{+}] $C_{13}H_{13}O_6$ requires 265.0712. The ^{1}H NMR spectrum of a solution of **4** in d^{6}-DMSO showed signals at δ 1.8 ppm (2H, quintet) corresponding to the aliphatic chain CH_2 at C(3), δ 2.23 ppm (5H, singlet) corresponding corresponding to the aliphatic chain CH_2 at C(4) and to the methyl group. δ 2.64 ppm (2H, triplet) corresponding to the aliphatic chain CH_2 at C(2). Three signals in the aromatic region at δ 7.10 (1H, doublet), δ 7.46 (1H, double of doublets) and δ 7.74 (1H, singlet) ppm are observed. The signal for the carboxylic –OH group occurs at δ12.6 ppm (2H, singlet) as broad spectrum. The^{13}C-NMR spectrum of **4** in d^{6}-DMSO showed signals at δ174.7 (aliphatic chain acid), δ169.8 (Methyl ketone), δ166.2 ppm (phenolic acid). δ148.9-124.2 ppm (aromatic CH groups), δ 33.9, 33.4, 26.6 (aliphatic –CH_2 groups) ppm and at 21.3 ppm (CH_3). The IR spectrum of the product showed two υ(C=O) bands, one at 1763 cm^{-1} due to the ester C=O stretch and one at 1686 cm^{-1} due to the carboxylic acid C=O stretch. The compound was obtained in good yield (40%) and excellent purity.

Compound **5** was obtained by esterification of **2** (55% yield), **Scheme 1.18.**

Scheme 1.18.

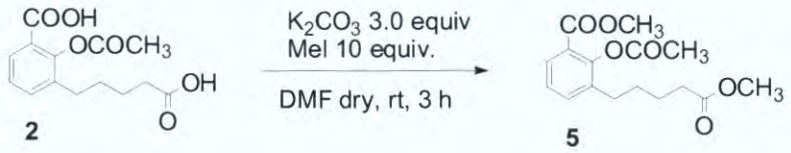

The structure of **5** was confirmed by HRMS, ^{1}H-NMR and ^{13}C-NMR data. HRMS; found 309.1341 [M+H^{+}] $C_{16}H_{21}O_6$ requires 309.1338. The ^{1}H NMR spectrum of a solution of **5** in d^{6}-DMSO showed signals (ppm) at δ 1.59-1.54 (4H, multiplet) corresponding to the aliphatic chain CH_2 at C(3) and CH_2 at C(4), δ 2.27 (3H, singlet) corresponding to the methyl group, δ 2.34 (2H, triplet) corresponding to the aliphatic chain CH_2 at C(5), δ 2.64 (2H, triplet) corresponding to the aliphatic chain CH_2 at C(2). Two signals at δ 3.58 and δ 3.80 correspond to the two ester groups while three signals in the aromatic region at δ 7.14 (1H, doublet), δ 7.50 (1H, double of doublets) and δ 7.75 (1H, doublet) are observed. The ^{13}C-NMR spectrum of **5** in d^{6}-DMSO showed

signals at δ 173.3, 169.3 and 164.5 corresponding to three ester groups, δ 148.0-122.5 (aromatic CH groups), δ 52.2, 51.2 (ester CH_3), δ 33.7, 33.0, 30.1 and 23.9 (aliphatic – CH_2 groups) and at δ 20.7 (CH_3). The compound was obtained in good yield (55%) and excellent purity.

Compounds **3**, **4** and **5** were evaluated in platelet aggregation assays by Dr Anthony Chubb, Molecular & Cellular Therapeutics Department, RCSI. Compounds **3** and **4** were found to be inactive in platelet aggregation assays at the highest concentration tested (1000 μM). The platelet aggregation assay measures the increased light transmission through platelet rich plasma (PRP), freshly isolated from healthy volunteers, in response to addition of 1.5 mM arachidonic acid as agonist. Various concentrations of each compound (0.1-1000 μM; final DMSO concentration < 0.4%) were added to stirred PRP for 5 min prior to arachidonate addition.[137]

Compound **5**, however, was found to inhibit platelet aggregation, with a 50% maximal inhibition concentration (IC_{50}) of 720 ± 85 μM which is 15-fold less potent than aspirin (47 ± 27 μM). Molecular modelling shows that **5** is capable of interacting simultaneously with Arg120 and Tyr385 by hydrogen bonding while correctly positioning the acetyl group near Ser530 for acetyl transfer to occur, **Fig. 1.17 B.** Furthermore, the binding energy of -13.3 kcal/mol is similar to that of the dicarboxylate form **2.** Importantly, **5** had no effect on platelet aggregation stimulated by 2μM of the thromboxane analogue U46619, at the highest concentration of inhibitor used (1000 μM). This implies that inhibition is not due to non-specific destruction of human cells, and that its mechanism of action is specific to the cyclooxygenase pathway, downstream of arachidonate and upstream of thromboxane. Despite the poor correlation between docking studies and data, compound **5** is sufficiently diverse from aspirin to constitute a new starting point for investigation. In particular, compound **5** contains an extra aliphatic chain and two ester groups, offering the possibility of further derivatization at each of these sites. An added benefit of this type of derivative is that it is non-acidic and would not cause topical irritation as aspirin does due to the presence in its structure of an acidic carboxylic acid group. Finally, compound **5** has been shown by us to specifically inhibit the COX pathway of platelet activation. A possible mechanism for the activity of **5** involves interaction of the ester group in the side chain

with Arg120 by hydrogen bonding. This places the acetyl group adjacent to Ser530 and facilitates its transfer. Interaction between the ester group attached to the ring and Tyr385 may also be involved in this process, **Scheme 1.19.**

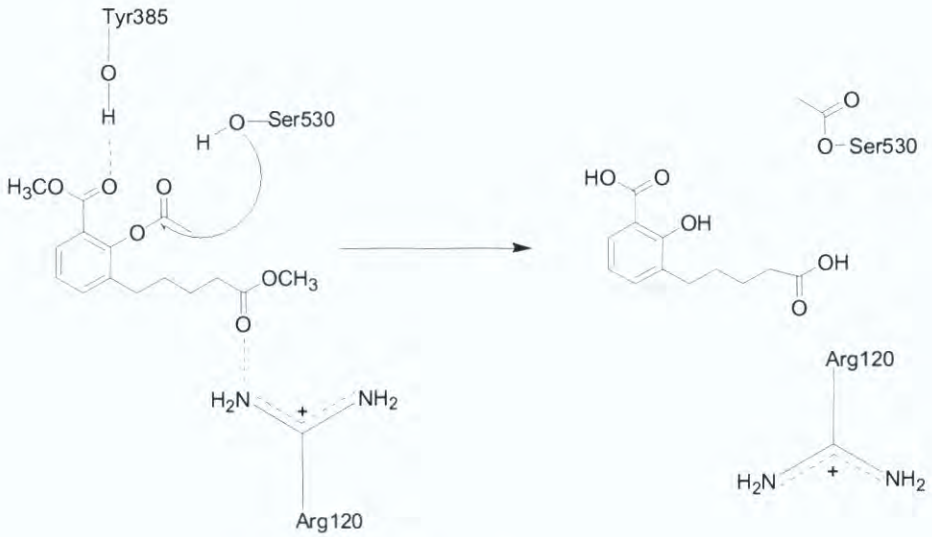

Scheme 1.19

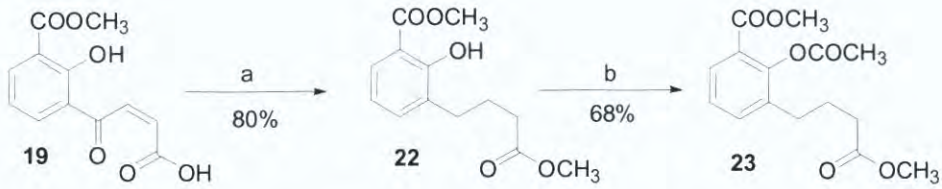

Scheme 1.20: Reagents and conditions: (a) H_2, Pd/C 0.1 equiv MeOH, 48 h, rt; (b) Ac_2O 1.2 equiv pyridine 1.2 equiv DCM dry, o/v

Compounds **22** and **23**, which are less polar than the previous compounds, were also synthesised, **Scheme 1.20.** Interestingly when the time period for the hydrogenation of **19** was extended from 12h to 24 h not only did reduction of double bond and keto group occur, as in the formation of **20**,[136] **Scheme 1.17**, but esterification of the acid group also occurred, giving **22** in 80% yield, **Scheme 1.20.** A tri-conversion similar to this has recently been reported in the literature. Acetylation of **22** gave **23** in in 68% yield, **Scheme 1.20.** The evaluation of these compounds in platelet aggregation assays will be undertaken.

The structure of **22** was confirmed by HRMS, ^{1}H-NMR and ^{13}C-NMR. HRMS; found 251.0915 [M-H^{+}] $C_{13}H_{15}O_5$ requires 251.0919. The ^{1}H NMR spectrum of a solution of **22** in $CDCl_3$ showed signals (ppm) at δ 1.94 (2H, quintet) corresponding to the aliphatic chain CH_2 at C(3), δ 2.34 (2H, triplet) corresponding to the aliphatic chain CH_2 at C(4), δ 2.6 (2H, triplet) corresponding to the aliphatic chain CH_2 at C(2), and δ 3.68 (3H, singlet) for the aliphatic chain (CH_3 ester group) and at δ 3.96 corresponding to the phenolic ester group. Three signals in the aromatic region at δ 6.92 (1H, doublet), δ 7.29 (1H, double of doublets) and δ 7.65 (1H, doublet) are observed. The signal for the phenolic –OH group occurs at δ 10.62 (1H, singlet). The^{13}C-NMR spectrum of **22** in $CDCl_3$ showed signals at δ173.9 (aliphatic ester) and δ170.5 (phenyl ring ester). δ 159.9-112.1 (aromatic CH groups), δ 34.1, 33.2 and 26.5 (aliphatic –CH_2 groups) and at δ 52.3, δ 51.6 (ester CH_3 groups). The compound was obtained in good yield (80%) and excellent purity.

The structure of **23** was confirmed by HRMS, ^{1}H-NMR and ^{13}C-NMR. HRMS; found 293.0622 [M-H^{+}] $C_{13}H_{15}O_5$ requires 293.0612. The ^{1}H NMR spectrum of a solution of **23** d^{6}-DMSO showed signals (ppm) at δ 1.9 (2H, quintet) corresponding to the aliphatic chain CH_2 at C(3), δ 2.26 (3H, singlet) corresponding to the O-C=O-C$\underline{H}_3$, δ 2.29 (2H, triplet) corresponding to the aliphatic chain CH_2 at C(4), δ 2.61 (2H, triplet) corresponding to the aliphatic chain CH_2 at C(2), δ 3.59 (3H, singlet) for the aliphatic chain (CH_3 ester group) and at δ 3.79 corresponding to the methyl protons of the phenolic ester group. Three signals in the aromatic region at δ 6.96 (1H, doublet), δ 7.31 (1H, double of doublets) and δ 7.77 (1H, doublet) are observed. The^{13}C-NMR spectrum of **23** in d^{6}-DMSO showed signals at δ173.6 (aliphatic ester) and δ169.8 (phenyl ring ester) and at δ 164.9 (acetyl carbonyl), δ 148.9-122.8 (aromatic CH groups) ppm, δ 34.2, 33.1 and 26.2 (aliphatic –CH_2 groups) and at δ 52.1, δ 51.5 and δ 20.9 (ester CH_3 groups). The compound was obtained in good yield (68%) and excellent purity.

1.10 Conclusions

We had predicted that a modification in the structure of aspirin by the introduction of an *n*-pentanoate group *meta* to the carboxylate group would lead to enhanced inhibition of the enzyme PGHS and improved therapeutic potency. An example of such a compound is **2.** Molecular modelling studies indicated that the side chain carboxylate could form a salt link with Arg120 at the active site of PGHS, while at the same time positioning the acetyl group close to Ser530, thus facilitating acetylation of this residue. The salicylate carboxylate group in this structure should also interact with Tyr385 at the active site. Although **2** was successfully synthesised it showed no activity in platelet aggregation assays. A number of other compounds were synthesised and the most active, albeit much less so than aspirin, was **5.** However the structure of **5** is sufficiently different from aspirin to make it a lead compound worthy of further investigation.

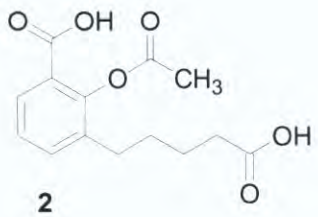

2

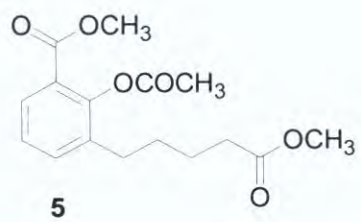

5

1.11 General Experimental Details

All reagents and solvents were used as purchased from Aldrich.

^{1}H and ^{13}C spectra were recorded on a Bruker DPX 400 spectrometer operating at 400 MHz at ambient temperatures. For ^{1}H NMR recorded in $CDCl_3$ or DMSO chemical shifts (δ_H) are quoted in parts per million (ppm) and referenced to the residual solvent peak. The following abbreviations are used: s, singlet; d, doublet; t, triplet; dd, doublet of doublet; m, multiplet; br, broad. Coupling constants (*J*) were measured in Hertz (Hz) to the nearest 0.5 Hz. Carbon spectra are supported by DEPT analysis. Infrared (IR) spectra were recorded as thin films between KCl plates. Absorption maxima (υ_{max}) are reported in wave numbers (cm^{-1}) and only selected peaks are reported. Flash chromatography was carried out using *silica gel 60* (0.040-0.063mm, 230-400mesh) as stationary phase. Thin layer chromatography was carried out on aluminium backed

plates pre-coated with *silica gel 60*, which were visualized by quenching of UV fluorescence (λ_{max} = 254 nm) or by staining with either 10% w/v ammonium molybdate in 2M sulphuric acid or basic potassium permanganate solution (followed by heat) as appropriate. Retention Factor (R_f value) are reported to ± 0.05.

1.12 Experimental - synthesis

2-Acetoxy-3-(4-carboxybutyl)benzoic acid, 2.

To a stirred solution of **11** (0.2 g, 0.84 mmol), in dry DMF (1 mL) under nitrogen at 0 °C was added acetic anhydride (0.8 mL, 8.4 mmol). The mixture was stirred for an additional 30 min then pyridine (6.8 mL, 84 mmol) was added dropwise at the same temperature. The resulting mixture was slowly warmed to room temperature and stirred for 3 h. To the reaction mixture water (10 mL) was added, followed by concentrated HCl. The mixture was then extracted with ethyl acetate (2 x 10 mL), washed with water (3 x 10 mL), dried over Na_2SO_4 , the solvent removed *in vacuo* and the residue washed twice with ether to afford **2** as a white solid (0.14 g, 0.5 mmol, 60%). ^{1}H NMR (400MHz, d^6-DMSO); δ 1.59-1.51 (4H, m), 2.23 (5H, m), 2.63 (2H, t, J = 7.2 Hz), 7.12-7.07 (1H, m), 7.45 (1H, dd, J = 8.4, J = 2.4 Hz), 7.73 (1H, d, J = 2.4 Hz), 12.59 (2H, br). ^{13}C NMR (400 MHz, d^6-DMSO); δ 20.8, 24.0, 30.2, 33.4, 33.9, 123.5, 123.6, 130.9, 133.5, 139.9, 148.2, 165.7, 169.3, 174.4. IR (KBr disc); υ_{max} 3435 br, 2919, 1754, 1695, 1434, 1304 cm^{-1}. Elemental Anal. Found: C, 60.54; H, 5.69. $C_{14}H_{16}O_6$ requires C, 59.99; H, 5.75%. HRMS found: 279.0882 [M-H$^+$] $C_{14}H_{15}O_6$ requires 279.0869. The compound was obtained in good yield (60%) and excellent purity.

2-Acetoxy-3-(4-carboxy-butyryl)-benzoic acid, 3.

To a stirred solution of **18** (0.5 g, 2 mmol), in dry DMF (3 mL) under nitrogen at 0 °C acetic anhydride was added (1.88 mL, 20 mmol) dropwise and stirred for 30 min. Dry pyridine (16 mL, 200 mmol) then added in the same way. The reaction mixture was warmed to room temperature and stirred over night. A saturated aqueous NH_4Cl solution (15 mL) was added and the resulting mixture was extracted with ethyl acetate (2 x 20 mL). The organic extract was washed with brine (30 mL) dried over Na_2SO_4 and concentrated under reduced pressure *in vacuo*. For further purification, the crude was dissolved in chloroform (5 ml), and washed with saturated sodium bicarbonate solution (2 x 10 mL), then acidified with 50% HCl, a white precipitate was obtained

after being washed with water which was dried over P_2O_5 to give **3** as a white solid (0.47 g, 1.6 mmol, 81%). R_f 0.2 (chloroform:methanol, 98:2). ^{1}H NMR (400MHz, d^6-DMSO); δ 1.84 (2H, q, J = 7.2 Hz), 2.28 (3H, s), 2.32 (2H, t, J = 7.6 Hz), 3.10 (2H, t, J = 7.2 Hz), 7.37 (1H, d, J = 8.4 Hz), 8.17 (1H, dd, J = 8.4, J = 2 Hz), 8.45 (1H, d, J = 2 Hz), 12.60 (2H, br). ^{13}C NMR (400 MHz, d^6-DMSO); δ 19.5, 21.3, 33.2, 37.6, 124.9, 125, 131.5, 133.7, 134.8, 153.9, 165.5, 169.4, 174.7, 198.5. IR (KBr disc); υ_{max} 3386-3000 br, 1783, 1707, 1600 cm^{-1}. Elemental Anal Found: C, 58.55; H, 5.31. $C_{14}H_{14}O_6$ requires C, 58.64; H, 5.30%. HRMS found: 293.0674 [M-H$^+$] $C_{14}H_{13}O_7$ requires 293.0661. The compound was obtained in good yield (81%) and excellent purity.

2-Acetoxy-3-(3-carboxy-propyl)-benzoic acid, 4.

To a stirred solution of **21** (0.5 g, 2.23 mmol) in dry DMF (5 mL) under N_2 atmosphere at 0 °C was added acetic anhydride (0.85 mL, 9 mmol) and stirred for an additional 30 min. Then pyridine was added (0.6 mL, 7.4 mmol) dropwise at the same temperature. The resulting mixture was slowly warmed to room temperature and stirred for 24 h. A saturated aqueous NH_4Cl solution (10 mL) was added and the resulting mixture was extracted with ethyl acetate (2 x 10 mL). The organic extract was washed with water (3 x 10 mL), brine and dried over Na_2SO_4. The solution was evaporated to dryness to give **4** (0.25 g, 0.9 mmol, 40%) as a pale yellow residue without purification. ^{1}H NMR (400MHz, d^6-DMSO); δ 1.80 (2H, q, J = 7.6 Hz), 2.23 (5H, s), 2.64 (2H, t, J = 7.6 Hz), 7.10 (1H, d, J = 8 Hz), 7.46 (1H, dd, J = 8.4, J = 2 Hz), 7.74 (1H, s), 12.60 (2H, br). ^{13}C NMR (400 MHz, d^6-DMSO); δ 21.3, 26.6, 33.4, 33.9, 124.2, 124.1, 131.5, 134.1, 140, 148.9, 166.2, 169.8, 174.7. IR (KBr disc); υ_{max} 3121, 1763, 1686, 1609, 1488, 1449 cm^{-1}. HRMS found: 265.0720 [M-H$^+$] $C_{13}H_{13}O_6$ requires 265.0712. The compound was obtained in good yield (40%) and excellent purity.

2-Acetoxy-3-(4-methoxycarbonyl-butyl)-benzoic acid methyl ester, 5.

To a solution of **2** (0.1 g, 0.36 mmol) in dry DMF (1 mL) under nitrogen was added dry potassium carbonate (0.15 g, 1.07 mmol) after grinding. The solution was heated at 60 °C, then allowed to cool to room temperature. Methyl iodide (0.22 mL, 3.6 mmol), was added in a dropwise fashion. The resulting mixture was stirred for over night, then poured into water (5 mL), and extracted with ethyl acetate (2 x 10 mL) DMF was

removed by washing the organic layer three times with water. The extract was dried over Na_2SO_4 and concentrated under reduced pressure. The mixture was purified by flash silica column chromatography (eluting with petroleum ether:ethyl acetate, 90:10) to give **5** as a pale brown oil (0.06 g, 0.2 mmol, 55%). R_f 0.70 (petroleum ether:ethyl acetate, 90:10). ^{1}H NMR (400MHz, d^6-DMSO); δ 1.59-1.54 (4H, m), 2.27 (3H, s), 2.34 (2H, t, J = 6.8 Hz), 2.64 (2H, t, J = 7.2 Hz), 3.58 (3H, s), 3.80 (3H, s), 7.14 (1H, d, J = 8.4 Hz), 7.50 (1H, dd, J = 8.4, J = 2.4 Hz), 7.75 (1H, d, J = 2 Hz). ^{13}C NMR (400 MHz, d^6-DMSO); δ 20.7, 23.9, 30.1, 33.0, 33.7, 51.2, 122.5, 123.8, 130.7, 134.0, 140.1, 148.0, 164.5, 169.3, 173.3. HRMS found: 309.1341 [M+H$^+$] $C_{16}H_{21}O_6$ requires 309.1338. The compound was obtained in good yield (55%) and excellent purity.

3-Chloro-2-hydroxybenzoic acid methyl ester, 8.

3-Chloro-2-hydroxybenzoic acid **6** (2 g, 11.6 mmol) was dissolved in (50 mL) methanol. Acetyl chloride (4 mL) was added dropwise to a methanolic solution at 0 °C. The resulting solution was warmed to room temperature then refluxed for over night. The solvent was removed by distillation to leave crude product. Saturated sodium bicarbonate solution (2 x 20 mL) was added then extracted with ethyl acetate (2 x 30 mL). The organic layer washed with brine (2 x 10 mL), dried over Na_2SO_4 and filtered. The solvent was removed *in vacuo* to leave **8** as yellow oil (2.2 g, 86%). ^{1}H NMR (400MHz, $CDCl_3$); δ 3.84 (3H, s), 6.71 (1H, q, J = 8 Hz), 7.41 (1H, d, J = 8 Hz), 7.63 (1H, d, J = 8 Hz), 11.22 (1H, s). ^{13}C NMR (400 MHz, $CDCl_3$); δ 52.8, 113.6, 119.3, 122.2, 128.4, 135.8, 157.3, 170.3. The compound was obtained in (86%) yield and excellent purity.[138]

3-(4-Carboxybutyl)-2-hydroxybenzoic acid methyl ester, 10.

To a stirred solution of **16** (2 g, 7.5 mmol) in trifuoroacetic acid (6 mL) under nitrogen atmosphere at 0 °C Et_3SiH was added (3.6 mL, 22.6 mmol) dropwise over 2 min. The mixture was then allowed to warm to room temperature and stirred vigorously for 48 h. TFA was removed under flow rate of nitrogen and the resulting oil was dissolved in ethyl acetate and washed twice with water. The product was then extracted with 20 mL of 10% NaOH solution. The aqueous layer was separated and acidified with 50% HCl solution and then extracted with ethyl acetate, dried over Na_2SO_4 and concentrated

under reduced pressure. The residue was purified by flash silica column chromatography (eluting with chloroform to chloroform:methanol, 98:2) to give 1.5 g (79%) of **10** as a white soild. R_f 0.52 (chloroform:methanol, 98:2). ^{1}H NMR (400MHz, d^6-DMSO); δ 1.53-1.48 (4H, m), 2.22 (2H, t, J = 6.8 Hz), 2.53 (2H, t, J = 6.8 Hz), 3.87 (3H, s), 6.90 (1H, d, J = 8.4 Hz), 7.36 (1H, dd, J = 8.4, J = 2 Hz), 7.58 (1H, d, J = 2 Hz), 10.36 (1H, s), 12.04 (1H, s). ^{13}C NMR (400 MHz, d^6-DMSO); δ 24.0, 30.4, 33.4, 33.6, 52.4, 112.4, 117.3, 129, 132.9, 135.8, 158.2, 169.3, 174.4. IR (KBr disc); υ_{max} 3400-2900 br, 1706, 1665, 1608, 1587, 1481 cm^{-1}. HRMS found: 251.0921 [M-H$^+$] $C_{13}H_{15}O_5$ requires 251.0919. The compound was obtained in good yield (79%) and excellent purity.

3-(4-Carboxy-butyl)-2-hydroxy-benzoic acid, 11.

An aqueous solution (5 mL) of sodium hydroxide (0.16 g, 4 mmol) was added to **10** (0.25 g, 0.99 mmol). The resulting solution was refluxed for 2 h. TLC indicated the disappearance of the starting material, the mixture was cooled in ice bath and acidified with concentrated hydrochloric acid; the solid was filtered off and dried over P_2O_5 gave the acid, **11** as white solid (0.22 g, 0.92 mmol, 93%). ^{1}H NMR (400MHz, d^6-DMSO); δ 1.54-1.48 (4H, m), 2.23 (2H, t, J = 6.8 Hz), 2.53 (2H, t, J = 6.8 Hz), 6.87 (1H, d, J = 8.4 Hz), 7.35 (1H, dd, J = 8.4, J = 2.4 Hz), 7.59 (1H, d, J = 2.4 Hz), 11.11 (1H, br). ^{13}C NMR (400 MHz, d^6-DMSO); δ 24.0, 30.4, 33.4, 33.6, 112.4, 116.9, 129.3, 132.6, 135.8, 159.3, 171.9, 174.4. IR (KBr disc); υ_{max} 3183, 1680, 1594, 1485 cm^{-1}. HRMS found: 237.0763 [M-H$^+$] $C_{12}H_{13}O_5$ requires 237.0763. The compound was obtained in high yield (92%) and excellent purity.

2-Hydroxybenzoic acid methyl ester, 13.

Salicylic acid **12** (10 g, 72 mmol) was dissolved in methanol (100 mL). Acetyl chloride (10 mL) was added drop wise to a methanolic solution at 0 °C. The resulting solution was stirred for 1 h at the same temperature then refluxed for 24 h. The solvent was removed by distillation to leave crude product. Water (50 mL) was added and extracted with ethylacetate (2 x 50 mL).The extract was washed with saturated sodium bicarbonate solution (2 x 40 mL), dried over Na_2SO_4 and filtered. The solvent was removed *in vacuo* to give **13** in quantitative yield as yellow oil. ^{1}H NMR (400 MHz,

$CDCl_3$); δ 3.76 (3H, s), 6.70 (1H, t, J = 7.6 Hz), 6.82 (1H, d, J = 8.4 Hz), 7.30-7.25 (1H, m), 7.65 (1H, dd, J = 8, J = 1.2 Hz), 10.63 (1H, s). ^{13}C NMR (400 MHz, $CDCl_3$); δ 170.6, 161.6, 135.7, 129.9, 119.1, 117.5, 112.4, 52.2. IR (KBr disc); υ_{max} 3187, 2951, 1680, 1609, 1581, 1482, 1444 cm^{-1}. The compound was obtained in quatitative yield and excellent purity.[138]

5-Bromo-2-hydroxybenzoic acid methyl ester, 14.

To a stirred solution of **13** (5 g, 32.9 mmol) in chloroform (50 mL) was added bromine (1.86 mL, 36.2 mmol). The mixture was stirred at room temperature for 72 h. At the beginning the mixture turned black red then yellow at the end of the reaction. The solvent was concentrated and washed with saturated sodium bicarbonate solution (2 x 20 mL), then extracted with chloroform (2 x 30 mL), the organic layer was washed with brine (2 x 15ml), dried over Na_2SO_4 and concentrated under reduced pressure to give **14** (5.5 g, 23.8 mmol, 72%) as a white solid precipitate. ^1H NMR (400MHz, $CDCl_3$); δ 3.96 (3H, s), 6.88 (1H, d, J = 9 Hz), 7.53 (1H, dd, J = 9, J = 2.5 Hz), 7.94 (1H, d, J = 2.4 Hz), 10.71 (1H, s). ^{13}C NMR (400 MHz, $CDCl_3$); δ 52.2, 110.3, 113.3, 119.1, 131.7, 137.9, 160.1,169.0. IR(KBr disc); υ_{max} 3199, 1687, 1606, 1574, 1465, 1427cm^{-1}. The compound was obtained in good yield (72%) and excellent purity.

8-Chloro-2, 2-dimethylbenzo[1,3]dioxin-4-one, 15.

To an ice cold solution of **6** (0.5 g, 2.9 mmol) in trifluoroacetic acid (4 mL, 8.7 mmol) were added trifluoroacetic anhydride (2.5 mL, 8.7 mmol) and acetone (5 mL). The mixture was warmed slowly to room temperature and then stirred for 24 h. The slightly yellow mixture was then concentrated on the rotary evaporator, poured into a saturated solution of aqueous $NaHCO_3$, and extracted with ethyl acetate (2 x 20 mL), washed with water and brine, dried over Na_2SO_4, and concentrated to leave black solid which is purified by flash silica column chromatography (eluting with ethyl acetate:petroleum ether, 2:3) to give **15** in quantitative yield as black solid. ^1H NMR (400MHz, $CDCl_3$); δ 1.81 (6H, s), 7.09 (1H, t, J = 8 Hz), 7.63 (1H, d, J = 7.32 Hz), 7.9 (1H, d, J = 8 Hz). ^{13}C NMR (400 MHz, $CDCl_3$); δ 25.4, 106.7, 114.6, 121.9, 122.3, 127.6, 136.0, 151.6, 159.8. IR (KBr disc); υ_{max} 3454, 2989, 1732, 1550, 1477, 1445 cm^{-1}. The compound was obtained in quantitative yield and excellent purity.

3-(4-Carboxybutyryl)-2-hydroxybenzoic acid methyl ester, 16.

To a mixture of **13** (0.5 g, 3.3 mmol), glutaric anhydride (0.375 g, 3.3 mmol), and tetrachloroethane (2.6 mL), aluminum chloride (0.92 g, 6.9 mmol) was added in portions with stirring during 1 h under dry conditions using a tube of $CaCl_2$. The mixture was then gradually heated on an oil bath to 130 °C, and maintained at this temperature for 4 h. The reaction mixture color changed into red. It was cooled and poured into ice (10 g), and concentrated hydrochloric acid was then added to obtain pH 2-3. The organic layer was separated and the aqueous phase was extracted with ethyl acetate (2 x 15 mL), the combined organic phase was washed with water (20 mL), and extracted with saturated sodium carbonate solution (2 x 25 mL), after being washed with diethyl ether (2 x 25 mL), the aqueous layer was acidified to pH 2 with concentrated hydrochloric acid and extracted with ethyl acetate, the solvent was removed *in vacuo* yielding a black viscous solid, which was purified by passing through a silica gel column (elution with chloroform:methanol, 99:1) to give **16** (0.25 g, 29%) as yellow solid powder. R_f 0.2 (chloroform:methanol, 99:1). ^{1}H NMR (400MHz, d^6-DMSO); δ 1.82 (2H, q, J = 7.2 Hz), 2.30 (2H, t, J = 7.2 Hz), 3.0 (2H, t, J = 7.2 Hz), 3.91 (3H, s), 7.09 (1H, d, J = 8.8 Hz), 8.10 (1H, dd, J = 8.8, J = 2 Hz), 8.35 (1H, d, J = 2,4 Hz), 11.03 (1H, s), 12.09 (1H, s). ^{13}C NMR (400 MHz, d^6-DMSO); δ 197.8, 174.8, 168.5, 163.5, 135.1, 131.3, 128.7, 118.2, 114.4, 53.1, 37.1, 33.3, 19.6. IR (KBr disc); υ_{max} 3160 br, 2951, 1697, 1669, 1603, 1587, 1439, 1449 cm^{-1}. Elemental Anal Found: C, 58.55; H, 5.31. $C_{13}H_{14}O_6$ requires C, 58.64 ; H, 5.30%. HRMS found: 267.0858 [M+H$^+$] $C_{13}H_{15}O_6$ requires 267.0869. The compound was obtained in low yield (29%) and excellent purity

Pentanedioic acid 2-methoxycarbonyl-phenyl ester methyl ester, 17.

To a solution of **13** (4 g, 26 mmol) in DCM (20 mL) were added 4-Chlorocarbonyl-butyric acid methyl ester (4.4 mL, 32 mmol), dimethylaminopyridine (4.6 g, 38 mmol) and pyridine as catalytic amounts (0.25 mL, 3.2 mmol). The resulting solution was stirred at room temperature for 48 h. Water (20 mL) was added and the mixture was extracted with DCM (2 x 30 mL), the extract washed with brine (2 x 15 mL), dried over Na_2SO_4 and concentrated *in vacuo* to give yellow liquid which was purified by flash silica column chromatography (eluting with petroleum ether:ethyl acetate, 8:2) to give

17 (5.6 g, 20 mmol, 77%) as a pale yellow oil. R_f 0.7 using (petroleum ether:ethyl acetate, 8:2). ^{1}H NMR (400MHz, $CDCl_3$); δ 2.06 (2H, q, J = 7.6 Hz), 2.46 (2H, t, J = 7.2 Hz), 2.68 (2H, t, J = 7.2 Hz), 3.64 (3H, s), 3.8 (3H, s), 7.06 (1H, d, J = 8 Hz), 7.28-7.24 (1H, m), 7.53-7.49 (1H, m), 7.96 (1H, d, J = 1.2 Hz). ^{13}C NMR (400 MHz, $CDCl_3$); δ 19.7, 32.8, 33.1, 51.6, 52.1, 123.1, 123.8, 126.0, 131.7, 133.9, 150.6, 164.8, 171.6, 173.4. IR (KBr disc); υ_{max} 2952, 1768, 1725, 1606, 1487, 1449 cm^{-1}. The compound was obtained in good yield (77%) and excellent purity.

3-(4-Carboxy-butyryl)-2-hydroxy-benzoic acid, 18.

A solution of **16** (0.5 g, 1.88 mmol), was added to an aqueous solution (5 mL) of sodium hydroxide (0.15 g, 3.76 mmol), the resulting solution was refluxed for 2 h. The mixture was cooled in ice bath and acidified with concentrated hydrochloric acid; the solid was filtered off and gave **18** as yellow solid (0.47 g, 1.87 mmol, 95%). ^{1}H NMR (400MHz, d^6-DMSO); δ 1.8 (2H, q, J = 7.2 Hz), 2.34 (2H, t, J = 7.2 Hz), 3.10 (2H, t, J = 7.2 Hz), 7.10 (1H, d, J = 8.8 Hz), 8.14 (1H, dd, J = 8.8, J = 2.4 Hz), 8.42 (1H, d, J = 2,4 Hz), 12.20 (2H, br). ^{13}C NMR (400 MHz, d^6-DMSO); δ 197.3, 174.3, 171.3, 164.5, 134.9, 130,9, 128.2, 117,5, 113,1, 36.6, 32.8, 19.2. IR (KBr disc); υ_{max} 3200, 1722, 1673, 1607, 1586, 1413 cm^{-1}. HRMS found: 251.0565 [M-H$^+$] $C_{12}H_{11}O_6$ requires 251.0556. The compound was obtained in high yield (95%) and excellent purity

3-(3-Carboxy-acryloyl)-2-hydroxy-benzoic acid methyl ester, 19.

To a mixture of **13** (3 g, 20 mmol), maleic anhydride (1 g, 20 mmol), and tetrachloroethane (10 mL), aluminum chloride (5.5 g, 42 mmol) was added in portions with stirring during 1 h under dry conditions using a tube of $CaCl_2$. The mixture was then gradually heated on an oil bath to 130 °C, maintained at this temperature for 2 h. TLC indicated the disappearance of the starting material, the mixture was cooled, and poured into ice (10 g) and concentrated hydrochloric acid was then added to obtain pH 2-3. The organic layer was separated and the aqueous phase was extracted with chloroform (2 x 30 mL), the combined organic phase was washed with water (20 mL), and extracted with saturated sodium carbonate solution (2 x 25 mL), after being washed with diethyl ether (2 x 25 mL), the aqueous layer was acidified to pH 2 with concentrated hydrochloric acid and extracted with ethyl acetate, the solvent was

removed *in vacuo* yielding a yellow solid which was purified with a silica gel column (eluting with petroleum ether:ethyl acetate, 1:1) to give **19** as yellow solid (2.2 g, 8.8 mmol, 44%). R_f 0.5 (eluting with ethyl acetate only). IR (KBr disc) υ_{max} 3184, 1710, 1666, 1585, 1493 cm^{-1}. ^1H NMR (400MHz, d^6-DMSO); δ 3.92 (3H, s), 6.67 (1H, d, J = 15.2 Hz), 7.13 (1H, d, J = 8.8 Hz), 7.86 (1H, d, J = 15.6 Hz), 8.17 (1H, dd, J = 8.8, J = 2.4 Hz), 8.38 (1H, d, J = 2 Hz), 11.21 (1H, s), 13.19 (1H, s). ^{13}C NMR (400 MHz, d^6-DMSO); δ 52.6, 114.5, 118.2, 127.7, 132.1, 132.6, 135.4, 135.8, 163.6, 166.3, 167.6, 186.9. HRMS found: 249.0408 [M-H$^+$] $C_{12}H_9O_6$ requires 249.0399 $C_{12}H_{10}O_6$. The compound was obtained in good yield (44%) and excellent purity.

3-(3-Carboxy-propyl)-2-hydroxy-benzoic acid methyl ester, 20.

To a solution of **19** (1 g, 4 mmol) in methanol (20 mL) was added 10% Pd/C (400 mg) in methanol (10 mL). The resulting suspension was hydrogenated at atmospheric pressure for 12 h. Filtration through Celite and concentration left **20** as a yellow semi solid (0.92 g, 3.9 mmol, 97%). ^1H NMR (400MHz, d^6-DMSO); δ 1.75 (2H, q, J = 7.2 Hz), 2.20 (2H, t, J = 7.2 Hz), 2.53 (2H, t, J = 7.2 Hz), 3.89 (3H, s), 6.92 (1H, d, J = 8.4 Hz), 7.35 (1H, dd, J = 8.8, J = 2.4 Hz), 7.58 (1H, d, J = 2 Hz), 10.39 (1H, s), 12.15 (1H, s). ^{13}C NMR (400 MHz, d^6-DMSO); δ 26.3, 32.9, 33.2, 52.4, 112.5, 117.4, 129.1, 132.4, 135.8, 158.3, 169.3, 174.2. IR (KBr disc); υ_{max} 3116 br, 2940, 1697, 1664, 1614, 1598, 1493 cm^1. HRMS found: 237.0760 [M-H$^+$] $C_{12}H_{13}O_5$ requires 237.0763. The compound was obtained in high yield (97%) and excellent purity

3-(3-Carboxy-propyl)-2-hydroxy-benzoic acid, 21.

To a solution of **20** (1.2 g, 5 mmol) in water (5 mL) was added an aqueous solution (5 mL) of sodium hydroxide (0.4 g, 10 mmol). The resulting solution was refluxed for over night. TLC indicated the disappearance of the starting material, the mixture was cooled in ice bath and acidified with concentrated hydrochloric acid; the solid was filtered off and gave **21** as a white solid (1 g, 4.5 mmol, 90%). ^1H NMR (400MHz, d^6-DMSO); δ 1.81 (2H, q, J = 7.6 Hz), 2.25 (2H, t, J = 7.6 Hz), 2.58 (2H, q, J = 7.6 Hz), 6.93 (1H, d, J = 8.4 Hz), 7.40 (1H, dd, J = 8.4, J = 2 Hz), 7.65 (1H, d, J = 2.4 Hz), 11.50 (1H, br). ^{13}C NMR (400 MHz, d^6-DMSO); δ 26.3, 32.8, 33.2, 112.4, 117.0, 129.4, 132.1, 135.8, 159.3, 171.9, 174.3. IR (KBr disc); υ_{max} 3200-2956 br, 1697,

1658, 1614, 1587, 1493 cm^{-1}. HRMS found: 223.0601 [M-H$^+$] $C_{11}H_{11}O_5$ requires 223.0606. The compound was obtained in high yield (90%) and excellent purity

2-Hydroxy-3-(3-methoxycarbonyl-propyl)-benzoic acid methyl ester, 22.

Compound **19** (1 g, 4 mmol) was dissolved in methnol (20 mL) and hydrogenated at room temperature under atmospheric pressure over 10% Pd/C (0.5 g) in methanol (10 mL) for 48 h. TLC indicated the disappearance of the starting material. Filtration through Celite and it was washed with methanol, which was then removed under reduced pressure to give **22** (0.8 g, 3.2 mmol, 80%) as a yellow oil. ^{1}H NMR (400MHz, $CDCl_3$); δ 1.94 (2H, q, J = 7.6 Hz), 2.34 (2H, t, J = 7.6 Hz), 2.60 (2H, t, J = 7.2 Hz), 3.68 (3H, s), 3.96 (3H, s), 6.92 (1H, d, J = 8.8 Hz), 7.29 (1H, dd, J = 8.4 and 2.4 Hz), 7.65 (1H, d, J = 2.4 Hz), 10.62 (1H, s). ^{13}C NMR (400 MHz, $CDCl_3$); δ 26.5, 33.2, 34.1, 51.6, 52.3, 112.1, 117.6, 129.2, 132.0, 136.1, 159.9, 170.5, 173.9. HRMS found: 251.0915 [M-H$^+$] $C_{13}H_{15}O_5$ requires 251.0919. The compound was obtained in good yield (80%) and excellent purity.

2-Acetoxy-3-(3-methoxycarbonyl-propyl)-benzoic acid methyl ester, 23.

To a solution of **22** (0.5 g, 2 mmol) in DCM (5 mL) was added acetic anhydride (0.23 mL, 2.4 mmol) at 0°C and the resulting mixture was stirred for an additional 30 min, then pyridine (0.2 mL, 2.4 mmol) was added in dropwise at the same temperature. The mixture was slowly warmed to room temperature and stirred over night. DCM was evaporated and the residue was dissolved in ethyl acetate (10 mL). The organic layer was washed with water (2 X 10 mL), brine and dried over Na_2SO_4, the solvent was removed *in vacuo* and the residue purified with a silica gel column (eluting with petroleum ether:ethyl acetate, 6:4) to give **23** (0.4 g, 1.4 mmol, 68%) as a light brown oil. R_f 0.6 using (petroleum ether:ethyl acetate, 6:4). ^{1}H NMR (400MHz, d^6-DMSO); δ 1.90 (2H, q, J = 7.6 Hz), 2.26 (3H, s), 2.29 (2H, t, J = 7.6 Hz), 2.61 (2H, t, J = 7.2 Hz), 3.59 (3H, s), 3.79 (3H, s), 6.96 (1H, d, J = 8.4 Hz), 7.31 (1H, dd, J = 8.4 and 2.4 Hz), 7.77 (1H, d, J = 2.4 Hz). ^{13}C NMR (400 MHz, DMSO); δ 20.9, 26.2, 33.1, 34.2, 51.5, 52.1, 122.8, 123.7, 131.5, 133.9, 139.3, 148.9, 164.9, 169.8, 173.6. HRMS found: 293.0622 [M-H$^+$] $C_{13}H_{15}O_5$ requires 293.0612. The compound was obtained in good yield (68%) and excellent purity.

1.13 References

1. S. Willoughby, A. Holmes, J. Loscalzo, *Eur J. Cardio. Nurs.*, 2002, **1**, 273-288.

2. S. P. Jackson, N. Mistry, Y. Yuan, *Trends Cardiovasc. Med.,* 2000, **10** (5), 192-197.

3. A. S. Weyrich, S. Lindemann, G. A. Zimmerman, *J. Thromb. Haemost,* 2003, **1**, 1897-1905.

4. P. Harrison, *Blood Rev.* 2005, **19**, 111–123

5. Y. Huo, K. F. Ley, *Tresnds. Cardiovasc. Med.,* 2004, **14**, 18-22.

6 D. L. Bhatt, E. J. Topol, *J. Nat. Rev. Drug Discov.*, 2003, **2**, 15-28.

7. H. D. Shah, R. K. Goyal, *Indian J. Pharmacol.*, 2004, **36**, 133-139.

8. A. J. Lusis, *Nature*, 2000, **407**, 233-241.

9. S. Willoughby, L. Chirkova, Y. Chirkov, J. Horowitz. *Platelets*, 1996, **7**, 329-333.

10. M. Nishikawa, P. de Lanerolle, T. M. Lincoln and R. S. Adelstein, *J. Biol. Chem.*, 1984, **259**, 13, 8429-8436.

11. E. J. Topoll, P. W. Serruys, *Circulation*, 1998, **98**, 1802-1820.

12. M. W. H. Behan, R. F. Storey, *Postgrad Med J.*, 2004, **80**, 155-164.

13. S. P. Jackson and S. M. Schoenwaelder, *Nat. Rev. Drug Discov.*, 2003, **2**, 1-15.

14. A. J. Marcus, 1994. *Multicellular eicosanoid and other metabolic interactions of platelets and other cells.* Third Edition, R. W. Colman, J. Hirsh, V. J. Marder, E. W. Salzmann, editors. JB Lippincott, Philadelphia, 590-602.

15. J. M. Dogne, X. de Leval, J. Delarge, J. L. David, B. Masereel, *Curr. Med. Chem.*, 2000, **7**, 609-628.

16. W. L. Smith, *Biochem J.*, 1989, **259** (2), 315-324.

17. J. M. Dogne, X. de Leval, J. Hanson, M. Frederick, B. Lambermont, A. Ghuysen, A. Casini, B. Maserreel, K. Ruan, B. Pirotte, P. Kolh, *Curr. Med. Chem.*, 2004, **11**, 1223-1241.

18. J. B. Smith, A. L. Wills, *Nature New Biol.*, 1971, **231**, 235-237.

19. Z. M. Ruggeri, *J. Clin. Invest*, 1997, **99**, 559-564.

20. J. E. Sadler, *Thromb. Haemost*, 2000, **84**, 160-174.

21. A. J. Marcus, *Semin. Hematol*, 1994, **31**, 261-269.

22. J. A. Lopez, R. K. Andrews, V. Afshar, M. C. Berndt., *Blood*, 1998, **91**, 4397-4418.

23. M. H. Kroll, A. I. Schafer, *Blood*, 1989, **74** (4), 1181-1195.

24. Z. M. Ruggeri, *Nature Med.*, 2002, **8**, 1227-1234.

25. G. J. Hankey, J. W. Eikelboom, *Medical Journal of Australia*, 2003, **178**, 568-574.

26. E. H. Awtry, J. Loscalzo, *Circulation*, 2000, **101**, 1206-1218.

27. Antithrombotic Trialists' Collaboration, *Brit. Med. J.,* 2002, **324**, 71-86.

28. C. Patrono, G. Ciabattoni, P. Patrignani, F. Pugliese, P. Fillabozi, F. Catella, G. Davi, L. Forni, *Circulation.*, 1985, **72**, 1177-1184.

29. M. J. Quinn, D. J. Fitzgerald, *Circulation*, *1999*, **100**, 1667-1672.

30. S. Noble, K. L. Goa, *Drugs & Aging.*, 1996, **8**, 214-32.

31. CAPRIE Steering Committee, *Lancet*. 1996, **348**, 1329-39.

32. J. Hanson, S. Rolin, D. Reynaud, N. Qiao, L. P. Kelley, H. M. Reid, F. Valentin, J. Tippins, B. T. Kinsella, B. Masereel, C. Pace-Asciak, C. B. Pirotte, J. M. Dogne, *J. Pharmacol. Ex. Ther.*, 2005, **313**, 293-301.

33. R. A. Coleman, P. P. Humphrey, I. Kennedy, G. P. Levy, P. Lumley, *Brit. J. Pharmacol.*, 1981, **73**, 773-778.

34. V. Euler, U. S., *Arch. Exptl. Pathol. Pharmakol.*, 1934, **175**, 78-84.

35. L. J. Marnett, S. W. Rowlinson, D. C. Goodwin, A. S. Kalgutkar, C. A. Lanzo, *J. Biol. Chem.*, 1999, **274** (33), 22903-22906.

36. M. Hamberg, B. Samuelsson, *J. Biol. Chem.*, 1967, **242**, 5336–5343.

37. G. A. FitzGerald, C. Patrono, *N. Engl. J. Med.*, 2001, **345**, 433–442.

38. W. L. Smith, R. M. Garavito, D. L. DeWitt, *J. Biol. Chem.*, 1996, **271**, 33157–33160.

39. W. L. Smith, D. L. DeWitt, R. M. Garavito, *Annu. Rev. Biochem*, 2000, **69**, 145-182.

40. J. R. Vane, *Nature-New Biology*, 1971, **231**, 232-235.

41. S. C. C.Tam, D. H. S. Lee, E. Y. Wang, D. G. Munroe, C. Y. Lau, *J. Biol. Chem.*, 1995, **270**, 13948-13955.

42. L. Smith, P. Borgeat, F.A. Fitzpatrick. In: D.E. Vance, J. Vance, Editors, Biochemistry of Lipids Lipoproteins and Membranes, Elsevier, New York (1991), 297–325.

43. W. L. Smith, L. J. Marnett, D. L. DeWitt, *Pharmacol Ther.*, 1991, **49**, 153-179.

44. R. J. A. Helliwell, L. F. Adams, M. D. Mitchell, *Prostaglandins Leukot. Essent. Fatty Acids*, 2004, **70**, 101-113.

45. K. Watanabe, R. Yoshida, T. Shimizu, O. Hayaishi, *J. Biol. Chem.*, 1985, **260**, 7035-7041.

46. D. L. DeWitt, W. L. Smith, *J. Biol. Chem.*, 1983, **258**, 3285-3293.

47. J. M. Woods, A. Mogollon, M. A. Amin, R. J. Martinez, A. E. Koch, *Exp Mol Pathol.*, 2003, **74**, 282-290.

48. T. Murata, F. Ushikubi, T. Matsuoka, M. Hirata, A.Yamasaki,Y. Sugimoto, A. Ichikawa, Y. Aze, T. Tanaka, N. Yoshida, A. Ueno, S. Oh-ishi , S. Narumiya, *Nature*,1997, **388**, 678-682.

49. Goodman and Gilman's, *the Pharmacological Basis of Therapeutics*. McGraw-Hill, 1996.

50. G. R. Bernard, K. L. Brigham, *Chest.*, 1986, **89**, 594-600 http://www.chestjournal.org/content/89/4/594

51. S. M. Grant, K. L. Goa, *Drugs.*, 1992, **43**, 889-924.

52. Y. Boie, T. H. Rushmore, A. Darmon-Goodwin, R. Grygorczyk, D. M. Slipetz, K. M. Metters, M. Abramovitz, *J. Biol. Chem.*, 1994, **269**, 12173-12178.

53. R. C. Harris, J. A. McKanna, Y. Akai, H. R. Jacobson, R. N. Dubois, M. D. Breyer, *J. Clin. Invest*, 1994, **94**, 2504–2510.

54. T. Kobayashi, Y. Tahara, M. Matsumoto, M. Iguchi, H. Sano, T. Murayama, H. Arai, H. Oida, T. Yuruig-Kobaysahi, J. K. Yamashita, H. Katagiri, M. Majima, M. Yokode, T. Kita, S. Narumiya, *J. Clin. Invest*, 2004, **114**, 784-794.

55. S. Narumiya, Y. Sugimoto, F. Ushikubi, *Physiol. Rev.*, 1999, **79**, 1193-1226.

56. R. M. Garavito, D. L. DeWitt, *Biochim Biophys Acta*., 1999, **1441**, 278-287.

57. D. Picot, P. J. Loll, R. M. Garavito, *Nature*, 1994, **367**, 243-249.

58. C. Luong, A. Miller, J. Barnett, J. Chow, C. Ramesha, M. Browner, *Nat Struct Biol*., 1996, **3**, 927–933.

59. D. L. DeWitt, W. L. Smit, *Methods in Enzymology*, 1990, **187**, 469-479.

60. D. L. DeWitt, W. L. Smith, *Proc. Natl. Acad. Sci*. U.S.A., 1988, **85**, 1412–1416.

61. J. C. Otto, D. L. DeWitt, W.L. Smith, *J. Biol. Chem.,* 1993, **268**, 18234-18242.

62. D. Picot, R. M. Garavito, *FEBS Lett*, 1994, **346**, 21-25.

63. P. J. Loll, D. Picot, R. Garavito, *Biochemistry*, 1996, **35**, 7330-7340.

64. R. M. Garavito, M. G. Malkowski, D. L. DeWitt, *Prostaglandins Other Lipid Mediat*, 2002, **68-69**, 129-152.

65. P. J. Loll, D. Picot, R. M. Garavito, *Nat. Struct. Biol*., 1995, **2**, 637-643.

66. D. L. Simmons, R. M. Botting, T. Hla, *Pharmacol. Rev*., 2004, **56**, 387-437.

67. M. G. Malkowski, S. L. Ginell, W. L. Smith, R. M. Garavito, *Science*., 2000, **289**, 1933-1937.

68. E. D. Thuresson, K. M. Lakkides, C. J. Rieke, Y. Sun, B. A. Wingerd, R. Micielli, A. M. Mulichak, M. G. Malkowski, M. Garavito, W. L. Smith, *J. Biol. Chem*., 2001, **276**, 10347-10359.

69. W. Y. L. Wong, J. S. Richards, 1991, *Mol. Endocrinol.,* **5**, 1269–1279.

70. M. K. O'Banion, H. B. Sadowski, V. Winn, D. A. Young, *J. Biol. Chem*., 1991, **266**, 23261–23267.

71. J. P. Merlie, D. Fagan, J. Mudd, P. Needleman, *J. Biol. Chem*., 1988, **263**, 3550-3553.

72. D. L. Simmons, R. M. Botting, P. M. Robertson, M. L. Madsen, J. R. Vane, *Proc. Natl. Acad. Sci.* USA., 1999, **96**, 3275–3280.

73. N. V. Chandrasekharan, H. Dai, K. L. Roos, N. K. Evanson, J. Tomsik, T. S. Elton, D. L. Simmons, *Proc. Natl. Acad. Sci. USA*., 2002, **99**, 13926-13931.

74. I. Morita, *Prostaglandins & Other Lipid Mediators*, 2002, **68-69**, 165-175.

75. I. Kudo, M. Murakami, *Prostaglandins & Other Lipid Mediat*, 2002, **68-69**, 3-58.

76. D. C. Zeldin, *J. Biol. Chem.*, 2001, **276**, 36059-36062.

77. G. Xiao, A. L. Tsai, G. Palmer, W. C. Boyar, P. J. Marshall, R. J. Kulmacz, *Biochemistry*, 1997, **36**, 1836-45.

78. W. L. Smith, W. E. M. Lands, *Biochemistry*, 1972, **11**, 3276–3285.

79. R. J. Kulmacz, W. A. Van der Donk, A. L. Tsai, *Prog. in Lipid Res.* 2003, **42**, 377-404.

80. L. M. Landino, B. C. Crews, J. K. Gierse, S. D. Hauser, L. J. Marnett, *J. Biol.* Chem., 1997, **272**, 21565-21574.

81. W. L. Smith, T. E. Eling, R. J. Kulmacz, L. J. Marnett, A. Tsai, *Biochemistry*, 1992, **31**, 3–7.

82. V. Koshkin, H. B. Dunford, *Biochim. Biophys Acta.*, 1999, **1430**, 341-348.

83. J. Zeng, R. E. Fenna, *J Mol. Biol.*, 1992, **226**, 185-207.

84. R. J. Kulmacz, *Prostaglandins.*, 1987, **34**, 225–40.

85. G. Lu, A. L. Tsai, H. E. Van Wart, R. J. Kulmacz, *J. Biol.* Chem., 1999, **274**, 16162-16167.

86. C. M. Markey, A. Alward, P. E. Weller, L. J. Marnett, *J. Biol. Chem.*, 1987, **262**, 6266-6279.

87. P. Ple, L. J. Marnett, *J. Biol. Chem.*, 1989, **264**, 13983-13993.

88. R. J. Kulmacz, R. B. Pendleton, W. E. Lands, *J. Biol. Chem.*, 1994, **269**, 5527–5536.

89. V. B. O'Donnell, B. Coles, M. J. Lewis, B. C. Crews, L. J. Marnett, B. A. Freeman, *J. Biol. Chem.*, 2000, **275**, 38239-38244.

90. M. B. Mattammal, R. Strong, V. M. Lakshmi, H. D. Chung, A. H. Stephenson, *J. Neurochem.*, 1995, **64**, 1645-1654.

91. A. M. Lambeir, C. M. Markey, H. B. Dunford, L. J. Marnett, *J. Biol. Chem.*, 1985, **260**, 14894–14896.

92. M. Bakovic, H. B. Dunford, *J. Biol. Chem.*, 1996, **271**, 2048-2056.

93. W-L. Lu, Q. Zhang, L. Zheng, H. Wang, R-Y. Li, L-F. Zhang, W-B Shen, X-D. Tu, *Biol. Pharm. Bull.*, **27**, 1515-1520, 2004.

94. D. L. DeWitt, *Mol. Pharmacol.*, 1999, **55**, 625–31.

95. O. Y. So, L. E. Scarafia, A. Y. Mak, O. H. Callan, D. C. Swinney, *J. Biol. Chem.*, 1998, **273**, 5801-5807.

96. R. J. Kurumbail, A. M. Stevens, J. K. Gierse, J. J. McDonald, R. A. Stegeman, J. Y. Pak, D. Gildehaus, J. M. Miyashiro, T. D. Penning, K. Seibert, P. C. Isakson, W. C. Stallings, (LONDON) *Nature*, 1996, **384**, 644-648.

97. G. P. Hochgesang, S. W. Rowlinson, L. J. J. Marnett, *J. Am. Chem. Soc.*, 2000, **122**, 6514-6515.

98. V. Colotta, F. Capelli, O. Lenzi, D. Catarzi, F. Varano, D. Poli, F. Vincenzi, K. Varani, P. A. Borea, D. Dal Ben, R. Volpini, G. Cristalli, G. Filacchioni, *Bioorg. Med. Chem.*, 2009, **17**, 401-410.

99. S. W. Rowlinson, J. R. Kiefer, J. Prusakiewicz, J. L. Pawlitz, K. R. Kozak, A. S. Kalgutkar, W. C. Stallings, R. G. Kurumbail, L. J. Marnett, *J. Biol. Chem.*, 2003, **278**, 45763-45769.

100. E. Wong, C. Bayly, H. L. Waterman, D. Riendeau, J. A. Mancini, *J. Biol. Chem.*, 1997, **272**, 9280–86.

101. F. Halter, A. S. Tarnawski, A. Schmassmann, B. M. Peskar, *Gut*, 2001, **49** (3), 443- 453.

102. M. D. Breyer, Y. Zhang, Y. Guan, C. Hao, R. L. Hebert, R. M. Breyer, *Kidney Internat.*, 1998, **54**, S88-S94.

103. P. K. Ramdial, D. K. Naidoo, *J. Clin. Path..*, 2009, **62**, 493-504.

104. L. M. Lichtenberger, *Biochem. Pharmaco*l., 2001, **61**, 631-637.

105. D. Bjorkman, *The American Journal of Medicine*, 1998, **105**, 17S-21S.

106. J. L. Wallace, P. R. Devchand, *Br. J. Pharmacol.*, 2005, **145**, 275-282.

107. R. Garcia-Nieto, C. Perez, A. Checa, F. Gago, *Rheumatology.*, 1999, **38**, 14-18.

108. G. Dannhardt, W. Kiefer, *J. Med. Chem.*, 2001, **36**,109-126.

109. C-C. Chan, S. Boyce, C. Brideau, S. Charleson, W. Cromlish, D. Ethier, J. Evans, A. W. Ford-Hutchinson, *et al.*, *J. Pharmacol. Exp. Ther.*, 1999, **290**, 551-560.

110. T. D. Penning, J. J. Talley, S. R. Bertenshaw, J. S. Carter, P. W. Collins, S. Docter, Y. Y. Zhang, P. C. Isakson, *J. Med. Chem.*, 1997, **40**, 1347-1365.

111. D. Riendeau, M. D. Percival, C. Brideau, S. Charleson, D. Dubé, D. Ethier, J.-P. Falgueyret, R. W. Friesen, R. Gordon, G. Greig, J. Guay, J. Mancini, M. Ouellet, E. Wong, L. Xu, S. Boyce, *J. Pharmacol. Exp. Ther.*, 2001, **296**, 2, 558-566.

112. A. S. Kalgutkar, S. W. Rowlinson, B. C. Crews, L. Marnett, J. *Bioorg. Med. Chem. Lett.*, 2002, **12**, 521-524.

113. A. Palomer, J. Pascual, M. Cabre, L. Borras, G. Gonzalez, M. Aparici, A. Carabaza, F. Cabre, M. L. Garcia, D. Mauleon, *Bio. Med.Chem. Letts.*, 2002, **12**, 533-537.

114. A. S. Kalgutkar, B. C. Crews, S. W. Rowlinson, A. B. Marnett, K. R. Kozak, R. P. Remmel, L. J. Marnett, *PNAS.*, 2000, **97**, 925-930.

115. F. MacRae, L. MacKenzie, K. McColl, D. Williams, *Pharmaceut. J.*, 2004, **272**, 187-189.

116. K. Seibert, Y. Z. Zhang, K. Leahy, S. Hauser, J. Masferrer, W. Perkins, L. Lee, P. Isakson, *Proc. Natl. Acad. Sci., USA* 1994, **91**, 12013-12017.

117. J. C. Bonner, A. B. Rice, J. L. Ingram, C. R. Moomaw, A. Nyska, A. Bradbury, A. R. Sessoms, P. C. Chulada, D. L. Morgan, D. C. Zeldin, R. Langenbach, *Am J Pathol.*, 2002, **161**, 459-470.

118. A. M. Simon, M. B. Manigrasso, J. P. O'Connor, *J Bone Miner. Res.*, 2002, **17**, 963–976.

119. T. Saito, I. W. Rodger, F. Hu, H. Shennib, A. Giaid, *Biochemical and Biophysical Research Communications.*, 2000, **273**, 772–775.

120. *Numbering*. The traditional ovine COX-1 numbering system is used in this report.

121. J. A. Mancini, D. Riendeau, J. P. Falgueyret, P. J. Vickers, G. P. O'Neill, *J Biol Chem.,* 1995, **270**, 29372-29377.

122. A. Alagha, E. Moman, M. F. A. Adamo, K. B. Nolan, A. J. Chubb, *Bioorg. & Med. Chem. Letts.*, 2009, **19** (15), 4213-4216.

123. Docking MOE-Dock 2008.10 function was used for docking. Ligand placement was performed using alpha sphere triangle matching, with London dG scoring. The top 30 hits were retained and refined using MMFF94x forcefield energy minimization with Generalized Born solvation model, allowing the receptor residues within 6 Å to relax around the mobile ligand. The receptor sidechains were tethered with a force constant of 1.0 kcal/(mol.Å^2). Energy minimization was stopped when the root-mean-squared gradient cutoff of 0.01 kcal/(mol.Å) was reached. Final poses were ranked using the London dG method to calculate the free energy of binding.

124. V. Colotta, F. Capelli, O. Lenzi, D. Catarzi, F. Varano, D. Poli, F. Vincenzi, K. Varani, P. A. Borea, D. DalBen, R. Volpini, G. Cristalli, G. Filacchioni, *Bioorg*

Med Chem., 2009, **17**, 401.

125. *Structure*. The ovine crystal structure 1DIY was used as there are no crystal structures of human PGHS-1.

126. K. Abderrahim, Z. Raymond, *J. Org. Chem.*, 2000, **65**, 3126-3134.

127. J. Clayden, N. Greeves, S. Warren, P. Wothers. Organic Chemistry, Oxford University Press (2001)

128. J. Rheinheimer, U. J. Vogelbacher, E. Bauman, H. König, M. Gerber, K-O Westphalen, H. Walter, U. S. *Patent* 5569640, Oct. 29, 1996.

129. http://www.organic-chemistry.org/namedreactions/fries-rearrangement.shtm

130. Vogel's Text book of Practical Organic Chemistry, 5th edition, Prentice Hall, 1996, p 976.

131. P. R. Vijayasarathy, R. B. Mane, G. S. Krishna Rao, *J. Chem. Soc., Perkin Trans.* 1977, **1**, 34-36.

132. B. Tomita, Y. Hirose, T. Nakatsuka, M. Gakkaishi, *Chem. Abstr*, 1969, **71**, 50250t.

133. A. V. Vorogushin, W. D. Wulff, H-J. Hansen, *J. Am. Chem. Soc.*, 2002, **124**, 6512-6513.

134. A. Yousef, P. Keykavous, *J. Org. Chem.*, 2005, **70** (33), 1100-1103.

135. G. V. Born, *Nature*, 1962, **194**, 927.

136. A. Mori, Y. Miyakawa, E. Ohashi, T. Haga, T. Maegawa, H. Sajiki, *Organic Letts.*, 2006, **8** (15), 3279-3281.

137. C. M. Dooley, M. Devocelle, B. McLoughlin, K. B. Nolan, D. J. Fitzgerald, C. T. Sharkey, *Mol. Pharmacol.*, 2003, **63**, 450-455.

138. K. R. West, R. Fred Ludlow, P. T. Corbett, P. Besenius, F. M. Mansfeld, P. A. G. Cormack, D. C. Sherrington, J. M. Goodman, M. C. A. Stuart, S. Otto, *Am. Chem. Soc.*, 2008, **130** (33),10834–10835.

Chapter 2

Acetylated Hydroxamic Acids as Prostaglandin-H-Synthase Inhibitors: Mode of Action Explained using Crystallography and *ex vivo* Studies

2.1 Chapter Overview 77

2.2 Aspirin 78

2.2.1 Biological Activity 78

2.2.2 Pharmacology and Pharmacokinetics 79

2.2.3 Side effects of aspirin 80

2.2.4 Inhibition of PGHS by aspirin, N-acetoxy-2-hydroxybenzamide (SalAc), 2, and N-acetoxy-N-acetyl-2-acetoxybenzamide ($SalAc_3$), 4 80

2.2.5 Towards 'Super Aspirin' 83

2.3 Acetylated pyridoxine (vitamin B6) derivatives as PGHS inhibitors 86

2.4 Experimental – synthesis 87

2.4.1 Salicylhydroxamic acid, 1. 87

2.4.2 N-acetoxy-2-hydroxybenzamide (SalAc), 2, and N-acetoxy-2-acetoxybenzamide ($SalAc_2$), 3. 87

2.4.3 N-acetoxy-N-acetyl-2-acetoxybenzamide ($SalAc_3$), 4. 89

2.4.4 Acetic acid 4-acetoxymethyl-5-hydroxy-6-methyl-pyridin-3-ylmethyl ester, 9. 89

2.4.5 Acetic acid 3-acetoxy-5-acetoxymethyl-2-methyl-pyridin-4-ylmethyl ester, 10. 90

2.5 Instrumentation 90

2.5.1 Infrared spectroscopy 90

2.5.2 ^{1}H, ^{13}C NMR spectroscopy 90

2.5.3 Single X-ray diffraction measurements 91

2.5.4 Mass spectroscopy 91

2.5.5 Elemental analysis 91

2.6 Results and Discussion 91

2.6.1 Salicylhydroxamic acid, 1. 91

2.6.2 N-acetoxy-2-hydroxybenzamide (SalAc), 2, and N-acetoxy-2-acetoxybenzamide ($SalAc_2$), 3. 92

2.6.3 N-acetoxy-N-acetyl-2-acetoxybenzamide ($SalAc_3$), 4. 97

2.6.4 Platelet aggregation studies 97

2.6.5 Acetic acid 4-acetoxymethyl-5-hydroxy-6-methyl-pyridin-3-ylmethyl ester, 9. 99

2.6.6 Acetic acid 3-acetoxy-5-acetoxymethyl-2-methyl-pyridin-4-ylmethyl ester, 10. 100

2.7 Conclusions 101

2.8 References 102

2.1 Chapter Overview

This chapter describes the synthesis of acetylated hydroxamic acids as inhibitors of prostaglandin-H-synthase (PGHS), also called cyclooxygenase (COX), the target for aspirin. Aspirin is not only an analgesic and anti-pyretic but also an anti-thrombotic agent which blocks the production of thromboxane A_2, which causes activation and aggregation of platelets, an early step in thrombosis. An introduction to platelets, thrombosis, prostaglandins and PGHS was given in chapter 1.

Previous work in our laboratory led to the synthesis or identification of acetylated salicylhydroxamate, **1**, derivatives that act as effective inhibitors of the COX site of PGHS. The first of these, N-acetoxy-2-hydroxybenzamide (SalAc, **2**), has less potency than aspirin, while N-acetoxy-2-acetoxybenzamide ($SalAc_2$, **3**), is the proposed reactive acetylating agent in the action of N-acetoxy-N-acetyl-2-acetoxybenzamide ($SalAc_3$, **4**) which is a 7-fold more potent inhibitor than aspirin. Based on site-directed mutagenesis studies, an X-ray structure of an enzyme-inhibitor complex and structure activity relationships a mechanism of action for SalAc, **2** similar to that of aspirin was proposed.[1] A mechanism for $SalAc_3$, **4** activity involving initial N-deacetylation followed by transfer of an acetyl group from the diacetylated metabolite $SalAc_2$, **3** to Ser530 was also suggested. We have synthesised $SalAc_2$, **3,** and studied its PGHS-inhibitory activity and compared this with the activity of **2** and **4**. This work and the crystal structures of $SalAc_2$, **3** and SalAc, **2,** are described in this chapter.

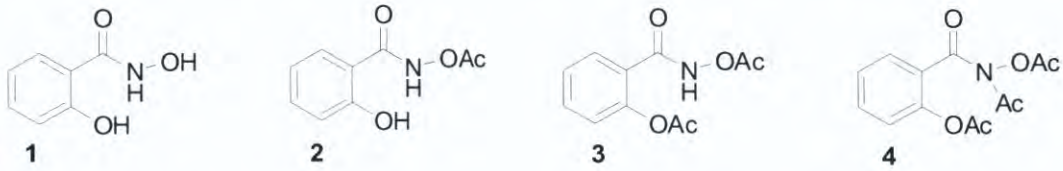

Fig. 1: Structures of salicylhydroxamic acid, **1** and PGHS inhibitor **2, 3** and **4**

As part of our research on acetylated derivatives as PGHS inhibitors we decided to acetylate vitamin B6 and to study its activity. This was based on a result obtained by Dr Anthony Chubb, Molecular & Cellular Therapeutics Department, RCSI, who showed using Autodock 4, that acetylation of vitamin B6 improves enzyme binding by

~3kcal/mol, with an improvement in inhibition of 140-fold. Although the compounds were synthesised they were inactive.

2.2 Aspirin

2.2.1 Biological Activity

Aspirin (acetylsalicylic acid) is the most widely used drug in the world. The history of aspirin goes back many thousands of years. It has been known since 400 BC that fevers can be lowered by chewing the bark of willow trees. The active agent in willow bark was found in 1827 to be salicin which in 1874 was used to reduce pain, fever and inflammation.[2] Salicin is further metabolised to salicylate, which could be converted by reaction with water into salicyl alcohol and then oxidized to salicylic acid. In 1859, salicylic acid was synthesised in Germany by Kolbe and consider more effective than salicin for reducing fevers and was also found to have analgesic and an anti-inflammatory properties.[3,4] Unfortunately, salicylic acid was too corrosive to the walls of the stomach. In 1895, Felix Hoffman a chemist from Bayer synthesised acetylsalicylic acid, which is less bitter than salicylic acid and was commercially marketed in tablet form in 1899 after successful clinical trials. The pharmacologist, Heinrich Dreser gave this the name 'Aspirin'; the "a" referring to the acetyl group and the "spirin" from the botanical name *Spiraea,* from which salicylates are extracted.[5,6]

Fig. 2: Structures of salicin, salicyl alcohol, salicylic acid and aspirin. Reproduced from R. Glaser, *J. Org. Chem.*, 2001, **66**, 771-779.

In 1971 Vane discovered that aspirin worked by inhibiting prostaglandin biosynthesis.[7] Smith, Willis *et al.* reported that aspirin could decrease PG production from aggregating platelets.[8] Aspirin has been reported to treat cardiovascular disorders,[9] cancer [10] and Alzheimer's disease.[11] It was reported that the incidence of cardiovascular disease was reduced by about 20% on aspirin administration. Low dose-aspirin (75

mg/day) has also been shown to reduce the risk of myocardial infarction, stroke or death in patients with asymptomatic ischemia.[12]

The anti-thrombotic effect of aspirin is because of inhibition of PGHS by irreversible acetylation of Ser530 (PGHS-1) or Ser516 (PGHS-2) at the active site,[13] and is ~170-fold more potent in inhibiting PGHS-1 than PGHS-2.[14] PGHS-1 is completely inactivated in the presence of aspirin whereas, PGHS-2 converts arachidonic acid not to PGH_2, but to 15-*R*-HETE.[15] The end result is that neither isoform converts arachidonic acid to PGH_2, a necessary step in the production of prostaglandins.

Inhibition of TxA_2 dependent aggregation and the prolongation of bleeding time, accounts for the anti-platelet effects of aspirin. Besides TxA_2 inhibition, aspirin also facilitates the inhibition of platelet activation by neutrophils, which is mediated by a nitric oxide NO/cGMP dependent process.[16] Aspirin may help in decreasing the progression of atherosclerosis by protecting LDL from oxidative modification,[17] and improves endothelial dysfunction in atherosclerotic vessels.[18] Aspirin can also act as an anti-oxidant by scavenging hydroxyl radicals to form 2,3- and 2,5- dihydroxybenzoate derivatives.[19,20]

2.2.2 Pharmacology and Pharmacokinetics

Aspirin is rapidly absorbed from the gastrointestinal (GI) tract and is effective within 60 minutes.[21] The plasma half life of aspirin is only 20 minutes.[22] Aspirin is hydrolyzed to salicylic acid, further metabolism of which gives glycine conjugates and glucuronides, and takes place mostly in the liver and their elimination occurs through renal excretion. Therapeutic benefit in a variety of cardiovascular disease situations has been reported with doses of 30-1500 (mg/day). However, the higher doses are associated with GI side effects.[21] The effect of daily doses is cumulative, although > 24 hours may be required to achieve maximal COX inhibition. Single doses below 100 mg result in a dose-dependent inhibition of thromboxane A_2 production, whereas a single dose of 100 mg almost completely inhibits the biosynthesis of thromboxane A_2.[23] Maintenance of the antiplatelet effects requires a dose as low as 40 mg daily.

Side effects of aspirin

Both the therapeutic and side effects of aspirin depend on the interaction with PGHS. The inhibition of prostaglandin synthesis is responsible for the anti-inflammatory effects of aspirin but also results in the loss of cytoprotective effect of PGE_2 on the gastric mucosa. Minor GI symptoms such as nausea, vomiting, heartburn, and indigestion have been reported in long term aspirin treatment and the major symptoms include peptic ulcers and GI bleeding. An overview of randomized experiments of aspirin therapy found that GI toxicity (minor and major) appears to be dose related, with daily doses between 30 and 1300 mg, [9, 24] however, even low doses of aspirin (50-75 mg/day) can cause GI bleeding.[25] Several clinical trials for aspirin have suggested an increased risk of stroke in patients receiving aspirin treatment for acute myocardial infarction. Aspirin is a relatively weak inhibitor of renal prostaglandin synthesis and at low to moderate doses does not affect renal function or blood pressure control.[26] However, at high doses (1500 mg/day), aspirin has the ability to reduce renal sodium excretion in patients with heart failure.[27] Aspirin at doses < 100 mg/day has little effect on ACE inhibitors whereas, higher doses of aspirin may attenuate the benefit of ACE inhibitors in patients with hypertension or heart failure.[28]

2.2.3 Inhibition of PGHS by aspirin, N-acetoxy-2-hydroxybenzamide (SalAc), 2, and N-acetoxy-N-acetyl-2-acetoxybenzamide ($SalAc_3$), 4.

The crystal structure of PGHS-1 inactivated by 2-bromoacetoxybenzoic acid (bromoaspirin), was solved in 1995 by Loll and co workers.[13] Aspirin inhibits PGHS by acetylating Ser530 in the COX site near Tyr385, the residue responsible for forming a radical species and abstracting the 13-pro-S hydrogen from arachidonic acid during catalysis. The bromoacetyl group introduced by bromoaspirin extends outward into the channel below Tyr385, sterically preventing any substrate e.g arachidonic acid from interacting with Tyr385. Aspirin is thought to behave similarly. Once aspirin has acetylated the Ser530 residue it generates salicylic acid as leaving group. The carboxylic acid of salicylic acid is well positioned to interact with the guanidinium group of Arg120 with which it forms a salt bridge and approaches to within hydrogen–bonding distance of the hydroxyl group of Tyr355. The aromatic ring of aspirin binds in approximately the same position of the cyclooxygenase channel. It is thought that

aspirin initially binds weakly at this site and then diffuses 5 Å upward along the channel in order to be in a position for Ser530 to attack the acetyl carbon and effect transacetylation. The whole channel is lined by hydrophobic amino acid side chains with the exception of Arg120 and its salt bridge pair Glu524 suggesting that the concentration of water in the channel is very low, further reducing the chance of hydrolysis, explaining the stability of acetylated PGHS toward hydrolysis.[29]

Previous work in our laboratory involved attempted synthesis of the hydroxamic acid analogue of aspirin from salicylhydroxamic acid.[1] This caused acetylation of the hydroxamate rather than the phenolic group leading to N-acetoxy-2-hydroxy-benzamide (SalAc), **2.** This was found to be less active than aspirin as a PGHS inhibitor. Ser530 Ala and Arg120 Glu mutagenesis resulted in loss of inhibition and a crystal structure of the enzyme inhibitor complex confirmed acetylation of Ser530 by this new inhibitor, **Fig. 3.** It is clear that **2** acts in the same way as aspirin, forming a salt linkage with Arg120 and transferring its acetyl group to Ser530. It was also shown that the pK_a of **2** is 5.27 (25°C) confirming that it is negatively charged at physiological pH.

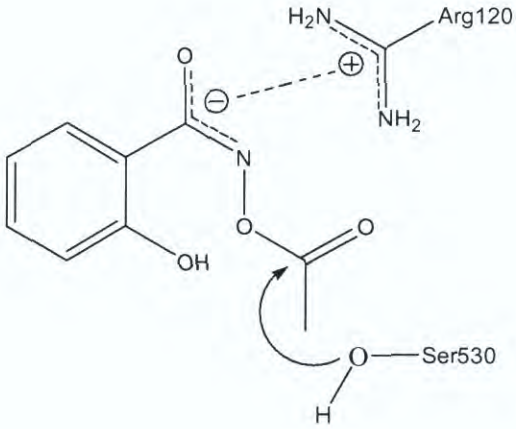

(a)

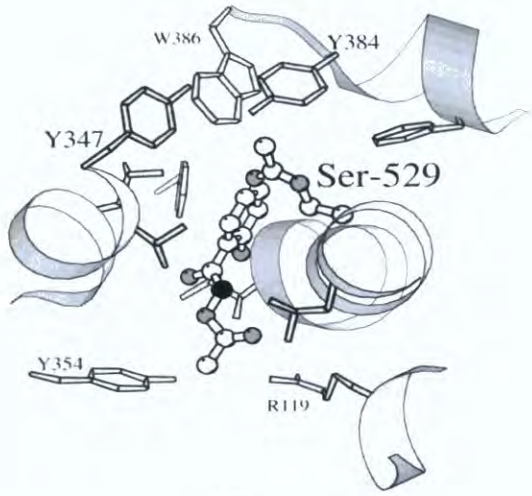

(b)

Fig. 3: PGHS-1 Ser530 is acetylated by N-acetoxy-2-hydroxybenzamide (SalAc, 2). (a) Proposed mechanism of AcSHA for acetylation of Ser530. (b) Crystal structure of *ovine* PGHS-1 treated with AcSHA showing Ser530 residue acetylated and an intact molecule of the inhibitor in the COX active site. Reproduced from C. J. Marmion, D. Griffith, K. B. Nolan, *Eur. J. Inorg. Chem.*, 2004, **15**, 3003-3016.

Following this study fully acetylated salicylhydroxamic acid i.e. N-acetoxy-N-acetyl-2-acetoxybenzamide ($SalAc_3$), **4**, was synthesised. This was found to be a much more effective PGHS inhibitor than aspirin and mutagenesis studies similar to the above as well as a study of related compounds, **5-7**, which proved to be inactive, established that the N-acetyl and 2-acetoxy group were essential for activity, **Fig. 4**. This suggested a mechanism for inhibition shown in **Fig. 5.** This mechanism involves N-deacetylation giving N-acetoxy-2-acetoxybenzamide ($SalAc_2$), **3**, as active acetylating agent which transfers the phenolic acetyl group to the enzyme.[30]

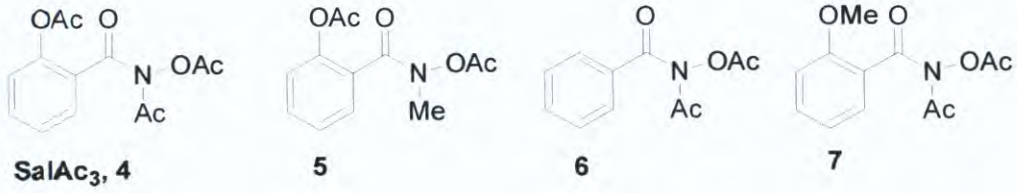

Fig. 4: Structures of PGHS inhibitor **4** and inactive **5, 6** and **7.** Reproduced from C. M. Dooley, M. Devocelle, B. McLoughlin, K. B. Nolan, D. J. Fitzgerald, C. T. Sharkey, *Mol. Pharmacol.*, 2003, **63**, 450-455.

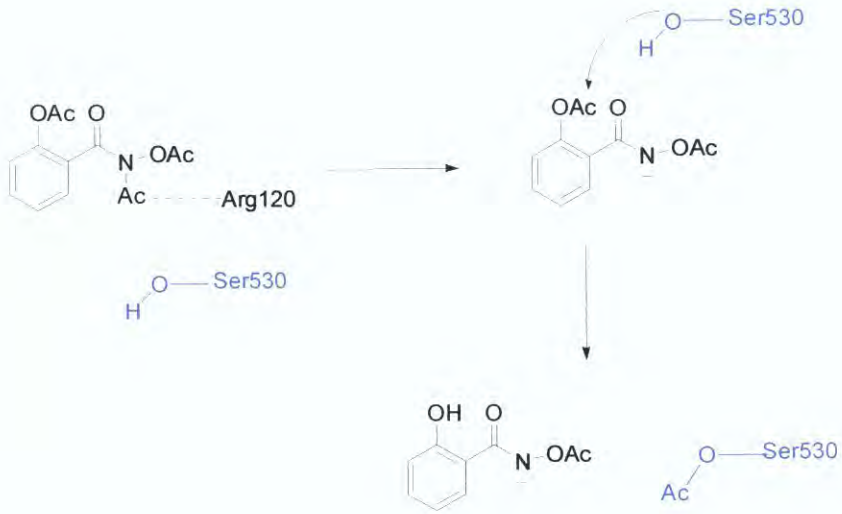

Fig. 5: Mechanism for inhibition of PGHS by ($SalAc_3$), **4**

2.2.5 Towards 'Super Aspirin'

Aspirin irreversibly inhibits PGHS by acetylating a serine residue in the active site. Two isoforms of PGHS exist, PGHS-1 which is responsible for physiological protection and PGHS-2, which causes pathological responses. The side effects of aspirin and other NSAIDs are because of inhibition of PGHS-1. Therefore, selective inhibitors of PGHS-2 should maintain the therapeutic effects without causing side effects. The development of selective PGHS-2 inhibitors was based on the presence of the smaller Val at position 523 in PGHS-2 compared to Ile in PGHS-1. Several PGHS-2 selective inhibitors have been developed such as celecoxib and nimesulide. Although initial results with these selective COX-2 inhibitors were promising, fatalities due to cardiovascular effects soon became widespread and some of these such as Vioxx were withdrawn.[31]

Another approach has been to develop dual COX and POX site inhibitors. The hydroxamic acid Tepoxalin is such an inhibitor. The rationale for the synthesis of hydroxamic acid analogues of aspirin is that (i) the hydroxamic acid group is less acidic than the carboxylic acid group and causes less topical irritation, (ii) acetylated hydroxamic acids like aspirin, inhibits the COX site by acetylation of Ser530, (iii) they should also inhibit the POX site since hydroxamic acids are known to inhibit

peroxidises, (iv) hydroxamic acids are potential NO donors.[32] The development of NO-releasing compounds is advantageous because NO reduces gastric acid secretion, increases cytoprotection, has anti-thrombotic activity and protects the gastric mucosa. Wallace and co-workers have reported such compounds i.e. nitrate esters of aspirin, NCX-4215 which have anti-thrombotic activity without gastric irritation and NCX-4016 which almost completely inhibited TxA_2 production and AA induced platelet aggregation.[33]

Triflusal, is an antiplatelet salicylate derivative which produces the active 2-hydroxy-4-trifluoromethylbenzoic acid (HTB) metabolite. It inhibits platelet arachidonic acid metabolism through PGHS with reduced risk of GI bleeding.[34]

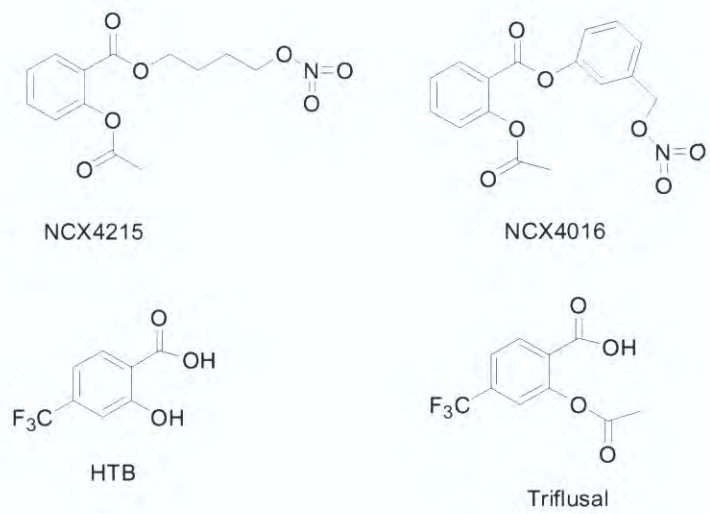

Fig. 6: Structure of NO-Aspirin NCX4215 and NCX4016 which both inhibit PGHS without damage to the gastric mucosa. HTB, a triflusal antiplatelet agents. Reproduced from K. D. Rainsford, *aspirin and related drugs*., 2004, 770 pages.

In our laboratory anthranilic hydroxamic acids as POX site inhibitors have been developed. This arose from the knowledge that peracids are efficient oxidants of myeloperoxidase (MPO) and that hydroxamic acids are structurally similar to peracids with a tendency for hydrogen bonding and metal binding.[35] From X-ray studies on the interactions between peroxidases and hydroxamates it was shown that the hydroxamate does not directly bind to the haem iron but interacts with various distal residues. This

indicates that the mode of inhibition of hydroxamic acids is not by chelation of the iron but competition with the reducing co-substrate for binding at this active site.[36] The salicylhydroxamic acid (SHA) binding affinity for haem-containing mammalian peroxidases is approximately three orders of magnitude greater than benzohydroxamic acid (BHA) due to extra interactions caused by the hydroxyl group.[37]

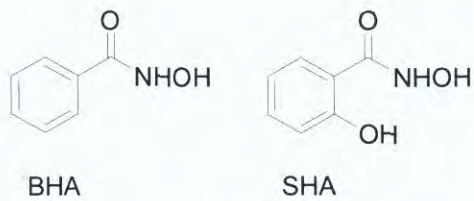

Fig. 7: Structures of BHA and SHA. Reproduced from J. Lee, A. J. Chubb, E. Moman, B. M. McLoughlin, C. T. Sharkey, J. G. Kelly, K. B. Nolan, M. Devocelle, D. J. Fitzgerald, *Org. Biomol. Chem.*, 2005, **3**, 3678–3685.

Tepoxalin **Fig. 8(a)**, a modified bis-substituted pyrazole, attached to a hydroxamic acid group, was found to be a dual inhibitor of both the COX and POX activities of PGHS-1.[38] It was suggested initially that inhibition of the POX site was due to chelation of the haem but later it was reported that its action was as a reducing co-substrate. However because of the high affinity of hydroxamates for Fe(III) it is possible that the chelation of the metal at the active site may play a key role in the inhibition of POX activity by tepoxalin.[39]

A non-hydroxamate dual POX and COX-site inhibitor is Resveratrol (3,5,4′-trihydroxy-*trans*-stilbene) **Fig. 8(b)**, a natural polyphenolic molecule found in grapes and in red wine, which has anti-inflammatory, cardiovascular and chemo-protecting properties. It inhibits both catalytic sites of PGHS-1 but only weakly inhibits the peroxidase site of PGHS-2. Structure activity relationships showed that the *m*-hydroquinone moiety is required for irreversible inactivation of PGHS-1. Resveratrol is a suicide substrate for the peroxidase site of the enzyme and also acts as a reducing co-substrate. Inactivation of the enzyme is by oxidation at the peroxidase site.[40,41]

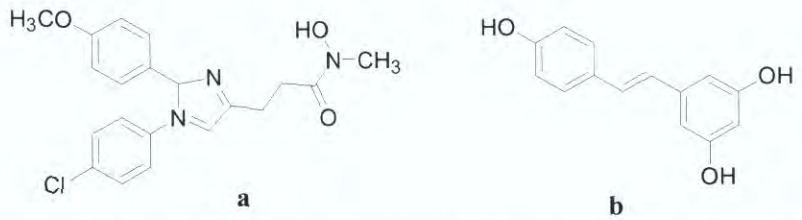

Fig. 8: (a) Tepoxalin and (b) Resveratrol an inhibitors of the peroxidase site of PGHS. Reproduced from M. Ouellet, S. M. Aitken, A. M. English, M. D. Percival, *Archives of Biochemistry and Biophysics*., **431** (1), 2004, 107-118.

It has been reported recently by Lee *et al.* in our research group that anthranilic hydroxamic acid inhibited the POX activity of PGHS with an IC_{50} of 72 μM and that derivatives substituted with two halogen groups improved activity. These compounds were shown to act as reducing co-substrates except for 3,5-diiodoanthranilic hydroxamic acid, **Fig. 9**, for which IC_{50} = 10.5 μM was shown to be a true PGHS-peroxidase inhibitor.[37]

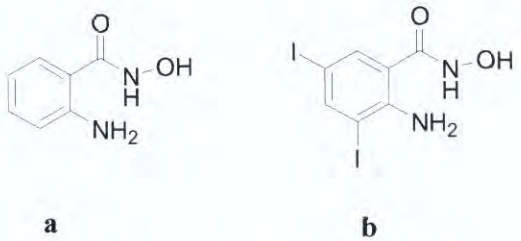

Fig. 9: (a) Anthranilic hydroxamic Acid, (b) 3,5-diiodoanthranilinic hydroxamic acid. Reproduced from J. Lee, A. J. Chubb, E. Moman, B. M. McLoughlin, C. T. Sharkey, J. G. Kelly, K. B. Nolan, M. Devocelle, D. J. Fitzgerald, *Org. Biomol. Chem*., 2005, **3**, 3678–3685.

2.3 Acetylated pyridoxine (vitamin B6) derivatives as PGHS inhibitors

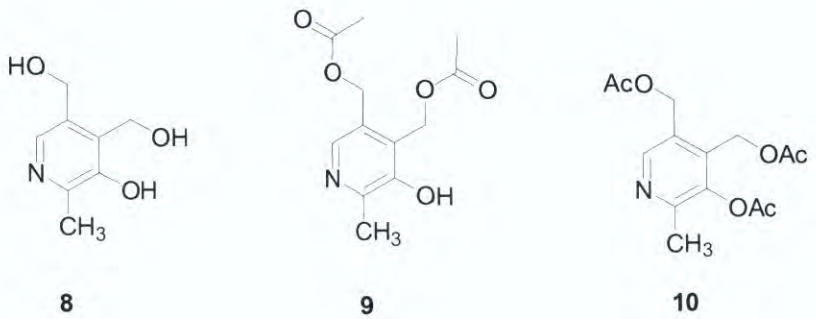

Pyridoxine (4,5-bishydroxymethyl-2-methylpyridin-3-ol), **8**, is a water-soluble vitamin used in the prophylaxis and treatment of vitamin B6 deficiency and peripheral neuropathy. The co-enzyme form of vitamin B6, pyridoxal 5'-phosphate (PLP), has been reported to be a weak inhibitor of ADP, epinephrine, collagen, arachidonic acid and thrombin induced platelet aggregation *in vitro*.[42] The co-enzyme form of vitamin B6 is also involved in a wide range of biochemical reactions, including the metabolism of amino acids and glycogen, the synthesis of nucleic acids, haemoglobin and the neurotransmitters serotonin, dopamine, norepinephrine and gamma-aminobutyric acid (GABA).[43] Vitamin B6 is an approved drug which is readily absorbed from the gastrointestinal tract, almost non toxic (LD50 = 4gm/kg in rats), and with good bioavailability (only 22% protein binding) and water solubility. As part of our research on acetylated derivatives as PGHS inhibitors we decided to acetylate vitamin B6 and to study its activity. Dr Anthony Chubb, Molecular & Cellular Therapeutics Department, RCSI, has shown, using Autodock 4, that acetylated derivatives of vitamin B6 improves enzyme binding by ~3kcal/mol, with an improvement in inhibition of 140-fold.

2.4 Experimental - synthesis

All reagents and solvents were purchased from Sigma-Aldrich and were used without further purification.

2.4.1 Salicylhydroxamic acid, 1.

The compound was prepared by a modification of a previously reported method. Hydroxylamine hydrochloride (2.74 g, 39.4 mmol), was added to sodium hydroxide (3.15 g, 79 mmol), in deionised water (25 mL). Then the solution was added to methyl salicylate (3 g, 19.7 mmol) in methanol (50 mL). The resulting solution was refluxed for 48 hours. TLC indicated the disappearance of starting material. The solution was acidified to pH 5.5 with 50% HCl. The solvent was removed *in vacuo,* yielding a red solid. Methanol (50 mL) was added and the sodium chloride filtered off. The solvent was removed *in vacuo* and the residue recrystallised from water to give **1** (2.3 g, 15 mmol, 76%) as brown crystals. ^{1}H NMR (400MHz, d^{6}-DMSO); δ 12.25 (1H, s), 11.45 (1H, s), 9.35 (1H, s), 7.6 (1H, dd, J = 1.6 and 8 Hz), 7.38 (1H, t, J = 1.6 Hz), 6.91-6.84 (2H, m). ^{13}C NMR (400 MHz, d^{6}-DMSO); δ 166.2, 159.4, 133.4, 126.9, 118.6, 117.2,

113.9. IR (KBr disc); υ_{max} 3291, 2692, 1610, 1526, 1493 cm^{-1}. The compound was obtained in good yield (76%) and excellent purity.[44]

2.4.2 N-acetoxy-2-hydroxybenzamide (SalAc), 2, and N-acetoxy-2-acetoxy benzamide ($SalAc_2$), 3.

Salicylhydroxamic acid (3 g, 19.6 mmol) was dissolved with stirring in dry dimethyl formamide (7 mL) under a nitrogen atmosphere to give a pink-colored solution which was cooled to 0 °C. Acetic anhydride (4 mL, 43.1 mmol) was then added dropwise over a 30 min period. Dry pyridine (8.7 mL, 107.8 mmol) was next added and the reaction mixture was warmed to room temperature and stirred for 20 hours. A saturated aqueous NH_4Cl solution (50 mL) was then added and the resulting mixture was extracted with ethyl acetate (2 x 50 ml). The organic phase was washed with brine (30 mL), dried over Na_2SO_4 and taken to dryness using a rotary evaporator. TLC using a petroleum ether and ethyl acetate (1:1) solvent system indicated two spots with R_f 0.75 for SalAc, **2**, R_f 0.65 for $SalAc_2$, **3.** The residue was purified by flash silica column chromatography (eluting with petroleum ether:ethyl acetate, 3:1) to give two fractions which were collected and taken to dryness.

SalAc, **2**, was obtained as a white solid (0.82 g, 4.2 mmol, 22% yield). mp 139 °C. HRMS found: 194.0456 [M-H$^+$], $C_9H_9NO_4$ requires 194.0453. ^{1}H NMR (400MHz, d^6-DMSO); δ 12.11 (1H, s), 11.39 (s, 1H), 7.74 (1H, dd, J = 1.6 and 8 Hz), 7.44 (1H, t, J = 1.6 Hz), 6.92-6.98 (2H, m), 2.24 (3H, s). ^{13}C NMR (400 MHz, d^6-DMSO); δ 168.5, 165.4, 158.0, 134.0, 128.8, 119.1, 117.1, 114.7, 18.1. IR (KBr disc); υ_{max} 3321, 2579, 1790, 1769, 1643, 1606 cm^{-1}. $SalAc_2$, **3**, was also obtained as a white solid (1.7 g, 7.2 mmol, 37% yield). mp 115 °C. HRMS found: 236.0556, [M-H$^+$] $C_{11}H_{11}NO_5$ requires 236.0559. ^{1}H NMR (400MHz, d^6-DMSO); δ 12.15 (1H, s), 7.63-7.58 (2H, m), 7.39 (1H, td, J = 15.2, 7.6 and 0.8 Hz), 7.25 (1H, d, J = 8 Hz), 2.23 (3H, s) and 2.21 (3H, s). ^{13}C NMR (400 MHz, d^6-DMSO); δ 168.8, 168.3, 162.7, 148.19, 132.3, 129.2, 126.0, 125.8, 123.7, 20.7, 18.1. IR (KBr disc); υ_{max} 3192, 2939, 1814, 1761, 1656, 1604, 1504, 1477 cm^{-1}. Tiny white crystals of **2** suitable for X-ray analysis were obtained by dissolving **2** in hot ethyl acetate, adding a few drops of petroleum ether and standing at room temperature overnight. Diamond-shaped crystals of **3** suitable for X-ray analysis

were obtained in the same way as **2**. The crystal structures of **2** and **3** are shown in **Figs. 10** and **11** respectively and the bond lengths and angles are compared in **Tables 3** and **4**. Crystallographic details and data collection parameters are given in Appendix **Table 1** and **Table 2**. A complete list of bond lengths (Å), bond angles (°), hydrogen bonds (Å and°) and torsion angles for **2** and **3** are listed in Appendix, **Table 1**, **Table 2**, respectively.

2.4.3 N-acetoxy-N-acetyl-2-acetoxybenzamide ($SalAc_3$), 4.

This compound was prepared by a modification of a previously reported method.[30] Acetic anhydride (10 mL, 98.0 mmol), and concentrated sulfuric acid (1 drop) were added to salicylhydroxamic acid (2 g, 13 mmol). The mixture was stirred at 80 °C under nitrogen for 48 hours. Ethyl acetate (40 mL) was added to the resulting dark orange solution. The organic phase was twice washed with 0.5 M sodium hydroxide (25 mL), water (25 mL), 0.5 M citric acid (25 mL), and brine. The organic layer was dried over Na_2SO_4 and evaporated to dryness using a rotary evaporator. The oily residue was purified by column chromatography on silica gel with a mixture of petroleum ether and ethyl acetate (4:1) as eluent. **4** was obtained as a brown oil (1.68 g, 6.02 mmol, 46%). HRMS found: 280.0825 [M-H$^+$], $C_{13}H_{14}NO_6$ requires 280.0821. ^{1}H NMR (400MHz, $CDCl_3$); δ 7.54-7.46 (2H, m), 7.29 (1H, td, J = 15.2, 7.6 and 1.2 Hz), 7.21 (1H, dd, J = 8.4 and 0.8 Hz), 2.56 (3H, s), 2.28 (3H, s), 2.0 (3H, s). ^{13}C NMR (400 MHz, $CDCl_3$); δ 168.8, 167.4, 166.7, 165.8, 147.3, 132.2, 128.2, 126.5, 125.8, 123.2, 24.9, 20.9, 17.6. IR (KBr disc); υ_{max} 3073, 3019, 2944, 1812, 1693br, 1608, 1483, 1369 cm^{-1}.

2.4.4 Acetic acid 4-acetoxymethyl-5-hydroxy-6-methyl-pyridin-3-ylmethyl ester, 9.

Pyridoxine (Vitamin B6), **8**, was purchased from Sigma-Aldrich and was used without further purification. To a stirred solution of pyridoxine (0.5 g, 2.96 mol), in dry DMF (2 mL) under nitrogen at 0 °C was added acetic anhydride (0.62 mL, 6.5 mol). The mixture was stirred for an additional 30 min, then pyridine (0.79 mL, 9.70 mol) was added dropwise at the same temperature. The resulting mixture was slowly warmed to room temperature and stirred for 4 hours. Water (10 mL) was added to the reaction mixture followed by saturated aqueous NH_4Cl solution (10 mL). Following extraction

into ethyl acetate (2 x 10 mL), and washing with water (2 x 10 mL), the solution was dried over Na_2SO_4, then the solvent removed *in vacuo*. The resulting residue was purified by flash chromatography using petroleum ether:ethyl acetate (80:20) as eluent to give **9** (0.26 g, 1.0 mol, 35 %) as a light brown solid, R_f =0.65. HRMS found: 252.0869 [M-H$^+$], $C_{12}H_{14}NO_5$ requires 252.0872. ^{1}H NMR (400 MHz, d^6-DMSO); δ 2.07 (3H, s), 2.08 (3H, s), 2.47 (3H, s), 5.17 (2H, s), 5.19 (2H, s), 8.06 (1H, s), 9.34 (1H, s). ^{13}C NMR (400 MHz, d^6-DMSO); δ 169.9, 168.7, 150.7, 145.8, 144.1, 135.1, 134.4, 58.3., 56.6, 20.3, 20.3, 19.1.

2.4.5 Acetic acid 3-acetoxy-5-acetoxymethyl-2-methyl-pyridin-4-ylmethyl ester, 10.

To a stirred solution of pyridoxine, **8**, (0.5 g, 2.96 mol), in dry DMF (2 mL) under nitrogen at 0 °C was added acetic anhydride (0.92 mL, 9.7 mol). The mixture was stirred for an additional 30 min, then pyridine (1.1 mL, 13.0 mol) was added dropwise at the same temperature. The resulting mixture was slowly warmed to room temperature and stirred for 3 hours. Water (10 mL) was added to the reaction mixture followed by saturated aqueous NH_4Cl solution (10 mL). Following extraction with ethyl acetate (2 x 10 mL), and washing with water (2 x 10 mL), the solution was dried over Na_2SO_4 , then taken to dryness *in vacuo* and washed twice with ether to afford **10** (0.77 g, 2.6 mol, 88 %) as yellow oil. HRMS found: 296.1139 [M-H$^+$], $C_{14}H_{18}NO_6$ requires 296.1134. ^{1}H NMR (400 MHz, $CDCl_3$); δ 1.97 (3H, s), 2.02 (3H, s), 2.33 (3H, s), 2.36 (3H, s), 5.10 (2H, d, J = 5.6 Hz), 5.21 (2H, s), 8.39 (1H, s). ^{13}C NMR (400 MHz, $CDCl_3$); δ 170.4, 170.2, 168.6, 153.1, 147.0, 144.6, 135.6, 129.4, 61.2, 56.8, 20.79, 20.5, 20.5, 19.53.

2.5 Instrumentation

2.5.1 Infrared spectroscopy

Infrared spectroscopic measurements were obtained using a Bruker Tensor 27 spectrometer. The spectra obtained were analysed using WinFIRST software. All KBr discs were made using FTIR grade KBr purchased from Aldrich.

2.5.2 ^{1}H, ^{13}C NMR spectroscopy

^{1}H NMR spectra were recorded on a Bruker DPX 400 spectrometer operating at 400 MHz at ambient temperatures. The Bruker DPX spectrometer was also used to record ^{13}C at 101 MHz. The spectra obtained were analysed using WIN NMR software.

2.5.3 Single X-ray diffraction measurements

Single-crystal X ray diffraction experiments on **2** and **3** were carried out by Dr Thomas McCabe, School of Chemistry, Trinity College Dublin, Ireland on a Bruker Smart Apex CCD diffractometer at 100 K using monochromated Mo-K_{α} radiation, (λ= 0.71073 Å) and the ϕ-ω scan method. The structure was solved by direct methods (SHELXS-97) and refined by full-matrix least squares using SHELXL 97-2.[45]

2.5.4 Mass spectrometry

Liquid chromatography-mass spectrometry experiments were performed by Dr. Dilip Rai in University College Dublin on a Quattro Micro quadrupole electrospray mass spectrometer (Micromass, Waters Corp., USA). 10 µL of the samples were injected in 300 µL of water: methanol (50:50, v/v). The mass spectrometry data were acquired both in positive and negative ion modes.

2.5.5 Elemental analysis

Elemental analysis were performed at the Microanalytical Laboratory, School of Chemistry and Chemical Biology, University College Dublin.

2.6 Results and Discussion

2.6.1 Salicylhydroxamic acid, 1,

Salicylhydroxamic acid, **1**, was prepared by a modification of a previously reported method,[44] using the reaction of methyl salicylate, (Aldrich), with hydroxylamine generated *in situ* by addition of NaOH to the hydrochloride. Salicylhydroxamic acid was qualitatively identified using a ferric chloride test as hydroxamates form an intense purple complex with iron (III).[46]

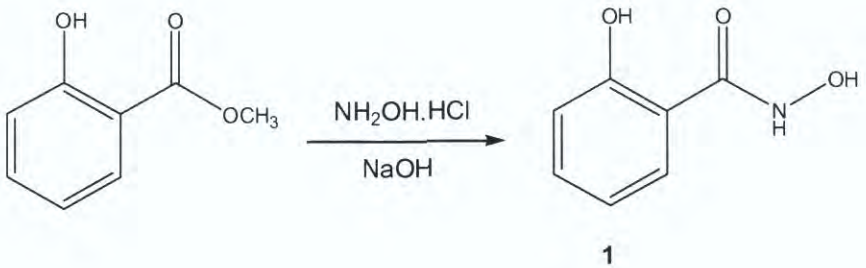

Scheme 1: Synthesis of salicylhydroxamic acid, **1**

The structure of **1** was confirmed by ^{1}H-NMR, ^{13}C-NMR and IR data. The ^{1}H NMR spectrum of a solution of **1** in d^{6}-DMSO showed signals at δ 12.25 ppm (1H, singlet) corresponding to the hydroxamate–NH group, δ 11.45 ppm (1H, singlet) for the phenolic –OH group and at δ 9.35 ppm (1H, singlet) for the hydroxamate -OH. Three signals in the aromatic region at δ 7.6 (1H, double of doublets), δ 7.38 (1H, triplet) and δ 6.91-6.84 (2H, multiplet) ppm are observed. The^{13}C-NMR spectrum of **1** in d^{6}-DMSO showed signals at δ 166.2 ppm (hydroxamte C=O) and at δ159.4-113.9 ppm (aromatic CH groups). The IR spectrum of the product showed a broad band at 3291 cm^{-1} due to ν(OH) and ν(NH) and a strong band at 1610 cm^{-1} due to the C=O stretch of the hydroxamte group.

2.6.2 N-acetoxy-2-hydroxybenzamide, SalAc, 2, and N-acetoxy-2-acetoxy benzamide, SalAc$_2$, 3.

N-acetoxy-2-hydroxybenzamide (SalAc), **2**, was synthesised by modification of a previously reported method,[47] by reaction of salicylhydroxamic acid, **1**, with 2.2 equivalent of acetic anhydride and an excess of pyridine in dry DMF under nitrogen. This produced a mixture of **2** and **3**, **Scheme 2.** Separation of **2** and **3** was performed by flash silica column chromatography (eluting with petroleum ether:ethyl acetate, 3:1) as eluent. Crystals of **2** suitable for X-ray analysis were obtained by recrystallisation from hot ethyl acetate, to which a few drops of petroleum spirit was added and standing at room temperature overnight. Diamond-shaped crystals of **3** suitable for X-ray analysis were similarly obtained.

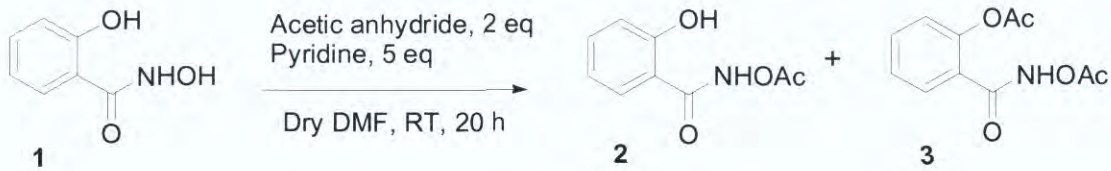

Scheme 2: The synthesis of SalAc, **2**, and $SalAc_2$, **3**

The structures of **2** and **3** were confirmed by HRMS, ^{1}H-NMR, ^{13}C-NMR, IR and finally by X-ray crystallographic data. The found HRMS [M-H$^+$] value of **2** 194.0456, was acceptably close to the theoretical, 194.0453. The ^{1}H NMR spectrum of a solution of **2** in d^6-DMSO showed signals at δ 2.24 ppm (3H, singlet) corresponding to the acetyl group protons. Three signals in the aromatic region at δ 6.92-6.98 (2H, multiplet), δ 7.44 (1H, triplet) and δ 7.74 (1H, double of doublets) ppm were observed while the signal for the phenolic –OH group occurred at δ11.39 ppm (1H, singlet) and for the hydroxamate –NH group at δ12.11 ppm (1H, singlet). The^{13}C-NMR spectrum of **2** in d^6-DMSO showed signals at δ 168.5 ppm (hydroxamte C=O), δ165.4 ppm (acetyl C=O), δ158.0-114.7 ppm (aromatic CH groups), and at δ 18.1 ppm due to the acetyl methyl group. The IR spectrum of the product showed a broad band at 3321 cm^{-1} due to ν(NH), two υ(C=O) bands at 1790 and 1769 cm^{-1} due to the acetyl group and a strong band at 1643 cm^{-1} due to the C=O stretch of the hydroxamate group.[48]

The found HRMS [M-H$^+$] value of **3**, 236.0556, was acceptably close to the theoretical value, 236.0559. The ^{1}H-NMR spectrum of a solution of **3** in d^6-DMSO showed the absence of the hydroxamate and phenolic OH groups and confirming that acetylation occurred at these sites, **Scheme 2.** The acetyl group protons gave singlets at δ 2.23 and 2.21 ppm indicating the presence of a di-acetylated product. A singlet at δ 12.15 ppm is due to the hydroxamate NH group and occurs in a similar position to that of the NH group in **2.** Three signals in the aromatic region at δ 7.25 (1H, doublet), δ 7.39 (1H, triple of doublets) and δ 7.63-7.58 (2H, multiplet) ppm were observed. The ^{13}C-NMR spectrum of **3** in d^6-DMSO showed signals at δ 168.8 (hydroxamate C=O), δ168.3 ppm (acetyl C=O), δ162.7 ppm (acetyl C=O), δ148.19-123.7 ppm (aromatic CH groups),

and at δ 20.7, 18.1 ppm (acetyl Methyl groups). The IR spectrum of the product showed a broad band at 3192 cm^{-1} for ν(NH), two υ(C=O) bands at 1814 and 1761 cm^{-1} corresponding to the acetyl groups and a strong bands at 1656 cm^{-1} due to the C=O stretch of the hydroxamate group.

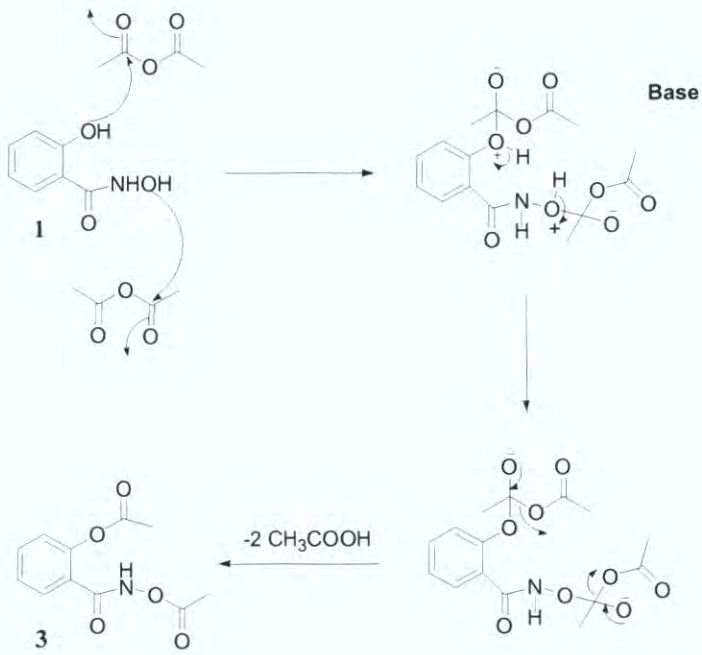

Scheme 3: The proposed mechanism of acetylation of salicylhydroxamic acid, **1**, and formation of N-acetoxy-2-N-acetoxy- benzamide ($SalAc_2$), **3**

The proposed mechanism of acetylation is shown in **Scheme 3.** This involves initial attack by the nucleophilic OH groups on the electrophilic carbon of the anhydride resulting in an unstable tetrahedral intermediate which, following elimination reaction of acetic acid yields the product. Pyridine removes H^+ formed during the reaction.

The structure of **2** is shown in **Fig. 10**, with selected bond lengths and angles given in the **Tables 3** and **4** and crystal data in **Table 1.** The structure of **2** was refined in the triclinic *P*-1 space group and high R factor obtained is due to twinning of the crystals. The crystal structure confirms that acetylation of the hydroxamate group and not the phenolic group of salicylhydroxamic acid occurred. The C(5)-O(1) = 1.369(4), C(7)-O(3) = 1.232(4) and N(1)-O(7) = 1.404(3) Å bond lengths are quite similar to the corresponding bond lengths found in salicylhydroxamic acid, 1.355(4), 1.258(4) and 1.390(4) Å,[44] respectively, the last two of these suggesting that there is similar

delocalization of the nitrogen lone pair of electrons into the hydroxamate π system in both cases. The C(7)-O(3) and C(7)-N(1) bond lengths, 1.232(4) and 1.341(4) Å are quite normal for hydroxamic acids.[49] The O(3)-C(7)-C(4) bond angle in SalAc, **2**, 121.5(3)° is similar to the corresponding bond angle in salicylhydroxamic acid i.e. 121.4(3)°. However the O(7)-N(1)-C(7) bond angle, 114.6(3)°, is much smaller than the corresponding bond angle in salicylhydroxamic acid i.e. 121.2°,[44] which may be due to the presence of the acetyl group instead of H on O(7) and the loss of H-bonding interactions.

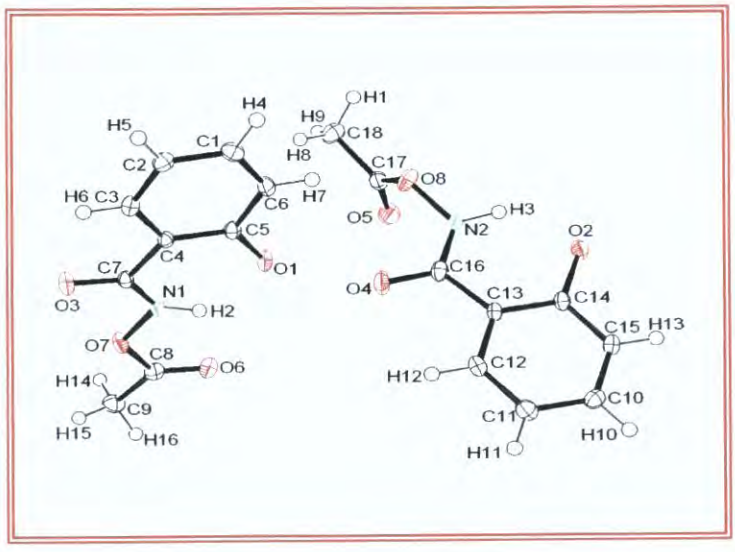

Fig. 10: Molecular structure and atomic labelling scheme for N-acetoxy-2-hydroxy-benzamide, SalAc, **2**

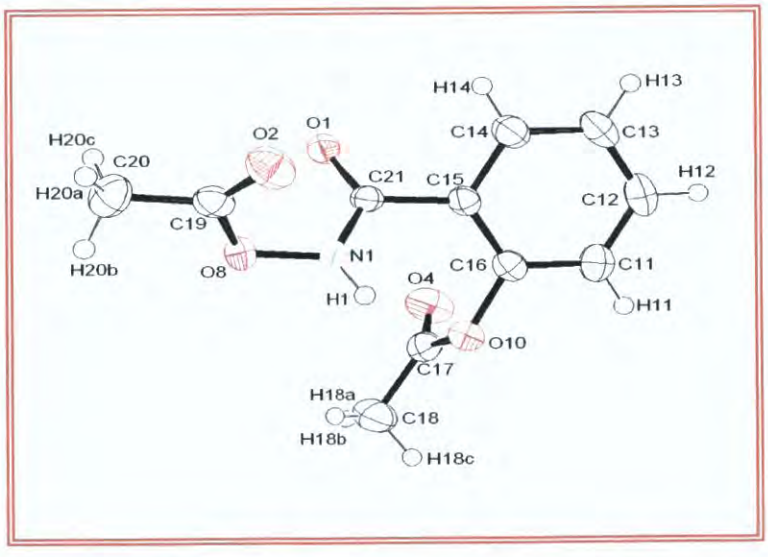

Fig. 11: Molecular structure and atomic labelling scheme for N-acetoxy-2-acetoxybenzamide, $SalAc_2$, **3**

Table 3: Bond lenghts (°) with estimated standard deviation for N-Acetoxy-2-hydroxybenzamide (SalAc), 2, compared with those of N-acetoxy-2-acetoxybenzamide ($SalAc_2$), 3

	Bond Length (Å) (SalAc),2	Bond Length (Å) ($SalAc_2$),3
O(1)-C(5) : O(10)-C(16)	1.369(4)	1.407(3)
C(4)-C(7) : C(15)-C(21)	1.493(4)	1.497(3)
O(3)-C(7) : O(1)-C(21)	1.232(4)	1.222(3)
N(1)-C(7) : N(1)-C(21)	1.341(4)	1.340(3)
O(7)-N(1) : O(8)-N(1)	1.404(3)	1.400(2)
O(7)-C(8) : O(8)-C(19)	1.365(4)	1.391(3)
O(6)-C(8) : O(2)-C(19)	1.205(4)	1.192(3)
C(8)-C(9) : C(19)-C(20)	1.493(5)	1.478(3)

Table 4: Bond angles (°) with estimated standard deviation for N-Acetoxy-2-hydroxybenzamide (SalAc), 2, compared with those of N-acetoxy-2-acetoxybenzamide ($SalAc_2$), 3

	Bond angles (°) (SalAc),2	Bond angles (°) ($SalAc_2$),3
O(1)-C(5)-C(4) : C(15)-C(16)-O(10)	120.2(3)	119.23(19)
O(3)-C(7)-C(4) : O(1)-C(21)-C(15)	121.5(3)	121.54(19)
C(7)-N(1)-O(7) : C(21)-N(1)-O(8)	114.6(3)	116.70(18)
O(6)-C(8)-C(9) : O(2)-C(19)-C(20)	128.5(3)	128.8(2)

The structure of **3** is shown in **Fig. 11**, with selected bond lengths and angles in **Tables 3** and **4** and crystal data in **Table 2.** The structure crystallizes in triclinic space group *P*–1 (#2). This compound in which the phenolic and hydroxamate groups are acetylated is the proposed active PGHS inhibitor derived from $SalAc_3$, **4**, discussed later. The hydroxamate C=O and C-N bond lengths, C(21)-O(1) = 1.222(3) Å and C(21)-N(1) = 1.340(3) Å, are both very similar to the corresponding bonds in **2** which is expected as the hydroxamate groups are acetylated in both cases. This is also true for the acetyl group C=O. The bond angles around the hydroxamate group are also similar for both compounds. The C(16)-O(10) bond in **3**, 1.407(3) Å is longer than the C(1)-O(5) bond in **2**, 1.369(4) Å due to acetylation of the O in **3.**

2.6.3 N-acetoxy-N-acetyl-2-acetoxybenzamide, $SalAc_3$, 4.

Treatment of salicylhydroxamic acid (SHA), **1**, with acetic anhydride at 80 °C for 48 h **Scheme 4** gave N-acetoxy-N-acetyl-2-acetoxybenzamide $SalAc_3$, **4**, as brown oil. The identity of the product **4** was confirmed by HRMS, ^{1}H-NMR, ^{13}C-NMR and IR data.

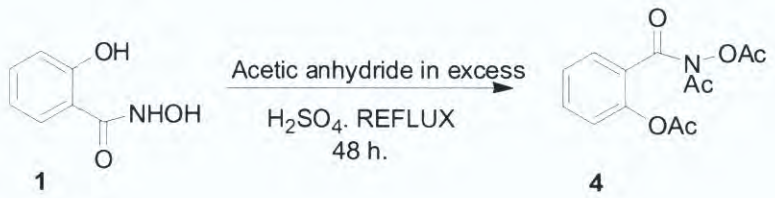

Scheme 4: Synthesis of **4**

The found HRMS value for [M-H$^+$], 280.0825, was acceptably close to the theoretical value of 280.0821 ($C_{13}H_{14}NO_6$). The ^{1}H NMR spectrum of a solution of **4** in $CDCl_3$ showed signals at δ 2.0 (3H), 2.28 (3H) and δ 2.56 (3H) ppm corresponding to the three acetyl groups. Three signals in the aromatic region at δ 7.21 (1H, double of doublets), δ 7.29 (1H, triple of doublets) and δ 7.54-7.46 (2H, multiplet) ppm were also observed. The^{13}C-NMR spectrum of **4** in $CDCl_3$ showed signals at δ 168.8-165.8 ppm corresponding to the four carbonyl groups, δ147.3-123.2 ppm (aromatic CH groups), and the acetyl methyl group signals at δ 24.9, 20.9 and 17.6 ppm. The IR spectrum of the product showed two υ(C=O) bands, one is very broad at ~1812 cm^{-1} due to the acetyl groups and another at 1693 cm^{-1} which is due to the υ(C=O) of the hydroxamate.

2.6.4 Platelet aggregation studies

Compounds **2** – **4** and aspirin, **Fig. 12**, were evaluated in platelet aggregation assays by Dr Anthony Chubb, Molecular & Cellular Therapeutics Department, RCSI. The platelet aggregation assay measures the increased light transmission through platelet rich plasma (PRP), freshly isolated from healthy volunteers, in response to addition of 1.5 mM arachidonic acid as agonist. Arachidonic acid induced platelet aggregation is inhibited by aspirin and other NSAIDs. Various concentrations of each compound (0.1-1000 μM; final DMSO concentration < 0.4%) were added to stirred PRP for 5 min prior to arachidonate addition. The results of these studies are shown in **Fig. 13.**

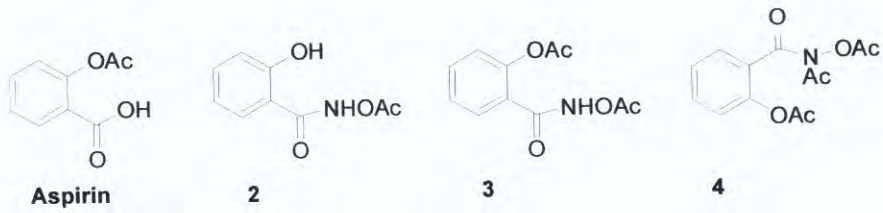

Fig. 12: Inhibition of platelet aggregation. Rotating human platelet rich plasma light transmission aggregation assays.

Compound **2**, was found to inhibit platelet aggregation, with a 50% maximal inhibition concentration (IC_{50}) of 599.9 ± 140.7 μM which is 13-fold less potent than aspirin, (IC_{50} = 47 ± 27 μM). Compounds **3** and **4** were found to inhibit platelet aggregation with an IC_{50} of 7.8 ± 5.5 μM and 12.3 ± 6.7 μM respectively, **Fig. 13.** Therefore compound **3** is 6-fold more active than aspirin and **4** is ~3.8 times more active. These results confirm the mechanism for PGHS inhibition of **4** shown in **Fig. 5** and also confirms that **4** is a pro-drug for **3.** The greater activity of **3** compared to **4** may be due to easier entry to the COX active site for steric reasons.

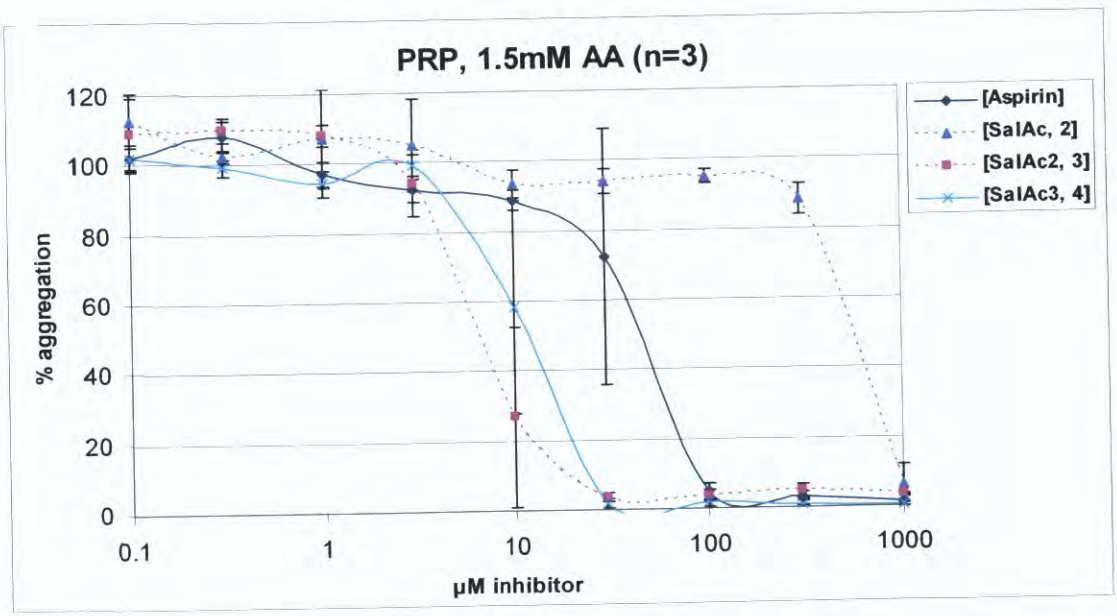

Fig. 13: Inhibition of platelet aggregation. Rotating human platelet rich plasma light transmission aggregation assays. Compounds were pre-incubated with platelets (DMSO = 0.8%) for 5 min prior to addition of 1.5 mM arachidonic acid and 3 min aggregation. Final inhibitor concentrations show in microMolar. Percentage aggregation normalized to DMSO control (n=3, SEM). Legend: Aspirin, diamond; SalAc, **2**, dashed diamond; $SalAc_2$, **3**, solid square; $SalAc_3$, **4**, dot-dashed circle.

2.6.5 Acetic acid 4-acetoxymethyl-5-hydroxy-6-methyl-pyridin-3-ylmethyl ester, 9.

Pyridoxine, **8**, was acetylated by reaction with two equivalents of acetic anhydride in the presence of pyridine as a base **Scheme 5.** Work-up involved addition of saturated aqueous NH_4Cl solution to neutralize the excess of base followed by extraction with ethyl acetate then flash chromatography for purification. TLC indicated the presence of two spots one major and one minor. Separation was completed on silica gel 60 using 20% ethyl acetate in petroleum ether. The fractions containing the major product were combined and taken to dryness under reduced pressure, which was shown to be the di-acetylated product, by HRMS, ^{1}H-NMR and ^{13}C-NMR and NOE.

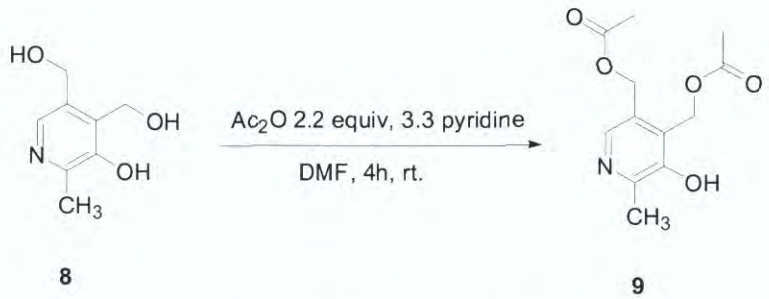

Scheme 5: Synthesis of **9**

The structure of **9** was confirmed by HRMS, ^{1}H-NMR, ^{13}C-NMR and NOE. HRMS; found 252.0869 [M-H$^+$], $C_{12}H_{14}NO_5$ requires 252.0872. The ^{1}H NMR spectrum of a solution of **9** in d^6-DMSO showed signals at δ 2.07 ppm (3H, singlet) for the methyl group, δ 2.08, 2.47 ppm corresponding to the methyl protons of the two acetyl groups, δ 5.17 ppm (2H, singlet) and δ 5.19 ppm (2H, singlet) corresponding to the aliphatic chain CH_2 groups. The signal for the N-CH proton occurs at δ 8.38 ppm (1H, singlet). The signal for the C-OH proton occurs at δ 9.34 ppm. The assignment of this signal was confirmed by the NOE spectrum carried out by Dr John O'Brien (TCD), see appendix. The^{13}C-NMR spectrum of **9** in d^6-DMSO showed signals at δ 169.9, 168.7 ppm corresponding to the acetyl group C=O peaks, δ 150.7-134.4 ppm due to the pyridoxine-CH groups, δ 58.3, 56.6 ppm due to the aliphatic $-CH_2$ groups while the acetyl group CH_3 signals appeared upfield at δ 20.3 and 20.3 ppm. The methyl group appeared at δ 19.1 ppm.

2.6.6 Acetic acid 3-acetoxy-5-acetoxymethyl-2-methyl-pyridin-4-ylmethyl ester, 10.

In order to ensure formation of the completely acetylated product **10**, over three equivalents of acetic anhydride were used. Product **10** was formed by the reaction of pyridoxine with acetic anhydride at room temperature in dry DMF in the presence of pyridine as base **Scheme 6.** Compound **10** was obtained after the workup as a yellow oil in 88% yield without any further purification.

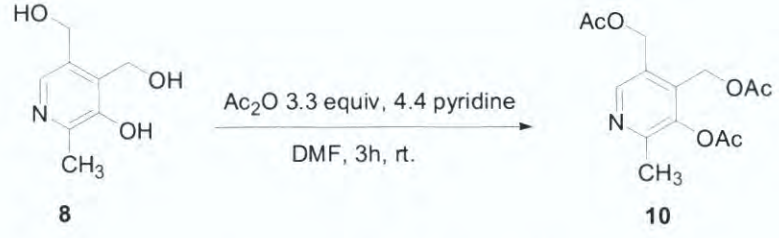

Scheme 6: Synthesis of **10**

The structure of **10** was confirmed by HRMS, ^{1}H-NMR and ^{13}C-NMR. HRMS; found 296.1139 [M-H^{+}], $C_{14}H_{18}NO_6$ requires 296.1134. The ^{1}H NMR spectrum of a solution of **10** in $CDCl_3$ showed signals at δ 1.97 ppm (3H, singlet) for the methyl group. δ 2.02, 2.33 and 2.36 (3H, singlet) ppm corresponding to the methyl protons of three acetyl groups, δ 5.10 ppm (2H, doublet) corresponding to the aliphatic chain CH_2, δ 5.21 ppm (2H, singlet) corresponding to the aliphatic chain CH_2. The signal for proton attached nitrogen group (N-C<u>H</u>) occurs at δ 8.39 ppm (1H, singlet). The^{13}C-NMR spectrum of **10** in $CDCl_3$ showed signals at δ 170.7, 170.2 and 168.6 ppm corresponding to the acetyl C=O peaks, δ 153.1-129.4 ppm (pyridoxine-CH groups), δ 61.2, 56.8 ppm (aliphatic –CH_2 groups), acetyl CH_3 peaks appeared upfield at δ 20.8, 20.5 and 20.5 ppm. Methyl group appeared at δ 19.53 ppm.

Compounds **9** and **10** were evaluated in platelet aggregation assays by Dr Anthony Chubb, Molecular & Cellular Therapeutics Department, RCSI. Unfortunately compounds **9** and **10** were found to be inactive in platelet aggregation assays at the highest concentration tested (1000 μM).

2.7 Conclusions

The work reported in this chapter has confirmed that $SalAc_2$, **3**, is the active acetylating agent in the inhibition of PGHS by $SalAc_3$, **4.** PGHS inhibition by the newly synthesised compound $SalAc_2$, **3**, was measured and compared with $SalAc_3$, **4**, and SalAc, **2.** $SalAc_2$, **3** is the most effective hydroxamate based PGHS inhibitor so far reported and because of the ease of optimising activity by introducing substituents on the aromatic ring is an excellent lead for the development of new inhibitors. The crystal structures of $SalAc_2$, **3**, and SalAc, **2**, were determined and are compared. The newly synthesised acetylated pyridoxine derivatives unfortunately were found to be inactive as PGHS inhibitors.

2.8 References

1. P. J. Loll, C. T. Sharkey, S. J. O'Connor, C. M. Dooley, E. O'Brien, M. Devocelle, K. B. Nolan, B. S. Selinsky, D. J. Fitzgerald., Molecular pharmacology, 2001, **60** (6), 1407-1413.

2. T. J. Maclagan, *Lancet*, 1876, **1**, 342–383.

3. J. R. Vane, R. M. Botting, *Thrombosis Research*, 2003, **110**, 255-258.

4. S. J. Padayatty, A. Katz, Y. Wang, P. Eck, O. Kwon, J-H. Lee, S. Chen, C. Corpe, A. Dutta, S. K. Dutta, M. Levine, *J. Am. Coll. Nutr.*, 2003, **22**, 18-35.

5. H. Dreser, *Pflugers Arch.*, 1899, **76**, 306–18.

6. S. Petit-Zeman, *Nat. Rev. Drug Discov.*, 2004, **3**, 726-727.

7. J. R. Vane, *Nature-New Biology*, 1971, **231**, 232-235.

8. J. B. Smith, A. L. Willis, *Nature*, 1971, **231**, 235–237.

9. E. H. Awtry, J. Loscalzo, *Circulation*, 2000, **101**, 1206-1218.

10. M. J Thun, S. J. Henley, C. Patrono, *J. Natl. Cancer Inst.*, 2002, **94**, 252–66.

11. F. Gao, K. R. Bales, R. C. Dodel, J. Liu, X. Chen, H. Hample, Farlow MR, Paul SM and Du Y, *Mol. Brain Res.*, 2002, **105**, 108-114.

12. I. Nyman, H. Larsson, L. Wallentin, *Lancet*, 1992, **340**, 497-501.

13. P. J. Loll, D. Picot, R. M. Garavito, *Nature Struct. Biol.*, 1995, **2**, 637–643.

14. J. R. Vane, Y. S. Bakhle, R. M. Botting. *Ann. Rev. Pharm. Tox.*, 1998, **38**, 97-120.

15. W. L. Smith, D. L. DeWitt, *Semin. Nephrol*, 1995, **15**, 179-194.

16. A. Lopez-Farre, C. Caramelo, A. Esteban, M. Alberola, I. Millas, M. Monton, S. Casado, *Circulation*, 1995, **91**, 2080–2088.

17. K. A. Steer, T. M. Wallace, C. H. Bolton, M. Hartog, *Heart.*, 1997, **77**, 333-337.

18. S. Husain, N. P. Andrews, D. Mulcahy, J. A. Panza, A. A. Quyyumi, *Circulation*, 1998, **97**, 211-218.

19. W. H. Betts, M. W. Whitehouse, L. G. Clelend, B. Vernon-Roberts, *J. Free Radic. Biol. Med.*, 1985, **1**, 273–280.

20. R. N. Pinckard, D. Hawkins, R. S. Farr, *Nature*, 1968, **219**, 68-69.

21. C. Patrono, B. Collar, J. Dalen, V. Fuster, M. Gent, L. Harker, J. Hirsh, *Chest.*, 1998, **114**, 470S-488S.

22. J. W. Burch, N. Stanford, P. W. Majerus, *J. Clin. Invest.*, 1978, **61** (2), 314–319.

23. H. Tohgi, S. Konno, K. Tamura, B. Kimura, K. Kawa, *Stroke*, 1992, **23**, 1400-1403.

24. P. J. Roderick, H. C. Wilkes, T.W. Meade, *Br. J. Clin. Pharmacol*, 1993, **35**, 219-226.

25. L. Hansson, A. Zanchetti, S. G. Carruthers, B. Dahlöf, D. Elmfeldt, S. Julius, J. Ménard, K. H. Rahn, *Lancet*, 1998, **351**, 1755-62.

26. P. Mene, F. Pugliese, C. Patrono, *Semin. Nephrol.*, 1995, **15**, 244–252.

27. G. A. Riegger, H. W. Kahles, D. Elsner, E. P. Kromer, K. Kochsiek, *Am J Med.*, 1991, **90** (5), 571–575.

28. J. J. Nawarskas, S. A. Spinler, *Pharmacotherapy*, 1998, **18**, 1041-1052.

29. D. Picot, P. J. Loll, R. M. Garavito, *Nature*, 1994, **367**, 243–249.

30. C. M. Dooley, M. Devocelle, B. McLoughlin, K. B. Nolan, D. J. Fitzgerald, C. T. Sharkey, *Mol. Pharmacol.*, 2003, **63**, 450-455.

31. Y. Cheng, M. Wang, Y. Yu, J. Lawson, C. D. Funk, G. A. Fitzgerald, *J Clin Invest.*, 2006, **116** , 1391-1399.

32. C. J. Marmion, D. Griffith, K. B. Nolan, *Eur. J. Inorg. Chem.*, 2004, **15**, 3003-3016.

33. J. L. Wallace, M. N. Muscara, W. McKnight, M. Dicay, P. Del Soldato, G. Cirin, *Thrombosis Research,* 1999, **93**, 43-50.

34. J. A. González-Correa, J. P. De La Cruz, *Cardiovascular Drug Reviews.*, 2006, **24** (1), 11–24.

35. A. Rockwell, M. Melden, R. A. Copeland, K. Hardman, C. P. Decicco, W. F. DeGrando, *J. Am. Chem. Soc.*, 1996, **118**, 10337-10338.

36. B. D. Howes, J. N. Rodriguez-Lopez, A. T. Smith, G. Smulevich, *Biochemistry*, 1997, **36**, 1532-1543.

37. J. Lee, A. J. Chubb, E. Moman, B. M. McLoughlin, C. T. Sharkey, J. G. Kelly, K. B. Nolan, M. Devocelle, D. J. Fitzgerald, *Org. Biomol. Chem.*, 2005, **3**, 3678–3685.

38. S. S. C. Tam, D. H. S. Lee, E. Y. Wang, D. G. Munroe, C. Y. Lau, *J. Biol. Chem.*, 199, **270**, 13948-13955.

39. M. Ouellet, S. M. Aitken, A. M. English, M. D. Percival, *Archives of Biochemistry and Biophysics*, 2004, **431** (1), 107-118.

40. D. L. Evers, X. Wang, S-M. Huong, D. Y. Huang, E-S. Huang, *Anti Viral Research*, 2004, **63** (2), 85-95.

41. L. M. Szewczuk, L. Forti, L. Stivala, T. Penning, *J. Biol. Chem.*, 2004, **279** (21), 22727-22731.

42. W. Zhang, et al., *Bioorg. Med. Chem. Lett.*, 2004, **14**, 4747-4750.

43. http://redpoll.pharmacy.ualberta.ca/drugbank/cgi-bin/getCard.cgi

44. I. K. Larsen, *Acta Crystallography*, 1978, **B34**, 962-964.

45. G. M. Sheldrick, SHELXTL-97, *Programme for Solution and Refinement of Crystal Structure* , Bruker –AXS, Madison, WI, USA, University of Göttingen, 1997.

46. H. L. Yale, *Chem. Rev.*, 1943, **33**, 209-256

47. E. C .O'Brien, S. L. Roy, J. Levaillain, D. J. Fitzgerald, *Inorg. Chim. Acta*, 1997, **266**, 117–120.

48. E. Farkas, D. A. Brown, R. Cittaro and W.K. Glass, *Journal of the Chemical Society, Dalton Trans.*, **18**, 1993, 2803-2807.

49. F. H. Allen, O. Kennard, D. G. Watson, L. Brammer, A. G. Orpen, *J. Chem. Soc., Perkin Trans.* 1987, **2**, S1-S19.

Chapter 3

Attempted Synthesis of a Dual POX/COX Site Inhibitor of PGHS. Synthesis and Crystal Structures of the Cyclic Hydroxamic Acid, 3-Hydroxy-2-methyl-3H-quinazolin-4-one (ChaH) and of its Fe(III), Co(II), Ni(II), Cu(II) and Zn(II) Complexes

3.1	Chapter overview	107
3.2	Metals in medicine – general	107
3.3	Metals in medicine and physiology	109
	3.3.1 Iron	110
	3.3.2 Cobalt	113
	3.3.3 Nickel	115
	3.3.4 Copper	116
	3.3.5 Zinc	118
3.4	Hydroxamic acids	121
	3.4.1 The chemistry of hydroxamic acids	121
	3.4.2 Hydroxamic acids in biology and medicine	127
	3.4.3 Cyclic hydroxamic acids	129
	3.4.4 Aims of the work in this chapter	129
3.5	Experimental - synthesis	131
	3.5.1 Methyl 4-aminobenzoate, 5.	131
	3.5.2 4-Aminophenylhydroxamic acid, 4-AphaH, 6.	131
	3.5.3 Anthranilic hydroxamic acid, 2-AphaH, 2.	132
	3.5.4 3-Hydroxy-2-methyl-3H-quinazolin-4-one (ChaH), 4.	133
	3.5.5 $Fe^{III}(4\text{-Apha})_3.C_2H_5OH$, 8.	133
	3.5.6 $Fe(Cha)_2(Cl)(H_2O).7/2H_2O$, 9.	134

3.5.7 $Co(Cha)_2(C_2H_5OH)_2.H_2O$, 10 and $Co(Cha)_2(C_2H_5OH)_2$, 11. 134

3.5.8 $Ni(Cha)_2(C_2H_5OH)_2$, 12. 135

3.5.9 $Cu(Cha)_2$, 13 and $Cu(Cha)H_2O(Cl)$, 14. 135

3.5.10 $[Zn(Cha)_2].2H_2O$, 15. 135

3.6 Experimental – instrumentation 136

3.6.1 Infrared spectroscopy 136

3.6.2 ^1H, ^{13}C NMR spectroscopy 136

3.6.3 Single crystal X-ray diffraction measurements 136

3.6.4 Mass spectrometry 136

3.6.5 Elemental analysis 137

3.7 Results and Discussion 137

3.7.1 Anthranilic hydroxamic acid, 2, and 4-Aminophenylhydroxamic acid, 6. 137

3.7.2 3-Hydroxy-2-methyl-3H-quinazolin-4-one (ChaH), 4. 139

3.7.3 $[Fe^{III}(4\text{-Apha})_3].C_2H_5OH$, 8. 143

3.7.4 Metal Complexes of the Cyclic Hydroxamic Acid, 3-Hydroxy-2-methyl-3H-quinazolin-4-one (ChaH), 4. 146

3.7.4.1 $Fe(Cha)_2(Cl)(H_2O).^7/_2H_2O$, 9. 147

3.7.4.2 $Co(Cha)_2(C_2H_5OH)_2.H_2O$, 10 and $Co(Cha)_2(C_2H_5OH)_2$, 11. 150

3.7.4.3 $Ni(Cha)_2(C_2H_5OH)_2$, 12. 152

3.7.4.4 $Cu(Cha)_2$, 13 and $Cu(Cha)H_2O(Cl)$, 14. 154

3.7.4.5 $[Zn(Cha)_2].2H_2O$, 15. 156

3.8 Conclusions 158

3.9 References 159

3.1 Chapter overview

Chapter 2 of this thesis described acetylated hydroxamate derivatives which inhibit the cyclooxygenase (COX) site of prostaglandin-H-synthase. In our laboratory inhibitors of the peroxidase (POX) site of this enzyme have also been synthesized. These are anthranilic acid and its derivatives. Since COX site activity is dependent on POX site activity, it was decided to use both of these structural features for the attempted synthesis of dual COX site and POX site inhibitors. The synthesis of acetylated anthranilic hydroxamic acid was therefore attempted in the hope that it would inhibit the COX site by acetylation of Ser530 and that the anthranilic acid group would inhibit the POX site. Unfortunately acetylation of anthranilic hydroxamic acid gave not the desired product but instead the cyclic hydroxamic acid, 3-hydroxy-2-methyl-3H-quinazolin-4-one (ChaH). The formation and structure of this and several of its metal complexes are described in this chapter.

3.2 Metals in medicine – general

Inorganic chemistry has made an important contribution to medical science and human health in the past half century.[1] It has long been known that many metal ions, dissolved in biological fluids, play critical roles in living systems. Whereas metal ions are electron deficient, most biomolecules such as proteins and DNA are electron rich and the combination of the two, giving metal complexes, perform important biological functions.[2]

Indeed, medicinal inorganic chemistry has been practiced for almost 5000 years.[3] The therapeutic applications of metal-based drugs spans diverse disease areas such as treatment of anaemia with iron compounds, of rheumatoid arthritis with gold compounds, of ulcers with bismuth compounds, of diabetes with vanadium compounds, of cancer with cisplatin and related compounds and of bipolar disorder with lithium compounds. Metal complexes such as those of gadolinium(III) have been widely used for a considerable time in imaging. Without doubt, the most well-known metal based drug is cisplatin, *cis*-$[PtCl_2(NH_3)_2]$, discovered in the 1960s.[4] Examples of metal complexes used in medicine are listed in **Table 1.**[5-7] As well as their applications as constituents of drugs, metal ions are also important in biochemistry and physiology.

Metals which are essential for mammalian biochemistry include Na, Mg, K, Ca, V, Cr, Mn, Fe, Co, Ni, Cu, Zn, Se, Mo and Sn while essential non-metallic elements include H, C, N, O, F, P, S, Cl and I. However there is debate about the essentiality of a lot of these elements such as nickel, chromium, silicon and tin.[8]

In the case of metal-based drugs it is important to know which component of the drug is essential for its activity; the metal itself, the ligand(s) or the metal-ligand complex. This is so that improvements in the drug can be achieved by structural modifications and also enables dealing, if necessary, with biodistribution and body clearance issues of toxic metal ions.[9] The use of metals in drugs is not universally popular due to the high molecular weight of metal complexes. According to some, the criteria for any new drug candidate is that it be metal free, neutral, hydrophilic and have a molecular weight less than 400 Dalton.[10]

Table 1: Examples of some metal compounds having medicinal applications. Reproduced from Rosette M Roat-Malone, *Metals in Medicine* in *Bioinorganic Chemistry, A Short Course*, John Wiley & Sons Inc., 2002, Chapter 7.

Metal Present in Drug	Drug Name	Active Compound in the Product	Medicinal Usage
Li	Camcolit	Li_2CO_3	Manic depression
Mg	Magnesia	MgO	Antacid, laxative
Co	Cobaltamin S	Coenzyme vitamin B_{12}	Dietary vitamin supplement
Zn		Zn undecanoate	Antifungal agent e.g. to treat athlete's foot
Sb	Triostam	NaSb(V) gluconate	Antileishmanial (antiprotozoal)
Fe		Fe(II) fumarate,succinate	Dietary iron supplement
Gd	Magnevist™	$[Gd(III)(DTPA)(H_2O)].2DTPA$ DTPA= Diethylenetriamine pentaacetic acid	MRI contrast agent
Pt	Platinol, cisDDP	*cis*-$[Pt(NH_3)_2Cl_2]$	Anticancer agent
Au	Auranofin	$Au(I)(PEt_3)$(acetylthioglucose)	Antiarthritic agent
Bi	De-Nol	$K_3[Bi(III)(citrate)_2]$	Antacid, antiulcer agent

3.3 Metals in medicine and physiology

Metal ions are required for many functions in the human body and deficiency of some metal ions can give rise to ill-health. A well known example is anemia due to iron deficiency. Metal ions, e.g. heavy metal poisons such as lead and mercury, can also cause toxicity. Metal compounds are also used as drugs and one of the best known examples is the anti-cancer drug cisplatin as well as its second generation derivatives oxaliplatin and carboplatin, which also possess anti-cancer activity, **Fig. 1.**

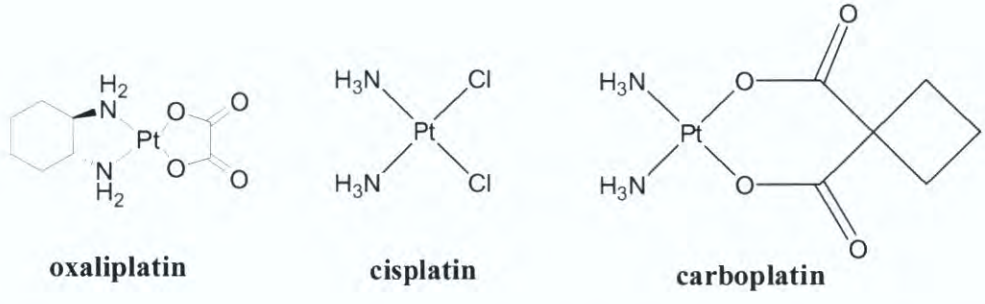

Fig. 1: Platinum antitumor compounds. Reproduced from L. Wei-Ping, Y. Qing-Song, Y. Yao, Chen. Xi-Zhu, H. Shu-Qian, *et al*, *Platinum Metals Review*., **52** (3), 2008, 163-171.

Cisplatin is used in the treatment of a number of solid malignancies and is effective against testicular cancer, making this disease up to 90% curable relative to the previous situation when it was almost completely fatal.[11] Unfortunately, the advent of cisplatin did not bring about a universal cure for cancer, since it is quite inactive against certain types of tumours. The clinical applications of cisplatin have significant side effects such as ototoxicity, nephrotoxicity and acquired or intrinsic resistance.[12] Therefore, much attention has focused on designing new platinum drugs with improved pharmaceutical properties and a broader range of antitumor activity. Thousands of platinum compounds have been tested for antitumor activity in the last 30 years but only less than 30 have reached clinical trials. Strategies for improving activity include the introduction of carrier groups for targeting tumor cells with high specificity.[13]

3.3.1 Iron

Iron is an essential element for almost all living cells. The functions of iron-containing proteins vary widely and include: (1) deoxyribose synthesis, (2) oxygen and electron transport e.g. hemerythrin, haemoglobin, myoglobin, (3) oxygen activation e.g. catechol dioxygenase, cytochrome P-450, (4) phosphoester hydrolysis e.g. uteroferrin, (5) phosphorous storage and transport e.g. phosvitin, (6) iron transport e.g. transferrin, phosvitin, and iron storage e.g. ferritin, phosvitin. Iron also occurs in many diverse metalloenzymes such as oxidases, hydrogenases and reductases.[14]

Iron is the second most abundant metal, after Al, and the fourth most abundant element in the earth's crust. Iron forms compounds in a wide range of oxidation states from –II to +VI, and the most important physiologically are +II and +III, although the +IV and +V states are thought to play roles in the cycles of some haemoprotein catalysed reactions. Most iron(III) complexes are octahedral e.g. $[Fe(H_2O)_6]^{3+}$ although square-pyramidal and trigonal bipyramidal iron(III) complexes are also common.[15]

Haemoglobin (Hb) and myoglobin (Mb) are important in the transport and storage of dioxygen in human body. Each of these proteins bind one molecule of O_2 per Fe^{2+}. The porphyrin present in both is protoporphyrin(IX). In both cases the iron is bound to the porphyrin forming a haem group and a proximal histidine residue from the protein chain completes square pyramidal coordination around the iron. The haem group in deoxymyoglobin and deoxyhaemoglobin contains 5-coordinate iron(II), which is high spin and lies out of the porphyrin plane towards the His residue. Upon oxygenation, Fe^{II} changes from high spin to low spin and moves into the plane of the porphyrin ring and pulls the proximal His residue with it. The movement, resulting from the binding of the first oxygen to haemoglobin, which is difficult because of the taut state caused by salt linkages between the subunits, gives rise to breakage of some of these linkages and opening-up of the structure, allowing the second, third and fourth oxygens to bind more easily. This is known as cooperativity and is very important in the physiological functioning of haemoglobin. Myoglobin does not exhibit this since it is comprised of only one protein chain.

Other examples of haem proteins are cytochromes, which are catalysts for redox reactions. Cytochrome P-450 is the name given to a group of enzymes which act as monooxygenases, catalyzing reactions in which one atom from molecular oxygen is used for substrate hydroxylation and the other atom ends up as water. These enzymes are involved in drug metabolism and other reactions. The active site in cytochrome P-450 is an iron(III)-protoporhyrin IX haem group in which the metal is 6-coordinate and low spin. A cysteinate residue from the protein acts as a fifth ligand and a water ligand completes hexacoordination. The organic substrate binds to the protein near the water ligand and this causes a spin change on the metal from low to high, followed by a one electron reduction of Fe(III) to high spin Fe(II). Binding of dioxygen to the metal occurs at this point and following an intramolecular redox reaction to give Fe(III)-($O_2^{\cdot-}$) and $1e^-$-reduction of the superoxide to a peroxo ligand, heterolytic cleavage of the peroxo ligand gives water and an Fe(V)=O species. This active oxidant transfers one atom of oxygen to the substrate to give the hydroxylated metabolite.[14]

Hemerythrin is a non-haem Fe protein which binds O_2 reversibly and is responsible for O_2 transport in the blood in marine invertebrates such as mollusks and arthropods. The active site consists of two iron atoms, bound to the protein by five His side chain residues leaving a vacant coordination site where dioxygen binds.[16]

The two main iron storage compounds in the human body are ferritin and haemosiderin. Ferritin is important in iron homeostasis, and is made up of an octahedral Fe(III) core with bridging oxide and/or hydroxide ions. Haemosiderin is thought to be a degradable product of ferritin.[17] In mammals, the transport of iron to haemoglobin inside the body is carried out by transferrin, a glycoprotein that binds iron reversibly. The iron(II) after passage through the stomach and uptake into the blood is oxidised to iron(III), which is a more stable form under physiological conditions. It is then picked up by transferrin and transported to other sites of the body i.e. transferrin transports ~ 40 mg of iron to the bone marrow per day.[14]

The poor solubility of iron(III) and precipitation of $Fe(OH)_3$ in aqueous media has forced living systems particularly bacteria to solubilise environmental iron by chelation.

This uses chelators called siderophores (iron-sequestering agents), which are produced by many microorganisms under iron-deficient conditions. Siderophores usually incorporate bi- or multidentate oxygen donors which have high affinities for iron(III). Examples of siderophores are catecholates such as enterobactin, or hydroxamates such as desferrioxamine.[18]

Iron-sulfur enzymes are relatively low molecular weight compounds whose main function is to act in electron transfer processes, in nitrogen fixation, in catalytic sites in hydrogenases and in the oxidation of NADH to $[NAD]^+$. Iron-sulfur proteins contain high spin Fe(III) or Fe(II) coordinated tetrahedrally by four S donors, from either S^{2-} or Cys residues in the protein. Ferredoxins possess several types of Fe/S clusters e.g. Fe_4S_4, Fe_2S_2 and Fe_3S_4. The FeS_4 centres occur singly in rubredoxins but are combined into di-, tri-, or tetra-iron units in ferredoxins, **Fig. 2.**[19]

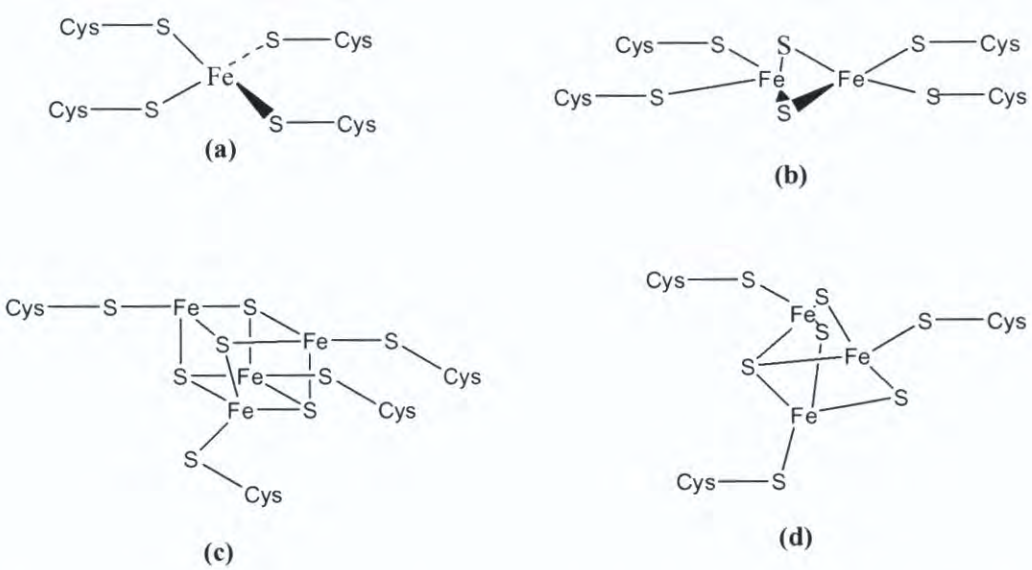

Fig. 2: Structures of Fe/S clusters (a) in rubredoxin and (b)-(d) in ferrodoxins. Reproduced from H. Beinert, *J Biol.Inorg. Chem.*, 2000, **5** (1), 2-15.

Iron compounds are also an important group of organometallic drugs. The discovery of ferrocene, an Fe(II) compound coordinated to two cyclopentadienyl rings, in 1951 opened up a new area of research in organo-metallic chemistry. Ferrocene derivatives have been used in drug design, usually as substitutes for phenyl or alkyl groups. Ferrocene is more lipophilic and electron donating than benzene and its incorporation

into a drug molecule enhances membrane permeability. Ferrocene is also used to deliver iron to biological systems.[17]

3.3.2 Cobalt

Cobalt is a relatively rare element and the concentration of Co (like Ni) in human serum is below 1 μg/L compared with 100 μg/L for zinc, iron and copper.[15] Cobalt always occurs in nature in association with Ni and As. Cobalt forms compounds in a number of oxidation states but the most common are +II, which are mainly octahedral e.g. the pink-coloured $[Co(H_2O)_6]^{2+}$ or tetrahedral e.g. the blue $[CoCl_4]^{2-}$, and +III, nearly all of which are low-spin octahedral. Cobalt(III) shows a particularly high affinity for N donors such as NH_3 and organic amines and its complexes are synthesised by oxidation of Co(II) in solution in the presence of these ligands. All Co(I) complexes have π-acid ligands which stabilize the low oxidation state. The well-recognized biological activity of cobalt is largely confined to vitamin B_{12} the structure of which is shown in **Fig. 3.**

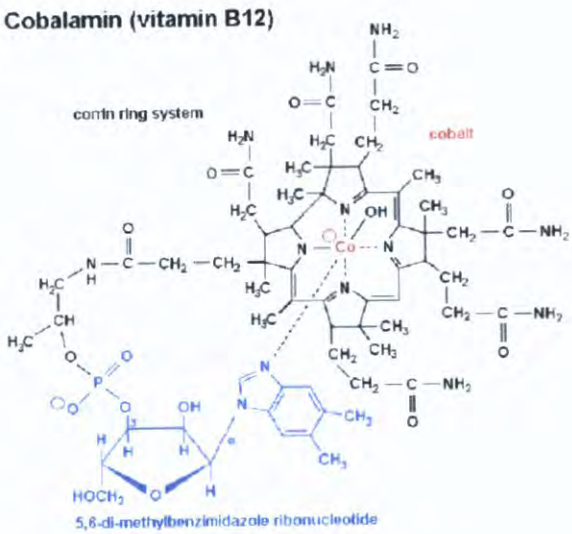

Fig. 3: The structure of methylated coenzyme from vitamin B_{12} which contains cobalt. Reproduced from J.J.R.Frausto da Silva and R.J.P.Williams, *The Biological Chemistry of the Elements, The Inorganic Chemistry of Life, Chapter 16, Nickel and Cobalt*, 2nd Ed., Oxford University Press, 2001.

The cobalt in vitamin B_{12} which is bonded to a corrin ring is sometimes also bound to the side chains of protein residues. The hole in the centre of the corrin ring is smaller than in porphyrins to accommodate and stabilize the relatively small Co(III) by σ-

bonding. A list of some enzymes which contain vitamin B_{12}, either in the simple form or as a coenzyme is given in **Table 2.** With the exception of methyl CoA mutase which occurs in mammals most others are confined to bacteria. Non-vitamin B_{12} cobalt compounds in biological systems include, nitrile hydratase for -CN bond hydration, methionine amino peptidase for removal of terminal methionine from peptides and aldehyde decarbonylase.

Table 2: Some examples of cytosol-localised enzymes requiring B_{12} coenzyme. Reproduced from J.J.R.Frausto da Silva and R.J.P.Williams, *The Biological Chemistry of the Elements, The Inorganic Chemistry of Life, Chapter 16, Nickel and Cobalt,*, 2nd Ed., Oxford University Press, 2001.

Enzyme	Function
Methionine synthase	Conversion of homocysteine into methionine
Methylmalonyl-CoA-mutase	Conversion of methylmalonyl-CoA into succinyl-CoA
Glutamate mutase	Conversion of L-glutamate into L-threo-β-methylaspartate
Diol dehydratase	Conversion of diols into aldehydes
Lysine mutase	Conversion of D-lysine into 2,5-diaminohexanoic acid
Ethanolamine deaminase	Cleavage of amino group in substrate e.g. $NH_2CH_2CH_2OH \longrightarrow CH_3CHO+NH_3$
Ribonucleotide reductase	Reduction of ribonucleotides to the corresponding deoxyribonucleotides

Cobalt and nickel complexes are known to have been important in the electron-rich environment in which life began. This environment had an atmosphere of reducing gases and sulphide and organisms used cobalt and nickel compounds as catalysts to deal with gases such as CH_4, H_2, CO and H_2S.[15, 20] The change of environment to an electron poor one containing O_2, N_2 and CO_2 required a change of metal catalyst and cobalt and nickel compounds are now used mainly in archaebacteria which exist in extremophile environments.

Cobalt complexes also have the potential to modify drug properties. Matrix metalloproteases (MMPs) are a class of enzymes implicated in tumour metastasis and for this reason they are excellent targets for anticancer drugs. It was reported that a Co(III) complex with the tetradentate ligand tris(methylpyridyl)amine (tpa), can act as a

carrier system to deliver and activate the MMP inhibitor marimastat at tumour sites by chelating the hydroxamate functional group of the inhibitor.[21] Ware and Denny [22] have investigated Co(III) complexes of nitrogen mustards as hypoxia activated pro-drugs. The Co(III) complex provides an inert frame-work for transportation of the cytotoxic mustard, allowing cellular uptake by a cycle of reduction and re-oxidation. The hypoxic environment of tumor cells stops re-oxidation and the metal remains in the more labile +II oxidation state, allowing release of the mustard in its active form. This approach has been fairly successful in targeting hypoxic environments but the irreversibility of the redox cycle reduced the effectiveness of the pro-drug.

3.3.3 Nickel

Nickel is a relatively abundant element, comprising approximately 8% of the earth's core and 0.01% of the earth's crust. Organisms have obtained nickel by leaching the most abundant form, Ni^{2+}.[22] Ni(II) forms a large number of complexes with coordination numbers 6, 5, and 4, having octahedral, square pyramidal/trigonal bipyramidal and tetrahedral/square planar geometries respectively.[15] The most common six-coordinate complex in solution is the octahedral, green aqua ion $[Ni(H_2O)_6]^{2+}$. Nickel can exist under physiological conditions in the oxidation states I, II, and III.[15]

Nickel is an essential trace element and is a constituent of at least four types of proteins or enzymes. These include urease, carbon monoxide dehydrogenase (CODH, or acetyl coenzyme A synthese), hydrogenase, and methyl-*S*-coenzyme M reductase **Table 3.**[23,24] Urease, the first enzyme to be crystallized, was isolated from jack beans by Sumner in 1962. Urease catalyses the decomposition of urea to ammonia and carbamate, **equation 1.**[25]

$$(NH_2)_2C{=}O + H_2O \longrightarrow NH_3 + NH_2COO^- \text{ (carbamate)} \quad \text{---------- } \mathbf{1}$$

Table 3: Chemical and physical properties of nickel enzymes in nature. Reproduced from M. J. Kendrick, M. T. May, K. D. Robinson and M. P. Plishka, *Metals in biological systems*, Ellis Horwood, 1992.

Enzyme	Source/ligands	Cofactor/Function
Urease	Bacteria, plants/ O, N from protein.	2Ni/subunit, acid catalysis, water activation, hydrolysis of urea
Hydrogenase	Most bacteria/tetrathiolate	Ni, Fe-S site for H_2 binding and fragmentation
Methyl coenzyme M reductase	Methanogenic bacteria/ tetrapyrrole (F_{430})	Ni tetradesulfurization hydrocorphin (coenzymeF_{430})
Co dehydrogenase	Acetogenic bacteria/ mixed Ni/Fe cluster.	Ni, Zn, Fe-S carbonylation-clusters catalyst for C-C bond formation and cleavage

Urease is a trimer, each protein sub-unit of which contains a redox-inactive dinuclear nickel(II) site i.e. Ni_2^{II}. One of these nickel ions is in a distorted tetrahedral environment and the other in a distorted trigonal bipyramidal environment. One nickel ion is thought to polarize and activate the urea carbonyl group by complexation and the other nickel ion provides the coordinated hydroxo nucleophile, the conjugate base of an aqua ligand, for nuclephilic attach on the urea –C=O group. In contrast to the redox processes involved in other three enzymes in **Table 3**, there is no evidence of metal redox reactions in the Ni^{2+}-ureases catalysed hydrolysis of urea.[23]

Nickel-containing carbonyl dehydrogenase converts CO to CO_2 and also catalyses the synthesis of acetyl-coenzyme A, **equation 2.**[26]

$$CO + H_2O \longrightarrow CO_2 + 2H^+ + 2e^- \quad \text{----------} \quad \mathbf{2}$$

3.3.4 Copper

Copper is the third most abundant metal in the human body, following iron and zinc.[27] Copper was first shown to be an essential biological element in the 1920's,[28] and is present in many metalloproteins and metalloenzymes e.g. blue copper proteins for

electron transfer, haemocyanin for O_2 transport, oxidases or hydroxylases, lysine oxidase, cytochrome oxidase and nitrite reductase [29]

Copper compounds also influence specific gene expression in mammalian cells,[30] and are used as protection against free radicals. The very high ligand affinities of both copper (I) and (II) make them the most effective mono and divalent ions for binding biomolecules at pH 7. Copper (I) is capable of binding π-acid ligands which facilitates the binding of ligands like O_2.[31] The most common use of copper in biology is in electron transfer reactions which are carried out by a group of copper-containing proteins called 'blue copper' proteins due to their intense blue colours. There are three types of copper sites in blue copper proteins: type 1 which is distorted tetrahedral, type 2 which is trigonal bipyramidal and type 3 which has a dinuclear site of distorted tetrahedral copper ions linked by a hydroxo bridge. The geometries of these sites are designed to stabilise Cu(I) relative to Cu(II).[14]

The toxicity associated with platinum drugs which limits its extensive use in the treatment of cancer has prompted investigations of other metal complexes, including those of essential metal ions like Cu(II) for anti-cancer activity.[32] Copper can be toxic to the body when it deviates from its normal metabolism e.g. in Wilson's disease. Complexes of such metals may serve as effective cytotoxic agents.[33] Copper-thiosemicarbazone complexes such as the copper(II) complex of N-(2-benzyloxy-benzylidiene)pyridine-2-carboxamidrazone, PCM, **Fig. 4,** have shown anti-tumour activity against human breast cancer due to the generation of cytotoxic Cu(I) species through intracellular enzymatic reduction. The copper complexes interact with oestrogen receptors in breast cancer cells producing anti-proliferative effects.[33,34]

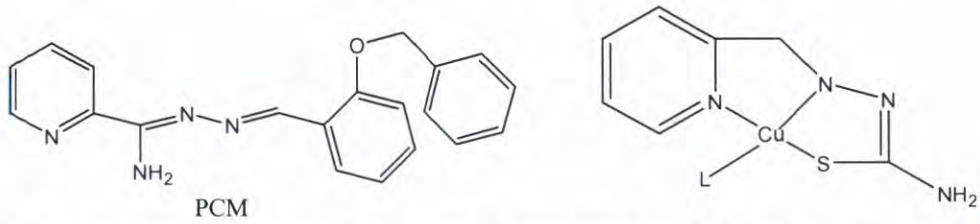

Fig. 4: Structure of an antitumour copper complex. Reproduced from M. Gielen and E. R. T. Tiekink, *Metallotherapeutic Drugs and Metal-based Diagnostic Agents: The Use of Metals in Medicine* Wiley, Chichester, 2005.

The anti-inflammatory role of copper has been attributed to its redox activity arising from the accessibility of the +I and +II oxidation states. For example the ability of copper in enzymes like superoxide dismutase (SOD) to remove the highly reactive superoxide radical O_2^-, by dismutation is summarized in **Scheme 1.**[31, 35]

$$Cu(II) + O_2^- \longrightarrow Cu(I) + O_2$$
$$Cu(I) + O_2^- + 2H^+ \longrightarrow Cu(I) + H_2O_2$$
$$\text{Net}: \ 2O_2^- + 2H^+ \longrightarrow H_2O_2 + O_2$$

Scheme 1

In this reaction SOD catalyses the dismutation of superoxide, which is a by-product of cellular respiration, in the cytoplasm. During dismutation, Cu(II) is reduced by the O_2^-, the resulting metabolites being O_2 and H_2O_2.[36] The most common form of this enzyme contains a dinuclear Cu(II), Zn(II) active site but other metallo forms are also known.

Cu(II) complexes of non-steroidal anti-inflammatory drugs (NSAIDs) play an important role in enhancing the pharmacological profile such as the activity and reduced toxicity of these drugs. There are no Cu(II) anti-inflammatory drugs currently available for oral human use. However an ethanolic gel-base of Cu-salicylate (Alcusal®) is available for topical relief of pain and inflammation in humans.[31] The binuclear copper(II) complex of diclofenac, $[Cu(L)_2 (H_2O)]_2 .2H_2O$, where diclofenac is HL, has been found to possess anti-inflammatory activity.[37]

3.3.5 Zinc

Zinc is the most abundant intracellular trace element, and plays a crucial role in a wide range of cellular processes, including cell proliferation, reproduction and immune function.[38,39] Zinc is essential to all forms of life, and its biochemical functions can be classified as catalytic, acting as a Lewis acid in some enzymes, structural and regulatory.[40] In the adult human body there is 2-3 g of zinc, as compared to 4 -6 g of iron and ~250 mg of copper. Zinc deficiency is associated with growth retardation.[41]

Zinc is required for the catalytic activity of more than 300 specific enzymes. Unlike copper and iron, zinc dose not participate in redox reactions, but functions as a Lewis acid activating complexed substrates.[40] Zinc(II) also stabilizes the tertiary structures of many zinc metalloenzymes and proteins. Common coordination environments of zinc in proteins and enzymes are shown in **Fig. 5.** [42]

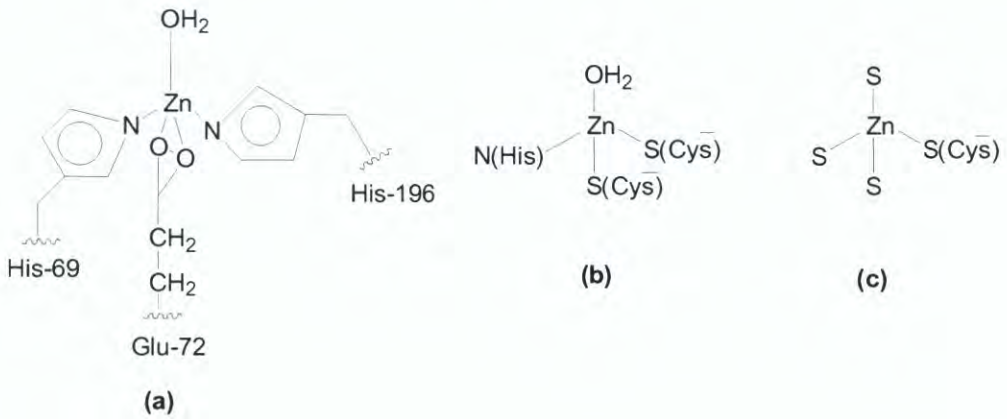

Fig. 5: Basic coordination geometries of Zn(II) in (a) carboxypeptidase A, (b) the catalytic zinc site in alcohol dehydrogenase and (c) the structural zinc site in alcohol dehydrogenase. Reproduced from W. Kaim and B. Schwederski, *Bioinorganic Chemistry: Inorganic Elements in the Chemistry of Life, Chapter 12,* Wiley, New York, 1991.

In addition, H_2O and its conjugate base OH^- are excellent ligands for Zn^{2+} in proteins and enzymes.[24] Therapeutic uses of zinc compounds include treatment of Wilson's disease, a genetic copper overload disorder, to decrease copper absorption. Zinc(II) induces metallothionein synthesis by intestinal mucosal cells and metallothionein has higher affinity for copper than zinc. The copper metallothionein complex is not absorbed but eliminated in the faeces during turnover of intestinal mucosal cells.[43]

The best known zinc enzymes are carbonic anhydrase, carboxypeptidase A, glycolysis enzymes, several proteases and isomerases. In 1940 carbonic anhydrase was the first enzyme shown to contain zinc and in 1955 carboxypeptidase was likewise shown to possess zinc.[44] Carbonic anhydrase, catalyses the hydration of CO_2, **equation 3.**

$$CO_2 + H_2O \rightleftharpoons HCO_3^- + H^+ \quad \text{----------} \quad \mathbf{3}$$

In carbonic anhydrase zinc(II) is bound to three histidine ligands and one water ligand in a distorted tetrahedral structure. The Lewis acidity of the zinc ion polarises the water

ligand, enhancing its acidity ($pK_a \sim 7$) thus ensuring appreciable quantities of the hydroxo conjugate base ligand at physiological pH. In the catalytic cycle of this enzyme the hydroxo ligand acts as a nucleophile attacking CO_2 which is positioned by interactions with the protein close to the zinc(II) , **Scheme 2.**[42] According to some evidence the CO_2 substrate may even be coordinated to the metal close to the hydroxo ligand nucleophile, thus facilitating reaction.

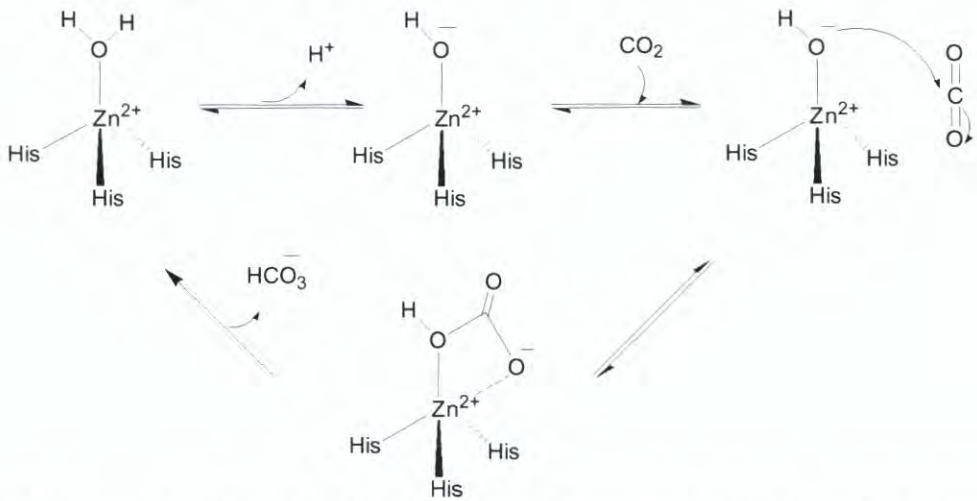

Scheme 2: Proposed mechanism for the formation of hydrogen carbonate from CO_2 at the active site of carbonic anhydrase. Modified from W. Kaim and B. Schwederski, *Bioinorganic Chemistry: Inorganic Elements in the Chemistry of Life, Chapter 12,* Wiley, New York, 1991.

Because Zn^{2+} is a d^{10}, non-redox active metal, it can easily substitute for other divalent cations present in proteins or enzymes. Such a substitution results in increased activity in some cases e.g. bovine superoxide dismutase (BSOD), which is dimeric enzyme that contains two Cu^{2+} ions and Zn^{2+} ions.[45]

3.4 Hydroxamic acids

3.4.1 The chemistry of hydroxamic acids

Hydroxamic acids, are weak organic acids of general formula RCON(R)OH, which have been known since 1869 with the discovery of oxalohydroxamic acid by Lossen.[46] Hydroxamic acids are generally considered to be derivatives of hydroxylamine and carboxylic acids. They have a wide number of applications in medicine and biology, many of which are due to their ability to form stable metal chelates,[47,48] and to release nitric oxide, NO.[49] Acetylated hydroxamic acids can act as effective aspirin analogues by prostaglandin-H-synthase inhibition.[50,51] Hydroxamic acids are used as potent and selective inhibitors of a range of other enzymes including matrix metalloproteases,[52,53] peroxidases,[54,55] hydrolases,[56,57] ureases,[58,59] lipoxygenases,[60] and as hypotensive,[61] anti-cancer,[62] anti-malarial,[63] anti-tuberculosis and antifungal agents.[18] They are also used as therapeutic agents targeting inflammation, cancer, cardiovascular diseases, HIV, Alzheimer's disease.[64,65] and as insecticides,[66] antimicrobials,[67] food additives,[68] and antioxidants.[69]

Hydroxamic acids are typically synthesised by the reaction between hydroxylamine or *O*/*N*-protected hydroxylamines, generated in situ by the addition of base to the hydrochlorides, and activated acyl groups such as carboxylic acid halides, esters, amides, anhydrides and imides, **equation 4.** A large number of solid phase synthetic methods for hydroxamic acids are now known, one of which is a convenient two-step procedure for the parallel synthesis of low molecular-weight hydroxamic acids from carboxylic acids and hydroxylamine with the use of polymer-supported 1-hydroxybenzotriazole.[47, 50]

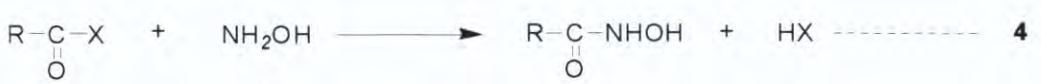

4

Hydroxamic acids can exist in two possible tautomeric forms, the keto tautomer, which is predominant under acidic conditions, and the enol form, which is the dominant form in alkaline medium, **Fig. 6.**[47] NMR studies have shown that each tautomer can exist as (*E*) and (*Z*) isomers in solution.[70] X ray studies have shown that the E form is the more

stable keto form in the solid state while the Z isomer is stabilized in aqueous solution by hydrogen bonding.[71] *Ab initio* molecular orbital calculations on acetohydroxamic acid and formohydroxamic acid found that stabilities follow the order E-keto> Z-keto > Z-enol > E-enol with the E-keto and Z-keto order being reversed on hydration, in agreement with a previous report .[72]

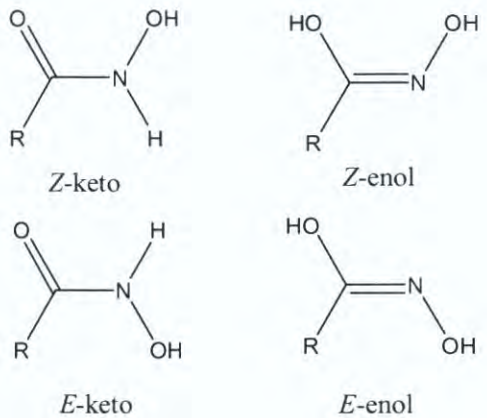

Fig. 6: E/Z keto and enol tautomeric forms of hydroxamic acids. Reproduced from C. J. Marmion, D. Griffith, K. B. Nolan, *Eur. J. Inorg. Chem.*, 2004, **15**, 3003-3016.

Hydroxamic acids form very stable complexes with a wide range of metal ions. The most common type of coordination by far is (O, O) bidentate involving the deprotonated hydroxamate and carbonyl oxygen atoms **Fig. 7.** This gives rise to a very stable 5-membered chelate ring. This structure is demonstrated by the tris-phenylhydroxamato iron(III) complex, **Fig. 8.**[47,73] Hydroxamic acids readily coordinate to a number of transition metal ions such as iron(III), cobalt(II) and nickel(II) in a bidentate manner,[74] generally forming 3:1 octahedral complexes while in the case of copper(II), 2:1 tetragonal complexes with two additional monodentate ligands axially coordinated are formed.

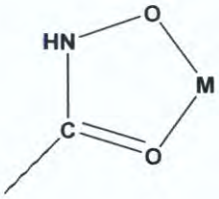

Fig. 7: (O,O)-chelating mode for hydroxamate ligands

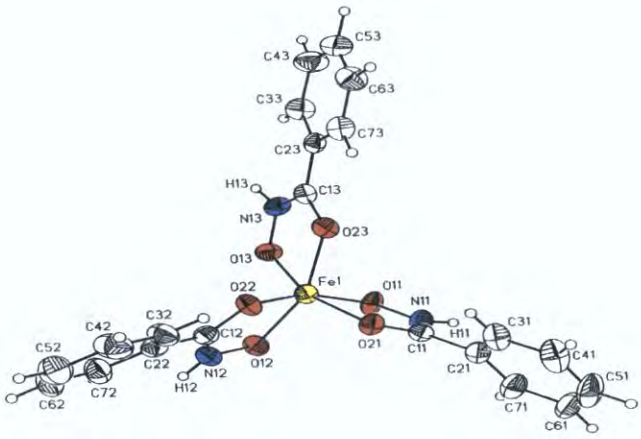

Fig. 8: Crystal structure of $Fe(PhCONHO)_3$

Other modes of coordination are also known but these require special environments. These include monodentate binding through the deprotonated oxygen, a form of binding observed when two adjacent coordination sites around the metal ion are not available. An example of this is the benzohydroxamato complex of octaethylporphyriniron(III), [Fe(OEP)PhCONHO].PhCONHOH, **Fig. 9 (a).**[75] An example of a monodentate nitrogen-bonded hydroxamate complex is the trifluoroacetohydroxamato complex of carbonic anhydrase, **Fig. 10,**[76] a type of coordination which is stabilized by other interactions such as F binding to the metal ion and hydrogen bonding interactions. Bidentate bridging coordination (O, μ-O), **Fig. 9 (b),** is also possible.[75]

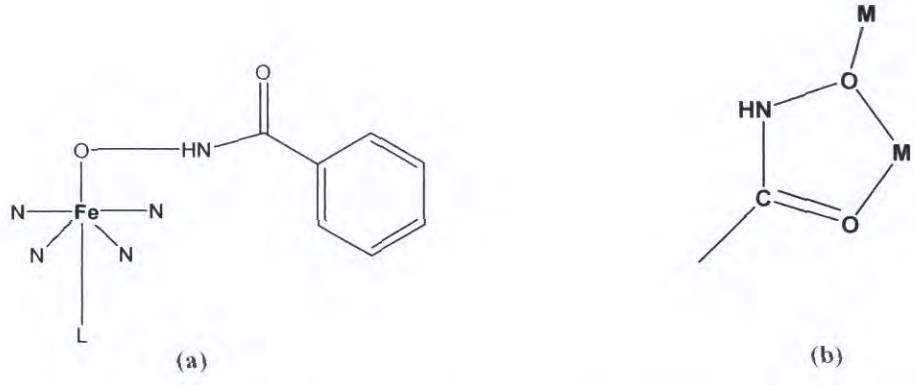

Fig. 9: (a) Monodentate O-bonded benzohydroxamate in [Fe(OEP)PhCONHO]·PhCONHOH. (b) (O,μ-O)-chelating mode. Reproduced from C. J. Marmion, D. Griffith, K. B. Nolan, *Eur. J. Inorg. Chem.*, 2004, **15**, 3003-3016.

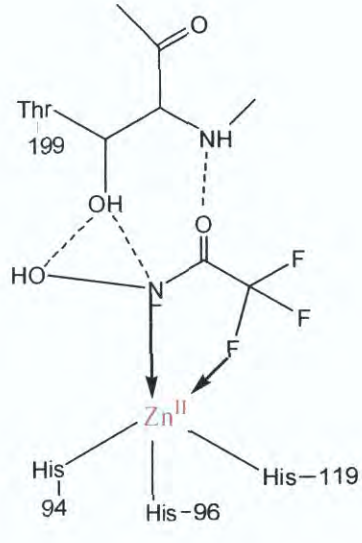

Fig. 10: Monodentate *N*-bonded trifluoroacetohydroxamate complex of carbonic anhydrase (a mimic of the hydrogen carbonate-enzyme product complex. Reproduced from C. J. Marmion, D. Griffith, K. B. Nolan, *Eur. J. Inorg. Chem.*, 2004, **15**, 3003-3016.

The coordination behaviour of the hydroxamate group can be enriched by the incorporation of secondary coordinating groups at adjacent sites. A typical example is that of the α-aminohydroxamic acids which can form O,O- or N,N-bidentate hydroxamate complexes depending on the metal ion and the pH of the medium. Under alkaline conditions, *N,N*- over *O,O*-coordination by copper(II) for α-aminohydroxamate ligands is preferred. Both types of coordination are observed in the dinuclear copper(II)

complex of alaninehydroxamic acid, **Fig. 11,** both alanine ligands forming five-membered rings.[77,78]

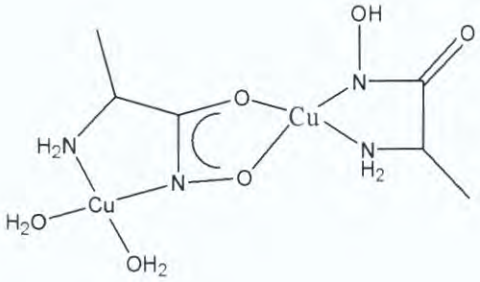

Fig. 11: Two distinct bidentate binding modes α-aminohydroxamic acids with copper(II)

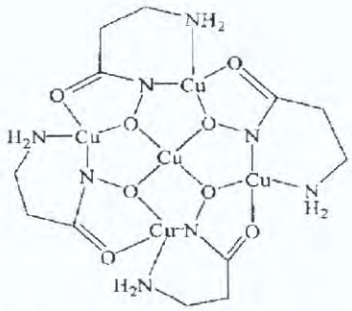

Fig. 12: Structure of the copper((II) metallacrown with β-alaninehydroxamic acid

The coordination properties of β-aminohydroxamic acids are similar to those of the derivatives. Potentially these can act as *N,N*-donors, giving 6-membered ring complexes or *O,O*-donors giving 5-membered ring complexes and in general the latter should be preferred by 1st row d-block metal ions. A remarkable structure was reported by Kozlowski and Farkas for the copper(II) complex with β-alaninehydroxamic acid.[79] This structure, referred to as a metallacrown, contains a twelve-membered ring made up of four copper(II) ions linked in pairs by doubly deprotonated NO groups of hydroxamate ligands and another copper(II) ion occupying a central cavity bonded to four hydroxamate oxygen atoms. The structure displays N,N and O,O binding by the ligand as well the hydroxamate oxygen acting as a bridge between metal ions. An extensive number of metallacrown complexes have since been described mainly by Pecoraro *et al.*[80]

A heptanuclear nickel(II) complex prepared in our laboratory,[81] contains a wide array of hydroxamate coordination modes. Reaction of 2-(dimethylamino)phenylhydroxamic acid (2-dmAphaH$_2$) with $NiSO_4 \cdot 6H_2O$ yielded a heptanuclear complex containing singly deprotonated (2-dmAphaH$^-$) and doubly deprotonated (2-dmApha^{2-}) hydroxamate ligands. This complex has the formula $[Ni_7(2\text{-dmApha})_2(2\text{-dmAphaH})_8(H_2O)_2]SO_4.15H_2O$ and contains a trigonal-bipyramidal array of nickel(II) ions with another two nickel(II) ions at each apex, **Fig. 13.** The complex exhibits four

distinct hydroxamate binding modes, two of which are novel, and these are doubly bidentate/triply bridging, bidentate/triply bridging, bidentate/bridging, and simply bridging, **Fig. 14.**[47,48]

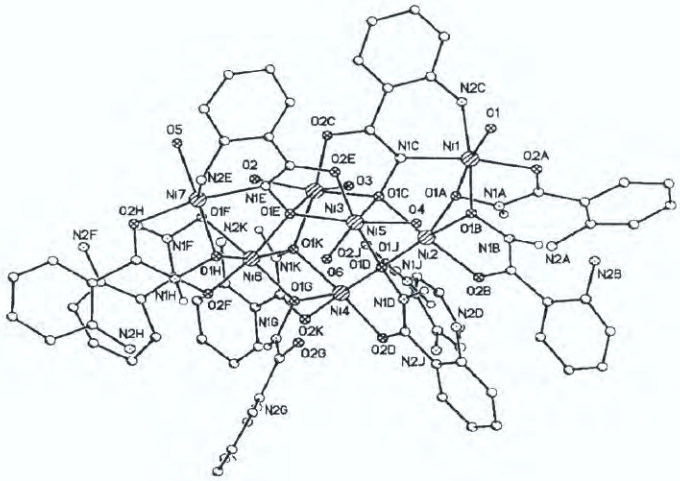

Fig. 13: Molecular structure of $[Ni_7(2\text{-dmApha}^{2-})_2(2\text{-dmAphaH}^-)_8(H_2O)_2]SO_4 \cdot 15H_2O$. From, D. Gaynor, Z. A. Starikova, S. Ostrovsky, W. Haase and K. B. Nolan, *Chem Commun.*, 2002, 506-507.

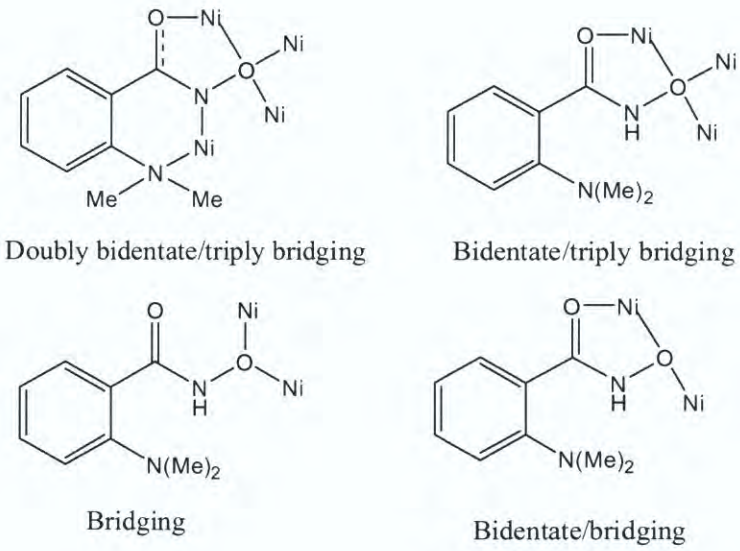

Fig. 14: Binding modes of hydroxamate ligands in $[Ni_7(2\text{-dmApha}^{2-})_2(2\text{-dmAphaH}^-)_8(H_2O)_2]SO_4 \cdot 15H_2O$. From, D. Gaynor, Z. A. Starikova, S. Ostrovsky, W. Haase and K. B. Nolan, *Chem Commun.*, 2002, 506-507.

3.4.2 Hydroxamic acids in biology and medicine

Hydroxamic acids are very important bioligands.[82] One example of this is their presence in siderophores, a class of low molecular weight iron-sequestering agents that possess hydroxamate (or catecholate) groups secreted by bacteria.[83] Organisms, mainly microbial and bacterial, have developed this method by which they increase absorption of iron, an essential element in demand but in poor supply due to its insolubility under physiological conditions.[84,85]

The high affinity and selectivity of siderophores for iron(III) makes them ideal for treatment of conditions related to iron overload.[86] An example is desferrioxamine B (Desferal), a trishydroxamate siderophore, **Fig. 15,** which has three hydroxamate functional groups capable of coordinating Fe(III) in an O,O-bidentate manner. This gives a water-soluble, high-spin, octahedral complex with a very high stability constant, $\log \beta = 30.4$. The iron siderophore complex once inside the cell can undergo reduction to allow utilization of the iron.[87,88]

The main therapeutic application of desferrioxamine B relates to treatment of iron-overload in transfusion-dependent patients such as those suffering from thalassaemia. Thalassaemia is an inherited disease which causes inability to properly synthesise haemoglobin and results in patients becoming anaemic.[89] Thalassaemic patients have regular blood transfusions to supplement their haemoglobin levels but prolonged transfusions leads to vastly elevated levels of iron in the blood and this accumulates in the heart, liver, endocrine glands and other vital organs resulting in death. Desferrioxamine B (Desferal), is administered by prolonged subcutaneous infusion 3 to 7 times per week or by daily intramuscular injections due to its instability in stomach acid. It forms a water soluble iron(III) complex at physiological pH, which can be excreted through the urine. Treatment of thalassaemic patients with regular blood transfusions increases life expectancy by about 20 years. It this treatment is supplemented with desferal it dramatically increases their life expectancy as shown in **Fig. 16.**[18,90]

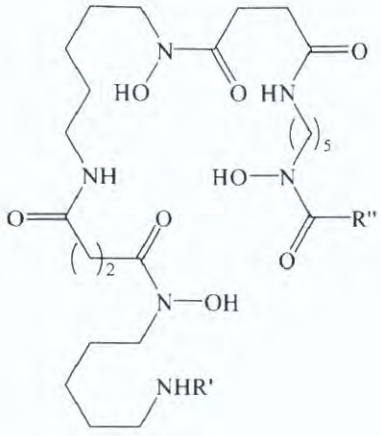

Fig. 15: Hydroxamate siderophore, Desferrioxamine B

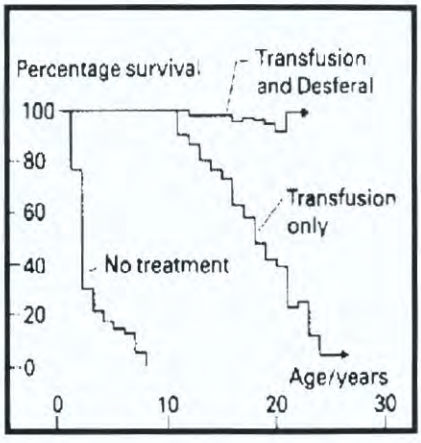

Fig. 16: Patient survival rate for treatment of thalasaemia by transfusion only and by both transfusion and administration of desferrioxamineB.[90]

Another biomedical application of hydroxamic acids is as matrix metalloprotease (MMP) inhibitors and anti-cancer agents. The MMPs are a family of zinc(II)-containing enzymes that are capable of degrading many proteinaceous constituents of the extracellular matrix. Over-expression of MMPs is linked to a number of diseases including arthritis and metastasis.[52,91] Examples are Batimastat and Marimastat which act as MMPs inhibitors and were once being investigated as anti-cancer agents.[92] These compounds contain a hydroxamic acid group, which inhibits the enzyme by O,O chelation of the catalytic zinc(II) ion and by interactions of other groups in the inhibitor with the protein.[52,93]

Other applications of hydroxamic acids derivatives in medicine include their use as inhibitors of histone deacetylase (HDACs),[94] e.g. suberoylanilide hydroxamic acid (SAHA). HDACs are involved in cell cycle progression and differentiation, and cancer. HDAC inhibitors are thought to be promising chemotherapeutic agents due to their low toxicity. Previous studies demonstrated that SAHA has antiproliferative effects on breast cancer cells.[95]

Some hydroxamic acid complexes have been shown to be anti-tumour active. An example of this is the significant cancer growth inhibition (65%) and increased life span

of tumour-bearing mice (150%) when treated with a copper(II)-benzohydroxamate complex.[96]

3.4.3 Cyclic hydroxamic acids

Cyclic hydroxamic acids, which contain the hydroxamate nitrogen and carbon as constituents of a ring, are found in nature. Examples of these include the antibiotics aspergillic acid, structure **1**, and norcadamine.[97-99] Indeed previous studies have shown that cyclic hydroxamic acids were much more effective antimicrobial agents than the structurally related lactams such as kanamycin.[100] Despite the importance of these compounds and the potential importance of their metal complexes there have been relatively few studies on their interaction with metal ions.[101-103] As well as their potential biomedical applications the effects of belonging to a ring system on the complexing properties of these ligands should be of interest.[104]

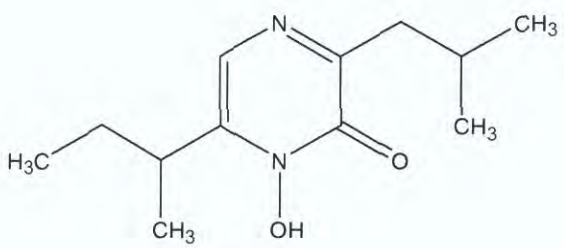

1

3.4.4 Aims of the work in this chapter

We have recently investigated hydroxamic acids as inhibitors of the enzyme prostaglandin-H-synthase (PGHS).[50,51] This enzyme catalyses the first two steps in the biotransformation of arachidonic acid to prostaglandin hormones. PGHS possesses two connected active sites,[105,106] a cyclooxygenase site (COX), which catalyses the addition of two oxygen molecules to arachidonic acid and a spatially distinct peroxidase site (POX), which catalyses the reduction of a hydroperoxide group to the corresponding alcohol. As part of a programme to develop new anti-inflammatory agents we have synthesised acetylated salicylhydroxamic acids which, like aspirin, inhibit the COX site and this by a mechanism similar to inhibition by aspirin,[50] and anthranilic hydroxamic acids which inhibit the POX site.[51] As a

logical extension to this work we attempted the acetylation of anthranilic hydroxamic acid, 2-AphaH, **2**, **Scheme 3**, as a possible dual COX/POX site inhibitor. We hoped that the product of this reaction would inhibit the COX site by acetylation of Ser530 and that the anthranilic acid group would inhibit the POX site. The attempted synthesis however afforded not the acetylated derivative, **3**, but instead the cyclic hydroxamic acid 3-hydroxy-2-methyl-3H-quinazolin-4-one (ChaH), **4**, **Scheme 4,** a compound previously reported.[107] In this chapter is reported the formation and X-ray structures of ChaH and of its complexes with Fe(III), Co(II), Ni(II), Cu(II) and Zn(II). The crystal structure of the related 4-aminophenylhydroxamate, complex $Fe(4\text{-}Apha)_3.C_2H_6O$ was also carried out for structural comparison.

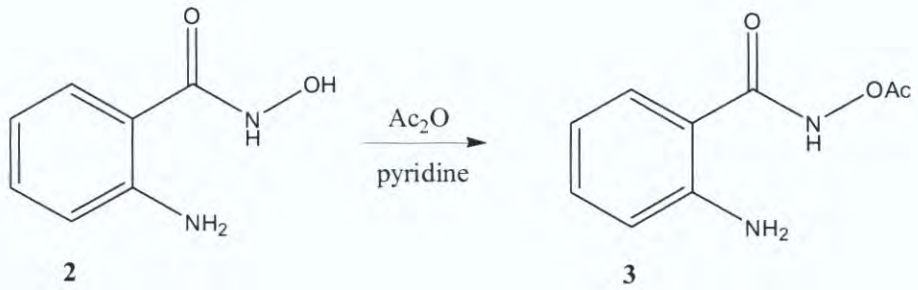

Scheme 3: Attempted Preparation of a Dual COX/POX Site Inhibitor: O-Acetylanthranilic hydroxamic acid

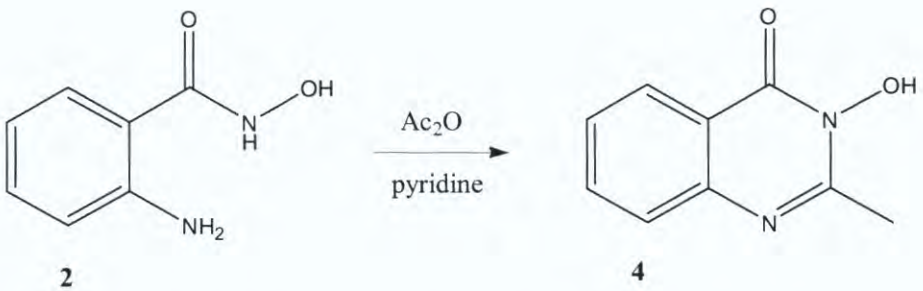

Scheme 4: Product of attempted acetylation of anthranilic hydroxamic acid

3.5 Experimental – synthesis

3.5.1 Methyl 4-aminobenzoate, 5.

Methyl 4-aminobenzoate, **5**, was synthesised as a precursor to 4-aminophenylhydroxamic acid, 4-AphaH, **6.** The synthesis was by modification of a previously reported method.[108,109] Thionyl chloride (7.4 mL, 100 mmol) was added dropwise to a methanolic solution (200 mL) of 4-aminobenzoic acid (10 g, 73 mmol) at 0 °C. The solution was warmed to room temperature and stirred for 24 hours. The solvent was distilled off and this was followed by the addition of water (100 mL) to the residue. A saturated solution of aqueous $NaHCO_3$ was then added and the resulting mixture was extracted with ethyl acetate (2 x 50 mL), dried over Na_2SO_4 and filtered. The filtrate was removed *in vacuo* to give **5** as a brown oil (5 g, 33 mmol, 45%). ^{1}H NMR (400MHz, $CDCl_3$); δ 3.9 (3H, s), 4.01 (2H, s), 6.51 (2H, d, J = 8.4 Hz), 7.7 (2H, d, J = 8.4 Hz). ^{13}C NMR (400 MHz, $CDCl_3$); δ 51.1, 113.3, 119.3, 131.1, 150.4, 166.8. IR (KBr disc); υ_{max} 3465 and 3369 (NH broad), 1683 (ester C=O), 1589, 1435, 1317 and 1288 (CN) cm^{-1}. The compound was obtained in good yield (45%) and excellent purity.[48]

3.5.2 4-Aminophenylhydroxamic acid, 4-AphaH, 6.

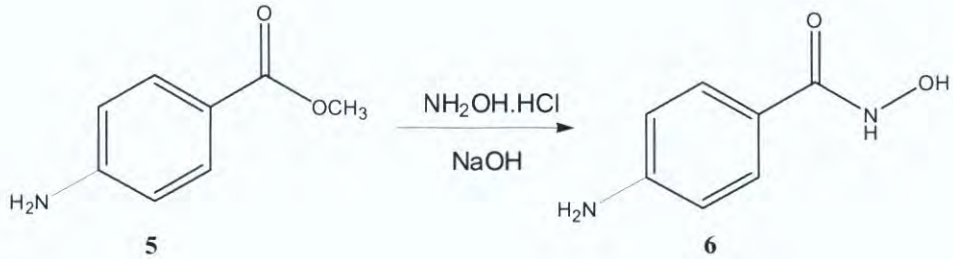

Scheme 5: Synthesis of 4-aminophenylhydroxamic acid, 4-AphaH, **6**

Hydroxylamine hydrochloride (3.475 g, 50 mmol), was added to sodium hydroxide (4 g, 100 mmol), in deionised water (30 mL). The solution was then added to **5** (3.775 g, 25 mmol) in methanol (50 mL) and the resulting solution was stirred for 72 hours, **Scheme 5.** TLC confirmed the disappearance of starting material. The resulting solution was acidified with 5% HCl to pH 6, then evaporated to half volume under reduced pressure and kept in the refrigerator overnight to give light orange crystals

which were collected and dried over P_2O_5 to give **6** (1.5 g, 10 mmol, 40%). ^{1}H NMR (400MHz, d^6-DMSO); δ 5.61 (2H, s), 6.52 (2H, d, J = 8.5 Hz), 7.47 (2H, d, J = 8.5 Hz), 8.68 (1H, s), 10.76 (1H, s). IR (KBr disc); υ_{max} 3414 and 3337 (NH), 1648 and 1603 (hydroxamate C=O), 1558 (CN) cm^{-1}. The compound was obtained in good yield (40%) and excellent purity.[48]

3.5.3 Anthranilic hydroxamic acid, 2-AphaH, 2.

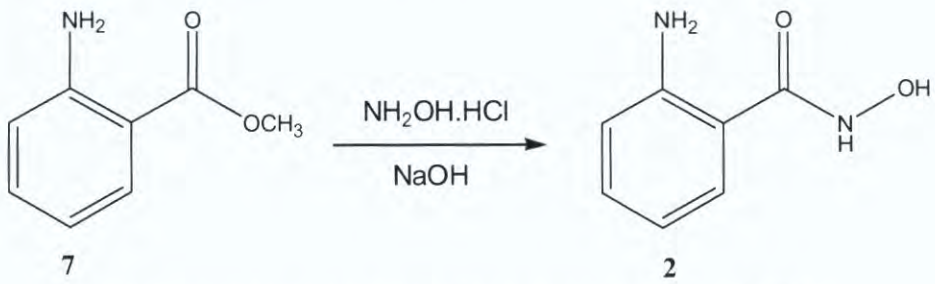

Scheme 6: Synthesis of anthranilic hydroxamic acid, 2-AphaH, **2**

Methyl 2-aminobenzoate, **7**, (purchased from Aldrich with 99% purity) was used without further purification. This ester was reacted with hydroxylamine, generated *in situ,* **Scheme 6**, to give the hydroxamic acid, 2-AphaH, **2**, by modification of a previously reported method.[106,107] Hydroxylamine hydrochloride (6.1 g, 88 mmol) was added to sodium hydroxide (7.0 g, 0.176 mol), in deionised water (50 mL). The solution was then added to methyl-2-aminobenzoate, **7**, (6.0 g, 40 mmol) in methanol (100 mL) and the resulting solution was refluxed for 48 hours and then acidified to pH 6 with 5% HCl. The solvent was removed *in vacuo* yielding an orange-yellow solid to which methanol (50 mL) was added and the sodium chloride removed by filtration. The filtrate was taken to dryness under reduced pressure. Recrystallisation of the residue was performed from hot water to give **2** (4.0 g, 26 mmol, 66%) as pink crystals which were collected by filtration and dried over P_2O_5. ^{1}H NMR (400MHz, d^6-DMSO); δ 6.23 (2H, s), 6.45 (1H, t, J = 7 Hz,), 6.67 (1H, d, J = 7.5 Hz), 7.15-7.1 (1H, m), 7.31 (1H, dd, J = 7.5 and 1 Hz), 8.87 (1H, s), 10.93 (1H, s). IR (KBr disc); υ_{max} 3472 and 3372 (NH), 1652, 1616 (C=O), 1583, 1561 (CN), 1491, 1413 cm^{-1}. The compound was obtained in good yield (66%) and excellent purity.[48]

3.5.4 3-Hydroxy-2-methyl-3H-quinazolin-4-one (ChaH), 4.

Anthranilic hydroxamic acid, **2**, (2 g, 13.16 mmol) was dissolved in dry pyridine (20 mL) under a nitrogen atmosphere and the solution was cooled to 0°C in an ice bath. Acetic anhydride (1.24 mL, 13.16 mmol) was then added slowly via a syringe and the resulting solution was stirred at 0 °C for 30 minutes and then at room temperature for 5 hours. This produced a white precipitate which was washed with 5% HCl (3 x 30 mL), then suspended in de-ionized water and stirred for 2 hours to remove remaining traces of pyridine. The precipitate was collected by filtration, dried over P_2O_5 and recrystallised from minimum hot ethanol to give **4** as white crystals. Yield (1.4 g, 61 %), m. p. 274 - 276 °C. Elemental analysis (%), calcd for $C_9H_8N_2O_2$: C, 61.33; H, 4.60; N, 15.90; found C, 60.79; H, 4.49; N, 15.75. ^{1}H NMR (d^6-DMSO); δ 2.52 (3H, s), 7.51-7.47 (1H, m), 7.62 (1H, d, J = 8.0 Hz), 7.77-7.81 (1H, m), 8.12 (1H, dd, J = 8.0 Hz, J = 1.2 Hz), 11.62 (1H, s). ^{13}C NMR (d^6-DMSO); δ 20.24, 133.90, 146.14, 121.35, 125.77, 126.01, 154.09, 157.66. IR (KBr disc); υ_{max} 3470br, 2571br, 1682vs, 1612s 1478s, 1463s, 1394s, 1239s, 1175s cm^{-1}.[110] The NMR spectra are shown in **Figs. 17-19.** The crystals obtained from the recrystallisation were used for an X-ray structure determination. Crystallographic details and data collection parameters are listed in **Table 4** (Appendix), with a complete list of bond lengths (Å), bond angles (°), hydrogen bonds (Å and°) and torsion angles. The structure is shown in **Fig. 20** with the most important bond lengths/angles in the legend.

3.5.5 [Fe^{III}(4-Apha)$_3$].C$_2$H$_5$OH, 8.

$FeCl_3.6H_2O$ (59.3 mg, 0.22 mmol) in water (5 mL), was added to a solution of 4-AphaH, **6**, (100 mg, 0.66 mmol) in ethanol (15 mL). The pH of the resulting solution was then raised to 5.7 using 0.1 M NaOH solution whereupon a dark red precipitate was obtained. This was removed by filtration and the filtrate was left to stand at room temperature for two months whereupon very dark red crystals were obtained. These were collected by filtration and dried. Yield (100 mg, 0.18 mmol, 82%). Elemental analysis (%), calcd $C_{23}H_{27}N_6O_7Fe$: C, 49.56; H, 5.26; N, 15.08; Fe, 10.02; found C 49.01, H 5.02, N 15.03, Fe 9.77. IR (KBr Disc); υ_{max} 3345br, 3211br, 1604s, 1525s, 1484s cm^{-1}. Crystallographic details and data collection parameters are listed in **Table 5**

(Appendix), with a complete list of bond lengths (Å), bond angles (°) and hydrogen bonds (Å and°) in **Table 13.** The structure is shown in **Fig. 21.**

3.5.6 $Fe(Cha)_2(Cl)(H_2O).^7/_2H_2O$, 9.

$FeCl_3.6H_2O$ (0.139 g, 0.51 mmol) in water (10 mL) was added to a solution of **4** (0.25 g, 1.56 mmol) in methanol (25 mL) at 40 °C. The resulting dark brown solution was left to stand at room temperature for two weeks during which time a dark brown/red crystalline product, suitable for X-ray structure determination was obtained. This was filtered, washed with water and dried. Yield (0.15 g, 0.24 mmol, 66%). Elemental analysis, (%) calcd. For $C_{18}H_{23}N_4O_{8.5}ClFe$: C, 41.36; H, 4.40; N, 10.72; Cl, 6.80, Fe, 10.68; found C 41.01, H 4.00, N 9.97, Cl 6.92, Fe 10.39. IR (KBr disc); υ_{max} 3500br, 3000s, 1614vs, 1569s, 1534vs, 1465s cm^{-1}. Crystallographic details and data collection parameters are listed in **Table 6** (Appendix), with a complete list of bond lengths (Å), bond angles (°), hydrogen bonds (Å and°) and torsion angles. The structure is shown in **Fig. 22** and the most significant bond lengths and angles are given in the legend.

3.5.7 $Co(Cha)_2(C_2H_5OH)_2.H_2O$, 10 and $Co(Cha)_2(C_2H_5OH)_2$, 11.

To a solution of $CoCl_2.6H_2O$ (0.05 g, 0.21 mmol) in water (3 mL) was added with stirring a solution of **4** (0.16 g, 0.92 mol) in hot ethanol (20 mL). The reaction solution was left to stand at room temperature for 2 months during which time a red precipitate was obtained. This was filtered, washed with ethanol and dried. Yield (0.09 g, 0.18 mmol, 86%). Elemental analysis, (%) calcd. for $C_{22}H_{28}N_4O_7Co$: C, 50.84; H, 5.45; N, 10.79, Co, 11.35; found C, 50.71; H, 4.73; N, 11.24, Co, 11.32. IR (KBr disc); υ_{max} 3067br, 1622vs, 1577vs, 1477vs cm^{-1}.[107] Amongst the precipitate described above a small quantity of red crystals of $Co(Cha)_2(C_2H_5OH)_2$, **11**, deposited. These were successfully extracted and were found to be suitable for X-ray structure analysis. Crystallographic details and data collection parameters are listed in **Table 7** (Appendix), with a complete list of bond lengths (Å), bond angles (°), hydrogen bonds (Å and°) and torsion angles. The structure of **11** is shown in **Fig. 23** and the most significant bond lengths and angles are given in the legend.

$Ni(Cha)_2(C_2H_5OH)_2$, 12.

To a solution of $NiCl_2.6H_2O$ (0.05 g, 0.21 mmol) in water (3 mL) was added a solution of **4** (0.081g, 0.46 mmol) in hot ethanol (20 mL). The reaction solution was left to stand at room temperature for 2 months during which time light green crystals suitable for X-ray structure structural analysis, were obtained. These were collected by filtration and washed with ethanol. Yield (0.06 g, 0.12 mmol, 57%). Elemental analysis, (%) calcd $C_{22}H_{26}N_4O_6Ni$: C, 50.87; H, 5.45; N, 10.79, Ni, 11.31; found C, 50.89; H, 5.86; N, 11.20; Ni, 11.83. IR (KBr disc); υ_{max} 3073br, 1607vs, 1577vs, 1472vs cm^{-1} Crystallographic details and data collection parameters are listed in **Table 8** (Appendix), with a complete list of bond lengths (Å), bond angles (°), hydrogen bonds (Å and°) and torsion angles. The structure of **12** is shown in **Fig. 24** and the most significant bond lengths and angles are given in the legend.

3.5.8 $Cu(Cha)_2$, 13 and $Cu(Cha)H_2O(Cl)$, 14.

To a solution of $CuCl_2.2H_2O$ (0.05 g. 0.29 mmol) in water (3 mL) was added with stirring a solution of **4** (0.11 g, 0.64 mmol) in hot ethanol (20 mL). This resulted in the immediate formation of a green precipitate which was collected by filtration and washed with ethanol. Yield: 0.07 g, 0.21 mmol, 73%. Elemental analysis, (%) calcd. for $C_{18}H_{16}N_4O_4Cu$: C, 51.98; H, 3.88; N, 13.47, Cu, 15.28; found C, 51.60; H, 3.57; N, 13.00; Cu, 15.16. IR (KBr disc); υ_{max} 3500-3200br, 1615vs, 1571vs, 1531vs, 1466s cm^{-1}. After two months standing at room temperature the filtrate above produced a very small amount of pale green crystalline material of $Cu(Cha)H_2O(Cl)$, **14**, suitable for X-ray analysis. Crystallographic details and data collection parameters are listed in **Table 9** (Appendix), with a complete list of bond lengths (Å), bond angles (°), hydrogen bonds (Å and°) and torsion angles. The structure of **14** is shown in **Fig. 25** and the most significant bond lengths and angles are given in the legend.

3.5.9 $[Zn(Cha)_2].2H_2O$, 15.

To a solution of $Zn(OAc)_2$ (0.05 g. 0.27 mmol) in water (3 mL) was added a solution of **4** (0.1 g, 0.60 mmol) in hot ethanol (20 mL). The reaction solution was left to stand at room temperature for 7 days during which white crystals suitable for X-ray structure analysis were obtained. These were collected by filtration and washed with ethanol.

Yield (0.08 g, 0.17 mmol, 62%). Elemental analysis, (%) calcd $C_{20}H_{22}N_4O_6Zn$: C, 49.96; H, 4.82; N, 11.65, Zn, 13.60; found C, 49.75; H, 4.53; N, 11.56; Zn, 14.13. IR (KBr disc); υ_{max} 3300-3000br, 1617vs, 1578vs, 1468vs cm^{-1}. Crystallographic details and data collection parameters are listed in **Table 10** (Appendix), with a complete list of bond lengths (Å), bond angles (°), hydrogen bonds (Å and°) and torsion angles. The structure of **15** is shown in **Fig. 24** and the most significant bond lengths and angles are given in the legend.

3.6 Experimental - instrumentation

3.6.1 Infrared spectroscopy

Infrared spectroscopic measurements were obtained using a Bruker Tensor 27 spectrometer. The spectra obtained were analysed using WinFIRST software. All KBr discs were made using FTIR grade KBr purchased from Aldrich.

3.6.2 ^{1}H, ^{13}C NMR spectroscopy

^{1}H NMR spectra were recorded on a Bruker DPX 400 spectrometer operating at 400 MHz at ambient temperatures. The Bruker DPX spectrometer was also used to record ^{13}C NMR spectra at 101 MHz. The spectra obtained were analysed using WIN NMR software.

3.6.3 Single crystal X-ray diffraction measurements

All single-crystal X ray diffraction experiments were carried out by Dr. Helge Müller-Bunz at University College Dublin on a Bruker Smart Apex CCD diffractometer at 100 K using monochromated Mo-K_α radiation, (λ= 0.71073 Å)[111] and the ϕ-ω scan method. The structure was solved by direct method (SHELXS-97)[111] and refined by full-matrix least squares using SHELXL 97-2 package.

3.6.4 Mass spectrometry

Liquid chromatography-mass spectrometry experiments were performed by Dr. Dilip Rai in University College Dublin on a Quattro Micro quadrupole electrospray mass spectrometer (Micromass, Waters Corp., USA). 10 μL of the samples were injected in

300 μL of water: methanol (50:50, v/v). The mass spectrometry data were acquired both in positive and negative ion modes.

3.6.5 Elemental analysis

Elemental analysis were performed at the Microanalytical Laboratory, School of Chemistry and Chemical Biology, University College Dublin.

3.7 Results and Discussion

3.7.1 Anthranilic hydroxamic acid, 2, and 4-Aminophenylhydroxamic acid, 6.

Hydroxamic acids are most conveniently synthesised by reacting activated carboxylic acid derivatives, e.g. an ester or acid chloride with hydroxylamine generated *in situ* by addition of base to one of its salt. In this reaction hydroxylamine acts as a nitrogen nucleophile attacking the carbonyl carbon, to give a tetrahedral intermediate which following loss of the leaving group gives the hydroxamic acid, **Scheme 7.**[108]

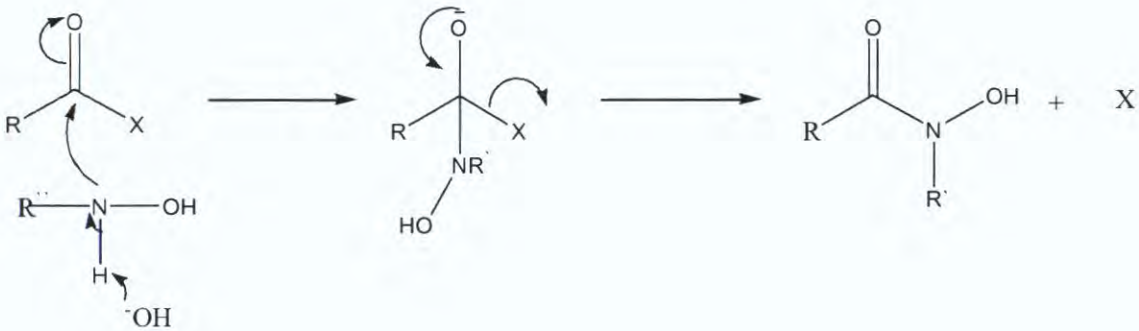

Scheme 7: Mechanism for hydroxamic acid formation from hydroxylamine and activated carboxylic acids.

In the work described in this chapter anthranilic hydroxamic acid, 2-AphaH, **2**, was prepared in ~ 66% yield by reaction of methyl anthranilate which was purchased from Aldrich, with hydroxylamine hydrochloride. 4-Aminophenylhydroxamic acid, 4-AphaH, **6**, was obtained in ~ 40% yield in the same way from methyl-4-aminobenzoate, **5**. This was conveniently obtained in ~45% yield by reaction of the carboxylic acid with thionyl chloride in methanol.[112] This ester was characterised by IR, ^{1}H and ^{13}C NMR data. The IR spectrum showed ν(N-H) bands at 3465 and 3369 cm^{-1}, a ν(C=O) band at 1683 cm^{-1} and a ν(C-N) band at 1317 cm^{-1}. The ^{1}H

NMR spectrum of **5** showed signals at 3.9 ppm due to the CH_3 of the ester group, 4.0 ppm due to the Ar-NH_2 and 6.5-7.7 ppm due to the four aromatic protons.

The hydroxamic acids **2** and **6** were qualitatively identified using a ferric chloride test as hydroxamates form an intense purple complex with iron(III),[113] while neither carboxylic acids or their esters produce such a colour. Each of the hydroxamic acids was characterised by IR, ^{1}H and ^{13}C NMR data. The IR spectra show overlapping ν(N-H), and ν(O-H) bands at ~ 3422 cm^{-1}, ν(C=O) hydroxamate bands at ~1650 cm^{-1} and ν(C-N) bands at ~1560 cm^{-1} , **Table 11.**[114]

Table 11: Infrared spectral data for 2-AphaH, 2, and 4-AphaH,6 .

Assignment	2-AphaH, 2	4-AphaH, 6
ν(N-H, OH)	~ 3422 cm^{-1}	~ 3422 cm^{-1}
ν(C=O)	1652 cm^{-1}	1648 cm^{-1}
ν(C-N)	1561 cm^{-1}	1558 cm^{-1}

The ^{1}H NMR spectra showed in each case a hydroxamate N-H group singlet at ~ 8.7 ppm, an O-H singlet at ~10.8 ppm, resonances due to the aromatic protons in the region ~6.45 – 7.47 and a singlet due to the –NH_2 group protons at ~5.61 for **6** and 6.23 ppm for **2**, **Table 12.**[115]

Table 12: ^{1}H NMR spectral data (δ in ppm) for 2-AphaH, 2, and 4-AphaH, 6.

Assignment	2-AphaH, 2	4-AphaH, 6
O-H (hydroxamate)	δ 10.93 (1H, s)	δ 10.76 (1H, s)
N-H (hydroxamate)	δ 8.87 (1H, s)	δ 8.68 (1H, s)
Aromatic protons	δ 6.45 (1H, t, J = 7 Hz), δ 6.67 (1H, d, J = 7.5 Hz, δ 7.15-7.10 (1H, m), δ 7.31 (1H, dd, J = 7.5 and 1 Hz)	δ 6.52 (2H, d, J = 8.5 Hz), δ 7.47 (2H, d, J = 8.5 Hz)
NH_2	δ 6.23 (2H, s)	δ 5.61 (2H, s)

3.7.2 3-Hydroxy-2-methyl-3H-quinazolin-4-one (ChaH), 4.

The acetylation of anthranilic hydroxamic acid, 2-AphaH, **2**, with one equivalent of acetic anhydride in dry pyridine, followed by recrystallisation of the product from hot ethanol yielded white crystals of the cyclic hydroxamic acid **4** rather than the acetylated product in ~61% yield. These crystals were suitable for structure determination. The proposed mechanism for formation of **4** is shown in **Scheme 8.** This involves acetylation of the amino group followed by nucleophilic attack by the deprotonated hydroxamato nitrogen on the acetyl group carbon giving a tetrahedral intermediate which, following further acetylation and loss of acetic acid, gives the product.

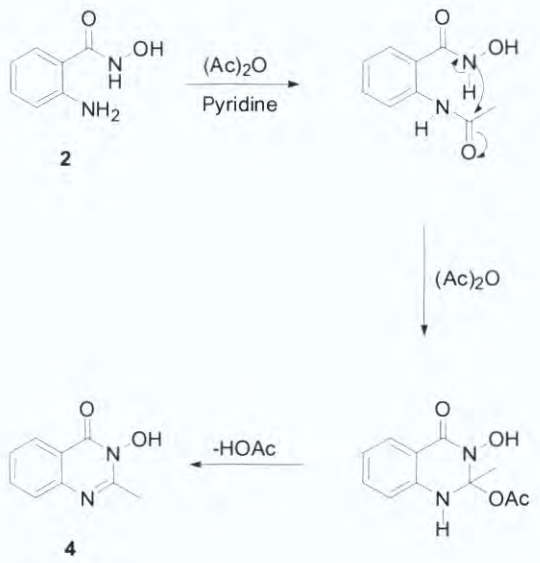

Scheme 8: Proposed mechanism for the formation of the cyclic hydroxamic acid (ChaH), **4**

The structure of **4** was confirmed by microanalysis, IR, ^{1}H-NMR, ^{13}C-NMR and X-ray structural data. Very satisfactory microanalysis was obtained for **4**. The IR spectrum showed clear bands at 3470 cm^{-1} corresponding to ν (OH), a strong absorption at 1682 cm^{-1} due to ν(C=O) of the hydroxamate group, and a strong ν (C=N) band at 1612 cm^{-1}. These IR assignments are based on a comparison with IR data for quinoline derivatives for example quinazoline,[116] which has a similar structure to **4**. The ν(C=O) band is at a much higher wave number than is normally observed for hydroxamic acids (~ 1625 cm^{-1}). This indicates reduced delocalisation of the nitrogen lone pair into the hydroxamate π system resulting in increased π

character of the C=O bond. A possible reason for the reduced delocalization is the presence of a second electron-withdrawing nitrogen in the ring. The ^{1}H NMR spectrum of **4, Figs. 17** and **18,** showed a singlet at δ 2.52 ppm corresponding to the CH_3 group, a multiplet for four aromatic protons between δ 7.51 -8.12 ppm and a very broad singlet at δ 11.62 ppm corresponding to the OH group. The ^{13}C NMR spectrum **Fig. 19,** displayed signals at δ 20.24 ppm for the CH_3 group, δ 133.90 ppm for the phenyl carbon next to the carbonyl group, δ 146.14 ppm for the phenyl carbon next to the nitrogen and signals for the remaining phenyl CH groups at δ 121.35, 125.77, 126.01 and 126.71 ppm. The C=N and C=O signals appeared at δ154.09 and 157.66 ppm respectively.

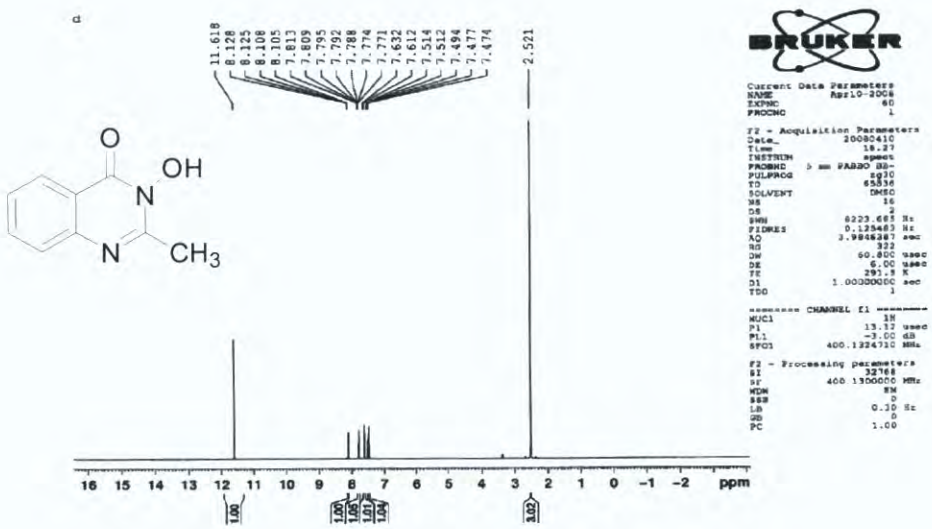

Fig. 17: ^{1}H NMR spectrum (d^6-DMSO, 400 MHz) of **4**

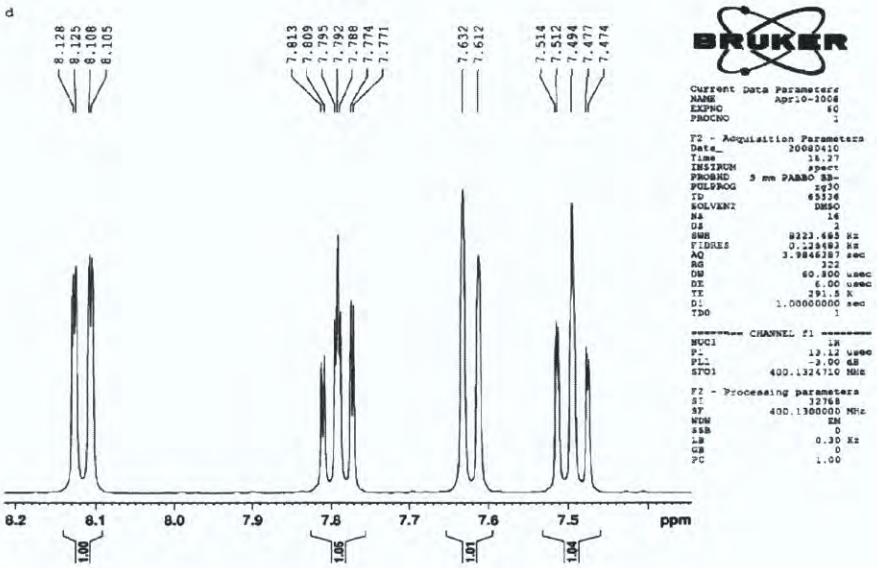

Fig. 18: ^{1}H NMR spectrum (d^{6}-DMSO, 400 MHz) of **4** in the aromatic region

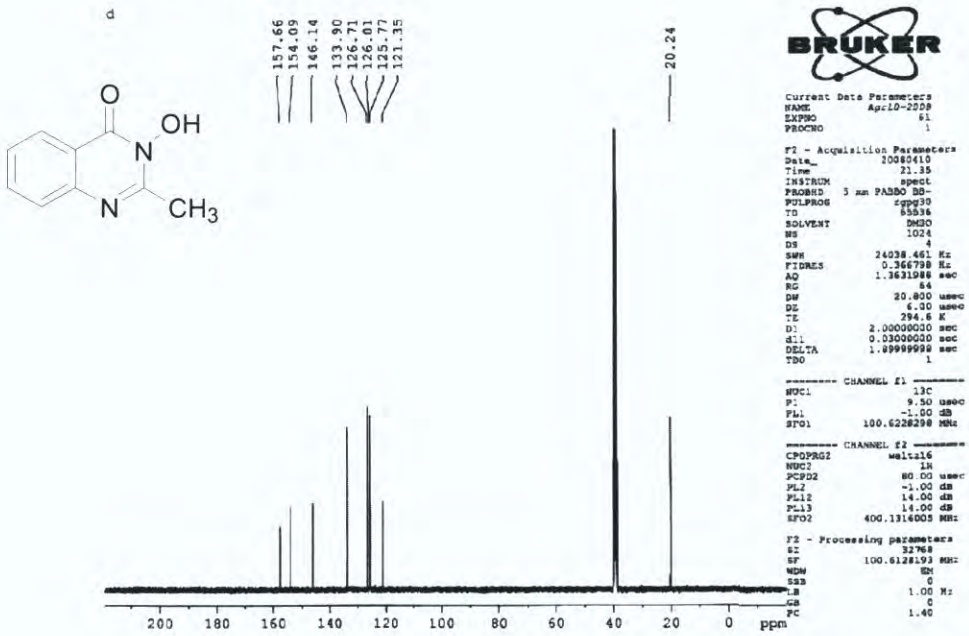

Fig. 19: ^{13}C NMR spectrum (d^{6}-DMSO, 400 MHz) of **4**

Crystals of **4** suitable for X-ray analysis were obtained by recrystallisation from ethanol. The structure of **4** is shown in **Fig. 20** with selected bond lengths and angles in the legend.

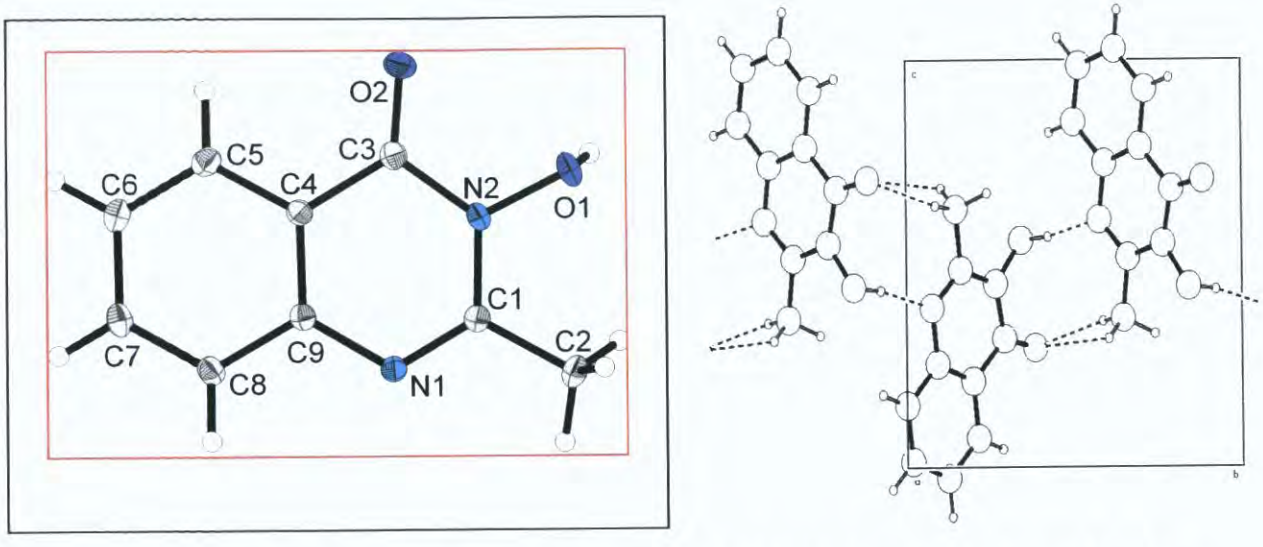

Fig. 20: Molecular structure and atomic labeling scheme for **4** and molecular packing viewed down the a-axis

Selected bond lengths (Å) and angles (°): C(3)–O(2) 1.2149(18), N(2)–O(1) 1.3823(14), N(1)–C(1) 1.3037(18), C(1)–N(2) 1.3689(17), N(2)–C(3) 1.3998(17), C(3)–C(4) 1.4608(17), N(1)–C(9) 1.3906(16); O(1)–N(2)–C(3) 116.60(11), O(2)–C(3)–N(2) 121.54(12), C(1)–N(1)–C(9) 118.67(11), N(1)–C(9)–C(4) 121.84(11), N(1)–C(1)–C(2) 120.34(12), C(5)–C(4)–C(3) 119.52(12), N(2)–C(1)–C(2) 117.70(12), N(1)–C(1)–N(2) 121.95(12), C(1)–N(2)–O(1) 117.90(11), C(1)–N(2)–C(3) 125.12(11), O(2)–C(3)–C(4) 125.99(12), N(2)–C(3)–C(4) 112.47(11), N(1)–C(9)–C(8) 119.15(12), C(9)–C(4)–C(3) 119.88(12). Dashed lines represent the O-H...N and C-H...O interactions within the lattice: O-H = 0.90(3), d = 1.75(3)Å, D=2.645(2) Å, θ= 171(3)° C-H2A = 0.9804Å, d = 2.4718Å, D=3.310(2) Å, θ= 143.23 (3)° C-H2C =0.9804 Å, d = 2.4717 Å, D=3.410(2) Å, θ = 160.29°.

This confirms the cyclic structure of the hydroxamic acid. The main feature of the structure is the length of the N(2)-C(3) bond, 1.3998(17) Å, which is significantly longer than normal (~1.33 Å,[117]) consistent with the IR evidence for reduced π electron delocalisation from N(2) to the hydroxamate group. This effect is also seen in the C(3)-O(2) bond length, 1.2149(18) Å, which is shorter than normal, (~1.25 Å,[117]). Indeed there may be significant π delocalisation from N(2) towards the imine group, since the C(1)-N(2) bond length, 1.3689(17) Å is much shorter that a C-N single bond,[117] and the C(1)-N(1) bond length, 1.3037(18) Å, is longer than normally observed for an imine. Intermolecular interactions involve hydroxamate OH to imine N and carbonyl oxygen to methyl H (H2A, H2C) hydrogen bonding. These interactions generate an infinite one dimensional chain along the base vector [010] giving the supramolecular architecture.

3.7.3 $[Fe^{III}(4\text{-Apha})_3].C_2H_5OH$, 8.

The complex $Fe(4\text{-AphaH})_3.C_2H_5OH$, **8**, was obtained as a dark red precipitate following addition of $FeCl_3.6H_2O$ in an aqueous solution to a solution of 4-AphaH, **6**, in ethanol **Scheme 9.** The complex was obtained in good yield (82%) and characterized by microanalysis, IR spectroscopy and finally by an X-ray crystal structure. The IR spectrum of **8** showed a sharp and intense hydroxamate ν(C=O) band at 1604 cm^{-1} which is shifted from that of the free ligand, 1648 cm^{-1} , upon coordination. This confirms involvement of the carbonyl oxygen atom in coordination to the metal ion. The appearance of a broad band at 3500-3000 cm^{-1} is due to overlapping ν(NH) and ν(OH) bands the latter from the ethanol in the lattice.

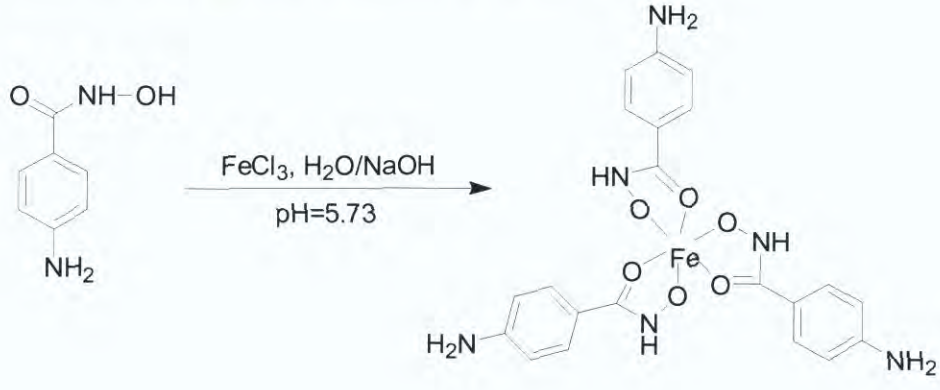

Scheme 9: Synthesis of tris(4-aminophenylhydroxamato)iron(III), 8

Single crystals of **8** suitable for X-ray structure determination were obtained by allowing the filtrate from the reaction mixture to stand at room temperature for two months after adjusting the pH ~ 5.7. The structure of **8** is shown in **Fig. 21** with selected bond lengths and angles in **Table 13.** The crystal structure shows that the iron(III) is in distorted octahedral environment surrounded by three hydroxamate ligands displaying normal bidentate (O, O) coordination to form stable 5-membered chelate rings. This is expected in view of the well known high affinity of Fe(III) for hydroxamic acids.[118,119] The Fe-O bond distances with the negative hydroxamate oxygen atoms are in the range 1.9615(14)-1.9822(14) Å while those with the neutral carbonyl oxygen atoms are in the range 2.0444(14)-2.0654 Å. The former distances are shorter due to charge effects. The mean ΔFe-O value is 0.0787 Å. All angles around the metal deviate, some significantly, from the ideal octahedral angles e.g. O(2)–Fe–

O(3) = 163.96(6)°, O(6)–Fe–O(1) = 162.99(6)°, O(4)–Fe–O(5) = 160.68(6)°, O(2)–Fe–O(6) = 90.72(6)°, O(1)–Fe–O(3) 89.21(5)°, O(5)–Fe–O(6) 78.92(5)°. The bond distances and angles in **8** are comparable to those in similar iron(III)-complexes such as tris(benzohydroxamato)iron(III) trihydrate.[73]

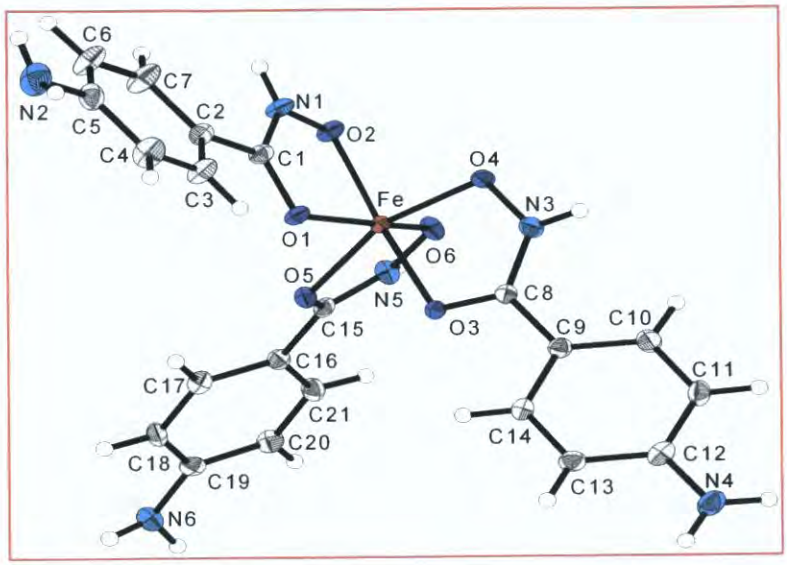

(a)

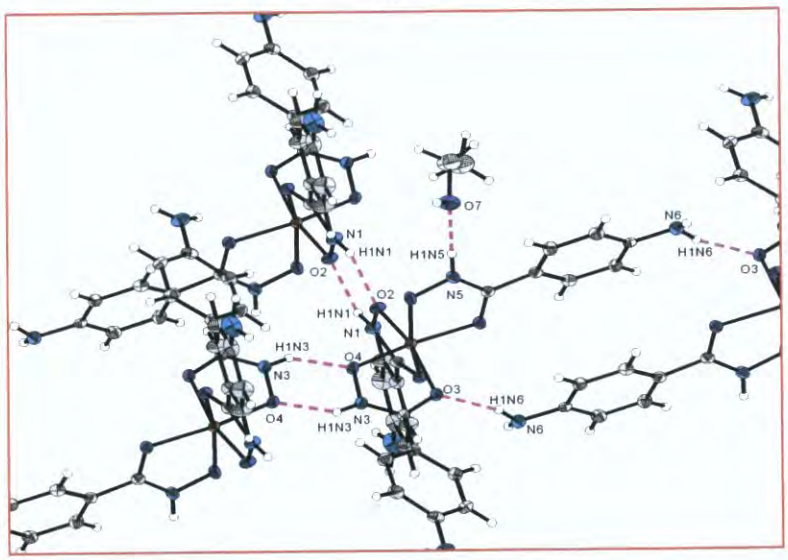

(b)

Fig. 21: (a) Molecular structure and atomic labeling scheme for **8** and (b) intermolecular hydrogen bonding interactions shown by dotted lines. Hydrogen atoms have been omitted for clarity

Intermolecular interactions giving rise to a polymer chain involve hydrogen bonding between (a) the ethanol O and hydroxamate N(5)H, (b) hydroxamate N(1)-H and hydroxamate O(2) of a neighbouring molecule, (c) hydroxamate N(3)-H and

hydroxamate O(4) of a neighbouring molecule and (d) amino group NH and hydroxamate O(3) of a neighbouring molecule chain.

Table 13: Selected bond lengths (Å) and angles (°) and hydrogen bonds (Å and°) for $Fe^{III}(4\text{-Apha})_3.C_2H_5OH$ with estimated standard deviations in parentheses

Fe–O(2)	1.9615(14)	O(6)–N(5)	1.379(2)
Fe–O(6)	1.9769(14)	N(5)–C(15)	1.313(3)
Fe–O(4)	1.9822(14)	C(15)–O(5)	1.285(2)
Fe–O(5)	2.0444(14)	C(15)–C(16)	1.474(3)
Fe–O(1)	2.0470(14)	C(16)–C(17)	1.396(3)
Fe–O(3)	2.0654(13)	C(16)–C(21)	1.400(3)
O(2)–N(1)	1.383(2)	C(19)–N(6)	1.381(3)
N(1)–C(1)	1.315(3)	O(4)–N(3)	1.378(2)
C(1)–O(1)	1.282(2)	N(3)–C(8)	1.304(3)
C(1)–C(2)	1.466(3)	C(8)–O(3)	1.283(2)
C(2)–C(3)	1.394(3)	C(8)–C(9)	1.470(3)
C(2)–C(7)	1.396(3)	C(9)–C(10)	1.398(3)
C(5)–N(2)	1.390(3)	C(9)–C(14)	1.401(3)
C(12)–N(4)	1.368(3)		

O(2)–Fe–O(6)	90.72(6)	N(2)–C(5)–C(4)	120.7(2)
O(2)–Fe–O(4)	92.73(6)	N(2)–C(5)–C(6)	121.0(2)
O(6)–Fe–O(4)	91.70(6)	N(3)–O(4)–Fe	111.77(11)
O(2)–Fe–O(5)	104.13(6)	C(8)–N(3)–O(4)	118.68(16)
O(6)–Fe–O(5)	78.92(5)	O(3)–C(8)–N(3)	117.74(17)
O(4)–Fe–O(5)	160.68(6)	O(3)–C(8)–C(9)	122.39(17)
O(2)–Fe–O(1)	79.40(5)	N(3)–C(8)–C(9)	119.87(17)
O(6)–Fe–O(1)	162.99(6)	C(8)–O(3)–Fe	113.04(12)
O(4)–Fe–O(1)	102.49(6)	C(10)–C(9)–C(14)	118.69(18)
O(5)–Fe–O(1)	90.01(6)	C(10)–C(9)–C(8)	121.53(18)
O(2)–Fe–O(3)	163.96(6)	C(14)–C(9)–C(8)	119.73(17)
O(6)–Fe–O(3)	102.91(6)	N(4)–C(12)–C(13)	121.5(2)
O(4)–Fe–O(3)	78.63(5)	N(4)–C(12)–C(11)	119.96(19)
O(5)–Fe–O(3)	86.98(5)	N(5)–O(6)–Fe	112.13(11)
O(1)–Fe–O(3)	89.21(5)	C(15)–N(5)–O(6)	117.38(16)
N(1)–O(2)–Fe	111.18(11)	O(5)–C(15)–N(5)	118.19(17)

C(1)–N(1)–O(2)	117.85(16)	O(5)–C(15)–C(16)	121.59(17)
O(1)–C(1)–N(1)	117.72(18)	N(5)–C(15)–C(16)	120.18(17)
O(1)–C(1)–C(2)	122.48(17)	C(15)–O(5)–Fe	113.19(12)
N(1)–C(1)–C(2)	119.79(17)	C(17)–C(16)–C(21)	118.42(18)
C(1)–O(1)–Fe	112.64(12)	C(17)–C(16)–C(15)	119.09(18)
C(3)–C(2)–C(7)	118.2(2)	C(21)–C(16)–C(15)	122.41(18)
C(3)–C(2)–C(1)	119.10(18)	N(6)–C(19)–C(20)	120.91(19)
C(7)–C(2)–C(1)	122.69(19)	N(6)–C(19)–C(18)	120.57(19)

D–H...A	d(D–H)	d(H...A)	d(D...A)	<(DHA)
O(7)–H(1O7)...O(6)#1	0.78(3)	1.91(3)	2.694(2)	175(3)
N(6)–H(1N6)...O(3)#2	0.84(2)	2.15(2)	2.968(2)	163.9(19)
N(5)–H(1N5)...O(7)	0.84(2)	1.91(2)	2.740(2)	176(2)
N(3)–H(1N3)...O(4)#3	0.86(3)	1.98(3)	2.755(2)	150(2)
N(1)–H(1N1)...O(2)#4	0.84(3)	1.99(3)	2.737(2)	149(2)

Symmetry transformations used to generate equivalent atoms:
#1 –x+1,–y+1,–z #2 –x+1,–y+1,–z+1 #3 –x,–y+1,–z

3.7.4 Metal Complexes of the Cyclic Hydroxamic Acid, 3-Hydroxy-2-methyl-3H-quinazolin-4-one (ChaH), 4.

Metal complexes of **4** were prepared by addition of an excess of **4** in hot ethanol to aqueous solutions of the metal chloride or the acetate in the case of zinc(II), **Scheme 10.** This resulted in the complexes either as crystals suitable for X-ray structure determination or as precipitates which, after filtration, gave filtrates from which suitable crystals were obtained, **Table 14.** Satisfactory microanalysis were obtained. The IR spectra of all of the complexes showed ν(C=O) hydroxamate bands at ~1607-1625 cm^{-1} which is in the normal range for hydroxamate complexes and is much lower than the free ligand indicative of involvement of this group in complex formation.

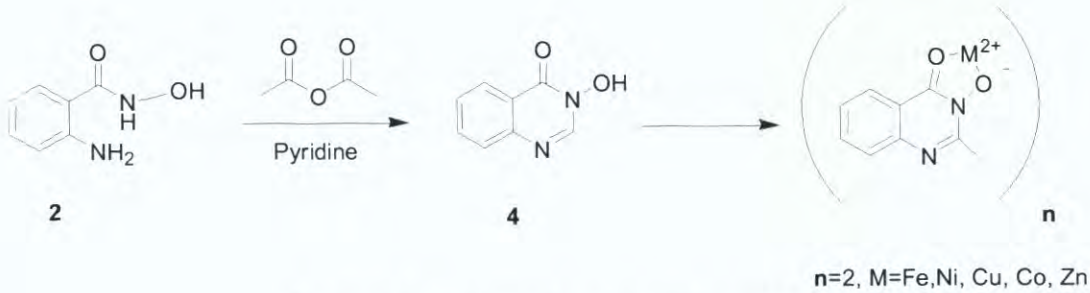

Scheme 10: Synthesis of metal complexes of **4**

Table 14: Crystalline complexes of cyclic hydroxamic acids obtained

Metal salt used	Solvent	Colour of product	Complex obtained
$FeCl_3.6H_2O$	Methanol	Dark-red/brown crystals	$Fe(Cha)_2(Cl)(H_2O).7/2H_2O$
$CoCl_2.6H_2O$	Ethanol	Red crystals	$Co(Cha)_2(C_2H_5OH)_2$
$NiCl_2.6H_2O$	Ethanol	Light green crystals	$Ni(Cha)_2(C_2H_5OH)_2$
$CuCl_2.2H_2O$	Ethanol	Pale green crystals	$Cu(Cha)H_2O(Cl)$
$Zn(OAc)_2$	Ethanol	White crystals	$Zn(Cha)_2.2H_2O$

3.7.4.1 $Fe(Cha)_2(Cl)(H_2O).^7/_2H_2O$, 9.

Complex **9** was obtained as a dark-red/brown crystalline product, in ~66% yield, after standing the reaction mixture at room temperature for a period of 2 weeks. Satisfactory microanalysis was obtained. The IR spectrum of the product showed clear absorption bands at ~3500 cm^{-1} (br) due to ν(O-H) of the aqua ligand and the lattice water, 1614 cm^{-1} (vs) due to ν(C=O) of the hydroxamate group, 1569 cm^{-1} (s) due to ν(C=N) of the imine stretch group. Absorption bands at 1534 cm^{-1} (s), 1465 cm^{-1} (vs) are due to the douple bonds of the aromatic ring. It is interesting to observe that the ν(C=O) band is at a wavenumber much lower than the free ligand (1682 cm^{-1}) indicating that the presence of the metal ion ensures normal delocalisation of the hydroxamate nitrogen lone pair into the hydroxamate π system.

The structure of **9** is shown in **Fig. 22 (a)** with selected bond lengths and angles in the legend and crystal data in **Table 6** (Appendix). The crystal structure shows that the iron(III) is in a pseudo-octahedral environment surrounded by two *cis* hydroxamate ligands displaying normal bidentate O,O-coordination. The two remaining *cis* coordination sites are occupied by a water molecule and a chloride ion. These two sites exhibit disorder with occupancy equally distributed with chloride, Cl / Cl', or water, O5 / O5'. Intermolecular hydrogen bonding involving lattice waters O1W-O5W with imine N, the Cl^- ligand and other lattice waters generate an infinite two dimensional supramolecular structure with large cavities along the base vectors [001] and [100] and along the plane (010), **Fig. 22 (b).** The Fe-O(hydroxamate) bond lengths, 1.964(2) Å and 1.981(2) Å, as expected on the basis of donor atom charges, are shorter than the Fe-O(carbonyl) lengths, 2.048(2) Å and 2.050(2) Å, giving ΔFe-O values of 0.084Å and 0.069Å. These bond lengths are similar to the corresponding bonds in

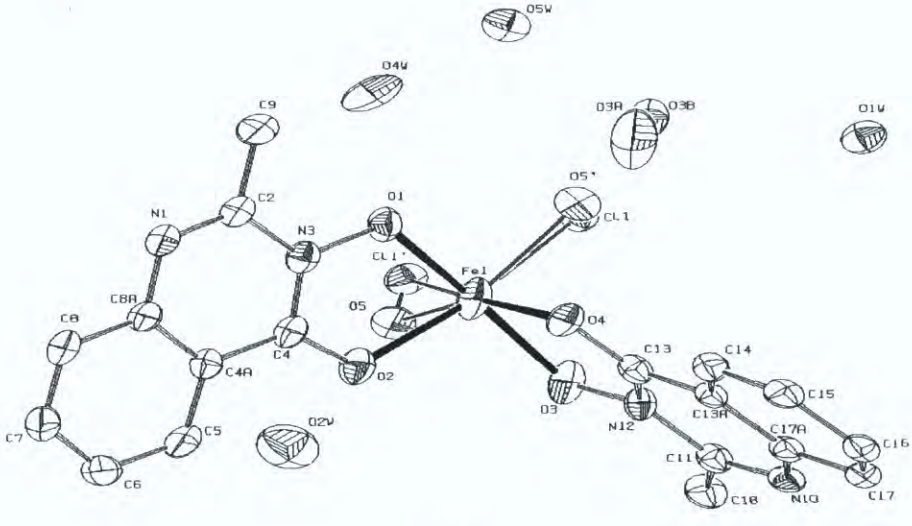

(a)

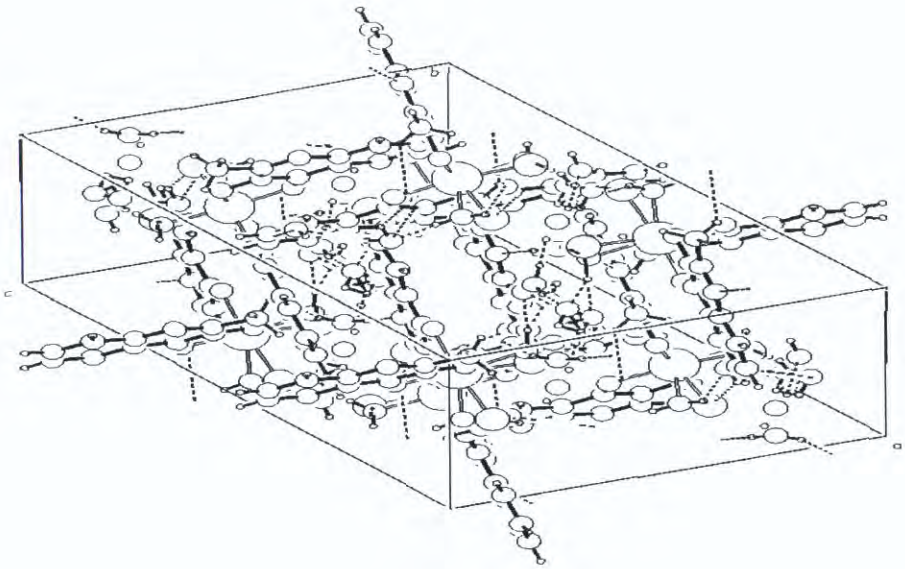

(b)

Fig. 22: (a) Molecular structure and atomic labeling scheme for complex **9** and (b) molecular packing viewed down the b axis

Selected bond lengths (Å) and angles (°): Fe(1)-O(1) 1.964(2), Fe(1)-O(2) 2.048(2), Fe(1)-O(3) 1.981(2), Fe(1)-O(4) 2.050(2), Fe(1)-O(5) 2.093(6), Fe(1)-O(5') 2.149(6), Fe(1)-Cl(1) 2.189(3), Fe(1)-Cl(1') 2.313(2), O(1)-N(3) 1.362(3), O(2)-C(4) 1.274(3), N(1)-C(2) 1.287(4), C(2)-N(3) 1.385(4), N(3)-C(4) 1.350(4); O(1)—Fe(1)—O(3) 170.72(9), O(5)—Fe(1)—O(2) 79.18(8), O(3)—Fe(1)—O(2) 95.11(9), O(1)—Fe(1)—O(4) 93.97(8), O(3)—Fe(1)—O(4) 78.61(8), O(2)—Fe(1)—O(4) 89.92(8), O(1)—Fe(1)—O(5) 103.9(2), O(3)—Fe(1)—O(5) 82.0(2), O(2)—Fe(1)—O(5) 79.65(17), O(4)—Fe(1)—O(5) 157.1(2), O(1)—Fe(1)—O(5') 82.82(18), O(2)—Fe(1)—O(5') 161.18(18), O(3)—Fe(1)—O(5') 102.00(18), O(4)—Fe(1)—O(5') 85.87(17), O(1)—Fe(1)—Cl(1) 94.37(8), O(3)—Fe(1)—Cl(1) 92.15(9), O(2)—Fe(1)—Cl(1) 170.46(9), O(4)—Fe(1)—Cl(1) 97.59(10), O(5)—Fe(1)—Cl(1) 95.27(19), O(1)—Fe(1)—Cl(1') 95.69(8), O(2)—Fe(1)—Cl(1') 98.37(8), O(3)—Fe(1)—Cl(1') 92.36(8), O(4)—Fe(1)—Cl(1') 168.29(8), O(5')—Fe(1)—Cl(1') 88.78(17), O(1)—N(3)—C(2) 119.3(2), O(2)—C(4)—N(3) 117.7(3).

$Fe(C_6H_5CONHO)_3$,[73] and in the 4-aminophenylhydroxamate complex **8** which are in the range 1.9689(18) Å – 1.9753(19) Å and 1.9615(14)-1.9822(14)Å respectively for the Fe-O(hydroxamate) bonds and 2.0356(18) Å – 2.0585(17)Å and 2.0444(14)-2.0654 Å respectively for the Fe-O(carbonyl) bonds. The mean ΔFe-O values are similar for all three complexes i.e. 0.0765 Å for **9**, 0.0787 Å for **8** and 0.0787Å for $Fe(C_6H_5CONHO)_3$. The difference in the Fe-Cl bond lengths, 2.189(3), and 2..313(2) Å, the latter of which is close to the reported average for Fe(III)–Cl bonds,[120] may be because of a *trans* influence, the longer bond being trans to the hydroxamate oxygen while the shorter is trans to the neutral carbonyl oxygen. The Fe-O(water) bond lengths 2.093(6) and 2.149(6) are close to the reported average

for Fe(III)-O(water) bonds.[120] The hydroxamate N to carbonyl C bond, N(12)-C(13) 1.361(4)Å, is shorter than the corresponding bond in **2** consistent with the IR evidence for increased delocalisation of the nitrogen lone pair of electrons into the hydroxamate π system in the complex. The bond angles around the metal 78.61(8) – 103.9(2)° and 161.18(18)-170.46(9)° indicate considerable distortion from octahedral geometry.

3.7.4.2 $Co(Cha)_2(C_2H_5OH)_2.H_2O$, 10 and $Co(Cha)_2(C_2H_5OH)_2$, 11.

Complexes **10** and **11** were obtained as a red precipitate and red crystals respectively from the reaction mixture after a period of two months. The red precipitate of **10** was obtained in ~86% yield. It gave a satisfactory microanalysis and its IR spectrum showed prominent absorption bands at ~3067 cm^{-1} (br) due to v(O-H) of the ethanol ligand and the lattice water, 1622 cm^{-1} (vs) due to v(C=O) of the hydroxamate group, 1577 cm^{-1} (s) due to v(C=N) of the imine and 1477 cm^{-1} due to the aromatic ring. The red crystals of **11** were suitable for X-ray structure analysis and the structure is shown in **Fig. 23 (a)** and **(b),** respectively with selected bond lengths and angles in the legend.

In **11** the metal ion lies in a pseudo-octahedral environment, which is the most commonly reported coordination geometry for Co(II),[120] containing two hydroxamate ligands displaying normal bidentate O,O-coordination and two *trans* ethanol ligands axially coordinated.

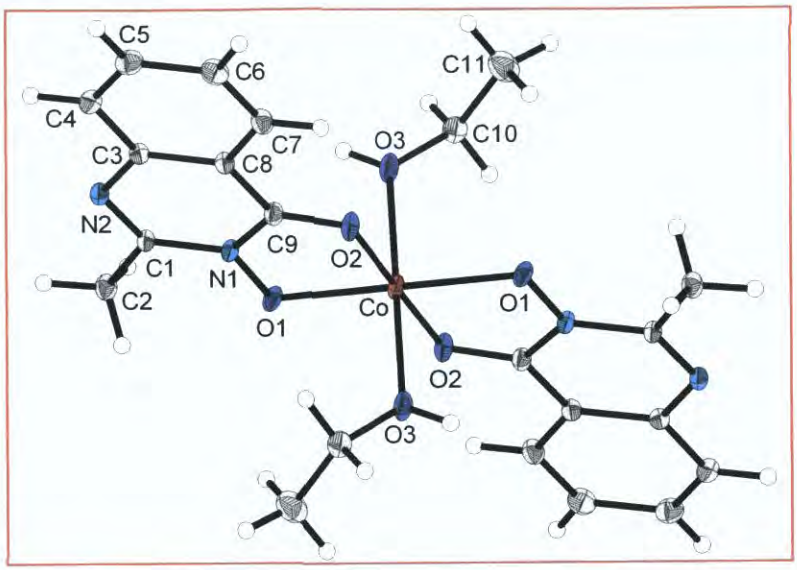

(a)

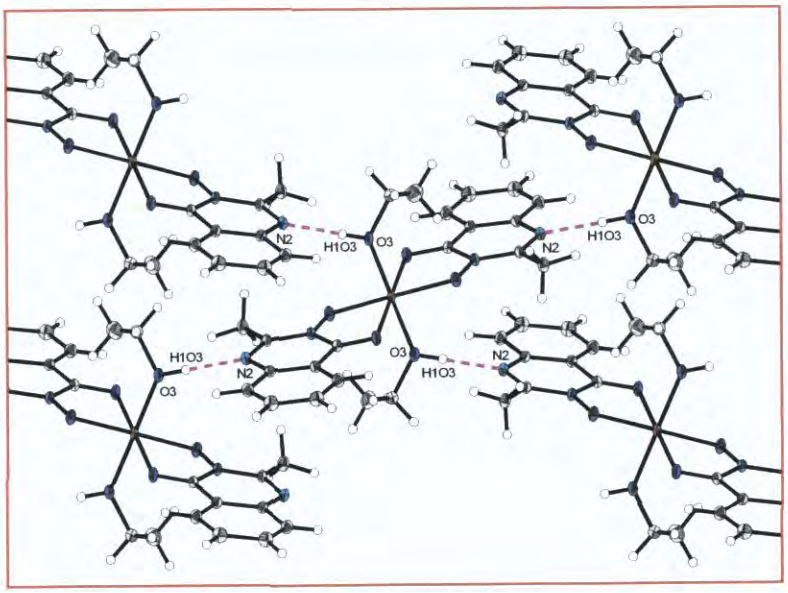

(b)

23: (a) Molecular structure and atomic labeling scheme for complex **11** and (b) molecular packing viewed down the b axis

Selected bond lengths (Å) and angles (°): Co–O(1) 2.0323(8), Co–O(2) 2.1253(8), Co–O(3) 2.1126(8), O(1)-N(1) 1.3576(10), N(1)–C(9) 1.3806(12), C(9)–O(2) 1.2501(12), N(1)–C(1) 1.3752(12), C(1)–N(2) 1.3083(13); O(1)–Co–O(1a) 180.0, O(1)–Co–O(3) 88.48(3), O(1a)–Co–O(3) 91.52(3), O(1)–Co–O(3a) 91.52(3), O(1a)–Co–O(3a) 88.48(3) O(3)–Co–O(3a) 180.0, O(1)–Co–O(2) 78.96(3), O(1a)–Co–O(2) 101.04(3) O(3)–Co–O(2) 87.33(3), O(3a)–Co–O(2) 92.67(3), O(1)–Co–O(2a) 101.04(3) O(1a)–Co–O(2a) 178.96(3) O(3)–Co–O(2a) 192.67(3), O(3a)–Co–O(2a) 187.33(3), O(2)–Co–O(2a) 180.0 O(2)–C(9)–C(8) 125.23(9) O(2)–C(9)–N(1) 119.55(9), O(1)–N(1)–C(9), 118.37(8).

As in the hydroxamate complexes discussed above and in others,[73] the M-O(hydroxamate) bonds, 2.0323(8) Å are shorter than the M-O(carbonyl) bonds,

2.1253(8) Å giving ΔCo-O = 0.0930 Å. The M-O(EtOH) bonds lengths are 2.1126(8) Å similar to the reported averages for octahedral complexes of cobalt(II) with neutral oxygen donor atoms.[120,121] The O-Co-O bond angles indicate relatively minor distortions from octahedral geometry. Intermolecular hydrogen bonding involving the imine nitrogens and EtOH ligands in **11** generate infinite two dimensional networks along the base vectors [0 0 1] & [0 1 0] and through the plane (-1 0 0).

The structure of **10** is likely to be similar to **11** but with a lattice water attached.

3.7.4.3 $Ni(Cha)_2(C_2H_5OH)_2$, 12.

Light green crystals of **12** were obtained in ~57% yield by allowing the reaction mixture to stand for 2 months at room temperature. The complex gave a satisfactory microanalysis and its IR spectrum showed clear absorption bands at ~3073 cm^{-1} (br) due to ν(O-H) of the ethanol ligand, 1607 cm^{-1} (vs) due to ν(C=O) of the hydroxamate group, 1577 cm^{-1} (s) due to ν(C=N) of the imine stretch group. Absorption bands at ~1472 cm^{-1} (vs) are due to the double bonds of the aromatic ring. The crystal structure of **12** is shown in **Fig. 24 (a)** and **24 (b)** with a list of important bond distances and angles given in the legend.

The structure of **12** is very similar to that of **11**. In **12** the metal ion is in a pseudo-octahedral environment, which is a very commonly reported geometry for Ni(II),[120] containing two hydroxamate ligands displaying normal bidentate O,O-coordination and two *trans* ethanol ligands axially coordinated. As in the case of the previously reported compexes the Ni-O(hydroxamate) bonds, 2.0181(10)Å, are shorter than the Ni-O(carbonyl) bonds, 2.0629(10) Å, giving ΔNi-O = 0.0448 Å. The Ni-O(EtOH) bonds lengths are 2.0794(11) Å similar to the reported averages for octahedral complexes of these metal ions with neutral oxygen donor atoms.[120,121] As is usually observed the Ni-O bond lengths are shorter than the corresponding Co-O bond lengths because of the higher charge density of Ni(II) relative to Co(II). The O-Ni-O bond angles in **12** e.g. O(1)–Ni–O(1a)= 180.0°, indicate relatively minor distortions from octahedral geometry. Intermolecular hydrogen bonding involving

the imine nitrogens and EtOH ligands generate infinite two dimensional networks along the base vectors [0 0 1] & [0 1 0] and through the plane (-1 0 0).

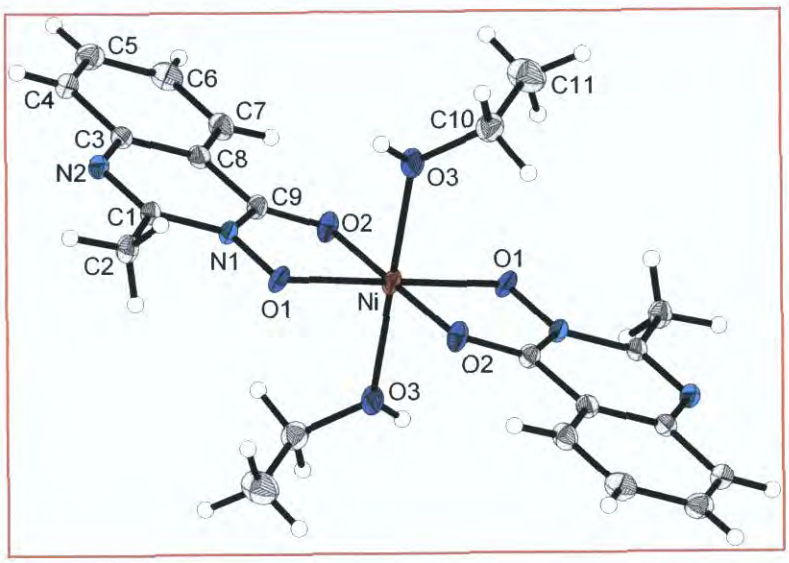

(a)

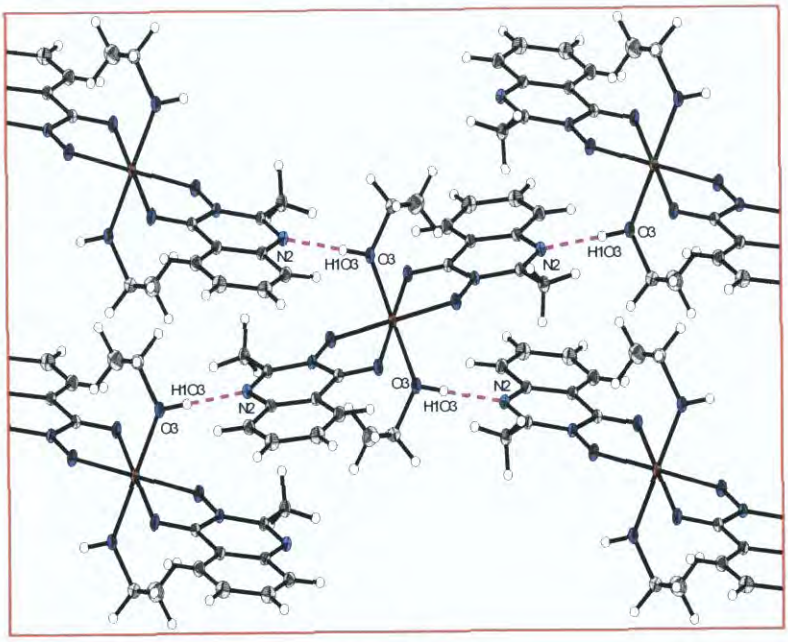

(b)

Fig. 24: (a) Molecular structure and atomic labeling scheme for complex **12** and (b) molecular packing viewed down the b axis

Selected bond lengths (Å) and angles (°): Ni–O(1) 2.0181(10) Ni–O(2) 2.0629(10), Ni–O(3) 2.0794(11) O(1)-N(1) 1.3565(14) , N(1)–C(9) 1.3778(17) , C(9)–O(2) 1.2509(17), N(1)–C(1) 1.3739(17), C(1)–N(2) 1.3070(17), O(1)–Ni–O(1a) 180.0, O(1)–Ni-O(3) 88.38(4), O(1a)–Ni–O(3) 91.62(4), O(1a)–Ni–O(3a) 88.38(4), O(1)–Ni–O(2) 80.68(4), O(1a)–Ni–O(2) 99.32(4), O(2)–Ni–O(3) 87.75(5), O(3a)–Ni–O(2) 92.67(3), O(1)–Ni–O(2a) 99.32(4), O(1a)–Ni–O(2a) 80.68(4), O(2)–Ni–O(3a) 92.25(5), O(3)–Ni–O(2a) 192.67(3).

3.7.4.4 $Cu(Cha)_2$ 13, and $Cu(Cha)H_2O(Cl)$, 14.

Complexes **13** and **14** were obtained as a green precipitate and pale green crystals respectively from the reaction mixture after a period of two months. The green precipitate of **13** was obtained in ~73% yield. It gave a satisfactory microanalysis and its IR spectrum showed clear absorption bands at ~3500-3200 cm^{-1} (br) due to ν(O-H) of the water ligand, 1615 cm^{-1} (vs) due to ν(C=O) of the hydroxamate group , 1571 cm^{-1} (vs) due to ν(C=N) of the imine stretch group and ~ 1531 cm^{-1} (vs), 1466 cm^{-1} (vs) for the double bonds of the aromatic ring. The pale green crystals of **14** were suitable for X-ray structure analysis and the structure is shown in **Fig. 25,** with selected bond lengths and angles in the legend.

In **14** the copper(II) lies in a square pyramidal environment, which is a commonly reported coordination geometry for Cu(II),[120,122] containing two hydroxamate ligands displaying normal bidentate O,O-coordination, a bridging chloride and a water ligand in the basal plane and a bridging chloride in the axial position. As in the previously discussed and other complexes containing hydroxamate ligands,[73] the M-O(hydroxamate) bond, 1.9198(15) Å, is shorter than the M-O(carbonyl) bond 1.9944(14) Å giving Δ(Cu-O) = 0.0746 Å. The Cu-O(water) bond length 1.9386(17) Å falls in the reported range for Cu-O(water) bonds in the basal position of square planar copper(II) complexes.[120,122] The Cu-Cl (basal) and Cu-Cl(axial) bond lengths, 2.2256(6) Å and 2.7080(6) Å are similar to those reported for copper(II) complexes e.g. $[Cu_2(\mu\text{-}Cl)_2(pabh)_2]\cdot 4H_2O$ (Hpabh is pyridine-2-carbaldehyde-benzoylhydrazone), which has both these types of bridging chloride ligand, 2.2177(11) Å 2.7821(13) Å.[123] The O-Cu-O and O-Cu-Cl bond angles 82.81(6)-95.92(5)° confirms the distorted square pyramidal geometry.

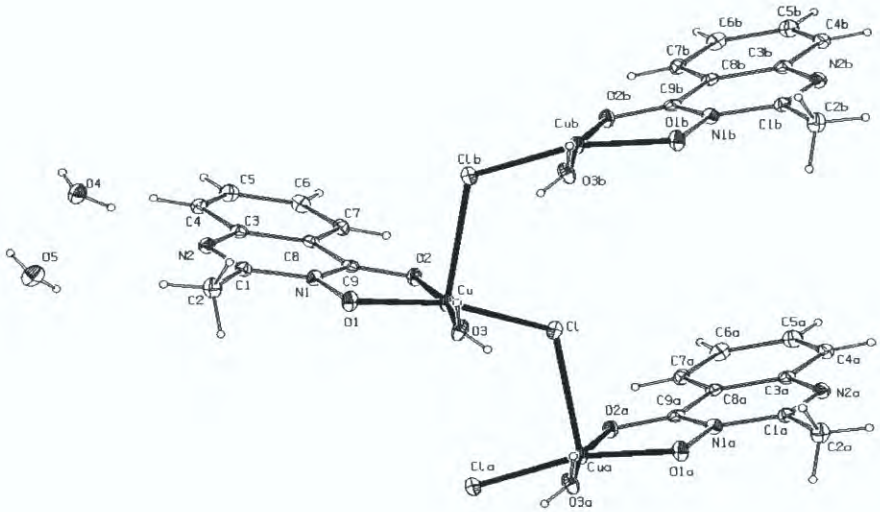

(a)

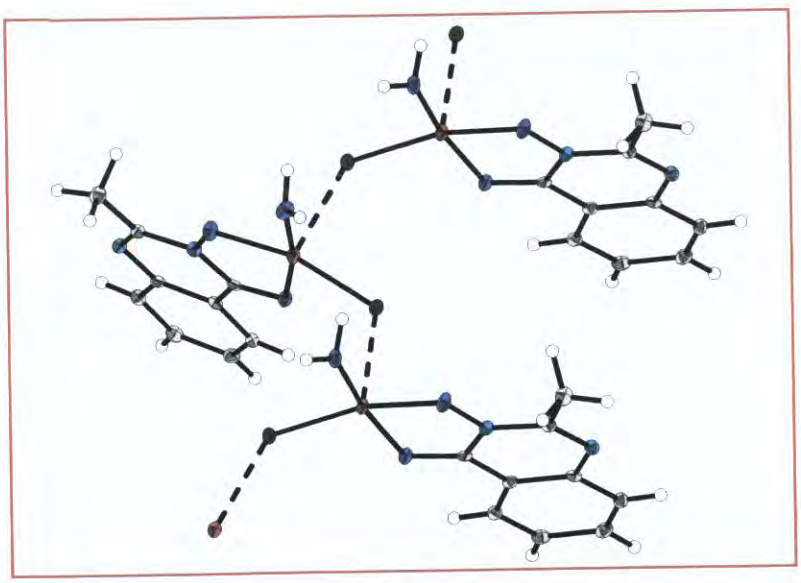

(b)

Fig. 25: (a) Molecular structure and atomic labeling scheme for complex **14** and (b) molecular packing viewed down the b axis

Selected bond lengths (Å) and angles (°): Cu–O(1) 1.9198(15), Cu–O(2) 1.9944(14), Cu–O(3) 1.9683(17), , Cu–Cl 2.2256(6), Cu-Clb 2.7080(6), N(1)–O(1) 1.362(2), N(1)–C(9) 1.355(3), O(2)–C(9) 1.272(3), N(1)–C(1) 1.383(3), C(1)–N(2) 1.296(3), C(8)–C(9) 1.431(3); O(1)–Cu–O(3) 86.63(7), O(1)–Cu–O(2) 82.81(6), O(1)–Cu–Cl 164.90(5), O1-Cu-Clb 95.92(5), O2-Cu-Clb 86.10(4), O3-Cu-Clb 96.45(6), O(3)–Cu–O(2) 169.34(7), O(2)–Cu–Cl 94.79(5), O(3)–Cu–Cl 95.03(6), O(1)–N(1)–C(1) 118.08(17), C(9)–N(1)–O(1) 118.06(17), O(2)–C(9)–N(1) 117.79(19), O(2)–C(9)–C(8) 126.32(19), N(1)–C(1)–C(2) 116.55(19).

3.7.4.5 $[Zn(Cha)_2].2H_2O$, 15.

Complex **15** was obtained as a white crystals in ~62% yield, from the reaction mixture after a period of one week. It gave a satisfactory microanalysis and its IR spectrum showed clear absorption bands at ~3300-3000 cm^{-1} (br) due to ν(O-H) of the water ligand, 1617 cm^{-1} (vs) due to ν(C=O) of the hydroxamate group, 1578 cm^{-1} (vs) due to ν(C=N) of the imine stretch group and ~1468 cm^{-1} (vs) due to the aromatic ring. The white crystals of **15** were suitable for X-ray structure analysis and the structure is shown in **Fig. 26** with selected bond lengths and angles in the legend.

In **15** the zinc(II) lies in a square pyramidal environment, containing O,O-bonded hydroxamate ligands in the basal plane and a water molecule located axially at 2.0167(15) Å. As in the previously discussed complexes and in other complexes with hydroxamate ligands,[73] the Zn-O(hydroxamate) bond, 1.9954(13) Å, is shorter than the Zn-O(carbonyl) bond 2.0789(13) Å, giving ΔZn-O of 0.0835 Å. The Zn-O(water) bond length 2.0167(15) Å falls in the reported range for Zn-O(water) bonds in zinc(II) complexes. The O-Zn-O bond angles in the basal plane range from 80.23(5) – 95.66(5)° indicating considerable distortion from square pyramidal geometry. The intermolecular hydrogen bonding involving O-H...O and O-H...N interactions within the lattice generate infinite one dimensional chain along the base vector [0 1 0]. These aggregates form two clusters each generating an infinite two dimensional network along the base vector [0 1 0] and [0 0 1] and along the plane (1 0 0).

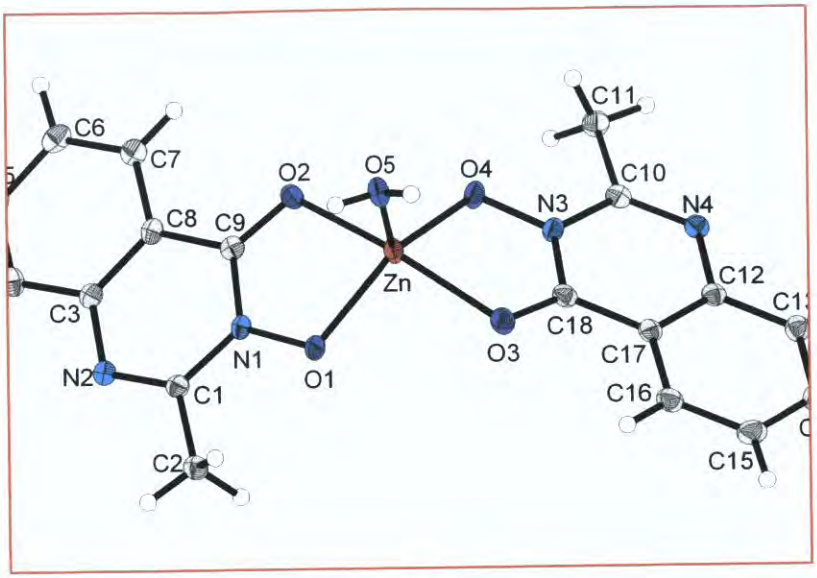

(a)

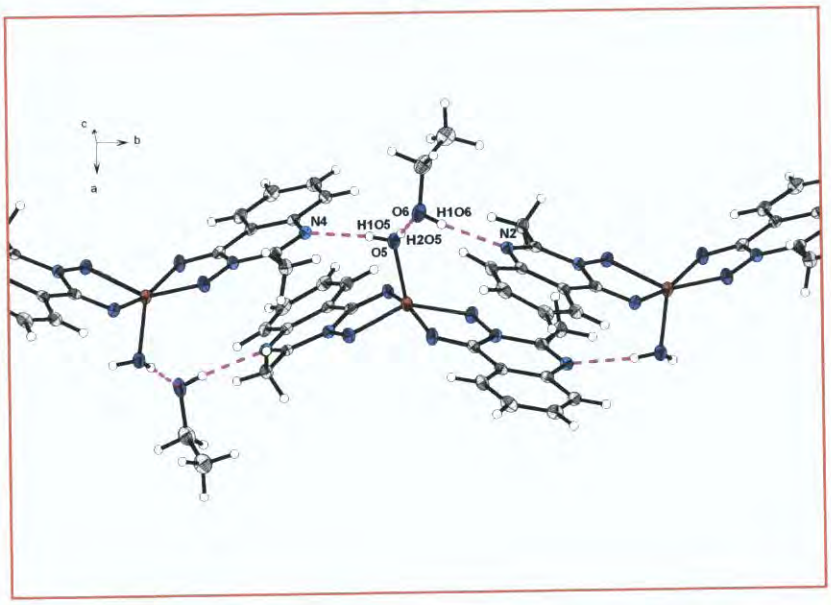

(b)

Fig. 26: (a) Molecular structure and atomic labeling scheme for complex **15** and (b) molecular packing viewed down the b axis

Selected bond lengths (Å) and angles (°): Zn–O(1) 1.9954(13), Zn–O(2) 2.0789(13), Zn–O(5) 2.0167(15), O(1)–N(1) 1.3551(19), N(1)–C(1) 1.370(2), C(1)–C(2) 1.492(3), N(1)–C(9) 1.375(2), C(9)–O(2) 1.252(2), C(1)–N(2) 1.304(2), O(1)–Zn–O(4) 140.06(6), O(1)–Zn–O(5) 104.00(6), O(1)–Zn–O(2) 80.63(5), O(1)–Zn–O(3) 95.66(5), O(5)–Zn–O(2) 97.30(6), O(4)–Zn–O(2) 91.11(5), O(5)–Zn–O(3) 100.96(6), O(3)–Zn–O(2) 161.72(5), O(4)–Zn–O(5) 115.83(6), O(4)–Zn–O(3) 80.23(5), O(2)–C(9)–C(8) 125.42(17), O(2)–C(9)–N(1) 119.16(17), O(1)–N(1)–C(9) 118.66(14).

3.8 Conclusions

The attempted synthesis of acetylated anthranilic hydroxamic acids as dual COX/POX site inhibitors in PGHS gave, instead of the desired product, cyclic hydroxamic acid **4**. The formation, spectra and crystal structures of this and of its Fe(III, Co(II), Ni(II), Cu(II) and Zn(II) complexes are reported, as well as the crystal structure of $[Fe^{III}(4\text{-}AphaH_{-1})_3](C_2H_6O)]$ for comparison. These structures expand the available information on hydroxamate complexes.

3.9 References

1. K. H. Thompson, C. Orvig, *Dalton Trans.*, 2006, **14**, 761-764.
2. E.I. Solomon, U.M. Sundaram, T.E. Machonkin, *Chem. Rev.*, 1996, **96** (7), 2563-2605.
3. P. J. Sadler, *Adv. Inorg. Chem.*, 1991, **36**, 1–48.
4. B. Rosenberg, L. V. Camp, T. Krigas, *Nature*, 1965, **205**, 698-699.
5. J. R. R. Frausto da Silva, R. J. P. Williams, *The Biological Chemistry of the Elements: The Inorganic Chemistry of Life*. Clarendon Press, New York, 1991.
6. S. Budavari, at el, *The Merck Index*, 13th ed., Merck & Co., Rahway, NJ, 2001.
7. R. M Roat-Malone, *Metals in Medicine* in *Bioinorganic Chemistry, A Short Course*, John Wiley & Sons Inc., 2002, Chapter 7.
8. M. Prak, Q. Li, N. Shcheynikov, S. Muallem, W.Zeng, *Cell Cycl.*, **4**, 2005, 24-26.
9. L. Ronconi, P. J. Sadler, *Coord. Chem. Rev.*, 2007, **251**, 1633-1648.
10. B. R. Cameron, I. R. Baird, *J. Inorg. Biochem*, 2001, **83**, 233-236.
11. L. Wei-Ping, Y. Qing-Song, Y. Yao, Chen. Xi-Zhu, H. Shu-Qian, *Platinum Metals Review*, 2008, **52** (3), 163-171.
12. M. A. Fuertes, C. Alonso and J. M. Perez, *Chem. Rev.*, 2003, **103**, 645-662.
13. M. D. Hall, T. W. Hambley, *Coord. Chem. Rev.*, 2002, **232**, 49-67.
14. C. E. Housecroft, A. G. Sharpe, *Inorganic Chemistry*, 1st edn., Prentice Hall, Harlow, 2001.
15. F. A. Cotton, G. Wilkinson, *Basic Inorganic Chemistry*, Wiley International Edn., John Wiley & Sons Inc., New York, 1976.
16. A. C. Rosenzweig, P. Nordlund, P. M. Takahara, C. A. Frederick, S. J. Lippard, *Nature*, 1993, **366**, 537-543.
17. P. J. Artymiuk, S. J. Yewdall, J. M. Smith, J. C. Livingstone, A. Treffry, A. Luzzago, S. Levi, P. Arosio, G. Cesareni, *Nature*, 1991, **349**, 541-544.
18. M. J. Miller, *Chem.* Rev., 1989, **89**, 1563 –1579 and references therein.
19. H. Beinert, *J. Biol. Inorg. Chem.*, 2000, **5** (1), 2-15.
20. J.J.R.Frausto da Silva and R.J.P.Williams, *The Biological Chemistry of the Elements, The Inorganic Chemistry of Life, Chapter 16, Nickel and Cobalt*, 2nd Ed., Oxford University Press, 2001.

21. T. W. Failes,C. Cullinane, C. I. Diakos, N. Yamamoto, J. G. Lyons, T. W. Hambley, *Chem. Eur. J.*, 2007, **13**, 2974–2982.

22. D. C. Ware, H. R. Palmer, F. B. Bruijn, R. F. Anderson, P. J. Brothers, W. A. Denny, W. R. Wilson, *Anti-Cancer Drug Des.*, 1998, **13**, 81–103.

23. H. E. Wages, K. L. Taft, S. J. Lippard, *Inorg. Chem.*, 1993, **32**, 4985-4987.

24. M. J. Kendrick, M. T. May, K. D. Robinson, M. P. Plishka, *Metals in Biological Systems*, Ellis Horwood, 1992.

25. J. B. Sumner, *Biochemistry*, 1962, **1**, 911-916.

26. R. H. Holm, *J. Am. Chem. Soc.*, 1991, **113**, 8458-8462.

27. F. A. Cotton, G. Wilkinson, *Advanced Inorganic Chemistry*, 5th edn., Wiley, New York, 1988.

28. E. B. Hart, H. Steenbock, J. Waddell, C. A. Elvehjem, *J. Biol, Chem.*, 1928, **77**, 777-795.

29. D. W. Cox, *British Medical Bulletin.*, 1999, **55** (3), 544-555.

30. R. Uauy, M. Olivares, M. Gonzales, *Am. J. Clin. Nutrit.*, 1998, **76**, S996.

31. J. E. Weder, C. T. Dillon, T. W. Hambley, B. J. Kennedy, P. A. Lay, J. R. Biffin, H. L. Regtop, N. M. Davies, *Coord. Chem. Rev.*, 2002, **232**, 95-126.

32. A. Shrivastav, N. K. Singh, S. M. Singh, *Bioorg. Med. Chem.*, 2002, **10**, 887-895.

33. M. Gielen, E. R. T. Tiekink, *Metallotherapeutic Drugs and Metal-based Diagnostic Agents : The Use of Metals in Medicine,* Wiley, Chichester, 2005.

34. Y. Li, M. A. Trush, *Carcinogenesis.*, 1993, **14**, 1303-1311.

35. M. B. Grisham, D. Jourd Heuil, D. A. Wink, *Am. J. Physiol.*, 1999, **276**, G315.

36. J. S. Valentine, *J. Chem. Educ.*, 1985, **62**, 925.

37. D. Kovala-Demertzi, *J. Inorg. Biochem*, 2000, **79**, 153-157.

38. T. M. Bray, W. J. Bettger, *Free Radic. Biol. Med.*, 1990, **8**, 281-291.

39. S. R. Powell, *J. Nutr.*, 2000, **130**, 1447S-1454S.

40. K. A. McCall, C. Huang, C. A. Fierke, *J. Nutr.*, 2000, **130**, 1437S-1446S.

41. B. L. Vallee, K. H. Falchuk, *Physiol. Rev.*, 1993, **73**, 79-118.

42. W. Kaim and B. Schwederski, *Bioinorganic Chemistry: Inorganic Elements in the Chemistry of Life, Chapter 12,* Wiley, New York, 1991.

43. D. W. Cox, E. A. Roberts, Sleisenger and Fordtrans *Gastrointestinal andLiver Disease*, Sleisenger (Eds), W. B. Saunders, St Louis, 2002, 1269-1277.

44. B. L. Vallee, D. S. Auld, *Faraday Discuss*, 1992, **93**, 47-65.

45. N. E. Dixon, A. M. Sargeson in *Roles for the Metal Ion in Reactions of Coordinated Substrates and in Some Metalloenzymes (Zinc Enzymes)*, ed. T. G. Spiro, John Wiley and Sons, New York, 1983, 254-266.

46. H. Lossen, *Liebigs Ann. Chem.*, 1869, **150**, 314.

47. C. J. Marmion, D. Griffith, K. B. Nolan, *Eur. J. Inorg. Chem.*, 2004, **15**, 3003-3016.

48. D. Gaynor, *synthesis of Aminophenylhydroxamic acids and their Metal Complexes. Synthesis, Structures, Magnetic Properties and Inhibition of Prostaglandin H_2 Synthesis*, PhD Thesis, NUI, 2002.

49. C. J. Marmion, T. Murphy, J. R. Docherty, K. B. Nolan, *Chem. Commun.*, 2000, 1153-1154.

50. C. M. Dooley, M. Devocelle, B. McLoughlin, K. B. Nolan, D. J. Fitzgerald, C. T. Sharkey, *Mol. Pharmacol.*, 2003, **63**, 450-455.

51. J. Lee, A. J. Chubb, E. Moman, B. M. McLoughlin, C. T. Sharkey, J. G. Kelly, K. B. Nolan, D. J. Fitzgerald, M. Devocelle, *Org. Biomol. Chem.*, 2005, **3**, 3678–3685.

52. E. M. F Muri, M. J. Nieto, R. D. Sindelar, J. S. Williamson, *Curr. Med. Chem.*, 2002, **9**, 1631-1653.

53. M. Sani, D. Belotti, R. Giavazzi, W. Panzeri, A. Volonterio, M. Zanda, *Tetrahedron Letters*, 2004, **45**, 1611-1615.

54. C.Indiani, E. Santoni, M. Becucci, A. Boffi, K. Fukuyama, G. Smulevich, *Biochemistry.*, 2003, **42**, 14066-14074.

55. E. C. O'Brien, E. Farkas, M. J. Gil, D. Fitzgerald, A. Castineras, K. B. Nolan, *J. Inorg. Biochem*, 2000, **79**, 47-51.

56. D. A. Brown, W. K. Glass, N. J. Fitzpatrick, T. J. Kemp, W. Errington, G. J. Clarkson, W. Haase, F. Karsten, A. H. Mahdy, *Inorg. Chim. Acta*, 2004, **357**, 1411-1436.

57. D. A. Brown, L. P. Cuffe, N. J. Fitzpatrick, A. T. Ryan, *Inorg. Chem.*, 2004, **43**, 297-302.

58. M. Arnold, D. A. Brown, O. Deeg, W. Errington, W. Haase, K. Herlihy, T. J. Kemp, H. Nimir, R. Werner, *Inorg. Chem.*, 1998, **37**, 2920-2925.

59. T. G. Barros, J. S. Williamson, O.A. C. Antunes, E. M. F. Muri, *Letters in Drug Design & Discovery.*, 2009, **6**, 186-192.

60. P. J. Connolly, S. K. Wetter, K. N. Beers, S. C. Hamel, R. H. Chen, M. P. Wachter, J. Ansell, M. M. Singer, M. Steber, D. M. Ritchie, D. C. Argentieri, *Bioorg. Med. Chem. Lett.*, 1999, **9**, 979-984.

61. R. Zamora, A. Grzesiok, H. Weber, M. Feelisch, *Biochem. J.*, 1995, **312** (Pt 2), 333-339.

62. W. P. Steward, A. L. Thomas, *Expert Opin. Investig. Drugs.*, 2000, **9**, 2913-2922.

63. R.C. Mishra, R. Tripathi, D. Katiyar, N. Tewari, D. Singh, R. P. Tripathi, *Bioorg. Med. Chem.*, 2003, **11**, 5363-5374.

64. J. El Yazal, Y. P. Pang, *J. Phys. Chem. A.*, 1999, **103**, 8346-8350.

65. J. El Yazal, Y. P. Pang, *J. Phys. Chem. B.*, 2000, **104**, 6499-6504.

66. A. K. Ghosh, *Proc Indian Natl. Sci. Acad.*, Part A, 1989, **55** (2), 253.

67. J. Hase, K. Kaboshi, N. Kawaguchi, K. Sakamoto, *Chem. Pharm, Bull.*, 1971, **19** (2), 363.

68. C. A. Chang, V. C. Sekhar, B. S. Garg, F. S. Guziec, T. C. Russon, *Inorg. Chem. Acta.*, 1987, **135**, 11-18.

69. J. Taira, M. Chika, Y. Aniya, *Biochem. Pharmacol*, 2002, **63** (5), 1019-1026.

70. A. E. Harvey, D. L. Manning, *J. Am. Chem. Soc.*, 1950, **72**, 4498.

71. D. A. Brown, R. A. Coogan, N. J. Fitzpatrick, W. K. Glass, D. E. Abukshima, L. Shiels, M. Ahlgrén, K. Smolander, T. T. Pakkanen, T. A. Pakkanen, M. Peräkylä, *J. Chem. Soc., Perkin Trans.* 1996, **2**, 2673-2679.

72. N. J. Fitzpatrick, R. Mageswaran, *Polyhedron.*, 1989, **8**, 2255-2263.

73. C. J. Marmion, T. Murphy, Z. Starikova, K. B. Nolan, *Acta Cryst.*, 2000, **C56**, e491-e492.

74. D. A. Brown, A. L. Roche, *Inorg. Chem.*, 1983, **22**, 2199-2202.

75. L. Cheng, M. A. Khan, R. W. Taylor, G. B. Richter-Addo, D. R. Powell, *Chem. Commun.*, 1999, **19**, 1941-1942.

76. E. Farkas, E. A. Enyedy, G. Micera, E. Garribba, *Polyhedron.*, 2000, **19**, 1727-1736.

77. B. Kurzak, K. Kurzak, J. Jezierska, *Inorg. Chim. Acta*, 1986, **125**, 77-82.

78. B. Kurzak, K. Kurzak, J. Jezierska, *Inorg. Chim. Acta.*, 1987, **130**, 189-193.

79. B. Kurzak, E. Farkas, T. Glowiak, H. Kozlowski, *J. Chem. Soc., Dalton Trans.*, 1991, **2**, 163-167.

80. V. L. Pecoraro, A. J. Stemmler, B. R. Gibney, J. J. Bodwin, H. Wang, J. W. Kampt, A. Barwinski, in *Prog. Inorg. Chem.*(Ed. K. Karlin), Pergamon Press, 1996, **45**, 83-177.

81. D. Gaynor, Z. A. Starikova, S. Ostrovsky, W. Haase, K. B. Nolan, *Chem. Commun.*, 2002, 506-507.

82. *Chemistry and Biology of Hydroxamic Acids*; H. Kehl, S. Karger: New York, 1982.

83. K. N. Raymond, *Coord. Chem. Rev.*, 1990, **105**, 135-153.

84. G. Winkelmann, D. van der Helm, J. B. Nielands, *Iron Transport in Microbes, Plants and Animals*, VCH Publishers, New York, 1987.

85. A. M. Albrecht-Gary, A. L. Crumbliss, *in Metal Ions in Biological Systems* (Eds.: A. Sigel, H. Sigel), Marcell Dekker, NewYork, 1998, **35**, 239.

86. D. A. Brown, M. V. Chidambaram, *in Metal Ions in Biological Systems*, **14**, Marcel Dekker, New York, 1982.

87. E. Farkas, E. A. Enyedy, L. Zekany, G. Deak, *J. Inorg. Biochem*, 2001, **83**, 107-114.

88. P. Rubini, A. Lakatos, D. Champmartin, T. Kiss, *Coord. Chem. Rev.*, 2002, **228**, 137-152.

89. L. Lo, S. T. Singer, *Pediatric Clinics of North America.*, 2002, **49**, 1165-1191.

90. P. S. Dobbin, R. C. Hider, *Chem. Br.*, 1990, **26**, 565-568.

91. S. Pikul, K. L. McDunham, N.G. Almstead, B. De, M.G. Natchus, M. V. Anastasio, S. J. McPhail, C. E. Snider, Y.O. Taiwo, T. Rydel, C. M. Dunaway, F. Gu, G. E. Mieling, *J. Med. Chem.*, 1998, **41** (19), 3568-3571.

92. B. Davies, P. D. Brown, N. East, M. J. Crimmin, F. R. Blackwill, *Cancer Rev.*, 1993, **53**, 2815-2822.

93. F. Grams, M. Crimmin, L. Hinnes, P. Huxley, M. Pieper, H. Tschesche, W. Bode, *Biochemistry*, 1995, **34**, 14012-20.

94. M. L. Curtin, R. B. Garland, H. R. Heyman, R. R. Fery, M. R. Michaelides, J. Li, L. J. Pease, K. B. Glaser, P. A. Marcotte, S. K. Davidsen. *Bioorg. Med. Chem. Letts.*, 2002, **12**, 2919-2923.

95. B. S. Mann, J. R. Johnson, M. H. Cohen, R. Justice, R. Pazdur, *Oncologist*, 2007, **12**, 1247-1252.

96. S. Natelson, P. Pantazis, E.A. Natelson, *Clin. Chim. Acta.*, 1994, **229**, 133-145.

97. J. C. MacDonald, *J. Biol. Chem.*, 1961, **236**, 512-514.

98. C. B. Schapira, S. Lamdan, *J. Heterocyclic Chem.*, 1972, **9**, 569-576.

99. K. Ebisui, A. Ishihara, H. Iwamura, *Plant Physiology and Biochemistry*, 2001, **39**, 27-35.

100. A. L. Davis, K. L. Hulme, G. T. Wilson, T. J. McCord, *Antimicrobial Agents and Chemotherapy*, 1978, **13**, 542-544.

101. K. L. Reddy, S. Srihari, P. Lingaiah, *Ind. J. Chem.*, 1985, **24A**, 318-322.

102. K. L. Reddy, A. R. Chandraiah, K. A. Reddy, *Ind. J. Che*m., 1989, **28A**, 622.

103. K. L. Reddy, S. Srihari, P. Lingaiah, *Ind. J. Chem.*, 1984, **23A**, 780.

104. A. L. Davis, O. H. P. Choun, D. E. Cook, T. J. McCord, *J. Med. Chem.*, 1964, **7**, 632.

105. W. L. Smith, D. L. DeWitt, R. M. Garavito, *Annu. Rev. Biochem*, 2000, **69**, 145-182.

106. S. S. C. Tam, D. H. S. Lee, E.Y. Wang, D. G. Munroe, C. Y. Lau, *J. Biol. Chem.*, 1995, **270**, 13948-13955.

107. D. S. Reddy, G. Shailaja, P. Pratap Reddy, P. S. N. Reddy, *Synthetic Comm.*, 1996, **26**, 2843-2846.

108. B. D. Hosangadi, R. H. Dave, *Tetrahedron Lett.*, 1996, **37**, 6375-6378.

109. D. Gaynor, Z. A. Starikova, W. Haase, K. B. Nolan, *Dalton Trans.*, 2001, 1578 - 1581.

110. E.C.O'Brien, *Synthesis of Aspirin Analogues, their Metal Complexing Properties and those of other Bioligands*, PhD Thesis, NUI, 1999.

111. G. M. Sheldrick, SHELXTL-97, *Programme for Solution and Refinement of Crystal Structures* , Bruker –AXS, Madison, WI, USA, University of Göttingen, 1997.

112. B. Van't Riet, G. L. Wampler, H. L. Elford, *J. Med. Chem.*, 1979, **22**, 589-592.

113. H. L. Yale, *Chem. Rev.*, 1943, **33**, 209-256.

114. R. T. Coutts, K. W. Hindmarsh, S. J. Powell, J. L. Pound, E. M. Smith, *Can. J. Pharm. Sci.*, 1968, **3**, 49.

115. V. A. Shenderovich, V. I. Ryaboi, E. D. Kriveleva, B. I. Ionin, I. A. Vainshenker, A. V. Dogadina, Zh. Obsh. Khim, 1979, **49**, 1746–1751.

116. C. J. Pouchert, *In The Aldrich Library of Infrared Spectra.*, 3rd ed, Aldrich Chemical Co, Milwakee, 1981, p 1405A.

117. F. H. Allen, O. Kennard, D. G. Watson, L. Brammer, A. G. Orpen.. *J. Chem. Soc. Perkin Trans.* **2**, 1987, S1-S19.

118. K. N. Raymond, E. A. Dertz, S. S. Kim, *Proc. Nat. Acad (USA)*, 2003, **100**, 3584-3588.

119. Z. D. Liu, R. C. Hider, *Coord. Chem. Rev.*, 2002, **232**, 151-171.

120. G. Kuppuraj, M. Dudev, C. Lim, *J. Phys. Chem. B.*, 2009, **113**, 2952–2960.

121. R. F. See, R. A. Kruse, W. M. Strub, *Inorg. Chem.*, 1998, **37**, 6369-5375.

122. C. Ramakrishnan, Y. S. Geetha, *Proc. Indian Acad. Sci. (Chem Sci).*, 1990, **102**, 481-496.

123. N. R. Sangeetha, S. Pal, *Polyhedron.*, 2000, **19**, 1593-1600.

Appendix

NMR and X-ray crystal structure data

Chapter 1: NMR Spectra

Chapter 2: NMR Spectra and lists of crystal data, bond lengths, bond angles and hydrogen bonds for:

N-acetoxy-2-hydroxybenzamide (SalAc), 2.

N-acetoxy-2-acetoxybenzamide ($SalAc_2$), 3.

Chapter 3: lists of crystal data, bond lengths, bond angles, torsion angles and hydrogen bonds for:

3-Hydroxy-2-methyl-3H-quinazolin-4-one (ChaH), 4.

$Fe^{III}(4\text{-}Apha)_3.C_2H_5OH$, 8.

$Fe(Cha)_2(Cl)(H_2O).7/2H_2O$, 9.

$Co(Cha)_2(C_2H_5OH)_2$, 11.

$Ni(Cha)_2(C_2H_5OH)_2$, 12.

$Cu(Cha)H_2O(Cl)$, 14.

$[Zn(Cha)_2].2H_2O$, 15.

NMR Spectra for Chapter 1

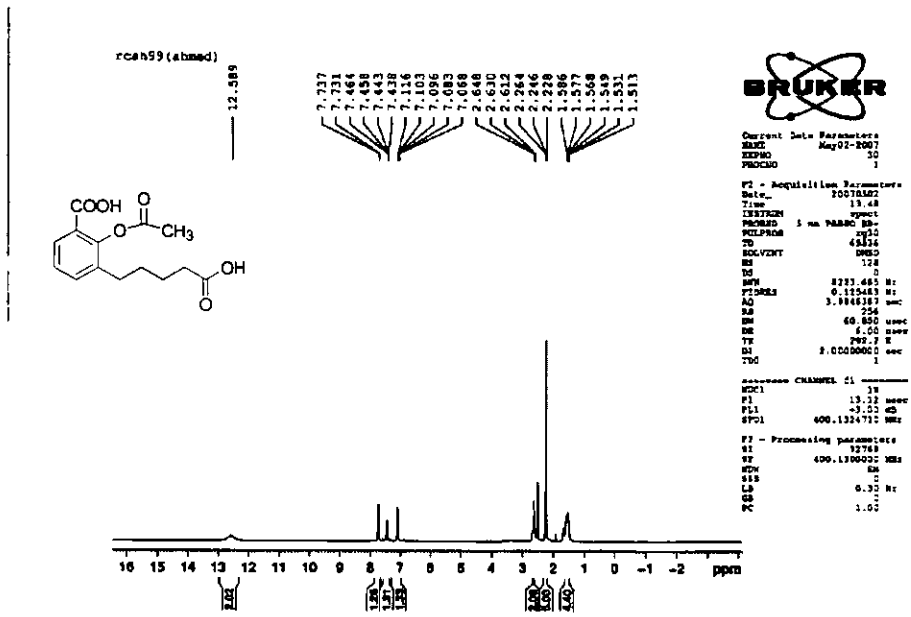

^{1}H-NMR of compound 2

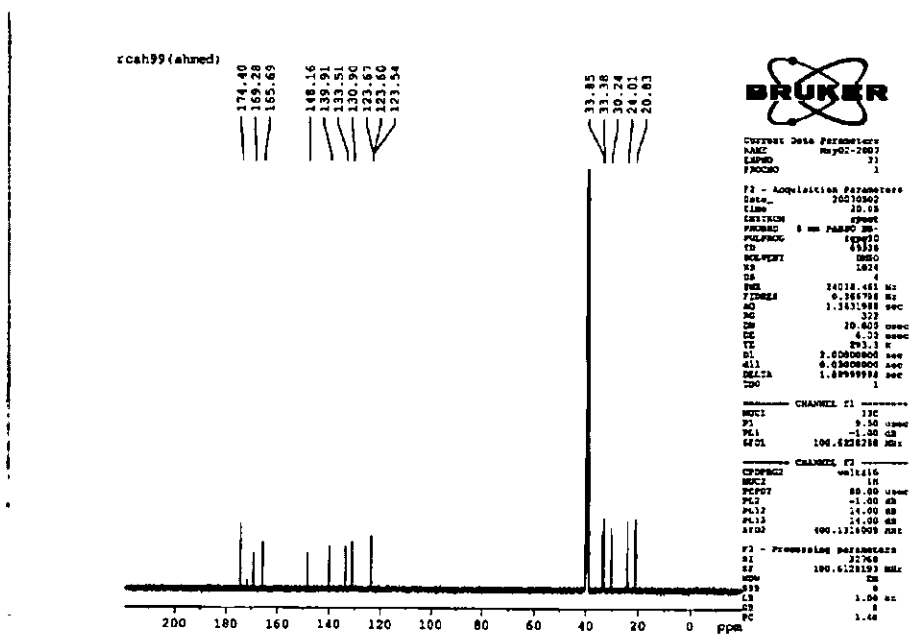

^{13}C-NMR of compound 2

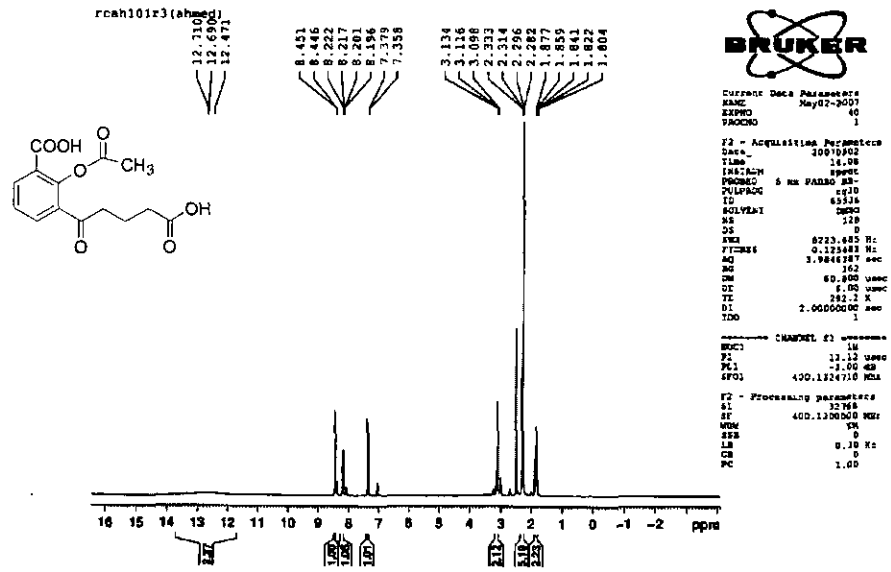

^{1}H-NMR of compound 3

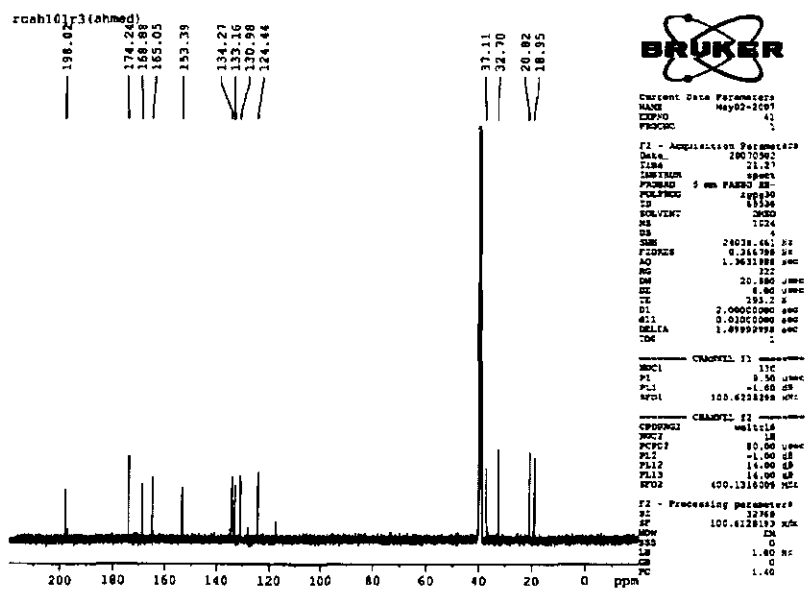

^{13}C-NMR of compound 3

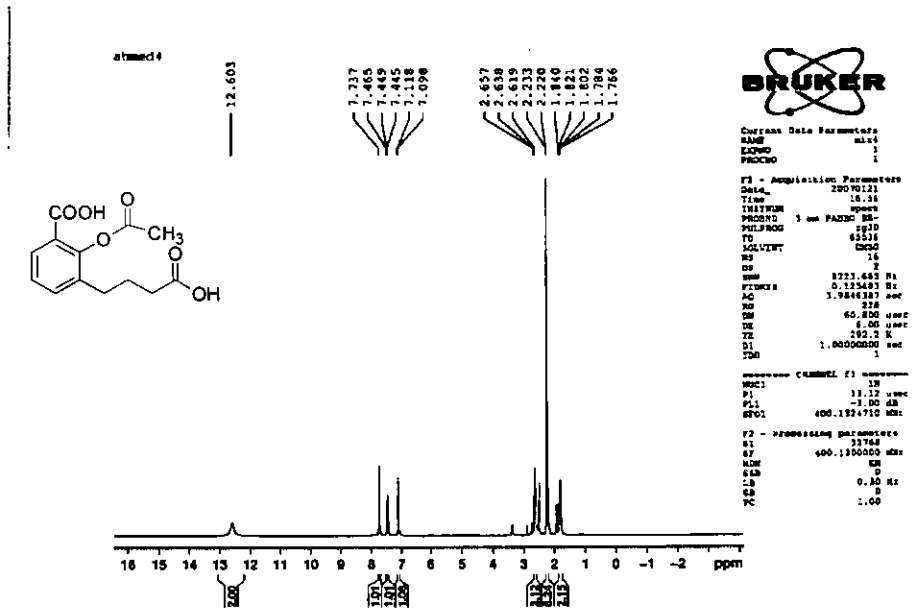

^{1}H-NMR of compound 4

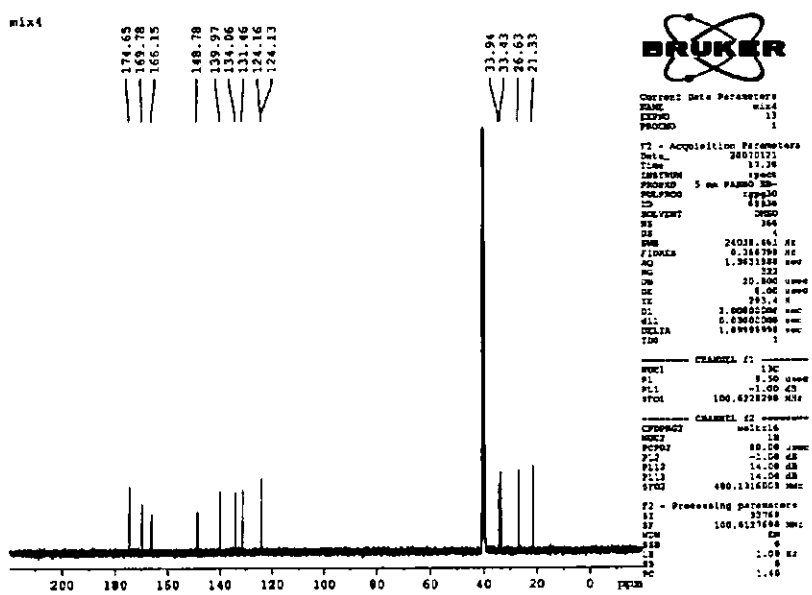

^{13}C-NMR of compound 4

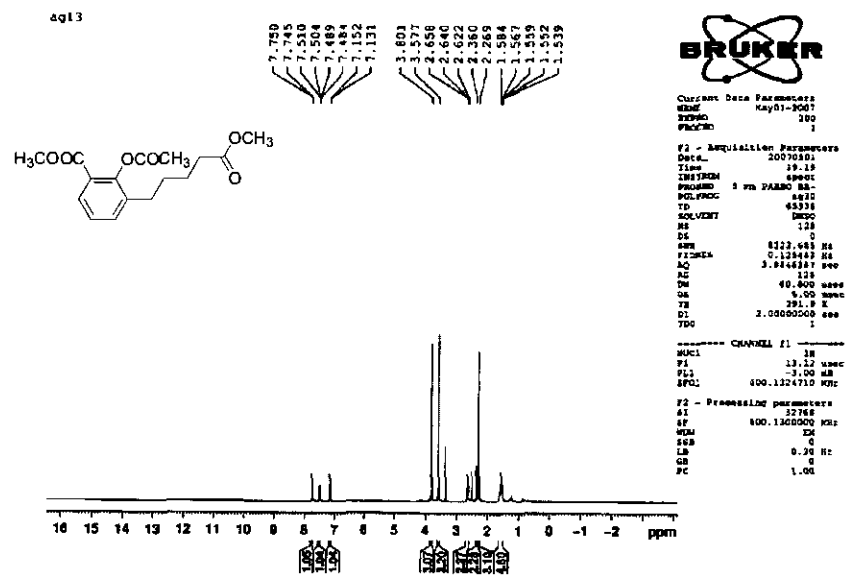

^{1}H-NMR of compound 5

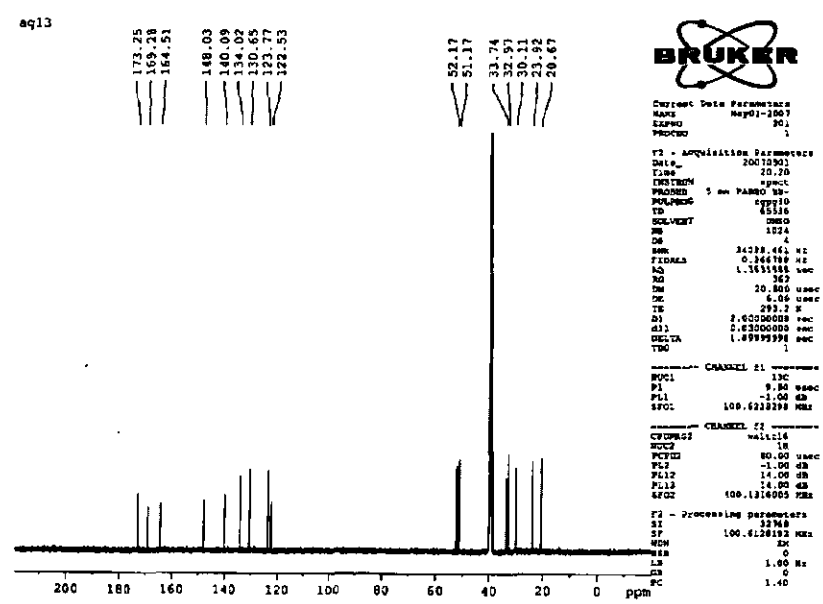

^{13}C-NMR of compound 5

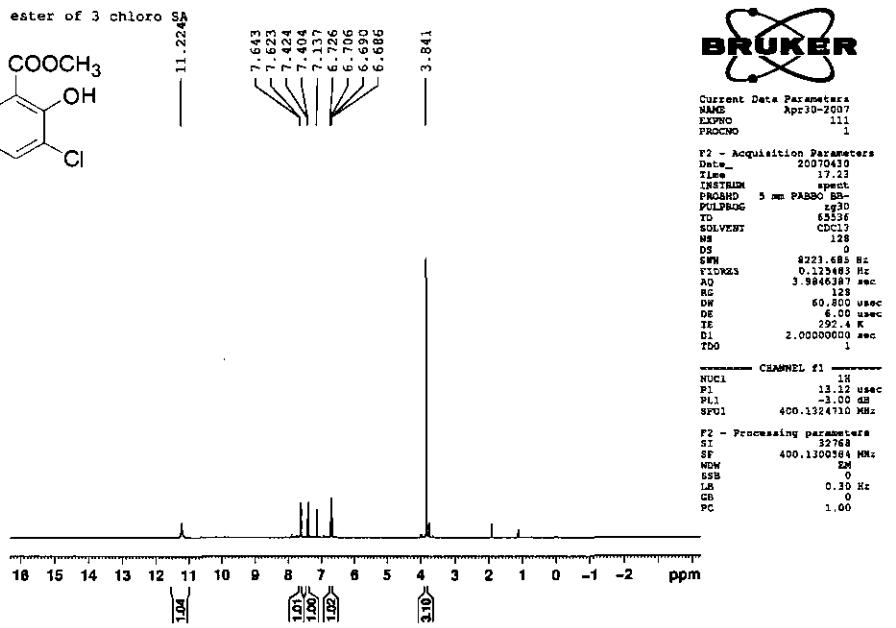

^{1}H-NMR of compound 8

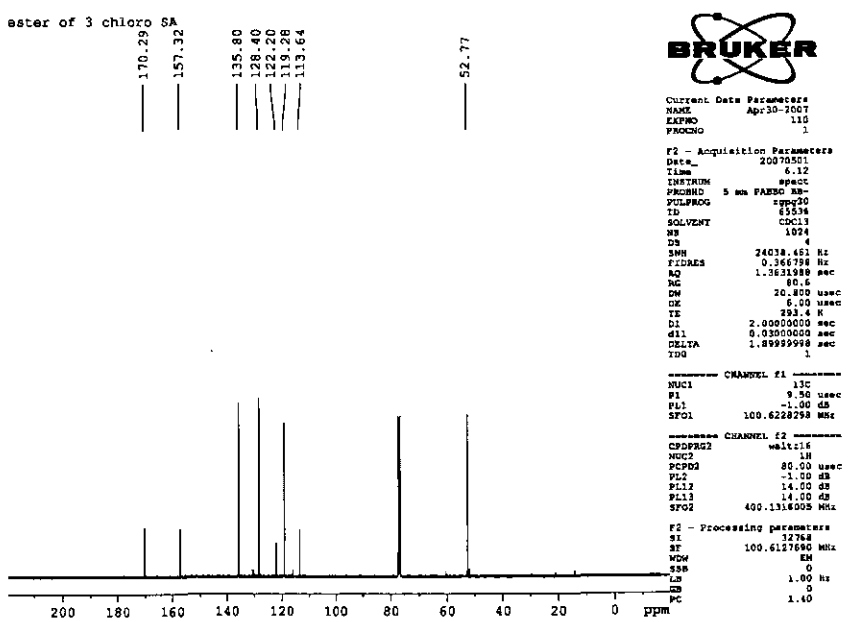

^{13}C-NMR of compound 8

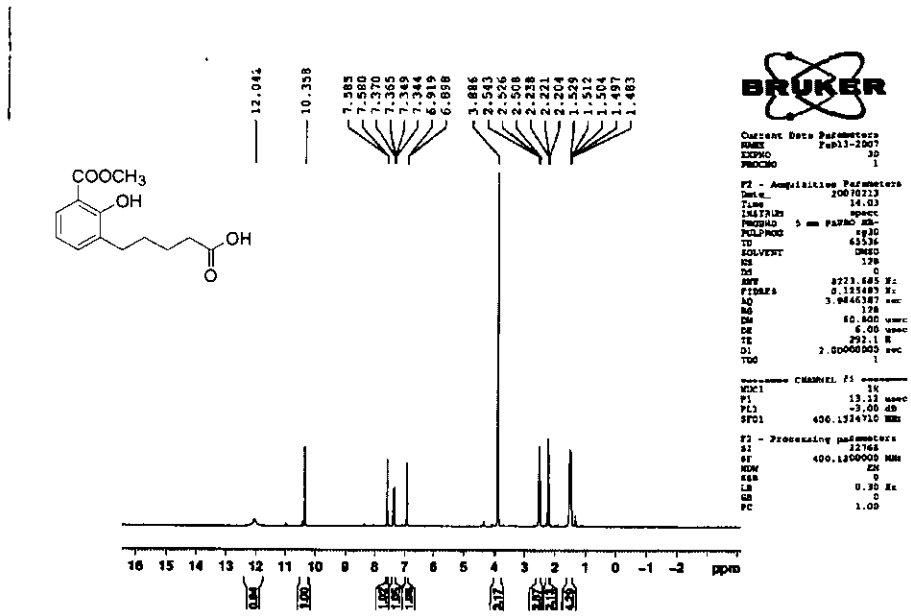

^{1}H-NMR of compound 10

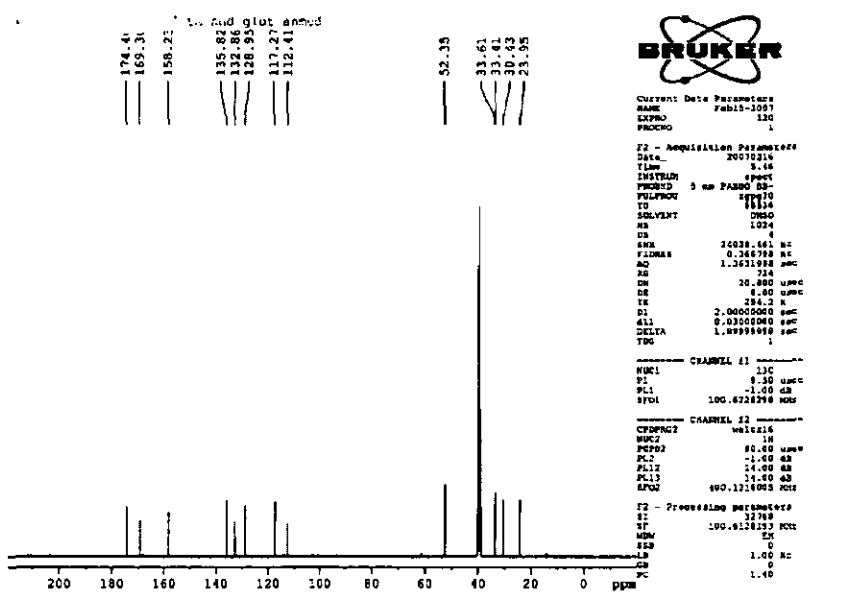

^{13}C-NMR of compound 10

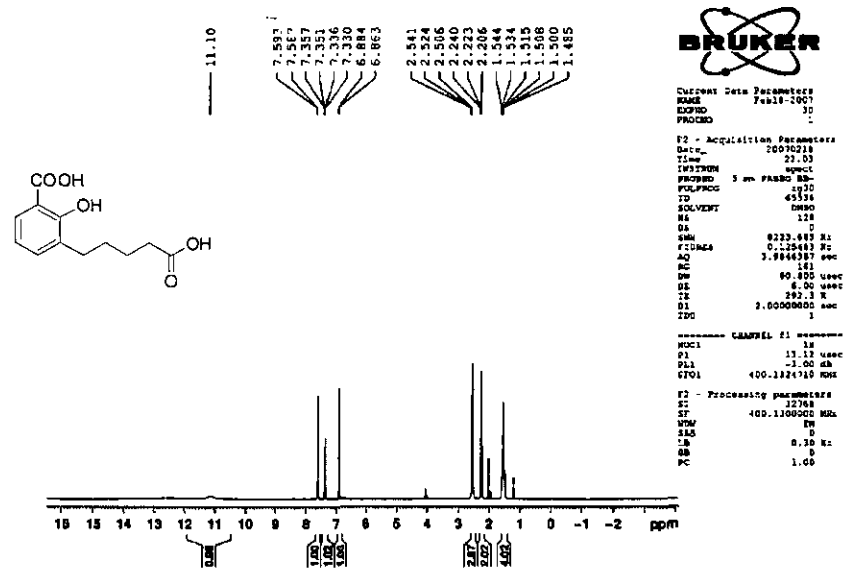

^{1}H-NMR of compound 11

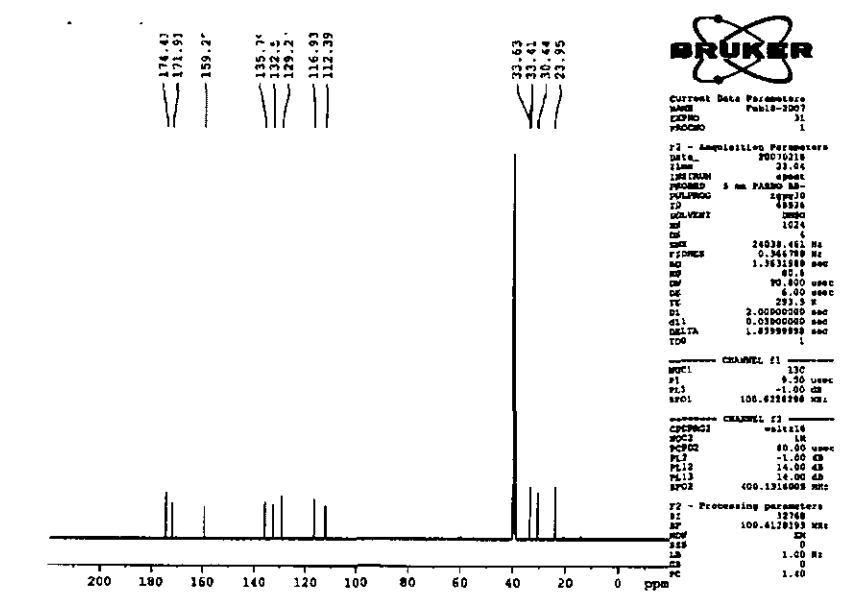

^{13}C-NMR of compound 11

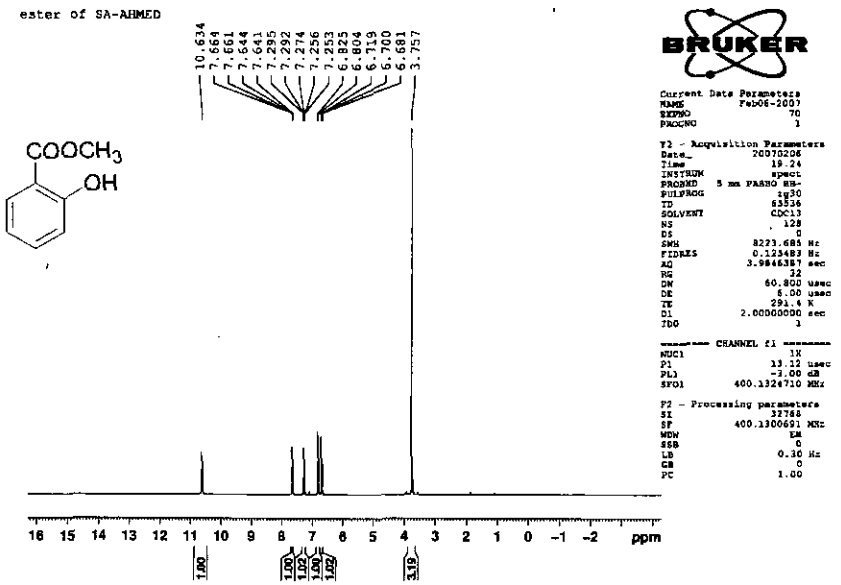

^{1}H-NMR of compound 13

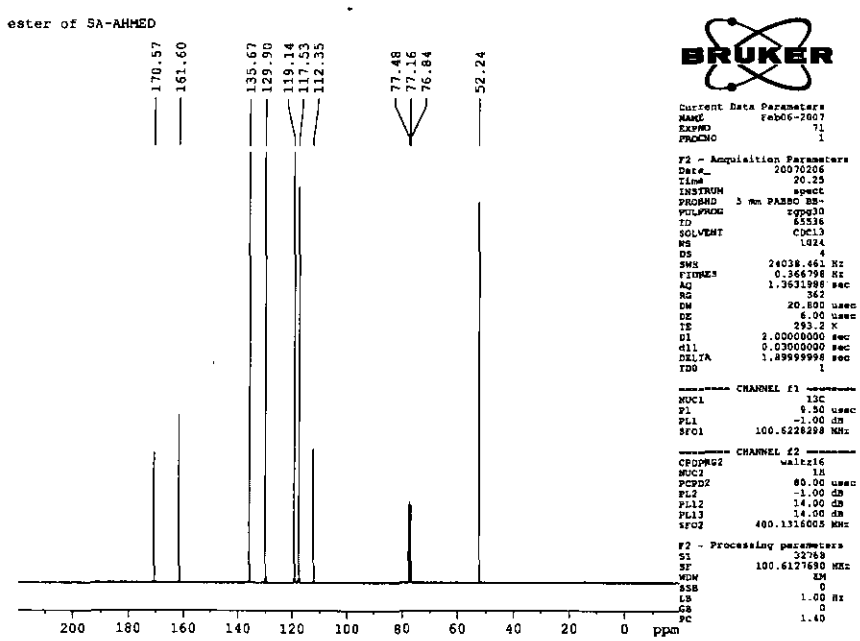

^{13}C-NMR of compound 13

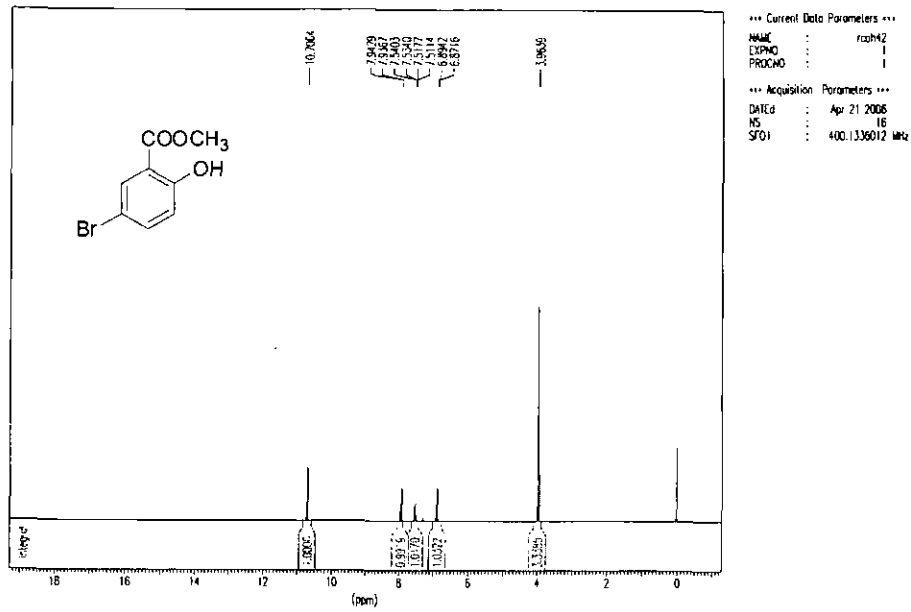

^{1}H-NMR of compound 14

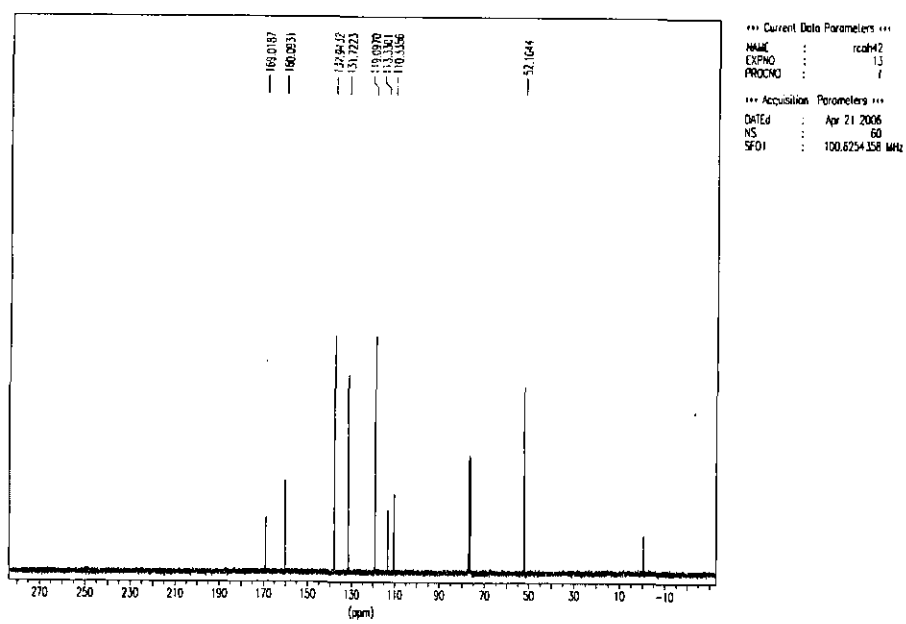

^{13}C-NMR of compound 14

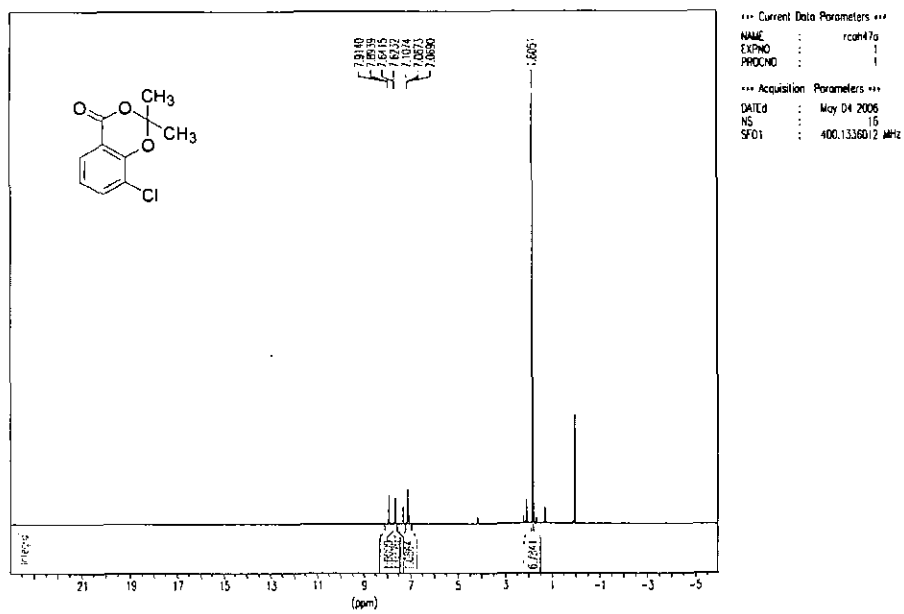

^{1}H-NMR of compound 15

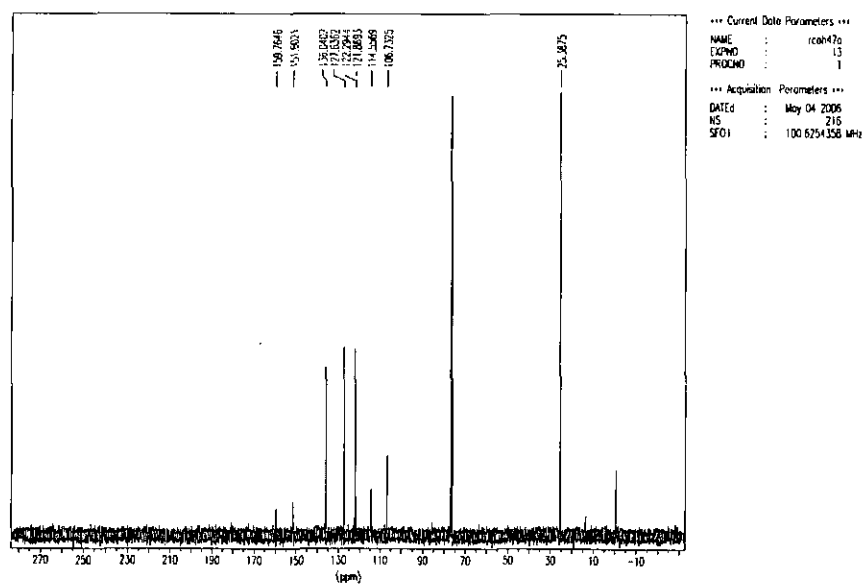

^{13}C-NMR of compound 15

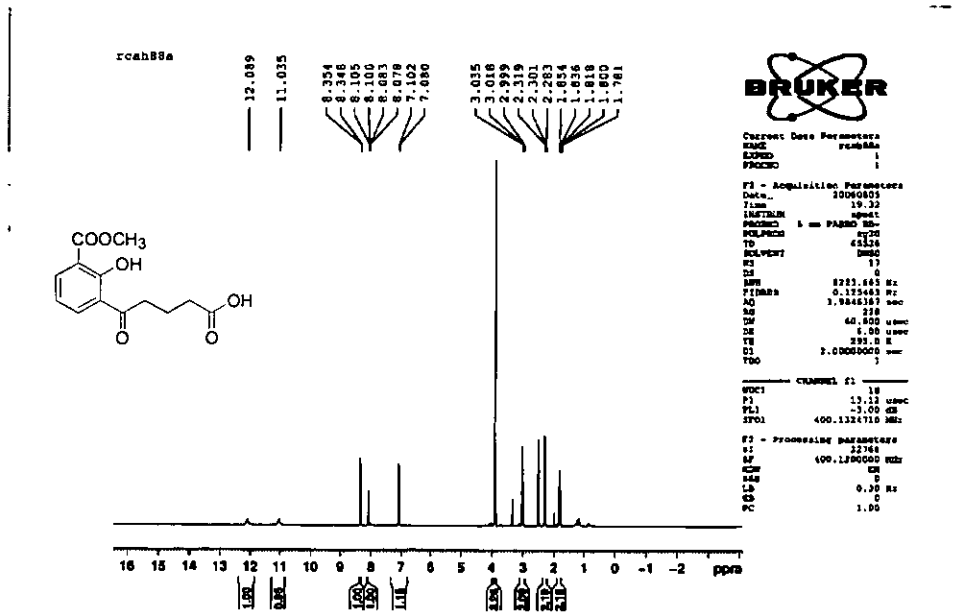

^{1}H-NMR of compound 16

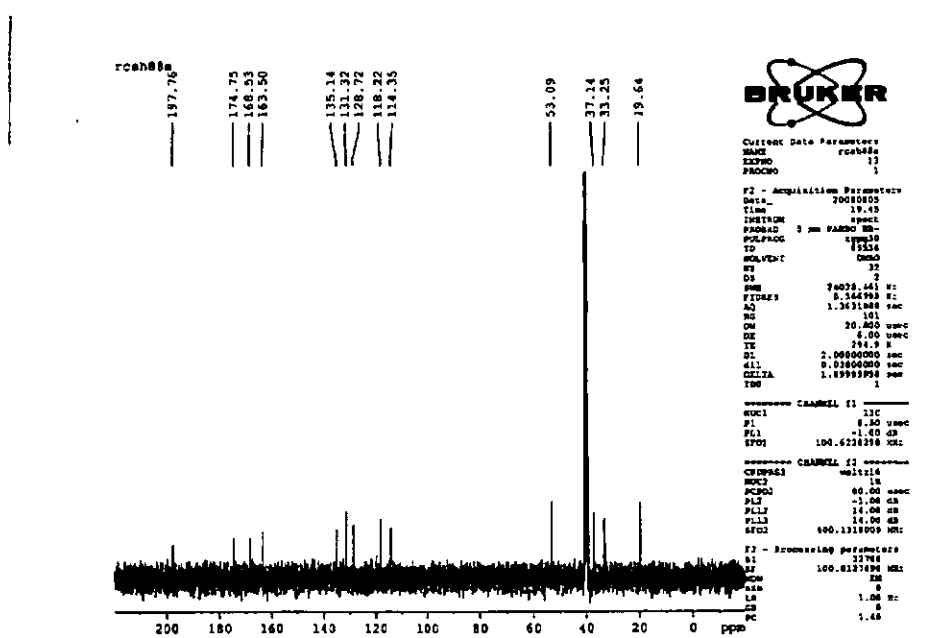

^{13}C-NMR of compound 16

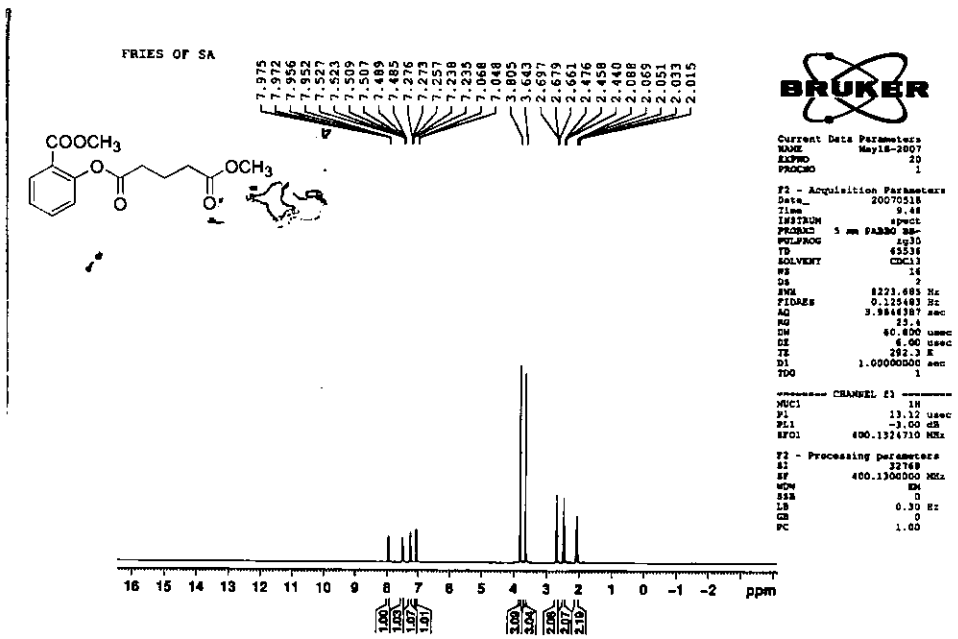

^{1}H-NMR of compound 17

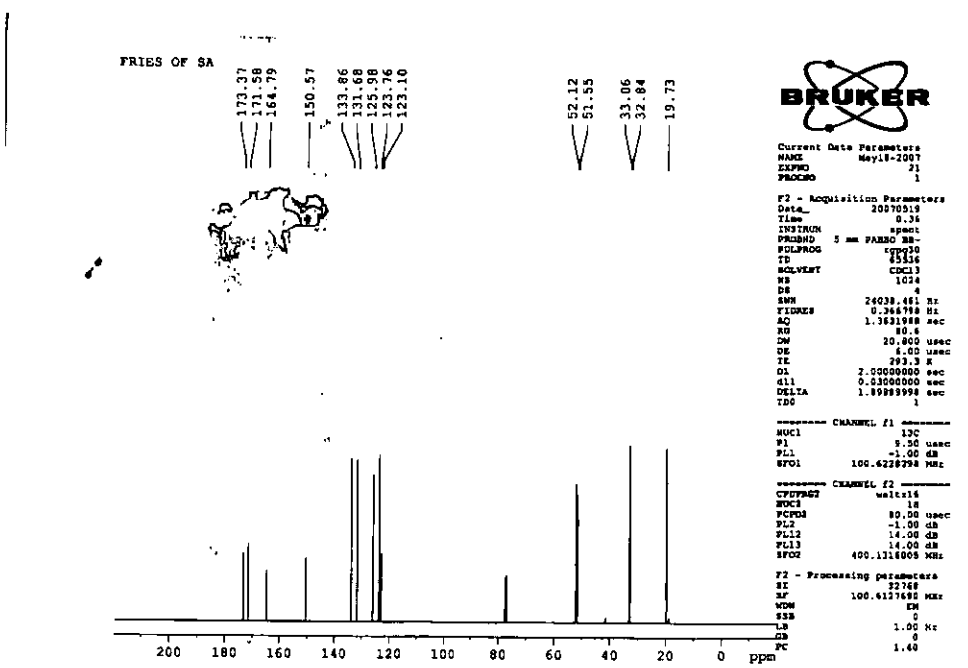

^{13}C-NMR of compound 17

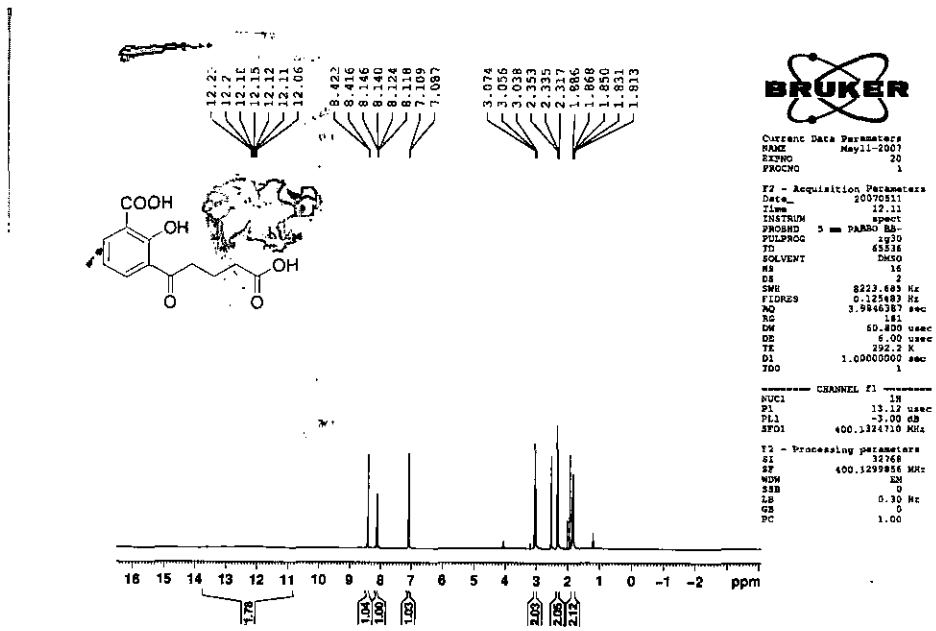

^{1}H-NMR of compound 18

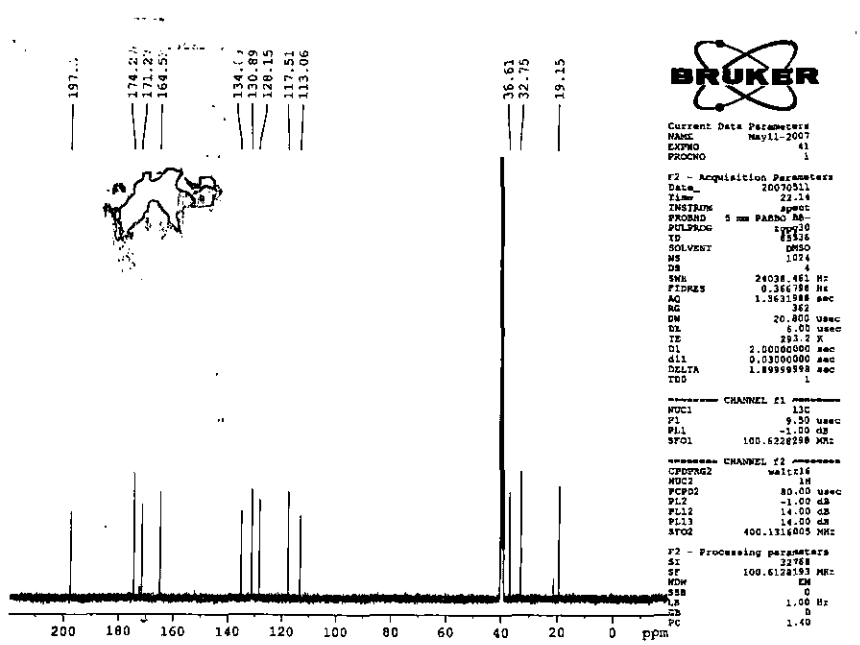

^{13}C-NMR of compound 18

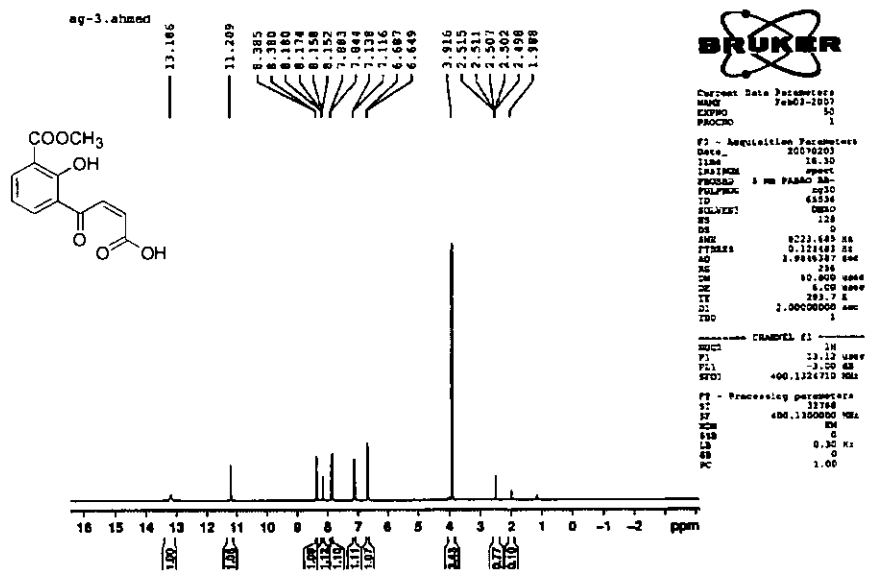

^{1}H-NMR of compound 19

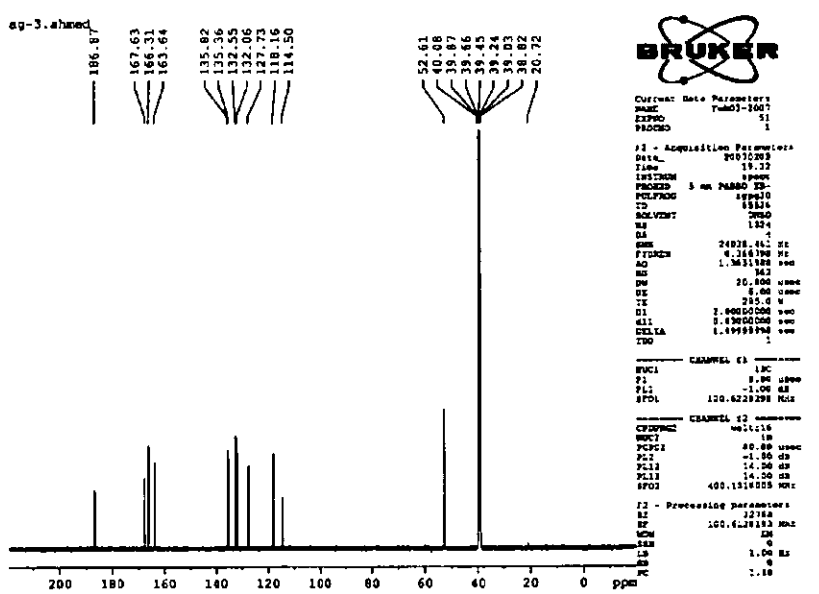

^{13}C-NMR of compound 19

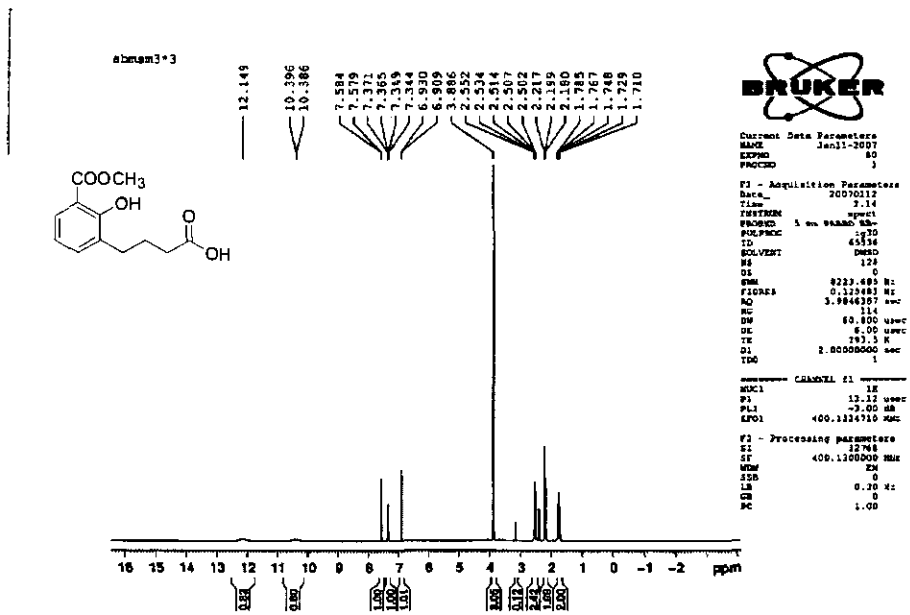

^{1}H-NMR of compound 20

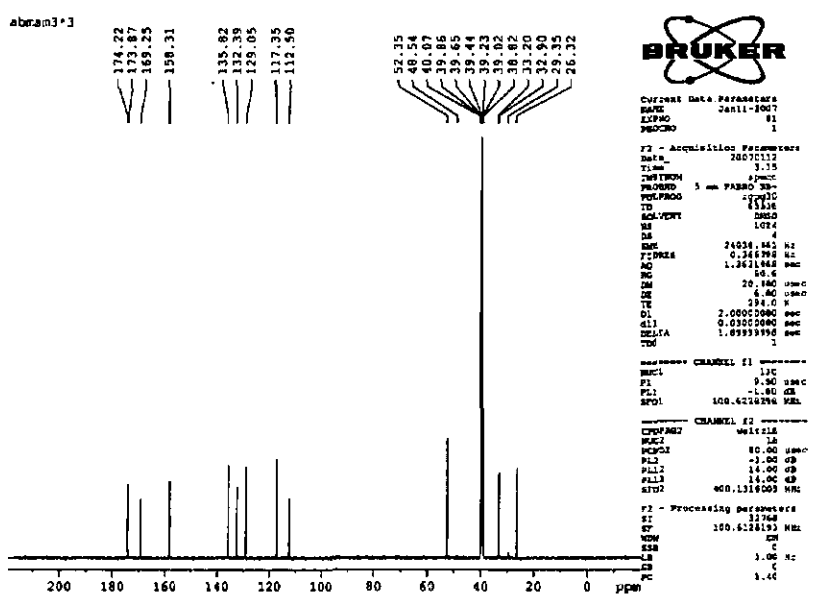

^{13}C-NMR of compound 20

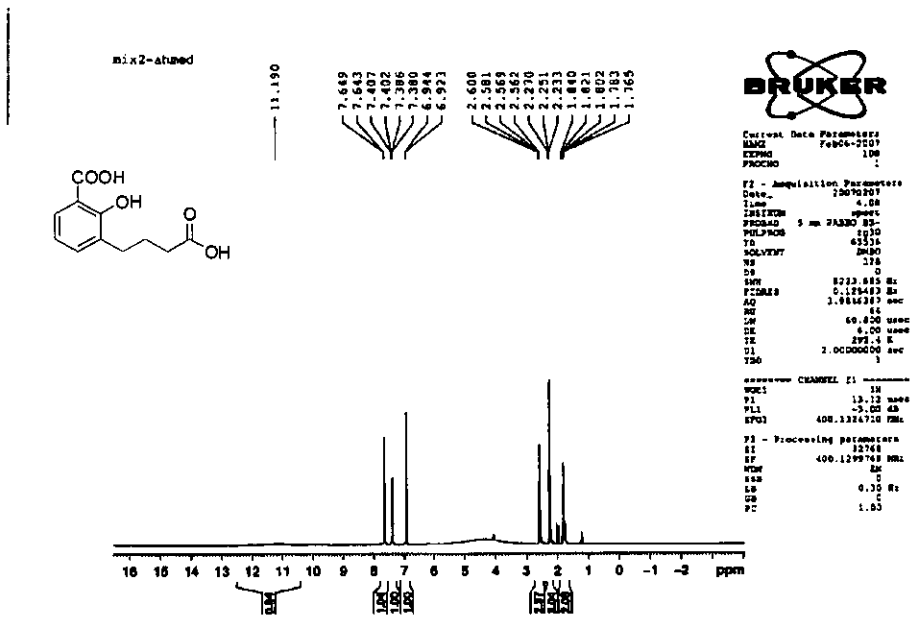

^{1}H-NMR of compound 21

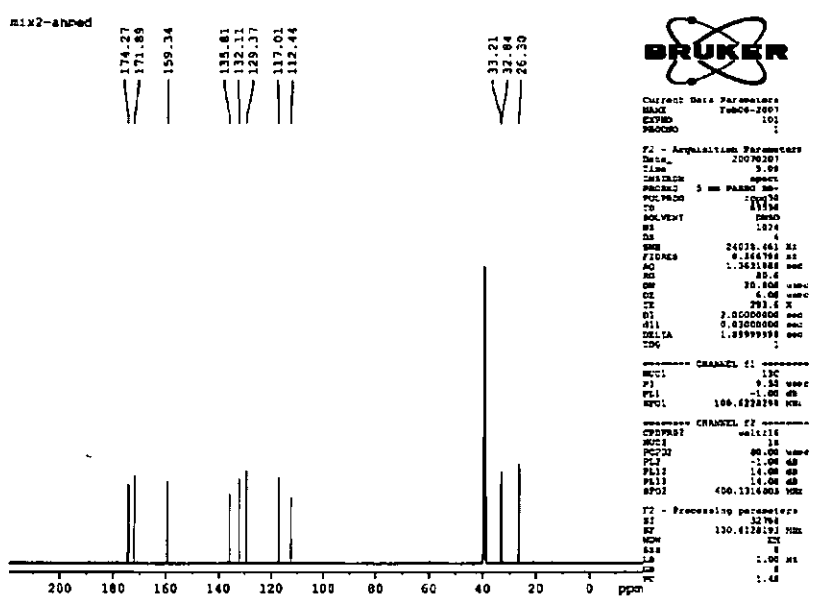

^{13}C-NMR of compound 21

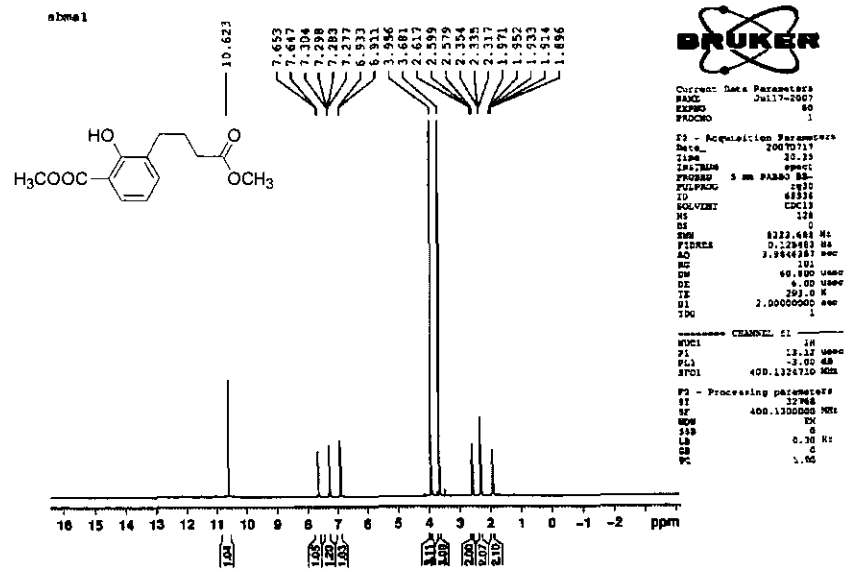

^{1}H-NMR of compound 22

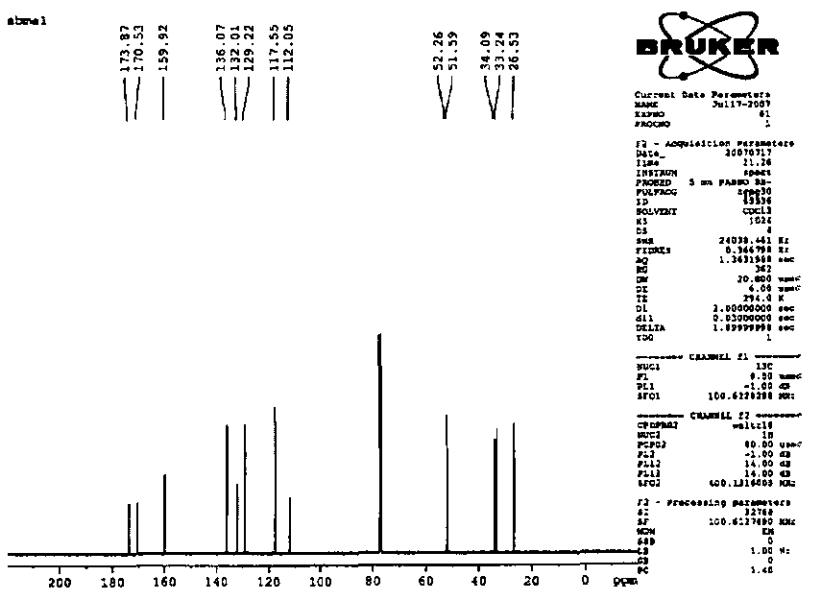

^{13}C-NMR of compound 22

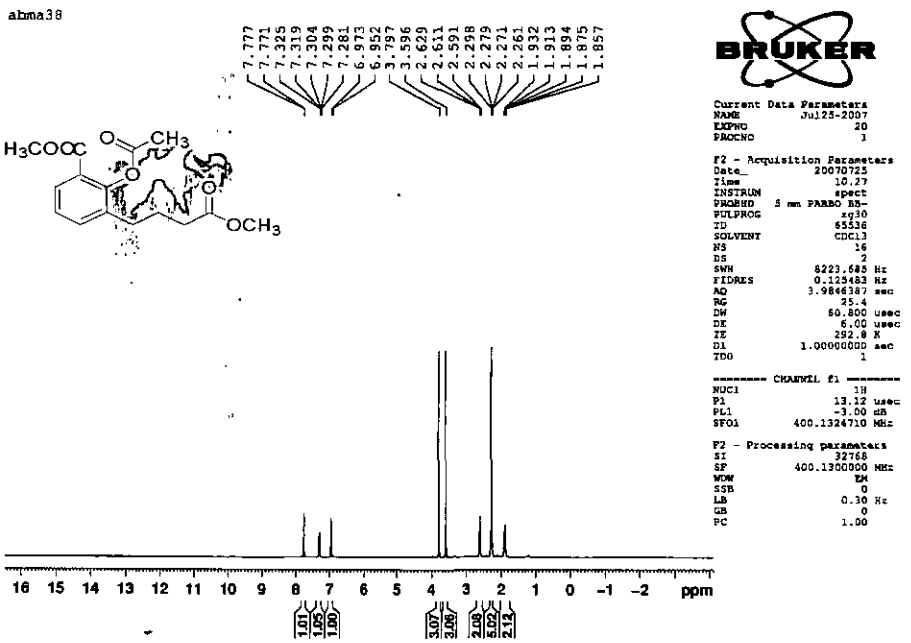

^{1}H-NMR of compound 23

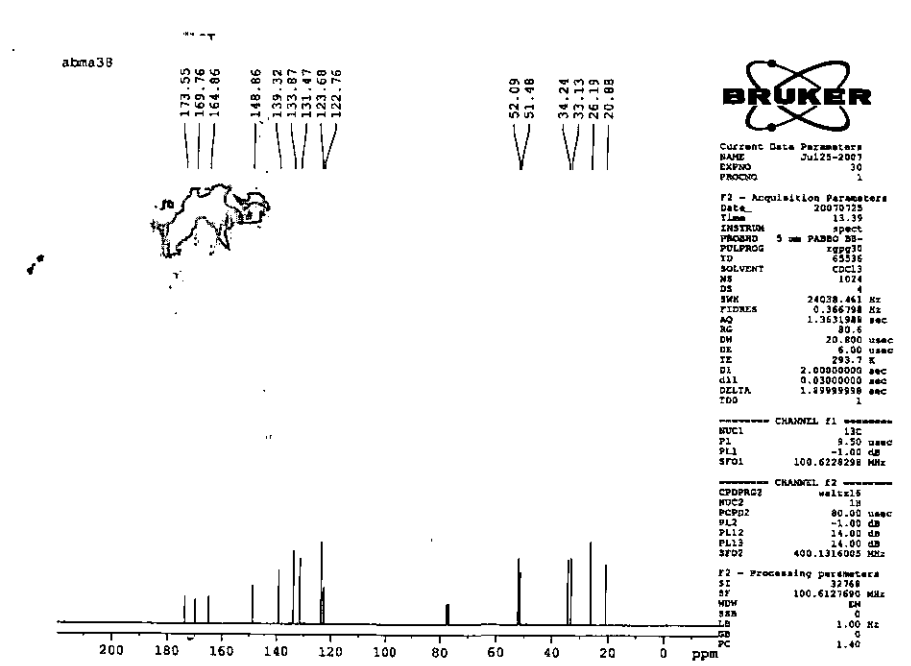

^{13}C-NMR of compound 23

Appendix Chapter 2

Chapter 2: NMR Spectra and lists of crystal data, bond lengths, bond angles and hydrogen bonds for:

N-acetoxy-2-hydroxy-benzamide (SalAc), 2.

N-acetoxy-2-acetoxybenzamide ($SalAc_2$), 3.

NMR Spectra for Chapter 2

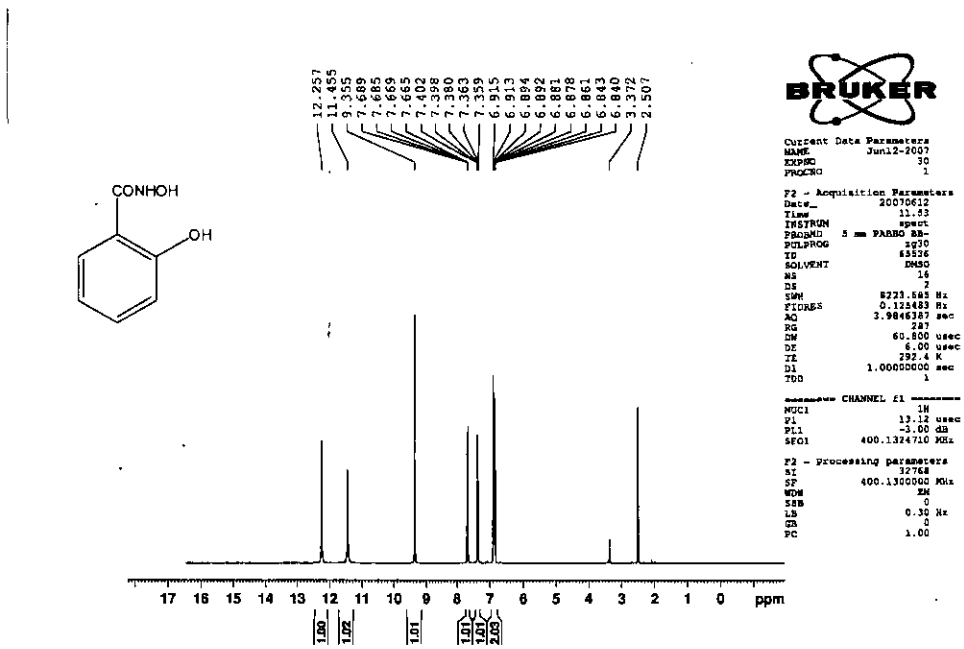

^{1}H-NMR of compound 1

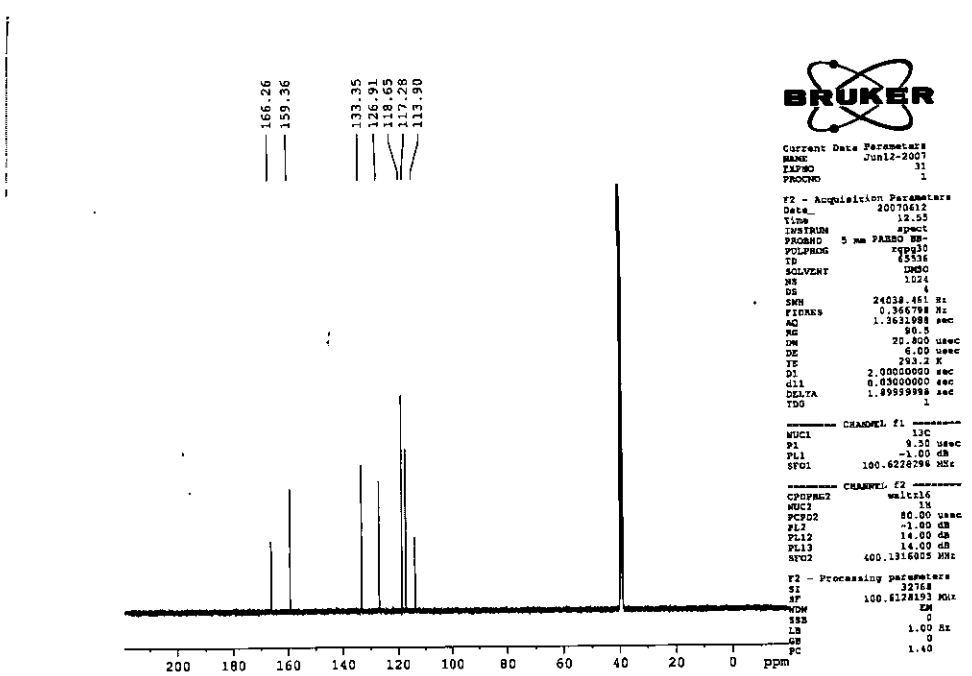

^{13}C-NMR of compound 1

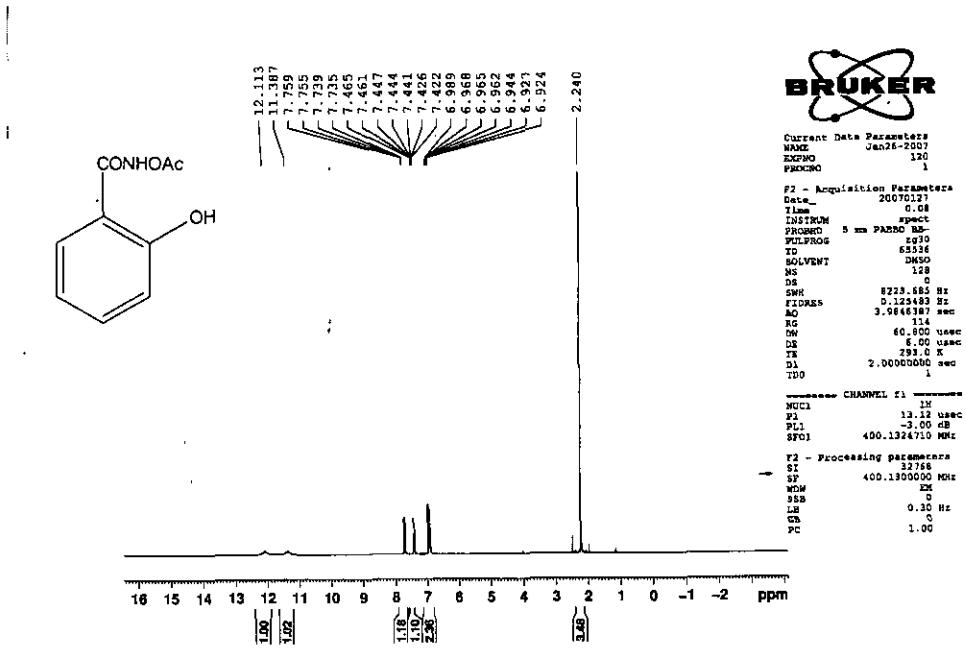

^{1}H-NMR of compound 2

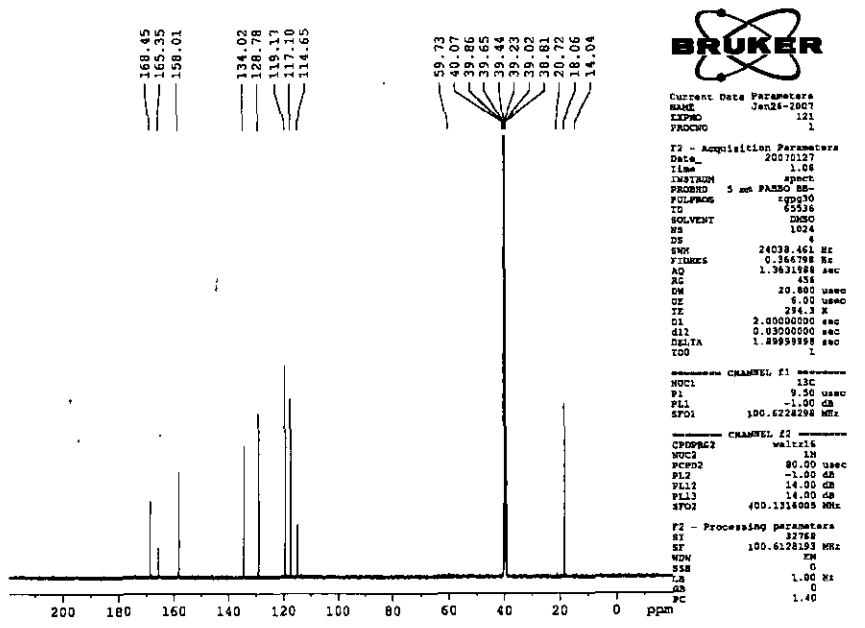

^{13}C-NMR of compound 2

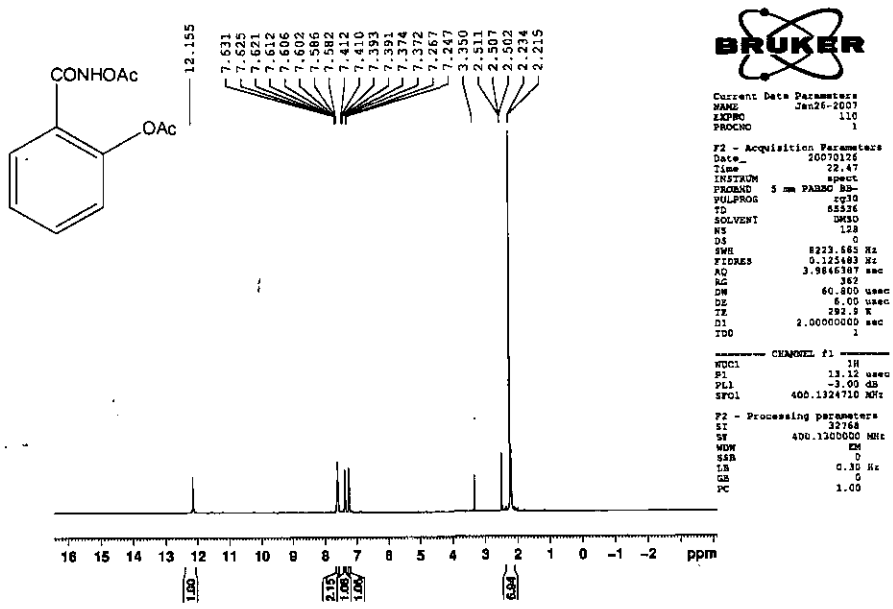

^{1}H-NMR of compound 3

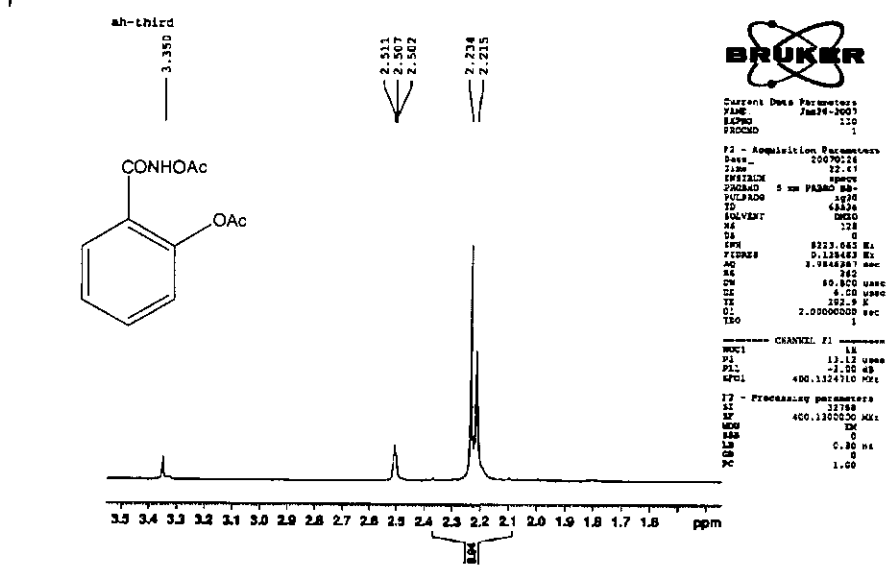

^{1}H-NMR of compound 3 (acetyl groups)

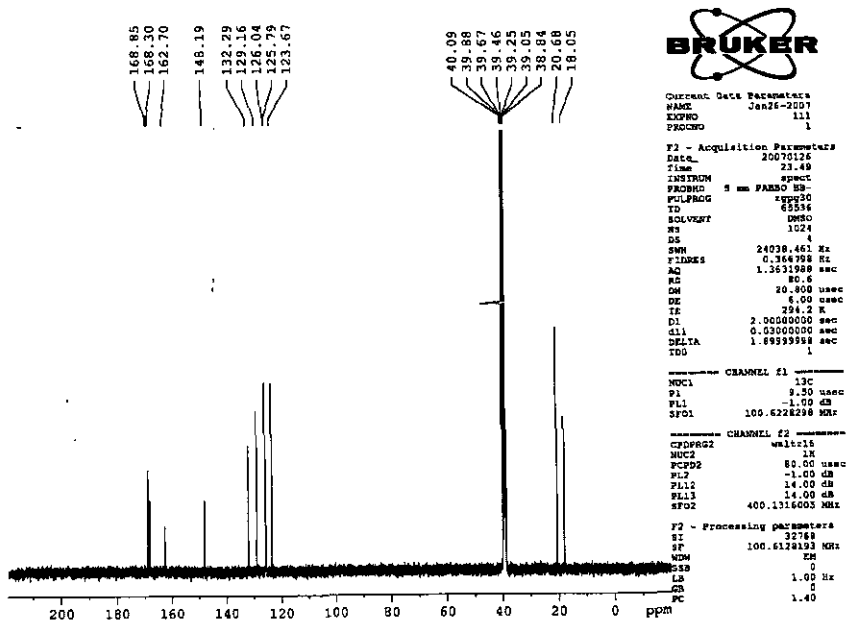

^{13}C-NMR of compound 3

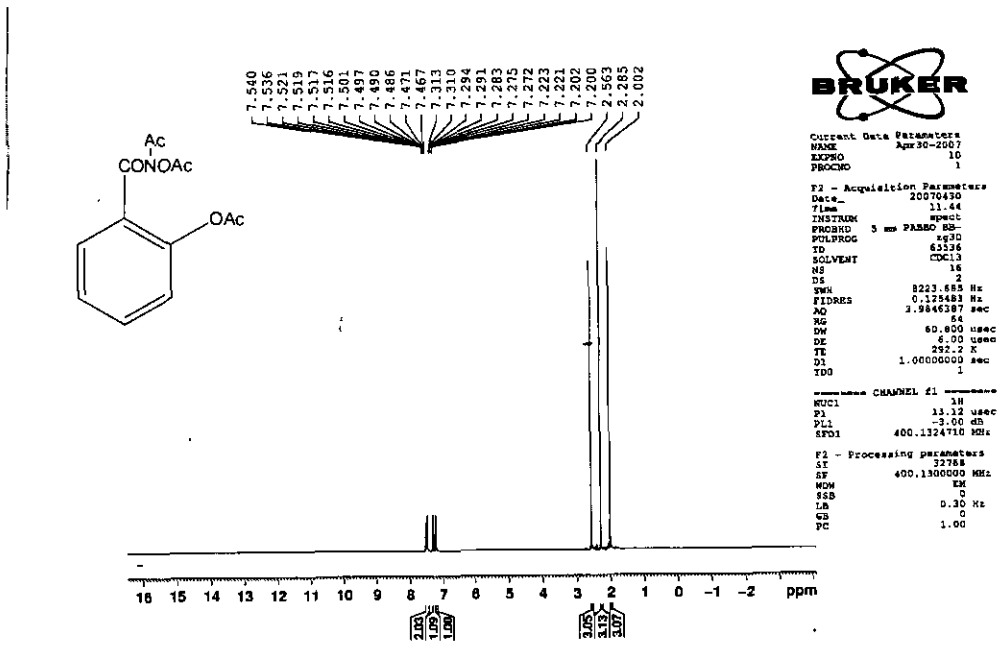

^{1}H-NMR of compound 4

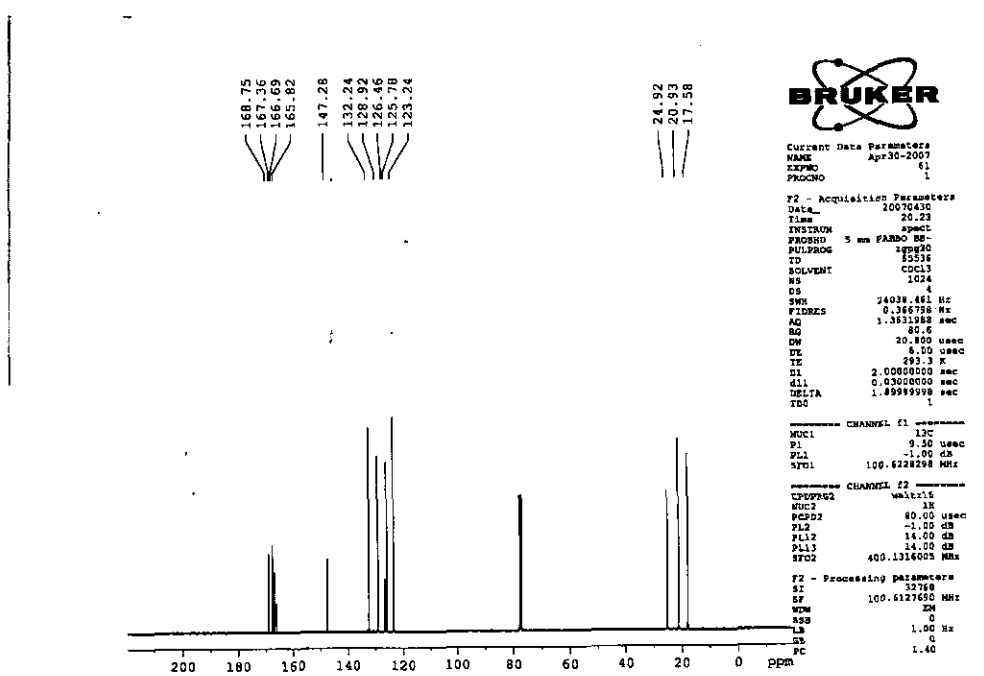

^{13}C-NMR of compound 4

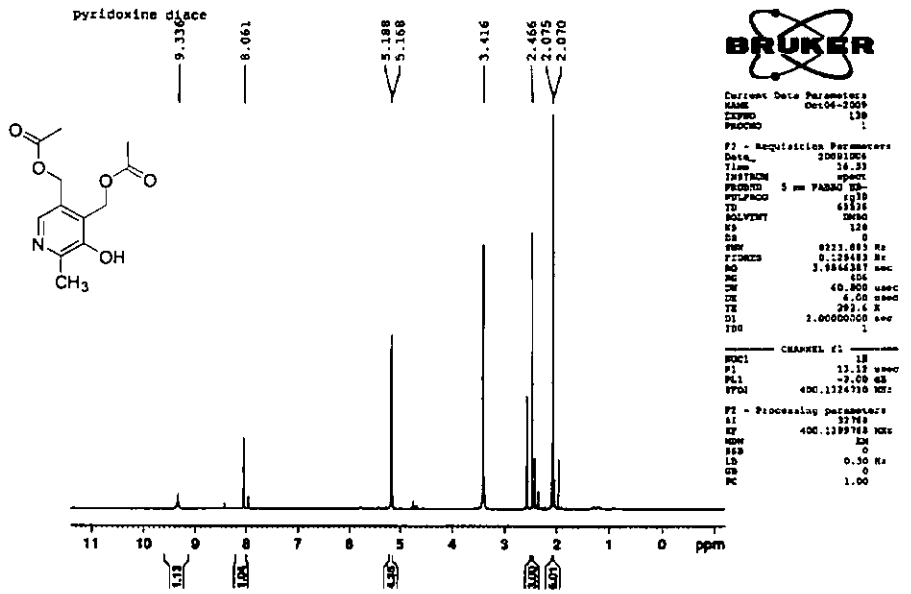

^{1}H-NMR of compound 9

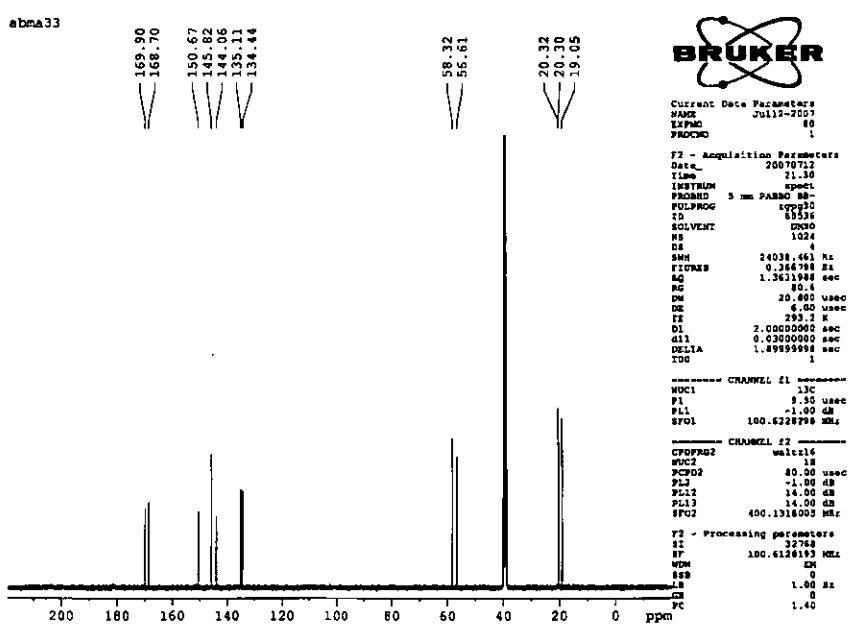

^{13}C-NMR of compound 9

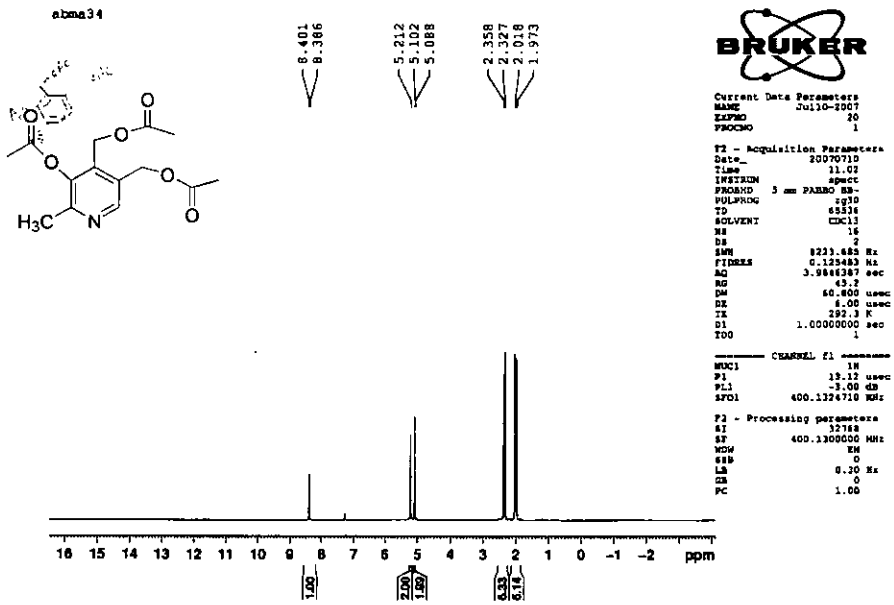

^{1}H-NMR of compound 10

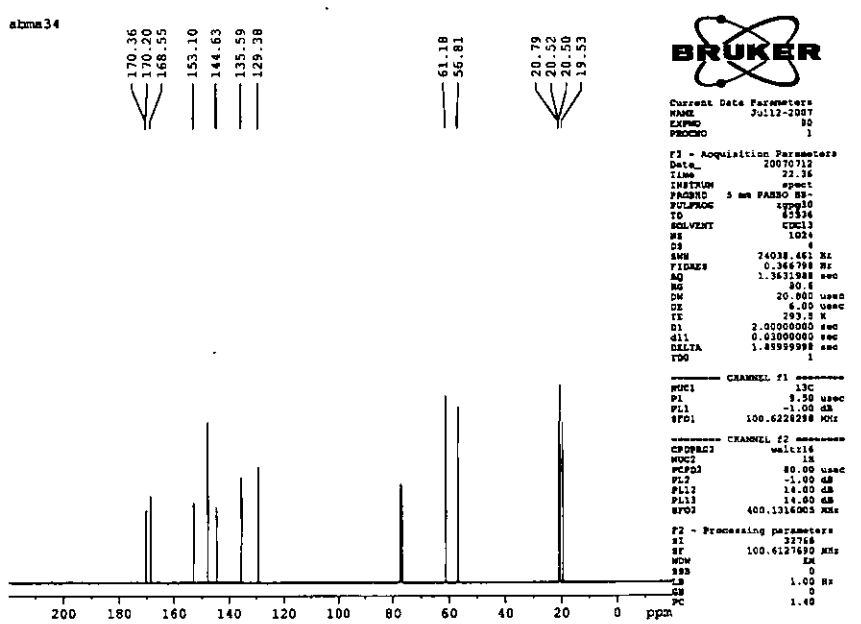

^{13}C-NMR of compound 10

Table 1: Crystal data for N-acetoxy-2-hydroxybenzamide (SalAc), 2

Compound	N-acetoxy-2-hydroxybenzamide SalAc
Empirical formula	$C_{36}H_{32}N_4O_{16}$
M_r	776.66
T/K	124(2)
Wavelength/ Å	0.71070
Crystal system	Triclinic
Space group	P-1
Unit cell dimensions	
a/Å	5.3529(6)
b/Å	12.6693(8)
c/Å	12.9339(18)
α/°	82.728(12)
β/°	89.823(12)
γ/°	88.140(9)
V/ Å^3	869.63(16)
Z	1
D_c/g cm^{-3}	1.483
μ/mm^{-1}	0.119
F(000)	404
Crystal size/mm	0.35x 0.25 x 0.20
θ range for data collection/°	3.43 to 28.26
Index ranges, hkl	$-7<=h<=7$, $-16<=k<=16$, $-17<=l<=17$
Reflections collected	15427
Independent reflections (R_{int})	4171 (0.0191)
Completeness to $\theta = 30.00°$	96.7 %
Refinement method	Full-matrix least-squares on F^2
Data / restraints / parameters	4171 / 0 / 255
Goodness–of–fit on F^2	1.067
Final R indices [$I > 2\sigma(I)$]	$R_1 = 0.0915$; $wR_2 = 0.2669$
R indices (all data)	$R_1 = 0.0928$; $wR_2 = 0.2675$
Largest diff. peak and hole/e nm^{-3}	0.817 and -0.476

Table 1: Atomic coordinates (x 10^4) and equivalent isotropic displacement parameters ($Å^2$x 10^3) for N-acetoxy-2-hydroxybenzamide (SalAc) U(eq) is defined as one third of the trace of the orthogonalized U^{ij} tensor.

Atom	x	y	z	U(eq)
O(1)	1754(4)	2745(2)	2088(2)	18(1)
O(3)	1475(5)	2011(2)	-971(2)	21(1)
O(6)	6870(5)	4146(2)	542(2)	21(1)
O(7)	4886(5)	3349(2)	-661(2)	19(1)
N(1)	3285(6)	2973(2)	156(2)	20(1)
C(1)	-3487(6)	941(3)	2237(3)	19(1)
C(2)	-3476(6)	652(3)	1235(3)	18(1)
C(3)	-1766(6)	1081(2)	511(2)	17(1)
C(4)	8(6)	1802(2)	780(2)	14(1)
C(5)	34(6)	2060(2)	1799(2)	14(1)
C(6)	-1742(6)	1640(3)	2522(2)	17(1)
C(7)	1672(6)	2252(2)	-82(2)	14(1)
C(8)	6673(6)	3988(3)	-353(3)	19(1)
C(9)	8190(7)	4422(3)	-1271(3)	23(1)
O(2)	2831(5)	2782(2)	7115(2)	19(1)
O(4)	3016(5)	2114(2)	4031(2)	25(1)
O(5)	1084(5)	4895(2)	3897(2)	25(1)
O(8)	-818(5)	3355(2)	4494(2)	22(1)
N(2)	1191(6)	3100(2)	5183(2)	21(1)
C(10)	8321(6)	975(3)	7167(3)	19(1)
C(11)	8314(6)	712(3)	6153(3)	20(1)
C(12)	6520(6)	1182(3)	5454(3)	18(1)
C(13)	4678(6)	1897(2)	5752(2)	14(1)
C(14)	4650(6)	2118(2)	6790(2)	14(1)
C(15)	6508(6)	1664(3)	7486(2)	17(1)
C(16)	2891(6)	2368(3)	4922(2)	17(1)
C(17)	-644(6)	4332(3)	3878(3)	19(1)
C(18)	-2935(7)	4512(3)	3209(3)	26(1)

Table 1: Bond lengths [Å] and angles [°] for N-acetoxy-2-hydroxybenzamide (SalAc)

Bond Atoms	Bond lengths [Å]	Bond Atoms	Bond lengths [Å]
O(1)-C(5)	1.369(4)	N(2)-H(3)	0.9623
O(3)-C(7)	1.232(4)	C(10)-C(15)	1.381(5)
O(6)-C(8)	1.205(4)	C(10)-C(11)	1.394(5)
O(7)-C(8)	1.365(4)	C(10)-H(10)	0.9500
O(7)-N(1)	1.404(3)	C(11)-C(12)	1.388(5)
N(1)-C(7)	1.341(4)	C(11)-H(11)	0.9500
N(1)-H(2)	0.9166	C(12)-C(13)	1.403(4)
C(1)-C(6)	1.390(5)	C(12)-H(12)	0.9500
C(1)-C(2)	1.391(5)	C(13)-C(14)	1.405(4)
C(1)-H(4)	0.9500	C(13)-C(16)	1.494(4)
C(2)-C(3)	1.381(5)	C(14)-C(15)	1.403(4)
C(2)-H(5)	0.9500	C(15)-H(13)	0.9500
C(3)-C(4)	1.413(4)	C(17)-C(18)	1.498(5)
C(3)-H(6)	0.9500	C(18)-H(1)	0.9800
C(4)-C(5)	1.398(4)	C(18)-H(8)	0.9800
C(4)-C(7)	1.493(4)	C(18)-H(9)	0.9800
C(5)-C(6)	1.400(4)		
C(6)-H(7)	0.9500	**Bond Atoms**	**Bond Angles [°]**
C(8)-C(9)	1.493(5)	C(8)-O(7)-N(1)	112.6(2)
C(9)-H(14)	0.9800	C(7)-N(1)-O(7)	114.6(3)
C(9)-H(15)	0.9800	C(7)-N(1)-H(2)	126.7
C(9)-H(16)	0.9800	O(7)-N(1)-H(2)	116.3
O(2)-C(14)	1.366(4)	C(6)-C(1)-C(2)	120.2(3)
O(4)-C(16)	1.237(4)	C(6)-C(1)-H(4)	119.9
O(5)-C(17)	1.189(4)	C(2)-C(1)-H(4)	119.9
O(8)-C(17)	1.390(4)	C(3)-C(2)-C(1)	119.9(3)
O(8)-N(2)	1.402(4)	C(3)-C(2)-H(5)	120.0
N(2)-C(16)	1.350(4)	C(1)-C(2)-H(5)	120.0

Continued: Table 1: Bond lengths [Å] and angles [°] for N-acetoxy-2-hydroxybenzamide (SalAc)

Bond Atoms	Bond Angles[°]	Bond Atoms	Bond Angles[°]
C(2)-C(3)-C(4)	120.8(3)	C(8)-C(9)-H(16)	109.5
C(2)-C(3)-H(6)	119.6	H(14)-C(9)-H(16)	109.5
C(4)-C(3)-H(6)	119.6	H(15)-C(9)-H(16)	109.5
C(5)-C(4)-C(3)	118.8(3)	C(17)-O(8)-N(2)	114.1(3)
C(5)-C(4)-C(7)	125.4(3)	C(16)-N(2)-O(8)	116.5(3)
C(3)-C(4)-C(7)	115.7(3)	C(16)-N(2)-H(3)	120.2
O(1)-C(5)-C(4)	120.2(3)	O(8)-N(2)-H(3)	118.2
O(1)-C(5)-C(6)	119.7(3)	C(15)-C(10)-C(11)	120.5(3)
C(4)-C(5)-C(6)	120.0(3)	C(15)-C(10)-H(10)	119.8
C(1)-C(6)-C(5)	120.2(3)	C(11)-C(10)-H(10)	119.8
C(1)-C(6)-H(7)	119.9	C(12)-C(11)-C(10)	119.2(3)
C(5)-C(6)-H(7)	119.9	C(12)-C(11)-H(11)	120.4
O(3)-C(7)-N(1)	122.4(3)	C(10)-C(11)-H(11)	120.4
O(3)-C(7)-C(4)	121.5(3)	C(11)-C(12)-C(13)	121.5(3)
N(1)-C(7)-C(4)	116.1(3)	C(11)-C(12)-H(12)	119.2
O(6)-C(8)-O(7)	121.7(3)	C(13)-C(12)-H(12)	119.2
O(6)-C(8)-C(9)	128.5(3)	C(12)-C(13)-C(14)	118.5(3)
O(7)-C(8)-C(9)	109.8(3)	C(12)-C(13)-C(16)	116.4(3)
C(8)-C(9)-H(14)	109.5	C(14)-C(13)-C(16)	125.1(3)
C(8)-C(9)-H(15)	109.5	O(2)-C(14)-C(15)	120.2(3)
H(14)-C(9)-H(15)	109.5	O(2)-C(14)-C(13)	120.0(3)
C(17)-C(18)-H(1)	109.5	C(15)-C(14)-C(13)	119.8(3)
C(17)-C(18)-H(8)	109.5	C(10)-C(15)-C(14)	120.5(3)
H(1)-C(18)-H(8)	109.5	C(10)-C(15)-H(13)	119.8
C(17)-C(18)-H(9)	109.5	C(14)-C(15)-H(13)	119.8
H(1)-C(18)-H(9)	109.5	O(4)-C(16)-N(2)	121.9(3)
H(8)-C(18)-H(9)	109.5	O(4)-C(16)-C(13)	121.0(3)
O(5)-C(17)-C(18)	127.9(3)	N(2)-C(16)-C(13)	117.0(3)
O(8)-C(17)-C(18)	108.3(3)	O(5)-C(17)-O(8)	123.8(3)

Symmetry transformations used to generate equivalent atoms:

Table 1: Anisotropic displacement parameters ($Å^2 x 10^3$) for N-acetoxy-2-hydroxybenzamide (SalAc) The anisotropic displacement factor exponent takes the form: $-2\pi^2[h^2 a^{*2} U^{11} + ... + 2 h k a^* b^* U^{12}]$

Atom	U^{11}	U^{22}	U^{33}	U^{23}	U^{13}	U^{12}
O(1)	25(1)	19(1)	11(1)	-2(1)	-2(1)	-5(1)
O(3)	29(1)	23(1)	12(1)	-5(1)	2(1)	-5(1)
O(6)	24(1)	22(1)	18(1)	-2(1)	-4(1)	-3(1)
O(7)	25(1)	22(1)	12(1)	-4(1)	5(1)	-8(1)
N(1)	24(1)	25(1)	11(1)	-3(1)	3(1)	-10(1)
C(1)	19(2)	18(2)	20(2)	0(1)	4(1)	-2(1)
C(2)	17(2)	19(2)	20(2)	-1(1)	-2(1)	-3(1)
C(3)	21(2)	15(1)	14(1)	-2(1)	-3(1)	-1(1)
C(4)	15(1)	14(1)	12(1)	-1(1)	0(1)	2(1)
C(5)	17(1)	12(1)	12(1)	0(1)	-1(1)	1(1)
C(6)	20(2)	19(1)	12(1)	-1(1)	2(1)	0(1)
C(7)	17(1)	13(1)	11(1)	-1(1)	-1(1)	1(1)
C(8)	19(2)	15(1)	21(2)	1(1)	-1(1)	1(1)
C(9)	20(2)	24(2)	24(2)	0(1)	4(1)	-3(1)
O(2)	24(1)	20(1)	13(1)	-3(1)	0(1)	6(1)
O(4)	33(1)	30(1)	11(1)	-3(1)	-2(1)	2(1)
O(5)	25(1)	27(1)	23(1)	0(1)	0(1)	-5(1)
O(8)	26(1)	19(1)	20(1)	3(1)	-9(1)	0(1)
N(2)	26(2)	23(1)	13(1)	-1(1)	-7(1)	4(1)
C(10)	18(2)	19(2)	18(2)	1(1)	-3(1)	0(1)
C(11)	22(2)	19(2)	19(2)	-2(1)	3(1)	1(1)
C(12)	21(2)	20(2)	14(1)	-3(1)	3(1)	-2(1)
C(13)	18(1)	15(1)	9(1)	0(1)	0(1)	-2(1)
C(14)	19(1)	12(1)	11(1)	-1(1)	0(1)	-1(1)
C(15)	21(2)	18(1)	12(1)	-3(1)	-2(1)	-2(1)
C(16)	21(2)	17(1)	13(1)	0(1)	-1(1)	-4(1)
C(17)	22(2)	20(2)	15(1)	-2(1)	1(1)	2(1)
C(18)	23(2)	25(2)	28(2)	3(1)	-5(1)	0(1)

Table 1: Hydrogen coordinates (x 10^4) and isotropic displacement parameters ($Å^2$x 10^3) for N-acetoxy-2-hydroxybenzamide (SalAc)

Atom	x	y	z	U(eq)
H(2)	3745	3097	811	24
H(4)	-4690	659	2729	23
H(5)	-4644	160	1048	22
H(6)	-1782	889	-175	20
H(7)	-1753	1834	3208	21
H(14)	7340	5060	-1632	34
H(15)	8388	3883	-1749	34
H(16)	9839	4606	-1035	34
H(3)	962	3206	5901	25
H(10)	9582	679	7643	22
H(11)	9522	216	5943	24
H(12)	6539	1016	4758	22
H(13)	6519	1832	8181	20
H(1)	-4427	4445	3651	39
H(8)	-2952	3982	2720	39
H(9)	-2925	5228	2819	39

Table 2: Crystal data for N-acetoxy-2-acetoxybenzamide ($SalAc_2$), 3

Compound	N-acetoxy-2-acetoxybenzamide ($SalAc_2$)
Empirical formula	$C_{44}H_{44}N_4O_{20}$
M_r	948.83
T/K	396(2)
Wavelength/ Å	0.71073
Crystal system	Triclinic
Space group	P-1
Unit cell dimensions	
a/Å	15.250(3)
b/Å	8.8357(16)
c/Å	8.4555(16)
α/°	90
β/°	95.548(4)
γ/°	90
V/ Å^3	1134.0(4)
Z	1
D_c/g cm^{-3}	1.389
μ/mm^{-1}	0.111
F(000)	496
Crystal size/mm	0.10 x 0.03 x 0.01
θ range for data collection/°	2.67 to 25.00
Index ranges, hkl	-16<=h<=18, -10<=k<=10, 10<=l<=10
Reflections collected	8765
Independent reflections (R_{int})	1996 (0.0602)
Completeness to θ = 30.00°	99.9 %
Refinement method	Full-matrix least-squares on F^2
Data / restraints / parameters	1996 / 0 / 156
Goodness–of–fit on F^2	1.110
Final R indices [I> 2σ (I)]	R_1 = 0.0551; wR_2 = 0.1132
R indices (all data)	R_1 = 0.0714; wR_2 = 0.1201

Table 2: Atomic coordinates (x 10^4) and equivalent isotropic displacement parameters ($Å^2$x 10^3) for N-acetoxy-2acetoxybenzamide ($SalAc_2$) U(eq) is defined as one third of the trace of the orthogonalized U^{ij} tensor.

Atom	x	y	z	U(eq)
O(1)	1826(1)	5971(2)	7778(2)	35(1)
O(2)	266(1)	7823(2)	5593(2)	49(1)
O(4)	4345(1)	5912(2)	6763(2)	52(1)
O(8)	1596(1)	8720(2)	6588(2)	32(1)
O(10)	3510(1)	6478(2)	4518(2)	32(1)
N(1)	1959(1)	7556(2)	5734(2)	37(1)
C(11)	3412(2)	3847(3)	3835(3)	38(1)
C(12)	2993(2)	2464(3)	3883(3)	43(1)
C(13)	2253(2)	2319(3)	4695(3)	41(1)
C(14)	1945(2)	3538(3)	5490(3)	36(1)
C(15)	2361(2)	4945(2)	5456(3)	27(1)
C(16)	3090(2)	5067(2)	4605(3)	29(1)
C(17)	4124(2)	6805(3)	5745(3)	35(1)
C(18)	4453(2)	8381(3)	5620(4)	53(1)
C(19)	680(2)	8690(3)	6448(3)	33(1)
C(20)	358(2)	9863(3)	7495(3)	45(1)
C(21)	2026(1)	6194(2)	6432(3)	26(1)

Table 2: Bond lengths [Å] and angles [°] for N-acetoxy-2-acetoxybenzamide ($SalAc_2$)

Bond Atoms	Bond lengths [Å]	Bond Atoms	Bond Angles[°]
O(1)-C(21)	1.222(3)	C(19)-O(8)-N(1)	112.65(17)
O(2)-C(19)	1.192(3)	C(17)-O(10)-C(16)	115.60(18)
O(4)-C(17)	1.192(3)	C(21)-N(1)-O(8)	116.70(18)
O(8)-C(19)	1.391(3)	C(21)-N(1)-H(1)	121.7
O(8)-N(1)	1.400(2)	O(8)-N(1)-H(1)	121.6
O(10)-C(17)	1.360(3)	C(16)-C(11)-C(12)	119.5(2)
O(10)-C(16)	1.407(3)	C(16)-C(11)-H(11)	120.2
N(1)-C(21)	1.340(3)	C(12)-C(11)-H(11)	120.2
N(1)-H(1)	0.8600	C(11)-C(12)-C(13)	119.9(2)
C(11)-C(16)	1.374(3)	C(11)-C(12)-H(12)	120.1
C(11)-C(12)	1.382(3)	C(13)-C(12)-H(12)	120.1
C(11)-H(11)	0.9300	C(14)-C(13)-C(12)	120.2(2)
C(12)-C(13)	1.382(4)	C(14)-C(13)-H(13)	119.9
C(12)-H(12)	0.9300	C(12)-C(13)-H(13)	119.9
C(13)-C(14)	1.376(3)	C(13)-C(14)-C(15)	120.7(2)
C(13)-H(13)	0.9300	C(13)-C(14)-H(14)	119.7
C(14)-C(15)	1.397(3)	C(15)-C(14)-H(14)	119.7
C(14)-H(14)	0.9300	C(16)-C(15)-C(14)	117.9(2)
C(15)-C(16)	1.386(3)	C(16)-C(15)-C(21)	124.23(19)
C(15)-C(21)	1.497(3)	C(14)-C(15)-C(21)	117.7(2)
C(17)-C(18)	1.488(4)	C(11)-C(16)-C(15)	121.8(2)
C(18)-H(18A)	0.9600	C(11)-C(16)-O(10)	119.0(2)
C(18)-H(18B)	0.9600	C(15)-C(16)-O(10)	119.23(19)
C(18)-H(18C)	0.9600	O(4)-C(17)-O(10)	122.4(2)
C(19)-C(20)	1.478(3)	O(4)-C(17)-C(18)	126.6(2)
C(20)-H(20A)	0.9600	O(10)-C(17)-C(18)	111.0(2)
C(20)-H(20B)	0.9600	C(17)-C(18)-H(18A)	109.5
C(20)-H(20C)	0.9600	C(17)-C(18)-H(18B)	109.5

Continued: Table 2: Bond lengths [Å] and angles [°] for N-acetoxy-2-acetoxybenzamide ($SalAc_2$)

Bond Atoms	Bond Angles[°]	Bond Atoms	Bond Angles[°]
H(18A)-C(18)-H(18B)	109.5	C(19)-C(20)-H(20B)	109.5
C(17)-C(18)-H(18C)	109.5	H(20A)-C(20)-H(20B)	109.5
H(18A)-C(18)-H(18C)	109.5	C(19)-C(20)-H(20C)	109.5
H(18B)-C(18)-H(18C)	109.5	H(20A)-C(20)-H(20C)	109.5
O(2)-C(19)-O(8)	122.2(2)	H(20B)-C(20)-H(20C)	109.5
O(2)-C(19)-C(20)	128.8(2)	O(1)-C(21)-N(1)	122.7(2)
O(8)-C(19)-C(20)	109.0(2)	O(1)-C(21)-C(15)	121.54(19)
C(19)-C(20)-H(20A)	109.5	N(1)-C(21)-C(15)	115.78(19)

Symmetry transformations used to generate equivalent atoms:

Table 3: Anisotropic displacement parameters ($Å^2 x 10^3$) for N-acetoxy-2-acetoxybenzamide ($SalAc_2$) the anisotropic displacement factor exponent takes the form: $-2\pi^2[h^2 a^{*2} U^{11} + ... + 2 h k a^* b^* U^{12}]$

Atom	U^{11}	U^{22}	U^{33}	U^{23}	U^{13}	U^{12}
O(1)	47(1)	29(1)	29(1)	1(1)	9(1)	-4(1)
O(2)	51(1)	45(1)	50(1)	-4(1)	-4(1)	-10(1)
O(4)	55(1)	49(1)	47(1)	9(1)	-11(1)	-12(1)
O(8)	36(1)	25(1)	36(1)	-3(1)	9(1)	3(1)
O(10)	33(1)	29(1)	34(1)	2(1)	3(1)	-2(1)
N(1)	54(1)	26(1)	33(1)	0(1)	21(1)	7(1)
C(11)	38(1)	38(2)	37(1)	-5(1)	3(1)	6(1)
C(12)	52(2)	31(1)	43(2)	-11(1)	-3(1)	8(1)
C(13)	51(2)	26(1)	44(2)	-4(1)	-4(1)	-6(1)
C(14)	41(2)	30(1)	39(2)	-1(1)	3(1)	-4(1)
C(15)	33(1)	23(1)	24(1)	2(1)	0(1)	1(1)
C(16)	31(1)	26(1)	29(1)	2(1)	-2(1)	1(1)
C(17)	33(1)	37(1)	34(1)	-3(1)	8(1)	-4(1)
C(18)	62(2)	43(2)	54(2)	-2(1)	8(2)	-17(1)
C(19)	39(1)	30(1)	31(1)	7(1)	3(1)	-2(1)
C(20)	39(2)	49(2)	47(2)	4(1)	8(1)	14(1)
C(21)	27(1)	26(1)	25(1)	1(1)	3(1)	-5(1)

Table 2: Hydrogen coordinates (x 10^4) and isotropic displacement parameters ($Å^2$x 10^3) for N-acetoxy-2-acetoxybenzamide ($SalAc_2$)

Atom	x	y	z	U(eq)
H(1)	2129	7708	4806	44
H(11)	3908	3952	3287	45
H(12)	3208	1631	3369	51
H(13)	1962	1394	4704	49
H(14)	1456	3423	6056	44
H(18A)	4859	8606	6529	79
H(18B)	3967	9074	5580	79
H(18C)	4747	8481	4671	79
H(20A)	-239	10120	7131	67
H(20B)	722	10748	7473	67
H(20C)	382	9483	8562	67

Appendix Chapter 3

Chapter 3: lists of crystal data, bond lengths, bond angles, torsion angles and hydrogen bonds for:

3-Hydroxy-2-methyl-3H-quinazolin-4-one (ChaH), 4.

Fe^{III}(4-Apha)$_3$.C_2H_5OH, 8.

Fe(Cha)$_2$(Cl)(H_2O).7/2H_2O, 9.

Co(Cha)$_2$(C_2H_5OH)$_2$, 11.

Ni(Cha)$_2$(C_2H_5OH)$_2$, 12.

Cu(Cha)H_2O(Cl), 14.

[Zn(Cha)$_2$].2H_2O, 15.

Table 4: Crystal data and structure refinement for $C_9H_8N_2O_2$ (ChaH), 4.

Complex	**3-Hydroxy-2-methyl-3H-quinazolin-4-one (ChaH), 4.**
Empirical formula	$C_9 H_8 N_2 O_2$
M_r	176.17
T/K	100(2)
Wavelength/ Å	0.71073
Crystal system	Monoclinic
Space group	$P2_1$ (#4)
Unit cell dimensions	
a/Å	4.3271(6)
b/Å	9.3902(13)
c/Å	9.6743(13)
α/°	90
β/°	95.837(3)
γ/°	90
V/ Å^3	391.05(9)
Z	2
D_c/g cm^{-3}	1.496
μ/mm^{-1}	0.109
F(000)	184
Crystal size/mm	0.50 x 0.20 x 0.10
θ range for data collection/°	2.12 to 32.01
Index ranges, hkl	$-6<=h<=6$, $-13<=k<=13$, $-13<=l<=14$
Reflections collected	9464
Independent reflections (R_{int})	1363 (0.0260)
Completeness to $\theta = 30.00°$	99.9 %
Absorption correction	none
Max./min. transmission	0.9892 and 0.9383
Refinement method	Full–matrix least–squares on F^2
Data / restraints / parameters	1363 / 1 / 123
Goodness–of–fit on F^2	1.036
Final R indices [$I > 2\sigma(I)$]	$R_1 = 0.0398$; $wR_2 = 0.1035$
R indices (all data)	$R_1 = 0.0411$, $wR_2 = 0.1046$
Largest diff. peak and hole/e nm^{-3}	0.535 and –0.158

Complete lists of bond lengths, bond angles, torsion angles and hydrogen bonds

Table 4a: Atomic coordinates (x 10^4) and equivalent isotropic displacement parameters ($Å^2$x 10^3) for $C_9H_8N_2O_2$ (ChaH). U(eq) is defined as one third of the trace of the orthogonalized U^{ij} tensor

Atom	x	y	z	U(eq)
N(1)	10455(3)	762(1)	3921(1)	13(1)
C(1)	9495(3)	1619(1)	4848(1)	13(1)
C(2)	10696(3)	1473(2)	6340(1)	17(1)
N(2)	7343(3)	2661(1)	4501(1)	13(1)
O(1)	6222(3)	3422(1)	5567(1)	17(1)
C(3)	5922(3)	2920(2)	3160(1)	14(1)
O(2)	3958(3)	3839(1)	2934(1)	20(1)
C(4)	7081(3)	1982(1)	2124(1)	13(1)
C(5)	5956(3)	2136(2)	720(2)	16(1)
C(6)	6995(3)	1234(2)	-258(1)	17(1)
C(7)	9169(3)	172(2)	150(2)	17(1)
C(8)	10295(3)	10(2)	1530(1)	15(1)
C(9)	9258(3)	923(1)	2541(1)	13(1)

Table 4b: Bond lengths [Å] and angles [°] for $C_9H_8N_2O_2$ (ChaH)

Bond Atoms	Bond lengths [Å]	Bond Atoms	Bond lengths [Å]
N(1)–C(1)	1.3037(18)	C(3)–C(4)	1.4608(17)
N(1)–C(9)	1.3906(16)	C(4)–C(9)	1.4012(18)
C(1)–N(2)	1.3689(17)	C(4)–C(5)	1.4022(18)
C(1)–C(2)	1.4899(18)	C(5)–C(6)	1.379(2)
C(2)–H(2A)	0.9800	C(5)–H(5)	0.9500
C(2)–H(2B)	0.9800	C(6)–C(7)	1.401(2)
C(2)–H(2C)	0.9800	C(6)–H(6)	0.9500
N(2)–O(1)	1.3823(14)	C(7)–C(8)	1.3820(19)
N(2)–C(3)	1.3998(17)	C(7)–H(7)	0.9500
O(1)–H(1O1)	0.90(3)	C(8)–C(9)	1.4074(18)
C(3)–O(2)	1.2149(18)	C(8)–H(8)	0.9500

Bond Atoms	Bond Angles[°]	Bond Atoms	Bond Angles[°]
C(1)–N(1)–C(9)	118.67(11)	C(9)–C(4)–C(5)	120.58(12)
N(1)–C(1)–N(2)	121.95(12)	C(9)–C(4)–C(3)	119.88(12)
N(1)–C(1)–C(2)	120.34(12)	C(5)–C(4)–C(3)	119.52(12)
N(2)–C(1)–C(2)	117.70(12)	C(6)–C(5)–C(4)	119.76(13)
C(1)–C(2)–H(2A)	109.5	C(6)–C(5)–H(5)	120.1
C(1)–C(2)–H(2B)	109.5	C(4)–C(5)–H(5)	120.1
H(2A)–C(2)–H(2B)	109.5	C(5)–C(6)–C(7)	120.01(12)
C(1)–C(2)–H(2C)	109.5	C(5)–C(6)–H(6)	120.0
H(2A)–C(2)–H(2C)	109.5	C(7)–C(6)–H(6)	120.0
H(2B)–C(2)–H(2C)	109.5	C(8)–C(7)–C(6)	120.76(13)
C(1)–N(2)–O(1)	117.90(11)	C(8)–C(7)–H(7)	119.6
C(1)–N(2)–C(3)	125.12(11)	C(6)–C(7)–H(7)	119.6
O(1)–N(2)–C(3)	116.60(11)	C(7)–C(8)–C(9)	119.88(13)
N(2)–O(1)–H(1O1)	105.6(18)	C(7)–C(8)–H(8)	120.1
O(2)–C(3)–N(2)	121.54(12)	C(9)–C(8)–H(8)	120.1
O(2)–C(3)–C(4)	125.99(12)	N(1)–C(9)–C(4)	121.84(11)
N(2)–C(3)–C(4)	112.47(11)	N(1)–C(9)–C(8)	119.15(12)
		C(4)–C(9)–C(8)	119.00(12)

Symmetry transformations used to generate equivalent atoms

Table 4c: Anisotropic displacement parameters ($Å^2 x 10^3$) for $C_9H_8N_2O_2$ (ChaH). The anisotropic displacement factor exponent takes the form: $-2\pi^2[h^2 a^{*2} U^{11} + ... + 2 h k a^* b^* U^{12}]$

Atom	U^{11}	U^{22}	U^{33}	U^{23}	U^{13}	U^{12}
N(1)	16(1)	12(1)	13(1)	1(1)	1(1)	1(1)
C(1)	14(1)	11(1)	13(1)	0(1)	2(1)	-2(1)
C(2)	20(1)	19(1)	12(1)	1(1)	1(1)	-2(1)
N(2)	15(1)	12(1)	13(1)	-3(1)	3(1)	0(1)
O(1)	21(1)	15(1)	16(1)	-5(1)	7(1)	-2(1)
C(3)	15(1)	13(1)	15(1)	-2(1)	1(1)	-2(1)
O(2)	21(1)	16(1)	23(1)	-2(1)	-1(1)	5(1)
C(4)	14(1)	11(1)	13(1)	-1(1)	1(1)	-1(1)
C(5)	17(1)	16(1)	15(1)	1(1)	-1(1)	-1(1)
C(6)	19(1)	20(1)	13(1)	0(1)	1(1)	-3(1)
C(7)	18(1)	17(1)	15(1)	-3(1)	4(1)	-4(1)
C(8)	18(1)	13(1)	15(1)	-1(1)	4(1)	0(1)
C(9)	14(1)	11(1)	13(1)	0(1)	2(1)	-1(1)

Table 4d: Hydrogen coordinates ($x 10^4$) and isotropic displacement parameters ($Å^2 x 10^3$) for $C_9H_8N_2O_2$ (ChaH)

Atom	x	y	z	U(eq)
H(2A)	9096	1038	6852	25
H(2B)	11229	2415	6728	25
H(2C)	12552	868	6421	25
H(1O1)	7350(60)	4230(30)	5650(30)	30(6)
H(5)	4483	2858	445	20
H(6)	6235	1334	-1210	21
H(7)	9879	-445	-529	20
H(8)	11765	-716	1796	18

Table 4e: Torsion angles [°] for $C_9H_8N_2O_2$ (ChaH)

C(9)–N(1)–C(1)–N(2)	0.33(19)	N(2)–C(3)–C(4)–C(5)	–178.11(12)
C(9)–N(1)–C(1)–C(2)	179.39(11)	C(9)–C(4)–C(5)–C(6)	0.1(2)
N(1)–C(1)–N(2)–O(1)	173.38(12)	C(3)–C(4)–C(5)–C(6)	–178.69(12)
C(2)–C(1)–N(2)–O(1)	–5.70(17)	C(4)–C(5)–C(6)–C(7)	–0.1(2)
N(1)–C(1)–N(2)–C(3)	0.8(2)	C(5)–C(6)–C(7)–C(8)	0.1(2)
C(2)–C(1)–N(2)–C(3)	–178.31(12)	C(6)–C(7)–C(8)–C(9)	–0.2(2)
C(1)–N(2)–C(3)–O(2)	177.74(13)	C(1)–N(1)–C(9)–C(4)	0.50(19)
O(1)–N(2)–C(3)–O(2)	5.04(19)	C(1)–N(1)–C(9)–C(8)	179.55(12)
C(1)–N(2)–C(3)–C(4)	–2.40(18)	C(5)–C(4)–C(9)–N(1)	178.86(12)
O(1)–N(2)–C(3)–C(4)	–175.10(10)	C(3)–C(4)–C(9)–N(1)	–2.31(19)
O(2)–C(3)–C(4)–C(9)	–177.09(14)	C(5)–C(4)–C(9)–C(8)	–0.19(19)
N(2)–C(3)–C(4)–C(9)	3.05(17)	C(3)–C(4)–C(9)–C(8)	178.63(12)
O(2)–C(3)–C(4)–C(5)	1.7(2)	C(7)–C(8)–C(9)–N(1)	–178.87(12)
		C(7)–C(8)–C(9)–C(4)	0.2(2)

Symmetry transformations used to generate equivalent atoms

Table 4f: Hydrogen bonds for $C_9H_8N_2O_2$ (ChaH) [Å and °]

D–H...A	d(D–H)	d(H...A)	d(D...A)	<(DHA)
O(1)–H(1O1)...N(1)#1	0.90(3)	1.75(3)	2.6451(17)	171(3)

Symmetry transformations used to generate equivalent atoms:

#1 –x+2,y+1/2,–z+1

Table 5: Crystal data and structure refinement for $Fe^{III}(4\text{-Apha})_3.C_2H_5OH$, 8.

Complex	**$Fe^{III}(4\text{-AphaH})_3.C_2H_5OH$, 8.**
Molecular formula	$C_{21}H_{21}N_6O_6Fe \times C_2H_6O$
Empirical formula	$C_{23}H_{27}N_6O_7Fe$
M_r	555.36
T/K	100(2)
Wavelength/ Å	0.71073
Crystal system	Triclinic
Space group	P–1 (#2)
Unit cell dimensions	
a/Å	10.6232(18)
b/Å	10.6455(18)
c/Å	13.225(2)
α/°	107.550(3)
β/°	91.085(4)
γ/°	112.217(3)
V/ Å^3	1305.1(4)
Z	2
D_c/g cm^{-3}	1.413
μ/mm^{-1}	0.631
F(000)	578
Crystal size/mm	0.30 x 0.20 x 0.03
θ range for data collection/°	1.63 to 27.11
Index ranges, hkl	$-13<=h<=13$, $-13<=k<=13$, $-16<=l<=16$
Reflections collected	24614
Independent reflections (R_{int})	5739 (0.0444)
Completeness to $\theta = 30.00°$	99.6 %
Absorption correction	Semi–empirical from equivalents
Max./min. transmission	0.9813 and 0.8825
Refinement method	Full–matrix least–squares on F^2
Data / restraints / parameters	5739 / 0 / 433
Goodness–of–fit on F^2	1.061
Final R indices [$I > 2\sigma(I)$]	$R_1 = 0.0396$; $wR_2 = 0.0905$
R indices (all data)	$R_1 = 0.0473$; $wR_2 = 0.0940$
Largest diff. peak and hole/e nm^{-3}	0.425 and –0.311

Table 5a: Atomic coordinates (x 10^4) and equivalent isotropic displacement parameters ($Å^2$x 10^3) for $Fe^{III}(4\text{-AphaH})_3.C_2H_5OH$ U(eq) is defined as one third of the trace of the orthogonalized U^{ij} tensor

Atom	x	y	z	U(eq)
Fe	1388(1)	3616(1)	1628(1)	12(1)
O(2)	665(1)	1614(1)	662(1)	18(1)
N(1)	–531(2)	780(2)	948(1)	19(1)
C(1)	–862(2)	1334(2)	1880(2)	16(1)
O(1)	–124(1)	2656(1)	2421(1)	16(1)
C(2)	–2049(2)	445(2)	2262(2)	18(1)
C(3)	–2669(2)	1117(2)	3040(2)	24(1)
C(4)	–3816(2)	325(3)	3394(2)	28(1)
C(5)	–4376(2)	–1172(2)	2994(2)	24(1)
N(2)	–5509(2)	–1970(3)	3375(2)	34(1)
C(6)	–3739(3)	–1848(2)	2234(2)	32(1)
C(7)	–2604(2)	–1056(2)	1865(2)	29(1)
O(4)	401(2)	4193(1)	686(1)	18(1)
N(3)	398(2)	5527(2)	1200(1)	19(1)
C(8)	1040(2)	6232(2)	2180(2)	15(1)
O(3)	1572(1)	5603(1)	2636(1)	15(1)
C(9)	1150(2)	7704(2)	2717(2)	15(1)
C(10)	1173(2)	8613(2)	2137(2)	20(1)
C(11)	1315(2)	10008(2)	2658(2)	21(1)
C(12)	1403(2)	10527(2)	3777(2)	18(1)
N(4)	1479(2)	11887(2)	4277(2)	24(1)
C(13)	1409(2)	9625(2)	4359(2)	18(1)
C(14)	1295(2)	8241(2)	3838(2)	17(1)
O(6)	3028(1)	4102(2)	902(1)	18(1)
N(5)	4160(2)	4154(2)	1468(1)	17(1)
C(15)	4028(2)	3985(2)	2410(2)	14(1)
O(5)	2846(1)	3730(1)	2723(1)	16(1)
C(16)	5226(2)	4146(2)	3095(2)	15(1)
C(17)	5013(2)	3612(2)	3950(2)	18(1)

Continued: Table 5a: Atomic coordinates (x 10^4) and equivalent isotropic displacement parameters (Å^{2}x 10^3) for [Fe^{III}(4-AphaH)$_3$](C_2H_5OH)]. U(eq) is defined as one third of the trace of the orthogonalized U^{ij} tensor.

Atom	x	y	z	U(eq)
C(18)	6104(2)	3822(2)	4653(2)	18(1)
C(19)	7457(2)	4587(2)	4530(2)	16(1)
N(6)	8551(2)	4808(2)	5240(2)	20(1)
C(20)	7675(2)	5081(2)	3657(2)	19(1)
C(21)	6581(2)	4880(2)	2957(2)	19(1)
O(7)	6287(2)	4191(2)	320(1)	30(1)
C(22)	6632(3)	2992(3)	–101(2)	45(1)
C(23A) [a)]	5904(9)	1809(6)	278(5)	48(2)
C(23B) [b)]	6799(14)	2255(11)	608(8)	52(3)

[a)] s.o.f. = 0.63(1) [b)] s.o.f. = 0.37(1) (s.o.f.: site occupation factor; the sum of the s.o.f.'s a) and b) is constrained to be 1)

Table 5b: Bond lengths [Å] and angles [°] for [Fe^{III}(4-AphaH)$_3$](C_2H_5OH)].

Bond Atoms	Bond lengths [Å]	Bond Atoms	Bond lengths [Å]	Bond Atoms	Bond lengths [Å]
Fe–O(2)	1.9615(14)	C(4)–C(5)	1.391(3)	C(9)–C(14)	1.401(3)
Fe–O(6)	1.9769(14)	C(4)–H(4)	0.94(3)	C(10)–C(11)	1.382(3)
Fe–O(4)	1.9822(14)	C(5)–N(2)	1.390(3)	C(10)–H(10)	0.92(2)
Fe–O(5)	2.0444(14)	C(5)–C(6)	1.395(3)	C(11)–C(12)	1.402(3)
Fe–O(1)	2.0470(14)	N(2)–H(1N2)	0.80(3)	C(11)–H(11)	0.95(2)
Fe–O(3)	2.0654(13)	N(2)–H(2N2)	0.90(3)	C(12)–N(4)	1.368(3)
O(2)–N(1)	1.383(2)	C(6)–C(7)	1.380(3)	C(12)–C(13)	1.402(3)
N(1)–C(1)	1.315(3)	C(6)–H(6)	0.96(3)	N(4)–H(1N4)	0.83(3)
N(1)–H(1N1)	0.84(3)	C(7)–H(7)	0.92(3)	N(4)–H(2N4)	0.90(3)
C(1)–O(1)	1.282(2)	O(4)–N(3)	1.378(2)	C(13)–C(14)	1.382(3)
C(1)–C(2)	1.466(3)	N(3)–C(8)	1.304(3)	C(13)–H(13)	0.90(2)
C(2)–C(3)	1.394(3)	N(3)–H(1N3)	0.86(3)	C(14)–H(14)	0.94(2)
C(2)–C(7)	1.396(3)	C(8)–O(3)	1.283(2)	O(6)–N(5)	1.379(2)
C(3)–C(4)	1.378(3)	C(8)–C(9)	1.470(3)	N(5)–C(15)	1.313(3)
C(3)–H(3)	0.93(3)	C(9)–C(10)	1.398(3)	N(5)–H(1N5)	0.84(2)

Continued: Table 5b: Bond lengths [Å] and angles [°] for $[Fe^{III}(4\text{-AphaH})_3](C_2H_5OH)]$.

Bond Atoms	Bond lengths [Å]	Bond Atoms	Bond Angles[°]	Bond Atoms	Bond Angles[°]
C(15)–O(5)	1.285(2)	O(2)–Fe–O(5)	104.13(6)	C(5)–N(2)–H(1N2)	114(2)
C(16)–C(17)	1.396(3)	O(6)–Fe–O(5)	78.92(5)	C(5)–N(2)–H(2N2)	112.1(19)
C(16)–C(21)	1.400(3)	O(4)–Fe–O(5)	160.68(6)	H(1N2)–N(2)H(2N2)	114(3)
C(17)–C(18)	1.377(3)	O(2)–Fe–O(1)	79.40(5)	C(7)–C(6)–C(5)	121.0(2)
C(17)–H(17)	0.96(2)	O(6)–Fe–O(1)	162.99(6)	C(7)–C(6)–H(6)	120.4(17)
C(18)–C(19)	1.400(3)	O(4)–Fe–O(1)	102.49(6)	C(5)–C(6)–H(6)	118.6(17)
C(18)–H(18)	0.92(2)	O(5)–Fe–O(1)	90.01(6)	C(6)–C(7)–C(2)	120.6(2)
C(19)–N(6)	1.381(3)	O(2)–Fe–O(3)	163.96(6)	C(6)–C(7)–H(7)	120.1(17)
C(19)–C(20)	1.396(3)	O(6)–Fe–O(3)	102.91(6)	C(2)–C(7)–H(7)	119.2(17)
N(6)–H(1N6)	0.84(2)	O(4)–Fe–O(3)	78.63(5)	N(3)–O(4)–Fe	111.77(11)
N(6)–H(2N6)	0.82(3)	O(5)–Fe–O(3)	86.98(5)	C(8)–N(3)–O(4)	118.68(16)
C(20)–C(21)	1.380(3)	O(1)–Fe–O(3)	89.21(5)	C(8)–N(3)–H(1N3)	127.3(17)
C(20)–H(20)	0.90(2)	N(1)–O(2)–Fe	111.18(11)	O(4)–N(3)–H(1N3)	113.2(17)
C(21)–H(21)	0.94(2)	C(1)–N(1)–O(2)	117.85(16)	O(3)–C(8)–N(3)	117.74(17)
O(7)–C(22)	1.417(3)	C(1)–N(1)–H(1N1)	129.3(18)	O(3)–C(8)–C(9)	122.39(17)
O(7)–H(1O7)	0.78(3)	O(2)–N(1)–H(1N1)	112.1(18)	N(3)–C(8)–C(9)	119.87(17)
C(22)–C(23B)	1.438(8)	O(1)–C(1)–N(1)	117.72(18)	C(8)–O(3)–Fe	113.04(12)
C(22)–C(23A)	1.446(5)	O(1)–C(1)–C(2)	122.48(17)	C(10)–C(9)–C(14)	118.69(18)
C(22)–H(22A)	0.9900	N(1)–C(1)–C(2)	119.79(17)	C(10)–C(9)–C(8)	121.53(18)
C(22)–H(22B)	0.9900	C(1)–O(1)–Fe	112.64(12)	C(14)–C(9)–C(8)	119.73(17)
C(22)–H(22C)	0.9900	C(3)–C(2)–C(7)	118.2(2)	C(11)–C(10)–C(9)	120.73(19)
C(22)–H(22D)	0.9900	C(3)–C(2)–C(1)	119.10(18)	C(11)–C(10)–H(10)	118.5(13)
C(23A)–H(22C)	1.5366	C(7)–C(2)–C(1)	122.69(19)	C(9)–C(10)–H(10)	120.7(13)
C(23A)–H(23A)	0.9800	C(4)–C(3)–C(2)	121.1(2)	C(10)–C(11)–C(12)	120.61(19)
C(23A)–H(23B)	0.9800	C(4)–C(3)–H(3)	119.6(17)	C(10)–C(11)–H(11)	118.6(13)
C(23A)–H(23C)	0.9800	C(2)–C(3)–H(3)	119.3(17)	C(12)–C(11)–H(11)	120.8(13)
C(23B)–H(23D)	0.9800	C(3)–C(4)–C(5)	120.8(2)	N(4)–C(12)–C(13)	121.5(2)
C(23B)–H(23E)	0.9800	C(3)–C(4)–H(4)	121.3(16)	N(4)–C(12)–C(11)	119.96(19)
C(23B)–H(23F)	0.9800	C(5)–C(4)–H(4)	117.9(16)	C(13)–C(12)–C(11)	118.58(18)
O(2)–Fe–O(6)	90.72(6)	N(2)–C(5)–C(4)	120.7(2)	C(12)–N(4)–H(1N4)	114.5(18)
O(2)–Fe–O(4)	92.73(6)	N(2)–C(5)–C(6)	121.0(2)	C(12)–N(4)–H(2N4)	117.8(18)
O(6)–Fe–O(4)	91.70(6)	C(4)–C(5)–C(6)	118.3(2)	H(1N4)–N(4)H(2N4)	125(3)

Continued: Table 5b: Bond lengths [Å] and angles [°] for $[Fe^{III}(4\text{-AphaH})_3](C_2H_5OH)]$.

Bond Atoms	Bond Angles[°]	Bond Atoms	Bond Angles[°]
C(14)–C(13)–C(12)	120.63(19)	C(20)–C(21)–H(21)	118.1(13)
C(14)–C(13)–H(13)	119.5(15)	C(16)–C(21)–H(21)	121.3(13)
C(12)–C(13)–H(13)	119.8(15)	C(22)–O(7)–H(1O7)	113(2)
C(13)–C(14)–C(9)	120.68(18)	O(7)–C(22)–C(23B)	118.2(4)
C(13)–C(14)–H(14)	119.0(13)	O(7)–C(22)–C(23A)	113.5(3)
C(9)–C(14)–H(14)	120.3(13)	C(23B)–C(22)–C(23A)	37.0(4)
N(5)–O(6)–Fe	112.13(11)	O(7)–C(22)–H(22A)	108.9
C(15)–N(5)–O(6)	117.38(16)	C(23B)–C(22)–H(22A)	73.0
C(15)–N(5)–H(1N5)	127.0(15)	C(23A)–C(22)–H(22A)	108.9
O(6)–N(5)–H(1N5)	114.4(15)	O(7)–C(22)–H(22B)	108.9
O(5)–C(15)–N(5)	118.19(17)	C(23B)–C(22)–H(22B)	129.9
O(5)–C(15)–C(16)	121.59(17)	C(23A)–C(22)–H(22B)	108.9
N(5)–C(15)–C(16)	120.18(17)	H(22A)–C(22)–H(22B)	107.7
C(15)–O(5)–Fe	113.19(12)	O(7)–C(22)–H(22C)	107.7
C(17)–C(16)–C(21)	118.42(18)	C(23B)–C(22)–H(22C)	107.9
C(17)–C(16)–C(15)	119.09(18)	C(23A)–C(22)–H(22C)	75.6
C(21)–C(16)–C(15)	122.41(18)	H(22A)–C(22)–H(22C)	136.9
C(18)–C(17)–C(16)	121.01(19)	H(22B)–C(22)–H(22C)	37.7
C(18)–C(17)–H(17)	120.6(14)	O(7)–C(22)–H(22D)	107.7
C(16)–C(17)–H(17)	118.4(14)	C(23B)–C(22)–H(22D)	107.6
C(17)–C(18)–C(19)	120.58(19)	C(23A)–C(22)–H(22D)	135.6
C(17)–C(18)–H(18)	118.3(15)	H(22A)–C(22)–H(22D)	39.5
C(19)–C(18)–H(18)	121.1(15)	H(22B)–C(22)–H(22D)	71.1
N(6)–C(19)–C(20)	120.91(19)	H(22C)–C(22)–H(22D)	107.1
N(6)–C(19)–C(18)	120.57(19)	C(22)–C(23A)–H(22C)	38.6
C(20)–C(19)–C(18)	118.49(18)	C(22)–C(23A)–H(23A)	109.5
C(19)–N(6)–H(1N6)	115.4(14)	H(22C)–C(23A)–H(23A)	142.0
C(19)–N(6)–H(2N6)	117(2)	C(22)–C(23A)–H(23B)	109.5
H(1N6)–N(6)–H(2N6)	115(2)	H(22C)–C(23A)–H(23B)	102.8
C(21)–C(20)–C(19)	120.82(19)	C(22)–C(23A)–H(23C)	109.5
C(21)–C(20)–H(20)	119.1(14)	H(22C)–C(23A)–H(23C)	76.8
C(19)–C(20)–H(20)	119.9(14)	C(22)–C(23B)–H(23D)	109.5
C(20)–C(21)–C(16)	120.62(19)	C(22)–C(23B)–H(23E)	109.5

Continued: Table 5b: Bond lengths [Å] and angles [°] for $[Fe^{III}(4\text{-AphaH})_3](C_2H_5OH)]$.

Bond Atoms	Bond Angles[°]
H(23D)–C(23B)–H(23E)	109.5
C(22)–C(23B)–H(23F)	109.5
H(23D)–C(23B)–H(23F)	109.5
H(23E)–C(23B)–H(23F)	109.5

Symmetry transformations used to generate equivalent atoms

Table 5c: Anisotropic displacement parameters ($Å^2 x\ 10^3$) for $[Fe^{III}(4\text{-AphaH})_3](C_2H_5OH)]$.
The anisotropic displacement factor exponent takes the form: $-2\pi^2[\ h^2\ a^{*2}U^{11} + ... + 2\ h\ k\ a^*\ b^*\ U^{12}\ ]$.

Atom	U^{11}	U^{22}	U^{33}	U^{23}	U^{13}	U^{12}
Fe	14(1)	10(1)	12(1)	3(1)	1(1)	5(1)
O(2)	19(1)	12(1)	19(1)	2(1)	7(1)	4(1)
N(1)	19(1)	11(1)	20(1)	0(1)	4(1)	3(1)
C(1)	16(1)	13(1)	19(1).	3(1)	1(1)	6(1)
O(1)	18(1)	10(1)	17(1)	2(1)	3(1)	4(1)
C(2)	18(1)	15(1)	20(1)	6(1)	2(1)	6(1)
C(3)	25(1)	14(1)	29(1)	5(1)	9(1)	5(1)
C(4)	28(1)	26(1)	32(1)	11(1)	15(1)	12(1)
C(5)	18(1)	25(1)	30(1)	16(1)	0(1)	4(1)
N(2)	23(1)	33(1)	45(1)	23(1)	6(1)	2(1)
C(6)	30(1)	15(1)	44(2)	10(1)	7(1)	2(1)
C(7)	30(1)	15(1)	38(1)	5(1)	13(1)	9(1)
O(4)	27(1)	13(1)	13(1)	0(1)	–2(1)	11(1)
N(3)	26(1)	17(1)	16(1)	3(1)	–1(1)	13(1)
C(8)	16(1)	14(1)	14(1)	5(1)	2(1)	6(1)
O(3)	19(1)	12(1)	14(1)	4(1)	–1(1)	6(1)
C(9)	16(1)	14(1)	16(1)	4(1)	2(1)	7(1)
C(10)	26(1)	19(1)	16(1)	6(1)	3(1)	11(1)
C(11)	25(1)	19(1)	23(1)	11(1)	4(1)	12(1)
C(12)	15(1)	15(1)	26(1)	7(1)	6(1)	6(1)
N(4)	33(1)	15(1)	24(1)	5(1)	8(1)	11(1)
C(13)	20(1)	17(1)	15(1)	3(1)	4(1)	7(1)
C(14)	19(1)	14(1)	18(1)	7(1)	3(1)	6(1)

Continued: Table 5c: Anisotropic displacement parameters ($Å^2$x 10^3) for $[Fe^{III}(4AphaH)_3](C_2H_5OH)]$. The anisotropic displacement factor exponent takes the form: $-2\pi^2[h^2 a^{*2}U^{11} + ... + 2 h k a^* b^* U^{12}]$.

Atom	U^{11}	U^{22}	U^{33}	U^{23}	U^{13}	U^{12}
O(6)	16(1)	25(1)	17(1)	11(1)	2(1)	9(1)
N(5)	15(1)	23(1)	18(1)	10(1)	5(1)	9(1)
C(15)	18(1)	10(1)	16(1)	4(1)	3(1)	6(1)
O(5)	16(1)	17(1)	16(1)	7(1)	3(1)	7(1)
C(16)	18(1)	14(1)	16(1)	5(1)	3(1)	9(1)
C(17)	18(1)	16(1)	20(1)	7(1)	5(1)	7(1)
C(18)	23(1)	20(1)	15(1)	9(1)	5(1)	11(1)
C(19)	20(1)	14(1)	14(1)	1(1)	2(1)	10(1)
N(6)	20(1)	25(1)	17(1)	8(1)	4(1)	10(1)
C(20)	14(1)	19(1)	21(1)	7(1)	5(1)	5(1)
C(21)	20(1)	20(1)	17(1)	9(1)	4(1)	7(1)
O(7)	37(1)	37(1)	33(1)	24(1)	20(1)	22(1)
C(22)	64(2)	50(2)	40(2)	22(1)	23(1)	37(2)
C(23A) [a)]	63(5)	36(3)	58(4)	23(3)	21(3)	26(3)
C(23B) [b)]	48(7)	39(5)	69(6)	15(4)	–16(5)	22(5)

[a)] s.o.f. = 0.63(1) [b)] s.o.f. = 0.37(1) (s.o.f.: site occupation factor; the sum of the s.o.f.'s a) and b) is constrained to be 1)

Table 5d: Hydrogen coordinates (x 10^4) and isotropic displacement parameters ($Å^2$x 10^3) for $[Fe^{III}(4\text{-}AphaH)_3](C_2H_5OH)]$.

Atom	x	y	z	U(eq)
H(1N1)	–870(30)	–70(30)	520(20)	35(7)
H(3)	–2310(30)	2110(30)	3310(20)	39(7)
H(4)	–4250(30)	780(30)	3910(20)	31(7)
H(1N2)	–5950(30)	–2770(30)	2960(20)	40(9)
H(2N2)	–6020(30)	–1470(30)	3640(20)	48(9)
H(6)	–4100(30)	–2880(30)	1980(20)	43(8)
H(7)	–2190(30)	–1520(30)	1360(20)	37(7)
H(1N3)	80(30)	5850(30)	780(20)	29(7)
H(10)	1160(20)	8320(20)	1403(18)	14(5)
H(11)	1350(20)	10600(20)	2244(17)	15(5)

H(1N4)	1650(30)	12170(30)	4940(20)	27(7)
H(2N4)	1610(30)	12470(30)	3880(20)	42(8)
H(13)	1480(20)	9950(30)	5080(20)	24(6)
H(14)	1290(20)	7650(20)	4247(17)	10(5)
H(1N5)	4800(20)	4120(20)	1112(18)	16(6)
H(17)	4080(20)	3110(20)	4045(18)	21(6)
H(18)	5920(20)	3460(30)	5211(19)	24(6)
H(1N6)	8350(20)	4670(20)	5823(18)	8(5)
H(2N6)	9270(30)	5490(30)	5290(20)	37(8)
H(20)	8540(20)	5590(20)	3568(17)	15(5)
H(21)	6770(20)	5270(20)	2400(17)	12(5)
H(1O7)	6510(30)	4730(30)	0(20)	30(7)
H(22A) [a)]	7633	3304	97	54
H(22B) [a)]	6425	2649	–893	54
H(22C) [b)]	5911	2283	–711	54
H(22D) [b)]	7502	3321	–395	54
H(23A) [a)]	5992	2168	1062	73
H(23B) [a)]	6297	1088	61	73
H(23C) [a)]	4929	1371	–32	73
H(23D) [b)]	7001	1432	207	77
H(23E) [b)]	5950	1914	912	77
H(23F) b)	7561	2917	1189	77

[a)] s.o.f. = 0.63(1) [b)] s.o.f. = 0.37(1) (s.o.f.: site occupation factor; the sum of the s.o.f.'s a) and b) is constrained to be 1)

Table 5e: Torsion angles [°] for $[Fe^{III}(4\text{-AphaH}_{-1})_3](C_2H_5OH)]$.

O(6)–Fe–O(2)–N(1)	175.55(12)	O(2)–Fe–O(4)–N(3)	166.76(12)
O(4)–Fe–O(2)–N(1)	–92.72(12)	O(6)–Fe–O(4)–N(3)	–102.43(12)
O(5)–Fe–O(2)–N(1)	96.80(12)	O(5)–Fe–O(4)–N(3)	–42.2(2)
O(1)–Fe–O(2)–N(1)	9.49(11)	O(1)–Fe–O(4)–N(3)	87.02(12)
O(3)–Fe–O(2)–N(1)	–36.0(3)	O(3)–Fe–O(4)–N(3)	0.40(11)
Fe–O(2)–N(1)–C(1)	–11.7(2)	Fe–O(4)–N(3)–C(8)	1.7(2)
O(2)–N(1)–C(1)–O(1)	6.1(3)	O(4)–N(3)–C(8)–O(3)	–4.0(3)
O(2)–N(1)–C(1)–C(2)	–174.36(16)	O(4)–N(3)–C(8)–C(9)	175.04(16)
N(1)–C(1)–O(1)–Fe	2.5(2)	N(3)–C(8)–O(3)–Fe	4.1(2)
C(2)–C(1)–O(1)–Fe	–176.99(14)	C(9)–C(8)–O(3)–Fe	–174.89(14)
O(2)–Fe–O(1)–C(1)	–6.88(13)	O(2)–Fe–O(3)–C(8)	–60.9(3)

O(6)–Fe–O(1)–C(1)	–62.3(2)	O(6)–Fe–O(3)–C(8)	86.72(13)
O(4)–Fe–O(1)–C(1)	83.59(13)	O(4)–Fe–O(3)–C(8)	–2.41(12)
O(5)–Fe–O(1)–C(1)	–111.26(13)	O(5)–Fe–O(3)–C(8)	164.62(13)
O(3)–Fe–O(1)–C(1)	161.76(13)	O(1)–Fe–O(3)–C(8)	–105.33(13)
O(1)–C(1)–C(2)–C(3)	20.6(3)	O(3)–C(8)–C(9)–C(10)	149.8(2)
N(1)–C(1)–C(2)–C(3)	–158.8(2)	N(3)–C(8)–C(9)–C(10)	–29.2(3)
O(1)–C(1)–C(2)–C(7)	–160.5(2)	O(3)–C(8)–C(9)–C(14)	–27.4(3)
N(1)–C(1)–C(2)–C(7)	20.0(3)	N(3)–C(8)–C(9)–C(14)	153.54(19)
C(7)–C(2)–C(3)–C(4)	–1.3(3)	C(14)–C(9)–C(10)–C(11)	–1.0(3)
C(1)–C(2)–C(3)–C(4)	177.7(2)	C(8)–C(9)–C(10)–C(11)	–178.25(19)
C(2)–C(3)–C(4)–C(5)	0.9(4)	C(9)–C(10)–C(11)–C(12)	–1.7(3)
C(3)–C(4)–C(5)–N(2)	178.1(2)	C(10)–C(11)–C(12)–N(4)	–177.0(2)
C(3)–C(4)–C(5)–C(6)	0.6(4)	C(10)–C(11)–C(12)–C(13)	2.9(3)
N(2)–C(5)–C(6)–C(7)	–179.2(2)	N(4)–C(12)–C(13)–C(14)	178.27(19)
C(4)–C(5)–C(6)–C(7)	–1.7(4)	C(11)–C(12)–C(13)–C(14)	–1.6(3)
C(5)–C(6)–C(7)–C(2)	1.3(4)	C(12)–C(13)–C(14)–C(9)	–1.0(3)
C(3)–C(2)–C(7)–C(6)	0.2(4)	C(10)–C(9)–C(14)–C(13)	2.3(3)
C(1)–C(2)–C(7)–C(6)	–178.7(2)	C(8)–C(9)–C(14)–C(13)	179.61(18)
O(2)–Fe–O(6)–N(5)	–100.53(12)	O(5)–C(15)–C(16)–C(17)	18.8(3)
O(4)–Fe–O(6)–N(5)	166.72(12)	N(5)–C(15)–C(16)–C(17)	–163.68(18)
O(5)–Fe–O(6)–N(5)	3.73(11)	O(5)–C(15)–C(16)–C(21)	–157.92(18)
O(1)–Fe–O(6)–N(5)	–46.5(3)	N(5)–C(15)–C(16)–C(21)	19.6(3)
O(3)–Fe–O(6)–N(5)	88.00(12)	C(21)–C(16)–C(17)–C(18)	1.2(3)
Fe–O(6)–N(5)–C(15)	–4.7(2)	C(15)–C(16)–C(17)–C(18)	–175.66(18)
O(6)–N(5)–C(15)–O(5)	2.6(3)	C(16)–C(17)–C(18)–C(19)	0.4(3)
O(6)–N(5)–C(15)–C(16)	–175.01(16)	C(17)–C(18)–C(19)–N(6)	179.44(18)
N(5)–C(15)–O(5)–Fe	0.8(2)	C(17)–C(18)–C(19)–C(20)	–2.4(3)
C(16)–C(15)–O(5)–Fe	178.37(13)	N(6)–C(19)–C(20)–C(21)	–178.92(19)
O(2)–Fe–O(5)–C(15)	85.37(13)	C(18)–C(19)–C(20)–C(21)	3.0(3)
O(6)–Fe–O(5)–C(15)	–2.56(12)	C(19)–C(20)–C(21)–C(16)	–1.4(3)
O(4)–Fe–O(5)–C(15)	–64.7(2)	C(17)–C(16)–C(21)–C(20)	–0.6(3)
O(1)–Fe–O(5)–C(15)	164.44(12)	C(15)–C(16)–C(21)–C(20)	176.07(18)
O(3)–Fe–O(5)–C(15)	–106.35(12)		

Symmetry transformations used to generate equivalent atoms:

Table 5f: Hydrogen bonds for $[Fe^{III}(4\text{-}AphaH_{-1})_3](C_2H_5OH)]$ [Å and °].

D–H...A	d(D–H)	d(H...A)	d(D...A)	<(DHA)
O(7)–H(1O7)...O(6)#1	0.78(3)	1.91(3)	2.694(2)	175(3)
N(6)–H(1N6)...O(3)#2	0.84(2)	2.15(2)	2.968(2)	163.9(19)
N(5)–H(1N5)...O(7)	0.84(2)	1.91(2)	2.740(2)	176(2)
N(3)–H(1N3)...O(4)#3	0.86(3)	1.98(3)	2.755(2)	150(2)
N(1)–H(1N1)...O(2)#4	0.84(3)	1.99(3)	2.737(2)	149(2)

Symmetry transformations used to generate equivalent atoms:

#1 –x+1,–y+1,–z #2 –x+1,–y+1,–z+1 #3 –x,–y+1,–z #4 –x,–y,–z

Table 6: Crystal data and structure refinement for $Fe(Cha)_2(Cl)(H_2O).^7/_2H_2O$, 9.

Complex	**$Fe(Cha)_2(Cl)(H_2O).^7/_2H_2O$, 9.**
Empirical formula	$C_{18}H_{23}N_4O_{8.5}ClFe$
M_r	522.70
T/K	113(2)
Wavelength/ Å	0.71073
Crystal system	Monoclinic
Space group	$C2/c$
Unit cell dimensions	
a/Å	16.031(7)
b/Å	25.745(12)
c/Å	12.726(6)
a/°	90
β/°	125.634(0)
γ/°	90
V/ Å^3	16.031(7)
Z	8
D_c/g cm^{-3}	1.613
μ/mm^{-1}	0.71072
F(000)	2160
Crystal size/mm	0.1 x 0.2 x 0.4
Reflections collected	19019
Independent reflections (R_{int})	5329 (0.0471)
Goodness–of–fit on F^2	0.958
Final R indices [$I > 2\sigma(I)$]	$R_1 = 0.0520$; $wR_2 = 0.1239$
R indices (all data)	$R_1 = 0.1020$; $wR_2 = 0.1459$
Largest diff. peak and hole/e nm^{-3}	1.031 and -0.624

Table 6a: Selected bond lengths (Å) and angles (°) and hydrogen bonds (Å and °) for $Fe(Cha)_2(H_2O)(Cl).7/2H_2O$, with estimated standard deviations in parentheses

Fe(1)-O(1)	1.964(2)	Fe(1)-O(3)	1.981(2)
Fe(1)-O(2)	2.048(2)	Fe(1)-O(4)	2.050(2)
Fe(1)-O(5)	2.093(6)	Fe(1)-O(5')	2.149(6)
Fe(1)-Cl(1)	2.189(3)	Fe(1)-Cl(1')	2.313(2)
O(1)-N(3)	1.362(3)	O(2)-C(4)	1.274(3)
O(3)-N(12)	1.357(3)	O(4)-C(13)	1.256(3)
N(1)-C(2)	1.287(4)	N(1)-C(8A)	1.406(4)
C(2)-N(3)	1.385(4)	C(2)-C(9)	1.483(4)
N(3)-C(4)	1.350(4)	C(4)-C(4A)	1.422(4)
N(10)-C(11)	1.294(4)	N(10)-C(17A)	1.385(3)
C(11)-N(12)	1.373(4)	N(12)-C(13)	1.361(4)
C(13)-C(13A)	1.425(4)	C(13A)-C(13)	1.125(4)
O(1)—Fe(1)—O(3)	170.72(9)	O(5)—Fe(1)—O(2)	79.18(8)
O(3)—Fe(1)—O(2)	95.11(9)	O(1)—Fe(1)—O(4)	93.97(8)
O(3)—Fe(1)—O(4)	78.61(8)	O(2)—Fe(1)—O(4)	89.92(8)
O(1)—Fe(1)—O(5)	103.9(2)	O(3)—Fe(1)—O(5)	82.0(2)
O(2)—Fe(1)—O(5)	79.65(17)	O(4)—Fe(1)—O(5)	157.1(2)
O(1)—Fe(1)—O(5')	82.82(18)	O(3)—Fe(1)—O(5')	102.00(18)
O(2)—Fe(1)—O(5')	161.18(18)	O(4)—Fe(1)—O(5')	85.87(17)
O(1)—Fe(1)—Cl(1)	94.37(8)	O(3)—Fe(1)—Cl(1)	92.15(9)
O(2)—Fe(1)—Cl(1)	170.46(9)	O(4)—Fe(1)—Cl(1)	97.59(10)
O(5)—Fe(1)—Cl(1)	95.27(19)	O(1)—Fe(1)—Cl(1')	95.69(8)
O(3)—Fe(1)—Cl(1')	92.36(8)	O(2)—Fe(1)—Cl(1')	98.37(8)
O(4)—Fe(1)—Cl(1')	168.29(8)	O(5')—Fe(1)—Cl(1')	88.78(17)
N(3)—O(1)—Fe(1)	112.91(16)	C(4)—O(2)—Fe(1)	113.03(19)
N(12)—O(3)—Fe(1)	113.14(16)	C(13)—O(4)—Fe(1)	113.79(18)
C(2)—N(1)—C(8A)	118.5(2)	N(1)—C(2)—N(3)	121.3(3)
O(1)—N(3)—C(2)	119.3(2)	O(2)—C(4)—N(3)	117.7(3)
O(2)—C(4)—C(4A)	126.2(3)	N(3)—C(4)—C(4A)	116.1(2)
C(11)—N(10)—C(17A)	118.8(2)	N(10)—C(11)—N(12)	121.3(2)
O(3)—N(12)—C(11)	119.8(2)	O(4)—C(13)—N(12)	118.1(3)
O(4)—C(13)—C(13A)	126.2(3)	N(12)—C(13)—C(13A)	116.1(2)

D-H…A	d(D-H)	d(H…A)	d(D…A)	<(DHA)
O(2W)-H(5OA)…O(5)	1.26(9)	1.38(9)	2.588(9)	159(7)
O(2W)-H(5OA)…O(2)	1.26(9)	2.49(8)	3.297(6)	119(5)
O(5')-H(5'A)…Cl(1'#1)	0.84(7)	2.45(7)	3.273(7)	163(6)
O(5')-H(5'A)…O(3WB)	1.03(9)	1.53(9)	2.520(9)	158(7)
O(1W)-H(1WA)…N(10#2)	0.88(3)	2.02(3)	2.851(3)	157(3)
O(2W)-H(2WA)…Cl(1'#3)	0.75(8)	2.65(9)	3.132(6)	124(9)
O(2W)-H(2WA)…Cl(1#3)	0.75(8)	2.90(9)	3.624(6)	163(8)
O(2W)-H(2WB)…O(2W#4)	0.54(4)	2.46(5)	2.791(10)	123(7)
O(3WA)-H(3WA)…O(1W)	1.03(9)	1.82(9)	2.480(8)	168(8)
O(3WA)-H(3WB)…O(5W#5)	1.02(8)	1.71(8)	2.542(11)	126(7)
O(3WA)-H(3WB)…O(5W)	1.02(8)	1.92(9)	2.833(11)	148(7)
O(3WB)-H(3WC)…O(5W#5)	1.37(5)	1.69(6)	2.701(10)	124(4)
O(3WB)-H(3WD)…O(1W)	0.78(12)	2.07(13)	2.838(8)	170(10)
O(5W)-H(5WA)…O(4W)	0.98(7)	1.85(8)	2.821(7)	172(6)
O(5W)-H(5WB)…O(3WB)	0.58(10)	2.30(11)	2.441(11)	169(14)
O(5W)-H(5WB)…O(3WA)	0.58(10)	2.30(11)	2.833(11)	156(14)

Symmetry transformations used to generate equivalent atoms:

#1 -x, y, -z+1/2 #2 x, -y+1, z+1/2 #3 -x, -y+1, -z

#4 -x, y, -z-1/2 #5 -x+1/2, -y+1/2, -z+1

Table 7: Crystal data and structure refinement for $Co(Cha)_2(C_2H_5OH)_2$, 11.

Complex	**$Co(Cha)_2(C_2H_5OH)_2$, 11.**
Empirical formula	$C_{22}H_{26}N_4O_6Co$
M_r	501.40
T/K	100(2)
Wavelength/ Å	0.71073
Crystal system	Monoclinic
Space group	$P2_1/c$ (#14)
Unit cell dimensions	
a/Å	9.3627(13)
b/Å	15.930(2)
c/Å	7.8111(11)
α/°	90
β/°	111.027(2)
γ/°	90
V/ Å^3	1087.4(3)
Z	2
D_c/g cm^{-3}	1.531
μ/mm^{-1}	0.837
F(000)	522
Crystal size/mm	0.70 x 0.60 x 0.60
θ range for data collection/°	2.33 to 31.97
Index ranges, hkl	$-13<=h<=13$, $-23<=k<=22$, $-11<=l<=11$
Reflections collected	12950
Independent reflections (R_{int})	3526 (0.0184)
Completeness to $\theta = 30.00°$	99.6 %
Absorption correction	Semi–empirical from equivalents
Max./min. transmission	0.6335 and 0.5237
Refinement method	Full–matrix least–squares on F^2
Data / restraints / parameters	3526 / 0 / 203
Goodness–of–fit on F^2	1.051
Final R indices [$I > 2\sigma(I)$]	$R_1 = 0.0318$; $wR_2 = 0.0833$
R indices (all data)	$R_1 = 0.0356$, $wR_2 = 0.0857$
Largest diff. peak and hole/e nm^{-3}	0.643 and –0.256

Table 7a: Atomic coordinates (x 10^4) and equivalent isotropic displacement parameters ($Å^2$x 10^3) for $[Co^{II}(ChaH_{-2})_2(C_2H_5OH)_2]$. U(eq) is defined as one third of the trace of the orthogonalized U^{ij} tensor.

Atom	x	y	z	U(eq)
Co	0	0	5000	13(1)
O(1)	–553(1)	1208(1)	5325(1)	15(1)
N(1)	617(1)	1590(1)	6665(1)	12(1)
C(1)	550(1)	2443(1)	6894(1)	12(1)
C(2)	–858(1)	2878(1)	5672(2)	16(1)
N(2)	1637(1)	2863(1)	8131(1)	13(1)
C(3)	2899(1)	2428(1)	9262(1)	13(1)
C(4)	4096(1)	2873(1)	10582(1)	16(1)
C(5)	5353(1)	2445(1)	11728(2)	19(1)
C(6)	5476(1)	1568(1)	11612(2)	19(1)
C(7)	4320(1)	1126(1)	10324(2)	16(1)
C(8)	3024(1)	1553(1)	9139(1)	13(1)
C(9)	1820(1)	1102(1)	7748(1)	13(1)
O(2)	1805(1)	329(1)	7473(1)	17(1)
O(3)	1388(1)	453(1)	3585(1)	20(1)
C(10)	1696(1)	27(1)	2147(2)	17(1)
C(11)	3212(2)	–416(1)	2874(2)	28(1)

Table 7b: Bond lengths [Å] and angles [°] for $[Co^{II}(ChaH_{-2})_2(C_2H_5OH)_2]$.

Bond Atoms	Bond lengths[Å]	Bond Atoms	Bond lengths[Å]	Bond Atoms	Bond lengths[Å]
Co–O(1)	2.0323(8)	N(1)–C(9)	1.3806(12)	C(3)–C(4)	1.4118(14)
Co–O(1)#1	2.0323(8)	C(1)–N(2)	1.3083(13)	C(4)–C(5)	1.3757(15)
Co–O(3)	2.1126(8)	C(1)–C(2)	1.4917(14)	C(4)–H(4)	0.960(16)
Co–O(3)#1	2.1126(8)	C(2)–H(2A)	0.984(17)	C(5)–C(6)	1.4086(16)
Co–O(2)	2.1253(8)	C(2)–H(2B)	0.950(17)	C(5)–H(5)	0.948(16)
Co–O(2)#1	2.1253(8)	C(2)–H(2C)	0.971(17)	C(6)–C(7)	1.3768(15)
O(1)–N(1)	1.3576(10)	N(2)–C(3)	1.3811(13)	C(6)–H(6)	0.945(18)
N(1)–C(1)	1.3752(12)	C(3)–C(8)	1.4057(14)	C(7)–C(8)	1.4087(14)

Continued. Table 7b: Bond lengths [Å] and angles [°] for $[Co^{II}(ChaH_{-2})_2(C_2H_5OH)_2]$.

Bond Atoms	Bond lengths[Å]	Bond Atoms	Bond Angles[°]	Bond Atoms	Bond Angles[°]
C(7)-H(7)	0.958(15)	N(2)-C(1)-N(1)	122.80(9)	C(9)-O(2)-Co	110.83(6)
C(8)-C(9)	1.4444(13)	N(2)-C(1)-C(2)	120.67(9)	C(10)-O(3)-Co	125.76(7)
C(9)-O(2)	1.2501(12)	N(1)-C(1)-C(2)	116.53(9)	C(10)-O(3)-H(1O3)	108.8(12)
O(3)-C(10)	1.4282(14)	C(1)-C(2)-H(2A)	112.6(10)	Co-O(3)-H(1O3)	118.9(12)
O(3)-H(1O3)	0.85(2)	C(1)-C(2)-H(2B)	109.7(10)	O(3)-C(10)-C(11)	110.82(10)
C(10)-C(11)	1.5024(17)	H(2A)-C(2)-H(2B)	108.7(15)	O(3)-C(10)-H(10A)	107.8(9)
C(10)-H(10A)	0.954(16)	C(1)-C(2)-H(2C)	110.7(10)	C(11)-C(10)-H(10A)	110.7(9)
C(10)-H(10B)	0.937(15)	H(2A)-C(2)-H(2C)	109.0(14)	O(3)-C(10)-H(10B)	106.2(9)
C(11)-H(11A)	0.988(19)	H(2B)-C(2)-H(2C)	105.9(14)	C(11)-C(10)-H(10B)	111.7(9)
C(11)-H(11B)	0.928(19)	C(1)-N(2)-C(3)	118.41(8)	H(10A)-C(10)-H(10B)	109.3(13)
C(11)-H(11C)	0.969(18)	N(2)-C(3)-C(8)	121.86(9)	C(10)-C(11)-H(11A)	110.6(10)
Bond Atoms	**Bond Angles[°]**	N(2)-C(3)-C(4)	119.22(9)	C(10)-C(11)-H(11B)	109.2(11)
O(1)-Co-O(1)#1	180.0	C(8)-C(3)-C(4)	118.92(9)	H(11A)-C(11)-H(11B)	110.9(17)
O(1)-Co-O(3)	88.48(3)	C(5)-C(4)-C(3)	119.80(10)	C(10)-C(11)-H(11C)	110.3(10)
O(1)#1-Co-O(3)	91.52(3)	C(5)-C(4)-H(4)	121.5(9)	H(11A)-C(11)-H(11C)	106.3(14)
O(1)-Co-O(3)#1	91.52(3)	C(3)-C(4)-H(4)	118.7(9)	H(11B)-C(11)-H(11C)	109.5(17)
O(1)#1-Co-O(3)#1	88.48(3)	C(4)-C(5)-C(6)	121.30(10)		
O(3)-Co-O(3)#1	180.0	C(4)-C(5)-H(5)	120.0(10)		
O(1)-Co-O(2)	78.96(3)	C(6)-C(5)-H(5)	118.7(10)		
O(1)#1-Co-O(2)	101.04(3)	C(7)-C(6)-C(5)	119.55(10)		
O(3)-Co-O(2)	87.33(3)	C(7)-C(6)-H(6)	121.0(11)		
O(3)#1-Co-O(2)	92.67(3)	C(5)-C(6)-H(6)	119.4(11)		
O(1)-Co-O(2)#1	101.04(3)	C(6)-C(7)-C(8)	119.98(10)		
O(1)#1-Co-O(2)#1	78.96(3)	C(6)-C(7)-H(7)	120.7(9)		
O(3)-Co-O(2)#1	92.67(3)	C(8)-C(7)-H(7)	119.3(9)		
O(3)#1-Co-O(2)#1	87.33(3)	C(3)-C(8)-C(7)	120.45(9)		
O(2)-Co-O(2)#1	180.0	C(3)-C(8)-C(9)	118.84(9)		
N(1)-O(1)-Co	110.47(6)	C(7)-C(8)-C(9)	120.70(9)		
O(1)-N(1)-C(1)	118.79(8)	O(2)-C(9)-N(1)	119.55(9)		
O(1)-N(1)-C(9)	118.37(8)	O(2)-C(9)-C(8)	125.23(9)		
C(1)-N(1)-C(9)	122.83(8)	N(1)-C(9)-C(8)	115.22(8)		

Symmetry transformations used to generate equivalent atoms: #1 –x,–y,–z+1

Table 7c: Anisotropic displacement parameters ($Å^2 x 10^3$) for for $[Co^{II}(ChaH_{-2})_2(C_2H_5OH)_2]$. The anisotropic displacement factor exponent takes the form: $-2\pi^2[h^2 a^{*2}U^{11} + ... + 2 h k a^* b^* U^{12}]$.

Atom	U^{11}	U^{22}	U^{33}	U^{23}	U^{13}	U^{12}
Co	18(1)	7(1)	15(1)	-1(1)	6(1)	-2(1)
O(1)	14(1)	10(1)	16(1)	-4(1)	1(1)	-3(1)
N(1)	13(1)	8(1)	13(1)	-1(1)	4(1)	-1(1)
C(1)	14(1)	9(1)	15(1)	-1(1)	6(1)	0(1)
C(2)	16(1)	12(1)	18(1)	0(1)	3(1)	2(1)
N(2)	14(1)	9(1)	15(1)	-1(1)	5(1)	1(1)
C(3)	14(1)	11(1)	14(1)	-1(1)	7(1)	0(1)
C(4)	16(1)	14(1)	17(1)	-3(1)	6(1)	-2(1)
C(5)	16(1)	21(1)	18(1)	-2(1)	4(1)	-3(1)
C(6)	15(1)	21(1)	19(1)	2(1)	4(1)	3(1)
C(7)	17(1)	14(1)	19(1)	1(1)	6(1)	3(1)
C(8)	14(1)	11(1)	14(1)	0(1)	6(1)	1(1)
C(9)	16(1)	10(1)	14(1)	1(1)	6(1)	1(1)
O(2)	21(1)	8(1)	19(1)	-1(1)	5(1)	1(1)
O(3)	32(1)	9(1)	25(1)	0(1)	18(1)	-1(1)
C(10)	20(1)	16(1)	16(1)	0(1)	7(1)	0(1)
C(11)	27(1)	25(1)	33(1)	8(1)	15(1)	9(1)

Table 7d: Hydrogen coordinates ($x 10^4$) and isotropic displacement parameters ($Å^2 x 10^3$) for $[Co^{II}(ChaH_{-2})_2(C_2H_5OH)_2]$.

Atom	x	y	z	U(eq)
H(2A)	-893(19)	3472(11)	6000(20)	31(4)
H(2B)	-1739(19)	2603(11)	5730(20)	30(4)
H(2C)	-938(18)	2842(10)	4400(20)	27(4)
H(4)	4008(17)	3470(10)	10660(20)	23(4)
H(5)	6151(18)	2741(10)	12630(20)	24(4)
H(6)	6350(20)	1291(11)	12420(20)	32(4)

Continued Table 7d: Hydrogen coordinates (x 10^4) and isotropic displacement parameters ($Å^2$x 10^3) for $[Co^{II}(ChaH\text{-}_2)_2(C_2H_5OH)_2]$.

H(7)	4396(17)	531(10)	10210(20)	20(3)
H(1O3)	1430(20)	977(13)	3430(20)	37(5)
H(10A)	1688(17)	433(10)	1250(20)	19(3)
H(10B)	886(16)	–351(10)	1640(20)	17(3)
H(11A)	3230(20)	–829(12)	3820(20)	37(5)
H(11B)	3980(20)	–22(10)	3340(30)	34(6)
H(11C)	3390(20)	–731(11)	1900(20)	33(4)

Table 7e: Torsion angles [°] for $[Co^{II}(ChaH\text{-}_2)_2(C_2H_5OH)_2]$.

O(3)–Co–O(1)–N(1)	–76.53(6)	C(4)–C(3)–C(8)–C(7)	0.46(14)	O(1)#1–Co–O(3)–C(10)	30.83(9
O(3)#1–Co–O(1)–N(1)	103.47(6)	N(2)–C(3)–C(8)–C(9)	2.05(14)	O(2)–Co–O(3)–C(10)	131.81(9
O(2)–Co–O(1)–N(1)	11.05(6)	C(4)–C(3)–C(8)–C(9)	–178.06(9)	O(2)#1–Co–O(3)–C(10)	–48.18(9
O(2)#1–Co–O(1)–N(1)	–168.95(6)	C(6)–C(7)–C(8)–C(3)	–0.16(16)	Co–O(3)–C(10)–C(11)	–98.29(11
O(1)–N(1)–C(1)–N(2)	–178.84(9)	C(1)–N(1)–C(9)–O(2)	179.56(9)	C(3)–C(4)–C(5)–C(6)	0.14(16
C(9)–N(1)–C(1)–N(2)	1.65(15)	O(1)–N(1)–C(9)–C(8)	179.77(8)	C(4)–C(5)–C(6)–C(7)	0.17(17
O(1)–N(1)–C(1)–C(2)	2.25(13)	C(1)–N(1)–C(9)–C(8)	–0.72(14)	C(5)–C(6)–C(7)–C(8)	–0.16(16
C(9)–N(1)–C(1)–C(2)	–177.27(9)	C(3)–C(8)–C(9)–O(2)	178.67(10)	N(2)–C(3)–C(8)–C(7)	–179.43(9
N(1)–C(1)–N(2)–C(3)	–0.63(15)	C(7)–C(8)–C(9)–O(2)	0.15(16)	O(1)#1–Co–O(2)–C(9)	168.57(7
C(2)–C(1)–N(2)–C(3)	178.24(9)	C(3)–C(8)–C(9)–N(1)	–1.04(13)	O(3)–Co–O(2)–C(9)	77.54(7
C(1)–N(2)–C(3)–C(8)	–1.21(14)	C(7)–C(8)–C(9)–N(1)	–179.56(9)	O(3)#1–Co–O(2)–C(9)	–102.46(7
C(1)–N(2)–C(3)–C(4)	178.90(9)	N(1)–C(9)–O(2)–Co	9.66(11)	O(1)–Co–O(3)–C(10)	–149.17(9
N(2)–C(3)–C(4)–C(5)	179.44(10)	C(8)–C(9)–O(2)–Co	–170.03(8)		
C(8)–C(3)–C(4)–C(5)	–0.45(15)	O(1)–Co–O(2)–C(9)	–11.43(7)		

Symmetry transformations used to generate equivalent atoms: #1 –x,–y,–z+1

Table 7f: Hydrogen bonds for for $[Co^{II}(ChaH\text{-}_2)_2(C_2H_5OH)_2]$[Å and °].

D–H...A	d(D–H)	d(H...A)	d(D...A)	<(DHA)
O(3)–H(1O3)...N(2)#2	0.85(2)	1.88(2)	2.7257(12)	177.1(18)

Symmetry transformations used to generate equivalent atoms: #1 –x,–y,–z+1 #2 x,–y+1/2,z–1/2

Table 8: Crystal data and structure refinement for $Ni(Cha)_2(C_2H_5OH)_2$, 12.

Complex	**$Ni(Cha)_2(C_2H_5OH)_2$, 12.**
Empirical formula	$C_{22}H_{26}N_4NiO_6$
M_r	501.18
T/K	100(2)
Wavelength/ Å	0.71073
Crystal system	Monoclinic
Space group	$P2_1/c$ (#14)
Unit cell dimensions	
a/Å	9.3851(8)
b/Å	15.8715(13)
c/Å	7.7661(7)
α/°	90
β/°	110.967(2)
γ/°	90
V/ Å^3	1080.21(16)
Z	2
D_c/g cm^{-3}	1.541
μ/mm^{-1}	0.947
F(000)	524
Crystal size/mm	0.40 x 0.30 x 0.03
θ range for data collection/°	2.32 to 28.29
Index ranges, hkl	$-12<=h<=12$, $-21<=k<=21$, $-10<=l<=10$
Reflections collected	10886
Independent reflections (R_{int})	2681 (0.0212)
Completeness to θ = 30.00°	99.9 %
Absorption correction	Semi–empirical from equivalents
Max./min. transmission	0.9722 and 0.8070
Refinement method	Full–matrix least–squares on F^2
Data / restraints / parameters	2681 / 0 / 203
Goodness–of–fit on F^2	1.049
Final R indices [$I > 2\sigma(I)$]	R_1 = 0.0318; wR_2 = 0.0890
R indices (all data)	R_1 = 0.0354, wR_2 = 0.0914
Largest diff. peak and hole/e nm^{-3}	0.531 and –0.223

Table 8a: Atomic coordinates (x 10^4) and equivalent isotropic displacement parameters ($Å^2$x 10^3) for $[Ni^{II}(ChaH_{-2})_2(C_2H_5OH)_2]$. U(eq) is defined as one third of the trace of the orthogonalized U^{ij} tensor.

Atom	x	y	z	U(eq)
Ni	0	0	5000	16(1)
O(1)	–592(1)	1203(1)	5262(1)	17(1)
N(1)	571(1)	1583(1)	6615(2)	14(1)
C(1)	497(2)	2437(1)	6863(2)	14(1)
C(2)	–915(2)	2873(1)	5646(2)	18(1)
N(2)	1584(1)	2858(1)	8102(2)	15(1)
C(3)	2847(2)	2422(1)	9224(2)	15(1)
C(4)	4043(2)	2867(1)	10544(2)	18(1)
C(5)	5301(2)	2439(1)	11678(2)	21(1)
C(6)	5427(2)	1561(1)	11550(2)	23(1)
C(7)	4274(2)	1118(1)	10265(2)	19(1)
C(8)	2975(2)	1545(1)	9087(2)	15(1)
C(9)	1775(2)	1095(1)	7687(2)	15(1)
O(2)	1765(1)	319(1)	7396(1)	20(1)
O(3)	1329(1)	447(1)	3553(2)	25(1)
C(10)	1685(2)	12(1)	2156(2)	23(1)
C(11)	3205(2)	–411(1)	2909(3)	36(1)

Table 8b: Bond lengths [Å] and angles [°] for $[Ni^{II}(ChaH_{-2})_2(C_2H_5OH)_2]$.

Bond Atoms	Bond lengths[Å]	Bond Atoms	Bond lengths[Å]	Bond Atoms	Bond lengths[Å]
Ni–O(1)#1	2.0181(10)	C(1)–C(2)	1.4940(19)	C(5)–H(5)	0.88(2)
Ni–O(1)	2.0181(10)	C(2)–H(2A)	0.96(2)	C(6)–C(7)	1.374(2)
Ni–O(2)#1	2.0629(10)	C(2)–H(2B)	0.91(2)	C(6)–H(6)	0.88(2)
Ni–O(2)	2.0629(10)	C(2)–H(2C)	0.95(2)	C(7)–C(8)	1.4087(19)
Ni–O(3)	2.0794(11)	N(2)–C(3)	1.3795(17)	C(7)–H(7)	0.89(2)
Ni–O(3)#1	2.0794(11)	C(3)–C(8)	1.4046(19)	C(8)–C(9)	1.4447(19)
O(1)–N(1)	1.3565(14)	C(3)–C(4)	1.4086(19)	C(9)–O(2)	1.2509(17)
N(1)–C(1)	1.3739(17)	C(4)–C(5)	1.373(2)	O(3)–C(10)	1.423(2)
N(1)–C(9)	1.3778(17)	C(4)–H(4)	0.89(2)	O(3)–H(1O3)	0.72(2)
C(1)–N(2)	1.3070(17)	C(5)–C(6)	1.405(2)	C(10)–C(11)	1.493(2)

Bond Atoms	Bond lengths[Å]	Bond Atoms	Bond Angles[°]
C(10)–H(10A)	0.92(2)	H(2B)–C(2)–H(2C)	107.8(18)
C(10)–H(10B)	0.97(2)	C(1)–N(2)–C(3)	118.50(11)
C(11)–H(11A)	1.01(2)	N(2)–C(3)–C(8)	121.73(12)
C(11)–H(11B)	0.93(2)	N(2)–C(3)–C(4)	119.33(12)
C(11)–H(11C)	0.99(2)	C(8)–C(3)–C(4)	118.94(13)
Bond Atoms	**Bond Angles[°]**	C(5)–C(4)–C(3)	119.81(13)
O(1)#1–Ni–O(1)	180.0	C(5)–C(4)–H(4)	120.5(12)
O(1)#1–Ni–O(2)#1	80.68(4)	C(3)–C(4)–H(4)	119.7(12)
O(1)–Ni–O(2)#1	99.32(4)	C(4)–C(5)–C(6)	121.36(14)
O(1)#1–Ni–O(2)	99.32(4)	C(4)–C(5)–H(5)	117.2(13)
O(1)–Ni–O(2)	80.68(4)	C(6)–C(5)–H(5)	121.4(13)
O(2)#1–Ni–O(2)	180.0	C(7)–C(6)–C(5)	119.57(14)
O(1)#1–Ni–O(3)	91.62(4)	C(7)–C(6)–H(6)	121.4(14)
O(1)–Ni–O(3)	88.38(4)	C(5)–C(6)–H(6)	119.0(15)
O(2)#1–Ni–O(3)	92.25(5)	C(6)–C(7)–C(8)	119.98(13)
O(2)–Ni–O(3)	87.75(5)	C(6)–C(7)–H(7)	120.1(13)
O(1)#1–Ni–O(3)#1	88.38(4)	C(8)–C(7)–H(7)	119.8(13)
O(1)–Ni–O(3)#1	91.62(4)	C(3)–C(8)–C(7)	120.35(13)
O(2)#1–Ni–O(3)#1	87.75(5)	C(3)–C(8)–C(9)	118.88(12)
O(2)–Ni–O(3)#1	92.25(5)	C(7)–C(8)–C(9)	120.75(13)
O(3)–Ni–O(3)#1	180.0	O(2)–C(9)–N(1)	119.57(12)
N(1)–O(1)–Ni	109.00(7)	O(2)–C(9)–C(8)	125.23(12)
O(1)–N(1)–C(1)	118.77(11)	N(1)–C(9)–C(8)	115.20(11)
O(1)–N(1)–C(9)	118.38(10)	C(9)–O(2)–Ni	110.86(9)
C(1)–N(1)–C(9)	122.85(11)	C(10)–O(3)–Ni	126.62(9)
N(2)–C(1)–N(1)	122.79(12)	C(10)–O(3)–H(1O3)	106.4(17)
N(2)–C(1)–C(2)	120.74(12)	Ni–O(3)–H(1O3)	119.3(17)
N(1)–C(1)–C(2)	116.47(12)	O(3)–C(10)–C(11)	111.81(15)
C(1)–C(2)–H(2A)	110.0(13)	O(3)–C(10)–H(10A)	108.5(14)
C(1)–C(2)–H(2B)	109.9(13)	C(11)–C(10)–H(10A)	108.3(13)
H(2A)–C(2)–H(2B)	108.6(19)	O(3)–C(10)–H(10B)	107.5(12)
C(1)–C(2)–H(2C)	110.8(13)	C(11)–C(10)–H(10B)	110.1(12)
H(2A)–C(2)–H(2C)	109.7(19)	H(10A)–C(10)–H(10B)	110.5(18)
C(10)–C(11)–H(11A)	107.0(13)	C(10)–C(11)–H(11C)	111.0(13)
C(10)–C(11)–H(11B)	103.8(15)	H(11A)–C(11)–H(11C)	105.5(18)

H(11A)–C(11)–H(11B)	116(2)	H(11B)–C(11)–H(11C)	113(2)

Symmetry transformations used to generate equivalent atoms:
#1 –x,–y,–z+1

Table 8c: Anisotropic displacement parameters ($Å^2$x 10^3) for $[Ni^{II}(ChaH_{-2})_2(C_2H_5OH)_2]$. The anisotropic Displacement factor exponent takes the form: $-2\pi^2[\, h^2\, a^{*2}U^{11} + ... + 2\, h\, k\, a^*\, b^*\, U^{12}\,]$

Atom	U^{11}	U^{22}	U^{33}	U^{23}	U^{13}	U^{12}
Ni	22(1)	8(1)	18(1)	–1(1)	8(1)	–2(1)
O(1)	18(1)	11(1)	19(1)	–4(1)	3(1)	–4(1)
N(1)	17(1)	10(1)	16(1)	–3(1)	6(1)	–2(1)
C(1)	17(1)	11(1)	17(1)	–1(1)	8(1)	0(1)
C(2)	19(1)	14(1)	20(1)	–1(1)	4(1)	2(1)
N(2)	16(1)	10(1)	18(1)	–1(1)	6(1)	1(1)
C(3)	16(1)	14(1)	17(1)	0(1)	8(1)	0(1)
C(4)	19(1)	15(1)	19(1)	–3(1)	8(1)	–2(1)
C(5)	17(1)	26(1)	19(1)	–2(1)	5(1)	–3(1)
C(6)	17(1)	27(1)	23(1)	5(1)	6(1)	6(1)
C(7)	21(1)	15(1)	23(1)	3(1)	10(1)	5(1)
C(8)	17(1)	14(1)	17(1)	0(1)	8(1)	1(1)
C(9)	20(1)	10(1)	18(1)	1(1)	9(1)	0(1)
O(2)	27(1)	10(1)	22(1)	–1(1)	8(1)	1(1)
O(3)	40(1)	9(1)	34(1)	1(1)	24(1)	–1(1)
C(10)	27(1)	20(1)	22(1)	–1(1)	10(1)	–2(1)
C(11)	35(1)	31(1)	47(1)	11(1)	22(1)	10(1)

Table 8d: Hydrogen coordinates (x 10^4) and isotropic displacement parameters ($Å^2$x 10^{-3}) for $[Ni^{II}(ChaH_{-2})_2(C_2H_5OH)_2]$.

Atom	x	y	z	U(eq)
H(2A)	–920(20)	3444(15)	6030(30)	39(6)
H(2B)	–1750(20)	2609(14)	5710(30)	31(5)
H(2C)	–980(20)	2859(13)	4400(30)	32(5)
H(4)	3970(20)	3420(13)	10650(30)	23(5)
H(5)	6020(20)	2735(13)	12490(30)	28(5)
H(6)	6240(30)	1305(14)	12320(30)	36(6)

H(7)	4370(20)	567(13)	10140(30)	25(5)
H(1O3)	1300(20)	889(15)	3320(30)	27(5)
H(10A)	1710(20)	398(14)	1270(30)	30(5)
H(10B)	890(20)	–403(13)	1620(30)	25(5)
H(11A)	3130(30)	–852(15)	3810(30)	44(6)
H(11B)	3880(30)	29(14)	3400(40)	41(7)
H(11C)	3420(30)	–725(14)	1930(30)	36(6)

Table 8e: Torsion angles [°] for $[Ni^{II}(ChaH_{-2})_2(C_2H_5OH)_2]$.

O(2)#1–Ni–O(1)–N(1)	–170.08(8)	C(1)–N(2)–C(3)–C(8)	–1.18(19)
O(2)–Ni–O(1)–N(1)	9.92(8)	C(1)–N(2)–C(3)–C(4)	178.77(12)
O(3)–Ni–O(1)–N(1)	–78.06(8)	N(2)–C(3)–C(4)–C(5)	179.50(13)
O(3)#1–Ni–O(1)–N(1)	101.94(8)	C(8)–C(3)–C(4)–C(5)	–0.5(2)
Ni–O(1)–N(1)–C(1)	171.47(9)	C(3)–C(4)–C(5)–C(6)	0.2(2)
Ni–O(1)–N(1)–C(9)	–8.71(13)	C(4)–C(5)–C(6)–C(7)	0.1(2)
O(1)–N(1)–C(1)–N(2)	–178.24(12)	C(5)–C(6)–C(7)–C(8)	0.0(2)
C(9)–N(1)–C(1)–N(2)	2.0(2)	N(2)–C(3)–C(8)–C(7)	–179.39(12)
O(1)–N(1)–C(1)–C(2)	2.48(18)	C(4)–C(3)–C(8)–C(7)	0.7(2)
C(9)–N(1)–C(1)–C(2)	–177.33(12)	N(2)–C(3)–C(8)–C(9)	2.3(2)
N(1)–C(1)–N(2)–C(3)	–0.9(2)	C(4)–C(3)–C(8)–C(9)	–177.68(12)
C(2)–C(1)–N(2)–C(3)	178.32(12)	C(6)–C(7)–C(8)–C(3)	–0.4(2)
C(6)–C(7)–C(8)–C(9)	177.92(13)	C(8)–C(9)–O(2)–Ni	–170.65(11)
O(1)–N(1)–C(9)–O(2)	–0.35(19)	O(1)#1–Ni–O(2)–C(9)	169.45(9)
C(1)–N(1)–C(9)–O(2)	179.47(13)	O(1)–Ni–O(2)–C(9)	–10.55(9)
O(1)–N(1)–C(9)–C(8)	179.44(11)	O(3)–Ni–O(2)–C(9)	78.18(10)
C(1)–N(1)–C(9)–C(8)	–0.75(18)	O(3)#1–Ni–O(2)–C(9)	–101.83(10)
C(3)–C(8)–C(9)–O(2)	178.51(13)	O(1)#1–Ni–O(3)–C(10)	29.13(13)
C(7)–C(8)–C(9)–O(2)	0.2(2)	O(1)–Ni–O(3)–C(10)	–150.87(13)
C(3)–C(8)–C(9)–N(1)	–1.26(18)	O(2)#1–Ni–O(3)–C(10)	–51.61(13)
C(7)–C(8)–C(9)–N(1)	–179.58(12)	O(2)–Ni–O(3)–C(10)	128.39(13)
N(1)–C(9)–O(2)–Ni	9.11(16)	Ni–O(3)–C(10)–C(11)	–96.69(16)

Symmetry transformations used to generate equivalent atoms:

#1 –x,–y,–z+1

Table 8f: Hydrogen bonds for for $[Ni^{II}(ChaH_{-2})_2(C_2H_5OH)_2]$ [Å and °].

D–H...A	d(D–H)	d(H...A)	d(D...A)	<(DHA)
O(3)–H(1O3)...N(2)#2	0.72(2)	2.02(2)	2.7354(16)	169(2)

Symmetry transformations used to generate equivalent atoms:

#1 –x,–y,–z+1 #2 x,–y+1/2,z–1/2

Table 9: Crystal data and structure refinement for $Cu(Cha)H_2O(Cl)$, 14.

Complex	**$Cu(Cha)H_2O(Cl)$, 14.**
Empirical formula	$C_9 H_{13} N_2 O_5 Cl Cu$
M_r	328.20
T/K	100(2)
Wavelength/ Å	0.71073
Crystal system	Monoclinic
Space group	$P2_1/c$ (#14)
Unit cell dimensions	
a/Å	9.5088(7)
b/Å	18.4349(13)
c/Å	6.8155(5)
α/°	90
β/°	90.643(1)
γ/°	90
V/ Å^3	1194.64(15)
Z	4
D_c/g cm^{-3}	1.825
μ/mm^{-1}	2.066
F(000)	668
Crystal size/mm	0.60 x 0.05 x 0.02
θ range for data collection/°	2.14 to 26.44
Index ranges, hkl	$-11<=h<=11$, $-23<=k<=23$, $-8<=l<=8$
Reflections collected	20966
Independent reflections (R_{int})	2452(0.0474)
Completeness to $\theta = 30.00°$	99.4 %
Absorption correction	Semi–empirical from equivalents
Max./min. transmission	0.9598 and 0.8071
Refinement method	Full–matrix least–squares on F^2
Data / restraints / parameters	2452 / 0 / 215
Goodness–of–fit on F^2	1.119
Final R indices [$I > 2\sigma(I)$]	$R_1 = 0.0286$, $wR_2 = 0.0628$
R indices (all data)	$R_1 = 0.0338$, $wR_2 = 0.0647$
Largest diff. peak and hole/e nm^{-3}	0.441 and –0.265

Table 9a: Atomic coordinates (x 10^4) and equivalent isotropic displacement parameters ($Å^2$x 10^3) for [Cu^{II} ($ChaH_{-1}$)(H_2O)$_2$Cl]. U(eq) is defined as one third of the trace of the orthogonalized U^{ij} tensor.

Atom	x	y	z	U(eq)
Cu	8884(1)	6820(1)	1812(1)	10(1)
Cl	8449(1)	7930(1)	674(1)	12(1)
N(1)	7982(2)	5440(1)	2254(3)	10(1)
O(1)	9226(2)	5798(1)	2076(2)	13(1)
C(1)	8023(2)	4701(1)	2600(3)	11(1)
C(2)	9433(2)	4360(1)	2675(4)	14(1)
N(2)	6886(2)	4323(1)	2825(3)	11(1)
O(2)	6881(2)	6501(1)	1697(2)	11(1)
C(3)	5608(2)	4672(1)	2657(3)	10(1)
C(4)	4372(2)	4265(1)	2891(3)	12(1)
C(5)	3088(2)	4592(1)	2688(3)	13(1)
C(6)	2976(2)	5337(1)	2256(3)	13(1)
C(7)	4169(2)	5749(1)	2038(3)	11(1)
C(8)	5499(2)	5423(1)	2239(3)	10(1)
C(9)	6777(2)	5825(1)	2036(3)	10(1)
O(3)	10940(2)	6941(1)	1904(3)	14(1)
O(4)	7439(2)	2989(1)	4774(3)	14(1)
O(5)	4862(2)	2539(1)	931(3)	18(1)

Table 9b: Bond lengths [Å] and angles [°] for[Cu^{II} ($ChaH_{-1}$)(H_2O)$_2$Cl]

Bond Atoms	Bond lengths[Å]	Bond Atoms	Bond lengths[Å]	Bond Atoms	Bond Angles[°]
Cu–O(1)	1.9198(15)	O(5)–H(1O5)	0.72(4)	C(4)–C(5)–H(5)	120.6(17)
Cu–O(3)	1.9683(17)	O(5)–H(2O5)	0.72(3)	C(6)–C(5)–H(5)	118.2(17)
Cu–O(2)	1.9944(14)	**Bond Atoms**	**Bond Angles[°]**	C(7)–C(6)–C(5)	120.0(2)
Cu–Cl	2.2256(6)	O(1)–Cu–O(3)	86.63(7)	C(7)–C(6)–H(6)	121.5(16)
Cu–Cl#1	2.7080(6)	O(1)–Cu–O(2)	82.81(6)	C(5)–C(6)–H(6)	118.5(16)
Cl–Cu#2	2.7080(6)	O(3)–Cu–O(2)	169.34(7)	C(6)–C(7)–C(8)	119.8(2)
N(1)–C(9)	1.355(3)	O(1)–Cu–Cl	164.90(5)	C(6)–C(7)–H(7)	119.9(16)
N(1)–O(1)	1.362(2)	O(3)–Cu–Cl	95.03(6)	C(8)–C(7)–H(7)	120.3(16)
N(1)–C(1)	1.383(3)	O(2)–Cu–Cl	94.79(5)	C(7)–C(8)–C(3)	120.1(2)

C(1)–N(2)	1.296(3)	O(1)–Cu–Cl#1	95.92(5)	C(7)–C(8)–C(9)	122.3(2)
C(1)–C(2)	1.480(3)	O(3)–Cu–Cl#1	96.45(6)	C(3)–C(8)–C(9)	117.65(19)
C(2)–H(2A)	0.95(3)	O(2)–Cu–Cl#1	86.10(4)	O(2)–C(9)–N(1)	117.79(19)
C(2)–H(2B)	0.99(3)	Cl–Cu–Cl#1	98.796(16)	O(2)–C(9)–C(8)	126.32(19)
C(2)–H(2C)	0.99(3)	Cu–Cl–Cu#2	117.71(2)	N(1)–C(9)–C(8)	115.89(19)
N(2)–C(3)	1.379(3)	C(9)–N(1)–O(1)	118.06(17)	Cu–O(3)–H(1O3)	119(2)
O(2)–C(9)	1.272(3)	C(9)–N(1)–C(1)	123.85(18)	Cu–O(3)–H(2O3)	126(2)
C(3)–C(4)	1.405(3)	O(1)–N(1)–C(1)	118.08(17)	H(1O3)–O(3)–H(2O3)	101(3)
C(3)–C(8)	1.417(3)	N(1)–O(1)–Cu	109.79(12)	H(1O4)–O(4)–H(2O4)	106(3)
C(4)–C(5)	1.368(3)	N(2)–C(1)–N(1)	121.79(19)	H(1O5)–O(5)–H(2O5)	106(3)
C(4)–H(4)	0.90(3)	N(2)–C(1)–C(2)	121.7(2)	C(4)–C(3)–C(8)	119.0(2)
C(5)–C(6)	1.409(3)	N(1)–C(1)–C(2)	116.55(19)	C(5)–C(4)–C(3)	120.0(2)
C(5)–H(5)	0.93(3)	C(1)–C(2)–H(2A)	108.2(15)	C(5)–C(4)–H(4)	122.1(17)
C(6)–C(7)	1.374(3)	C(1)–C(2)–H(2B)	108.9(17)	C(3)–C(4)–H(4)	118.0(17)
C(6)–H(6)	0.89(3)	H(2A)–C(2)–H(2B)	105(2)	C(4)–C(5)–C(6)	121.1(2)
C(7)–C(8)	1.405(3)	C(1)–C(2)–H(2C)	112.6(16)		
C(7)–H(7)	0.90(3)	H(2A)–C(2)–H(2C)	111(2)		
C(8)–C(9)	1.431(3)	H(2B)–C(2)–H(2C)	111(2)		
O(3)–H(1O3)	0.85(3)	C(1)–N(2)–C(3)	118.37(19)		
O(3)–H(2O3)	0.69(3)	C(9)–O(2)–Cu	110.98(13)		
O(4)–H(1O4)	0.76(4)	N(2)–C(3)–C(4)	118.58(19)		
O(4)–H(2O4)	0.73(3)	N(2)–C(3)–C(8)	122.38(19)		

Symmetry transformations used togenerate equivalent atoms:

#1 x,–y+3/2,z+1/2 #2 x,–y+3/2,z–1/2

Table 9c: Anisotropic displacement parameters ($Å^2 x 10^3$) for $[Cu^{II} (ChaH_{-1})(H_2O)_2Cl]$. The anisotropic displacement factor exponent takes the form: $-2\pi^2[h^2 a^{*2} U^{11} + ... + 2 h k a^* b^* U^{12}]$.

Atom	U^{11}	U^{22}	U^{33}	U^{23}	U^{13}	U^{12}
Cu	7(1)	8(1)	15(1)	0(1)	0(1)	–1(1)
Cl	13(1)	9(1)	14(1)	1(1)	–1(1)	–1(1)
N(1)	7(1)	10(1)	12(1)	0(1)	1(1)	–2(1)
O(1)	7(1)	10(1)	22(1)	0(1)	2(1)	–3(1)
C(1)	12(1)	10(1)	9(1)	–1(1)	0(1)	1(1)
C(2)	10(1)	13(1)	20(1)	0(1)	0(1)	2(1)
N(2)	10(1)	10(1)	11(1)	1(1)	0(1)	1(1)

O(2)	9(1)	9(1)	15(1)	0(1)	0(1)	–1(1)
C(3)	11(1)	12(1)	7(1)	–1(1)	–1(1)	1(1)
C(4)	13(1)	11(1)	11(1)	0(1)	1(1)	–2(1)
C(5)	11(1)	15(1)	14(1)	–1(1)	0(1)	–4(1)
C(6)	9(1)	16(1)	13(1)	–2(1)	–2(1)	3(1)
C(7)	14(1)	10(1)	10(1)	–2(1)	–1(1)	1(1)
C(8)	11(1)	11(1)	7(1)	–2(1)	1(1)	0(1)
C(9)	12(1)	11(1)	5(1)	–1(1)	–1(1)	–1(1)
O(3)	11(1)	12(1)	21(1)	4(1)	–1(1)	–4(1)
O(4)	11(1)	12(1)	19(1)	3(1)	1(1)	1(1)
O(5)	14(1)	19(1)	21(1)	5(1)	2(1)	1(1)

Table 9d: Hydrogen coordinates (x 10^4) and isotropic displacement parameters ($Å^2$x 10^3) for $[Cu^{II}(ChaH_{-1})(H_2O)_2Cl]$.

Atom	x	y	z	U(eq)
H(2A)	9310(30)	3850(15)	2760(40)	15(6)
H(2B)	9900(30)	4443(15)	1410(50)	32(8)
H(2C)	10020(30)	4543(15)	3780(40)	25(7)
H(4)	4460(30)	3791(15)	3190(40)	19(7)
H(5)	2270(30)	4327(15)	2820(40)	24(7)
H(6)	2130(30)	5534(13)	2180(40)	12(6)
H(7)	4100(30)	6222(15)	1720(40)	20(7)
H(1O3)	11380(30)	6911(15)	3000(50)	29(9)
H(2O3)	11310(30)	7215(17)	1450(40)	21(9)
H(1O4)	7240(40)	3335(19)	4230(50)	42(11)
H(2O4)	6780(30)	2839(16)	5160(40)	21(8)
H(1O5)	4450(30)	2777(18)	300(50)	31(10)
H(2O5)	4360(30)	2308(18)	1420(50)	26(9)

Table 9e: Torsion angles [°] for [Cu^{II} ($ChaH_{-1}$)(H_2O)$_2$Cl].

O(1)–Cu–Cl–Cu#2	–18.29(19)	N(1)–C(1)–N(2)–C(3)	1.8(3)
O(3)–Cu–Cl–Cu#2	77.45(6)	C(2)–C(1)–N(2)–C(3)	–177.40(19)
O(2)–Cu–Cl–Cu#2	–98.42(5)	O(1)–Cu–O(2)–C(9)	6.40(14)
Cl#1–Cu–Cl–Cu#2	174.789(10)	O(3)–Cu–O(2)–C(9)	14.2(5)
C(9)–N(1)–O(1)–Cu	6.1(2)	Cl–Cu–O(2)–C(9)	171.41(13)
C(1)–N(1)–O(1)–Cu	–175.49(14)	Cl#1–Cu–O(2)–C(9)	–90.07(13)
O(3)–Cu–O(1)–N(1)	174.96(13)	C(1)–N(2)–C(3)–C(4)	179.70(19)
O(2)–Cu–O(1)–N(1)	–6.49(12)	C(1)–N(2)–C(3)–C(8)	0.4(3)
Cl–Cu–O(1)–N(1)	–88.2(2)	N(2)–C(3)–C(4)–C(5)	–178.49(19)
Cl#1–Cu–O(1)–N(1)	78.81(12)	C(8)–C(3)–C(4)–C(5)	0.9(3)
C(9)–N(1)–C(1)–N(2)	–3.0(3)	C(3)–C(4)–C(5)–C(6)	–0.4(3)
O(1)–N(1)–C(1)–N(2)	178.63(18)	C(4)–C(5)–C(6)–C(7)	–0.2(3)
C(9)–N(1)–C(1)–C(2)	176.25(19)	C(5)–C(6)–C(7)–C(8)	0.3(3)
O(1)–N(1)–C(1)–C(2)	–2.1(3)	C(6)–C(7)–C(8)–C(3)	0.2(3)
C(6)–C(7)–C(8)–C(9)	–179.76(19)	C(1)–N(1)–C(9)–O(2)	–179.06(19)
N(2)–C(3)–C(8)–C(7)	178.52(19)	O(1)–N(1)–C(9)–C(8)	–179.93(17)
C(4)–C(3)–C(8)–C(7)	–0.8(3)	C(1)–N(1)–C(9)–C(8)	1.7(3)
N(2)–C(3)–C(8)–C(9)	–1.5(3)	C(7)–C(8)–C(9)–O(2)	1.3(3)
C(4)–C(3)–C(8)–C(9)	179.18(19)	C(3)–C(8)–C(9)–O(2)	–178.7(2)
Cu–O(2)–C(9)–N(1)	–4.9(2)	C(7)–C(8)–C(9)–N(1)	–179.58(19)
Cu–O(2)–C(9)–C(8)	174.25(17)	C(3)–C(8)–C(9)–N(1)	0.4(3)
O(1)–N(1)–C(9)–O(2)	–0.7(3)		

Symmetry transformations used to generate equivalent atoms:

#1 x,–y+3/2,z+1/2 #2 x,–y+3/2,z–1/2

Table 9f: Hydrogen bonds for for [Cu^{II} ($ChaH_{-1}$)(H_2O)$_2$Cl] [Å and °].

D–H...A	d(D–H)	d(H...A)	d(D...A)	<(DHA)
O(5)–H(2O5)...O(2)#3	0.72(3)	2.30(3)	3.013(3)	169(3)
O(5)–H(1O5)...O(2)#4	0.72(4)	2.28(4)	3.003(3)	178(3)
O(4)–H(2O4)...O(5)#5	0.73(3)	2.03(3)	2.759(3)	174(3)
O(3)–H(1O3)...O(4)#6	0.85(3)	1.89(3)	2.727(3)	168(3)
O(4)–H(1O4)...N(2)	0.76(4)	2.08(4)	2.843(3)	174(3)
O(3)–H(2O3)...O(4)#7	0.69(3)	2.04(3)	2.729(3)	175(3)

Symmetry transformations used to generate equivalent atoms:

#1 x,–y+3/2,z+1/2 #2 x,–y+3/2,z–1/2 #3 –x+1,y–1/2,–z+1/2

#4 –x+1,–y+1,–z #5 x,–y+1/2,z+1/2 #6 –x+2,–y+1,–z+1

#7 –x+2,y+1/2,–z+1/2

Table 10: Crystal data and structure refinement for $[Zn(Cha)_2].2H_2O$, 15.

Complex	**$[Zn(Cha)_2].2H_2O$, 15.**
Empirical formula	$C_{20}H_{22}N_4O_6Zn$
M_r	479.79
T/K	100(2)
Wavelength/ Å	0.71073
Crystal system	Monoclinic
Space group	$C2/c$ (#15)
Unit cell dimensions	
a/Å	15.594(2)
b/Å	15.511(2)
c/Å	17.437(2)
a/°	90
β/°	111.025(3)
γ/°	90
V/ Å^3	3936.7(10)
Z	8
D_c/g cm^{-3}	1.619
μ/mm^{-1}	1.296
F(000)	1984
Crystal size/mm	0.60 x 0.40 x 0.30
θ range for data collection/°	1.92 to 26.47
Index ranges, hkl	$-19<=h<=19$, $-19<=k<=19$, $-21<=l<=21$
Reflections collected	28789
Independent reflections (R_{int})	4068 (0.0444)
Completeness to $\theta = 30.00°$	99.8 %
Absorption correction	Semi–empirical from equivalents
Max./min. transmission	0.6972 and 0.5218
Refinement method	Full–matrix least–squares on F^2
Data / restraints / parameters	4068 / 19 / 368
Goodness–of–fit on F^2	1.039
Final R indices [$I > 2\sigma(I)$]	$R_1 = 0.0283$; $wR_2 = 0.0702$
R indices (all data)	$R_1 = 0.0343$, $wR_2 = 0.0727$
Largest diff. peak and hole/e nm^{-3}	0.385 and –0.273

Table 10a: Atomic coordinates (x 10^4) and equivalent isotropic displacement parameters ($Å^2$x 10^3)for $[Zn^{II}(ChaH_{-1})_2(C_2H_6O)]$. U(eq) is defined as one third of the trace of the orthogonalized U^{ij} tensor.

Atom	x	y	z	U(eq)
Zn	2423(1)	4052(1)	2152(1)	15(1)
O(1)	3026(1)	2908(1)	2203(1)	16(1)
N(1)	2590(1)	2452(1)	1509(1)	14(1)
C(1)	2897(1)	1636(1)	1445(1)	14(1)
C(2)	3669(1)	1311(1)	2175(1)	17(1)
N(2)	2546(1)	1161(1)	790(1)	14(1)
C(3)	1822(1)	1495(1)	138(1)	15(1)
C(4)	1455(1)	1002(1)	–584(1)	18(1)
C(5)	711(1)	1303(1)	–1223(1)	20(1)
C(6)	303(1)	2097(1)	–1170(1)	20(1)
C(7)	672(1)	2595(1)	–479(1)	17(1)
C(8)	1440(1)	2306(1)	178(1)	14(1)
C(9)	1853(1)	2822(1)	905(1)	14(1)
O(2)	1597(1)	3560(1)	1018(1)	17(1)
O(3)	3519(1)	4618(1)	3074(1)	19(1)
N(3)	3058(1)	5734(1)	2183(1)	14(1)
C(10)	3113(1)	6578(1)	1962(1)	15(1)
C(11)	2430(1)	6857(1)	1158(1)	19(1)
N(4)	3727(1)	7110(1)	2425(1)	15(1)
C(12)	4348(1)	6812(1)	3160(1)	14(1)
C(13)	5026(1)	7378(1)	3661(1)	17(1)
C(14)	5644(1)	7086(1)	4393(1)	19(1)
C(15)	5619(1)	6238(1)	4656(1)	21(1)
C(16)	4962(1)	5678(1)	4177(1)	18(1)
C(17)	4322(1)	5963(1)	3424(1)	14(1)
C(18)	3631(1)	5388(1)	2912(1)	15(1)
O(4)	2395(1)	5223(1)	1667(1)	18(1)
O(5)	1540(1)	3859(1)	2742(1)	19(1)
O(6)	1787(1)	4494(1)	4238(1)	23(1)
C(19)	1029(2)	4602(2)	4525(1)	28(1)
C(20)	177(2)	4970(2)	3888(2)	31(1)

Table 10b: Bond lengths [Å] and angles [°] for[$Zn^{II}(ChaH_{-1})_2(C_2H_6O)$].

Bond Atoms	Bond lengths [Å]	Bond Atoms	Bond lengths [Å]	Bond Atoms	Bond Angles[°]
Zn–O(1)	1.9954(13)	C(11)–H(11B)	0.972(16)	O(5)–Zn–O(2)	97.30(6)
`Zn–O(4)	1.9977(13)	C(11)–H(11C)	0.974(16)	O(3)–Zn–O(2)	161.72(5)
Zn–O(5)	2.0167(15)	N(4)–C(12)	1.381(2)	N(1)–O(1)–Zn	110.32(10)
Zn–O(3)	2.0748(14)	C(12)–C(17)	1.401(3)	O(1)–N(1)–C(1)	118.45(15)
Zn–O(2)	2.0789(13)	C(12)–C(13)	1.409(3)	O(1)–N(1)–C(9)	118.66(14)
O(1)–N(1)	1.3551(19)	C(13)–C(14)	1.371(3)	C(1)–N(1)–C(9)	122.88(16)
N(1)–C(1)	1.370(2)	C(13)–H(13)	0.952(15)	N(2)–C(1)–N(1)	122.99(17)
N(1)–C(9)	1.375(2)	C(14)–C(15)	1.399(3)	N(2)–C(1)–C(2)	120.82(17)
C(1)–N(2)	1.304(2)	C(14)–H(14)	0.945(15)	N(1)–C(1)–C(2)	116.19(16)
C(1)–C(2)	1.492(3)	C(15)–C(16)	1.373(3)	C(1)–C(2)–H(2A)	108.5(13)
C(2)–H(2A)	0.984(15)	C(15)–H(15)	0.948(16)	C(1)–C(2)–H(2B)	111.1(14)
C(2)–H(2B)	0.933(16)	C(16)–C(17)	1.405(3)	H(2A)–C(2)–H(2B)	109.0(19)
C(2)–H(2C)	0.954(16)	C(16)–H(16)	0.936(15)	C(1)–C(2)–H(2C)	111.4(14)
N(2)–C(3)	1.384(2)	C(17)–C(18)	1.436(3)	H(2A)–C(2)–H(2C)	107.4(19)
C(3)–C(8)	1.404(3)	O(5)–H(1O5)	0.77(3)	H(2B)–C(2)–H(2C)	109(2)
C(3)–C(4)	1.407(3)	O(5)–H(2O5)	0.76(3)	C(1)–N(2)–C(3)	118.05(16)
C(4)–C(5)	1.370(3)	O(6)–C(19)	1.450(3)	N(2)–C(3)–C(8)	122.01(17)
C(4)–H(4)	0.954(16)	O(6)–H(1O6)	0.75(3)	N(2)–C(3)–C(4)	118.83(17)
C(5)–C(6)	1.404(3)	C(19)–C(20)	1.506(3)	C(8)–C(3)–C(4)	119.16(17)
C(5)–H(5)	0.930(16)	C(19)–H(19A)	1.022(16)	C(5)–C(4)–C(3)	119.74(18)
C(6)–C(7)	1.372(3)	C(19)–H(19B)	1.024(17)	C(5)–C(4)–H(4)	121.9(13)
C(6)–H(6)	0.951(15)	C(20)–H(20A)	1.000(17)	C(3)–C(4)–H(4)	118.4(13)
C(7)–C(8)	1.401(3)	C(20)–H(20B)	0.989(17)	C(4)–C(5)–C(6)	121.17(19)
C(7)–H(7)	0.920(15)	C(20)–H(20C)	1.028(17)	C(4)–C(5)–H(5)	119.1(14)
C(8)–C(9)	1.441(3)	**Bond Atoms**	**Bond Angles[°]**	C(6)–C(5)–H(5)	119.7(14)
C(9)–O(2)	1.252(2)	O(1)–Zn–O(4)	140.06(6)	C(7)–C(6)–C(5)	119.60(19)
O(3)–C(18)	1.254(2)	O(1)–Zn–O(5)	104.00(6)	C(7)–C(6)–H(6)	122.7(14)
N(3)–O(4)	1.356(2)	O(4)–Zn–O(5)	115.83(6)	C(5)–C(6)–H(6)	117.7(14)
N(3)–C(18)	1.374(2)	O(1)–Zn–O(3)	95.66(5)	C(6)–C(7)–C(8)	120.26(19)
N(3)–C(10)	1.376(2)	O(4)–Zn–O(3)	80.23(5)	C(6)–C(7)–H(7)	120.6(13)
C(10)–N(4)	1.302(2)	O(5)–Zn–O(3)	100.96(6)	C(8)–C(7)–H(7)	119.2(13)
C(10)–C(11)	1.488(3)	O(1)–Zn–O(2)	80.63(5)	C(7)–C(8)–C(3)	119.98(17)
C(11)–H(11A)	0.965(16)	O(4)–Zn–O(2)	91.11(5)	C(7)–C(8)–C(9)	121.51(17)

Continued Table 10b: Bond lengths [Å] and angles [°] for $\{Zn^{II}(ChaH_{-1})_2(C_2H_6O)\}$.

Bond Atoms	Bond Angles[°]	Bond Atoms	Bond Angles[°]
C(3)–C(8)–C(9)	118.51(17)	C(16)–C(15)–H(15)	121.8(13)
O(2)–C(9)–N(1)	119.16(17)	C(14)–C(15)–H(15)	118.4(13)
O(2)–C(9)–C(8)	125.42(17)	C(15)–C(16)–C(17)	119.65(19)
N(1)–C(9)–C(8)	115.41(16)	C(15)–C(16)–H(16)	120.0(13)
C(9)–O(2)–Zn	111.23(12)	C(17)–C(16)–H(16)	120.4(13)
C(18)–O(3)–Zn	111.76(12)	C(12)–C(17)–C(16)	120.50(18)
O(4)–N(3)–C(18)	118.26(15)	C(12)–C(17)–C(18)	118.92(17)
O(4)–N(3)–C(10)	118.63(15)	C(16)–C(17)–C(18)	120.58(17)
C(18)–N(3)–C(10)	123.10(16)	O(3)–C(18)–N(3)	118.95(17)
N(4)–C(10)–N(3)	122.35(17)	O(3)–C(18)–C(17)	125.82(17)
N(4)–C(10)–C(11)	121.21(17)	N(3)–C(18)–C(17)	115.23(16)
N(3)–C(10)–C(11)	116.44(17)	N(3)–O(4)–Zn	110.78(10)
C(10)–C(11)–H(11A)	109.2(13)	Zn–O(5)–H(1O5)	108(2)
C(10)–C(11)–H(11B)	108.9(14)	Zn–O(5)–H(2O5)	122(2)
H(11A)–C(11)–H(11B)	111.1(19)	H(1O5)–O(5)–H(2O5)	110(3)
C(10)–C(11)–H(11C)	111.7(14)	C(19)–O(6)–H(1O6)	109(2)
H(11A)–C(11)–H(11C)	109.0(19)	O(6)–C(19)–C(20)	113.74(18)
H(11B)–C(11)–H(11C)	106.9(19)	O(6)–C(19)–H(19A)	109.7(15)
C(10)–N(4)–C(12)	118.63(16)	C(20)–C(19)–H(19A)	110.9(15)
N(4)–C(12)–C(17)	121.74(17)	O(6)–C(19)–H(19B)	119.3(16)
N(4)–C(12)–C(13)	119.22(17)	C(20)–C(19)–H(19B)	112.2(16)
C(17)–C(12)–C(13)	119.04(17)	H(19A)–C(19)–H(19B)	88(2)
C(14)–C(13)–C(12)	119.52(18)	C(19)–C(20)–H(20A)	113.9(15)
C(14)–C(13)–H(13)	121.5(13)	C(19)–C(20)–H(20B)	110.6(16)
C(12)–C(13)–H(13)	119.0(13)	H(20A)–C(20)–H(20B)	105(2)
C(13)–C(14)–C(15)	121.44(18)	C(19)–C(20)–H(20C)	109.9(15)
C(13)–C(14)–H(14)	118.8(13)	H(20A)–C(20)–H(20C)	110(2)
C(15)–C(14)–H(14)	119.7(13)	H(20B)–C(20)–H(20C)	107(2)
C(16)–C(15)–C(14)	119.84(19)		

Symmetry transformations used to generate equivalent atoms

Table 10c: Anisotropic displacement parameters ($Å^2 x 10^3$) for $[Zn^{II}(ChaH_{-1})_2(C_2H_6O)]$. The anisotropic displacement factor exponent takes the form: $-2\pi^2[h^2 a^{*2} U^{11} + ... + 2 h k a^* b^* U^{12}]$

Atom	U^{11}	U^{22}	U^{33}	U^{23}	U^{13}	U^{12}
Zn	19(1)	12(1)	14(1)	-1(1)	5(1)	0(1)
O(1)	17(1)	15(1)	12(1)	-4(1)	1(1)	0(1)
N(1)	14(1)	14(1)	12(1)	-3(1)	4(1)	-2(1)
C(1)	13(1)	14(1)	17(1)	1(1)	7(1)	-1(1)
C(2)	18(1)	16(1)	17(1)	-1(1)	4(1)	2(1)
N(2)	15(1)	14(1)	14(1)	-1(1)	5(1)	-1(1)
C(3)	15(1)	15(1)	15(1)	1(1)	7(1)	-3(1)
C(4)	23(1)	14(1)	19(1)	0(1)	10(1)	-3(1)
C(5)	26(1)	23(1)	12(1)	-3(1)	6(1)	-9(1)
C(6)	19(1)	23(1)	14(1)	5(1)	3(1)	-4(1)
C(7)	19(1)	17(1)	15(1)	3(1)	5(1)	-1(1)
C(8)	16(1)	15(1)	14(1)	0(1)	7(1)	-4(1)
C(9)	14(1)	15(1)	14(1)	2(1)	7(1)	-1(1)
O(2)	19(1)	13(1)	17(1)	-1(1)	5(1)	2(1)
O(3)	22(1)	13(1)	16(1)	2(1)	2(1)	0(1)
N(3)	15(1)	14(1)	13(1)	-1(1)	3(1)	-2(1)
C(10)	16(1)	15(1)	14(1)	1(1)	7(1)	2(1)
C(11)	20(1)	18(1)	15(1)	3(1)	2(1)	1(1)
N(4)	16(1)	15(1)	14(1)	0(1)	5(1)	1(1)
C(12)	14(1)	16(1)	14(1)	-1(1)	7(1)	2(1)
C(13)	18(1)	17(1)	19(1)	-1(1)	8(1)	-1(1)
C(14)	16(1)	23(1)	17(1)	-7(1)	4(1)	-3(1)
C(15)	19(1)	26(1)	15(1)	-2(1)	1(1)	5(1)
C(16)	19(1)	17(1)	15(1)	0(1)	4(1)	4(1)
C(17)	15(1)	15(1)	14(1)	-3(1)	6(1)	2(1)
C(18)	17(1)	15(1)	14(1)	-1(1)	6(1)	3(1)
O(4)	20(1)	14(1)	14(1)	-1(1)	0(1)	-3(1)
O(5)	25(1)	14(1)	18(1)	-3(1)	9(1)	-1(1)
O(6)	33(1)	16(1)	21(1)	-4(1)	10(1)	-6(1)
C(19)	34(1)	28(1)	23(1)	0(1)	11(1)	-6(1)
C(20)	33(1)	32(1)	29(1)	0(1)	10(1)	-3(1)

Table 10d: Hydrogen coordinates (x 10^4) and isotropic displacement parameters ($Å^2$x 10^{-3}) for $[Zn^{II}(ChaH_{-1})_2(C_2H_6O)]$.

Atom	x	y	z	U(eq)
H(2A)	4216(12)	1665(13)	2246(13)	21(6)
H(2B)	3802(15)	737(11)	2103(14)	25(6)
H(2C)	3534(16)	1364(15)	2665(12)	29(6)
H(4)	1748(14)	471(11)	–619(13)	20(6)
H(5)	478(15)	976(13)	–1700(12)	25(6)
H(6)	–234(12)	2260(14)	–1618(11)	20(6)
H(7)	428(14)	3127(11)	–446(13)	14(5)
H(11A)	2530(15)	7457(11)	1069(13)	22(6)
H(11B)	1815(12)	6766(15)	1164(14)	29(6)
H(11C)	2477(16)	6519(14)	705(12)	26(6)
H(13)	5044(14)	7954(11)	3481(13)	17(5)
H(14)	6085(13)	7475(12)	4732(12)	19(5)
H(15)	6066(13)	6064(13)	5163(11)	19(6)
H(16)	4947(14)	5108(11)	4349(13)	17(5)
H(1O5)	1444(18)	3369(19)	2736(16)	36(8)
H(2O5)	1620(20)	4044(18)	3168(19)	43(9)
H(1O6)	2008(18)	4923(17)	4245(16)	30(7)
H(19A)	890(18)	4029(12)	4745(16)	38(7)
H(19B)	1152(19)	4858(17)	5096(12)	49(8)
H(20A)	–50(17)	4633(15)	3365(12)	37(7)
H(20B)	–338(15)	4974(17)	4093(16)	42(7)
H(20C)	289(18)	5600(12)	3766(16)	41(7)

Table 10e: Torsion angles [°] for $[Zn^{II}(ChaH_{-1})_2(C_2H_6O)]$.

O(4)–Zn–O(1)–N(1)	–80.68(13)	C(8)–C(9)–O(2)–Zn	–178.87(14)
O(5)–Zn–O(1)–N(1)	95.00(11)	O(1)–Zn–O(2)–C(9)	–0.29(12)
O(3)–Zn–O(1)–N(1)	–162.20(10)	O(4)–Zn–O(2)–C(9)	140.43(12)
O(2)–Zn–O(1)–N(1)	–0.26(10)	O(5)–Zn–O(2)–C(9)	–103.35(12)
Zn–O(1)–N(1)–C(1)	–178.31(12)	O(3)–Zn–O(2)–C(9)	79.3(2)
Zn–O(1)–N(1)–C(9)	0.77(18)	O(1)–Zn–O(3)–C(18)	141.10(13)
O(1)–N(1)–C(1)–N(2)	–177.33(15)	O(4)–Zn–O(3)–C(18)	1.21(12)
C(9)–N(1)–C(1)–N(2)	3.6(3)	O(5)–Zn–O(3)–C(18)	–113.43(13)

O(1)–N(1)–C(1)–C(2)	2.5(2)	O(2)–Zn–O(3)–C(18)	63.9(2)
C(9)–N(1)–C(1)–C(2)	–176.55(16)	O(4)–N(3)–C(10)–N(4)	179.67(16)
N(1)–C(1)–N(2)–C(3)	–1.0(3)	C(18)–N(3)–C(10)–N(4)	1.2(3)
C(2)–C(1)–N(2)–C(3)	179.21(16)	O(4)–N(3)–C(10)–C(11)	–0.3(2)
C(1)–N(2)–C(3)–C(8)	–2.7(3)	C(18)–N(3)–C(10)–C(11)	–178.79(17)
C(1)–N(2)–C(3)–C(4)	177.89(17)	N(3)–C(10)–N(4)–C(12)	0.6(3)
N(2)–C(3)–C(4)–C(5)	176.91(17)	C(11)–C(10)–N(4)–C(12)	–179.46(17)
C(8)–C(3)–C(4)–C(5)	–2.6(3)	C(10)–N(4)–C(12)–C(17)	–1.2(3)
C(3)–C(4)–C(5)–C(6)	–0.2(3)	C(10)–N(4)–C(12)–C(13)	178.99(17)
C(4)–C(5)–C(6)–C(7)	2.2(3)	N(4)–C(12)–C(13)–C(14)	179.94(17)
C(5)–C(6)–C(7)–C(8)	–1.3(3)	C(17)–C(12)–C(13)–C(14)	0.1(3)
C(6)–C(7)–C(8)–C(3)	–1.4(3)	C(12)–C(13)–C(14)–C(15)	–0.1(3)
C(6)–C(7)–C(8)–C(9)	178.81(17)	C(13)–C(14)–C(15)–C(16)	0.0(3)
N(2)–C(3)–C(8)–C(7)	–176.07(17)	C(14)–C(15)–C(16)–C(17)	0.1(3)
C(4)–C(3)–C(8)–C(7)	3.4(3)	N(4)–C(12)–C(17)–C(16)	–179.82(17)
N(2)–C(3)–C(8)–C(9)	3.7(3)	C(13)–C(12)–C(17)–C(16)	0.0(3)
C(4)–C(3)–C(8)–C(9)	–176.86(17)	N(4)–C(12)–C(17)–C(18)	0.1(3)
O(1)–N(1)–C(9)–O(2)	–1.1(2)	C(13)–C(12)–C(17)–C(18)	179.96(17)
C(1)–N(1)–C(9)–O(2)	177.93(16)	C(15)–C(16)–C(17)–C(12)	–0.1(3)
O(1)–N(1)–C(9)–C(8)	178.59(14)	C(15)–C(16)–C(17)–C(18)	179.92(18)
C(1)–N(1)–C(9)–C(8)	–2.4(2)	Zn–O(3)–C(18)–N(3)	–0.9(2)
C(7)–C(8)–C(9)–O(2)	–1.7(3)	Zn–O(3)–C(18)–C(17)	179.53(15)
C(3)–C(8)–C(9)–O(2)	178.55(17)	O(4)–N(3)–C(18)–O(3)	–0.2(2)
C(7)–C(8)–C(9)–N(1)	178.63(16)	C(10)–N(3)–C(18)–O(3)	178.22(16)
C(3)–C(8)–C(9)–N(1)	–1.1(2)	O(4)–N(3)–C(18)–C(17)	179.37(15)
N(1)–C(9)–O(2)–Zn	0.8(2)	C(10)–N(3)–C(18)–C(17)	–2.2(3)
C(12)–C(17)–C(18)–O(3)	–178.94(18)	C(10)–N(3)–O(4)–Zn	–177.26(12)
C(16)–C(17)–C(18)–O(3)	1.0(3)	O(1)–Zn–O(4)–N(3)	–88.42(13)
C(12)–C(17)–C(18)–N(3)	1.5(2)	O(5)–Zn–O(4)–N(3)	96.24(12)
C(16)–C(17)–C(18)–N(3)	–178.58(17)	O(3)–Zn–O(4)–N(3)	–1.28(11)
C(18)–N(3)–O(4)–Zn	1.28(18)	O(2)–Zn–O(4)–N(3)	–165.10(11)

Symmetry transformations used to generate equivalent atoms:

Table 10f: Hydrogen bonds for $[Zn^{II}(ChaH_{-1})_2(C_2H_6O)]$ [Å and °].

D–H...A	d(D–H)	d(H...A)	d(D...A)	<(DHA)
O(5)–H(1O5)...N(4)#1	0.77(3)	1.98(3)	2.744(2)	171(3)
O(5)–H(2O5)...O(6)	0.76(3)	1.92(3)	2.683(2)	178(3)
O(6)–H(1O6)...N(2)#2	0.75(3)	2.05(3)	2.794(2)	173(3)

Symmetry transformations used to generate equivalent atoms:

#1 –x+1/2,y–1/2,–z+1/2 #2 –x+1/2,y+1/2,–z+1/2